ELECTROHYDRODYNAMIC DRYING (EHD) AND ITS ASSOCIATED EFFECTS ON CONFORMATION OF FOOD PROTEINS USING MOLECULAR MODELING CONCEPT

By

Ashutosh Singh

Department of Bioresource Engineering

McGill University, Montreal

Quebec, Canada

June 2014

A thesis submitted to McGill University in partial fulfillment of the requirements of the degree of Doctor of Philosophy

Abstract

Food and its constituents are subjected to various processing techniques including, thermal, mechanical, chemical, extraction, extrusion, high pressure, high electric field and irradiation. Some of these techniques are used to either improve their shelf life (e.g. heating, pasteurization) by removing or inactivating microbes and toxins, extract valuable compounds (e.g. isolation, purification, oil extraction) or modify their properties (gelling, foaming, improving digestibility) to derive large varieties of additional food products (e.g. bread, yogurt, beverages). These processing methods can be categorized as thermal or non-thermal. The thermal techniques process food by subjecting them to high temperature, e.g. roasting, frying, drying etc.; these techniques have both positive (improvement in texture, color, taste etc.) and negative (generation of acrylamide through Maillard reaction, loss of nutritional value etc.) effects. Non-thermal methods (high-pressure, electric field treatment, irradiation etc.) have been developed to combat these disadvantages of thermal processes.

Proteins, which are one of the most important macromolecular constituent of food are very sensitive to external stresses, arising from the aforementioned processing methods. Studies have shown that under the influence of external stress proteins undergo structural and conformational changes, which impacts its functionality. Some food proteins including wheat gluten, egg proteins, milk proteins etc. are involved in patho-physiology of several allergic reactions. The relation between external stresses and food protein functionality is well known at a macro level but the mechanisms involved at the atomistic and molecular level are not well known.

In this study, we have designed and developed an apparatus for investigating non-thermal electrohydrodynamic (EHD) drying technique in which an electric wind generated from a charged electrode is used to enhance the drying of a hygroscopic or non hygroscopic sample under ambient conditions. The efficiency and applicability of the designed EHD unit are tested by evaluating the effect of process parameters such as electrode gap, applied voltage and presence of air cross-flow under ambient condition on drying kinetics of sand (non-hygroscopic) and wheat (hygroscopic) samples. The results revealed that presence of air cross-flow under

ambient conditions improve the drying process. Also, an increase in applied voltage and a reduction of the gap between the electrodes resulted in faster drying rates. Evaluation was also done to learn the effect of EHD drying on conformation of wheat protein using Fourier Transform Infrared Scpectroscopy (FT-IR), in which it was concluded that the application of external electric field during EHD drying process significantly affected the conformation of wheat protein. Shift in high and low frequency bands were observed suggesting changes in hydrogen bonding pattern within the protein due to structural and conformational modification under external electric field.

In this study, molecular dynamics (MD) modeling technique was applied to explore the behavior of protein, at ambient conditions and under the influence of external electric field stress. MD simulations were performed on two proteins, soybean hydrophobic protein and wheat gliadin protein under electric field strength ranging from 0.002 V/nm to 3 V/nm. By performing these simulation a valuable insight into the effects of electric field on protein conformation was noted through application of nominal electric field of strength 0.002 V/nm - 0.004 V/nm which had no effect on the conformation and surface properties of proteins, but as the field strength was increased to 3 V/nm a complete unfolding of the protein was observed. Assessment of hydrogen bond evolution during the course of simulation suggested that external electric field affects the hydrogen bonding pattern. This observation was later validated by conducting an FT-IR study on formation of hydrated wheat gluten protein, where it was concluded that the application of an external electric field stress influences the hydrogen bonding pattern of the protein resulting in the occurrence of intramolecular hydrogen-bonded antiparallel β-sheet aggregates.

RÉSUMÉ

Les aliments et leurs constituants sont soumis à divers traitements/procédés de transformation avant d'arriver sur notre table. Les plus communs sont les procédés thermiques, mécaniques et chimiques, l'extraction, l'extrusion, la pression, les champs électriques élevés et l'irradiation. Ces technologies sont soit utilisées pour accroître leur durée de vie en éliminant les microbes et les toxines, soit pour extraire les composés actifs, ou encore pour modifier leurs propriétés. En général, on distingue deux grands types de procédés: des traitements thermiques et les traitements non thermiques. Les traitements thermiques consistent à soumettre les aliments à des températures élevées qui permettent d'améliorer la texture, la couleur, la digestibilité et le goût de ces derniers. Par contre, ils peuvent aussi engendrer la formation d'acrylamide par réaction de Maillard et la perte de leur valeur nutritive. Des méthodes non-thermiques (haute pression, traitement aux champs électriques, irradiation, et autres) ont été développées pour éviter ces inconvénients.

Les protéines sont l'une des constituantes macromoléculaires les plus importants de notre alimentation. Plusieurs études ont démontré que lorsqu'elles sont exposées à ces traitements, elles subissent des changements structuraux et de conformation qui affectent leur fonctionnalité. Lorsque les protéines comme le gluten de blé, les protéines d'œuf et les protéines de lait subissent des modifications, elles peuvent causer, chez certaines personnes, des réactions allergènes. La relation entre les contraintes externes et la fonctionnalité des protéines alimentaires est relativement bien connu au niveau macroscopique, mais les mécanismes impliqués aux niveaux moléculaire et atomistique sont très peu documentés.

Dans cette étude, un appareil a été conçu et développé pour étudier un nouveau mode de séchage non-thermique: le séchage par électrohydrodynamique (EHD). L'appareil crée un vent de particules électriques, produit à partir d'une électrode chargée, qui permet d'améliorer le séchage. L'efficacité et l'applicabilité de l'unité EHD a été testées en évaluant les effets des paramètres d'opération comme : la distance entre les électrodes, la tension appliquée et la présence d'un courant d'air forcé perpendiculaire au flux des particules électriques. Le montage a permis d'étudier, sous des conditions ambiantes de température et d'humidité relative, la cinétique de séchage d'échantillons de sable (matière non hygroscopique) et de blé (matière

hygroscopique). Les résultats ont indiqué que la présence de courant d'air forcé permettait d'améliorer le processus de séchage. De plus, l'augmentation de la tension appliquée aux électrodes ainsi que la diminution de la distance entre ces dernières a permis d'accroître la vitesse de séchage. L'appareil a aussi été utilisé pour étudier les effets du mode de séchage EHD sur la structure de la protéine de blé. L'analyse, par spectroscopie infrarouge à transformée de Fourier (FT-IR), des échantillons traités a révélé que le procédé EHD affectait la conformation de la protéine de blé. Les décalages observés dans certaines bandes, à hautes et à basses fréquences, ont suggéré des changements dans le profil des liaisons-hydrogène à l'intérieur de la protéine. Ces changements ont été associés à la modification de structure et de conformation de la protéine qui avait été exposée à un champ électrique élevé lors du séchage EHD.

La modélisation de la dynamique moléculaire (DM) a été utilisée pour étudier le comportement de la protéine, sous des conditions ambiantes et sous l'influence d'un champ électrique de haute intensité. Les simulations ont porté sur deux types de protéines : une protéine hydrophobe de soja et la gliadine de blé. Lors de ces essais, l'intensité du champ électrique était de 0,002 à 3 V / nm. Les resultants des simulations ont indiqué que les champs électriques dont l'intensité était de 0.002 à 0,004 V /nm n'avait pas d'effet sur la conformation et sur les propriétés de surface des protéines. Par contre, lorsque l'intensité du champ était augmentée à 3 V / nm, un déploiement complet de la protéine a été observée. L'évaluation de l'évolution des liaisons hydrogène a suggéré que le champ électrique externe affectait le mode de liaison des liaisons-hydrogène. Cette observation a été validée par une étude sur la formation de protéines de gluten de blé hydraté exposées à des champs électriques élevés. L'analyse par FT-IR des protéines a révélée que l'application de champs électriques élevés influence la distribution spatiale des liaisons-hydrogène résultant dans la formation intramoléculaire d'agrégats antiparallèles de structures-β reliées par des liaisons-hydrogène.

Acknowledgement

I would like to express my sincere gratitude towards my supervisor Dr. G.S.V. Raghavan, for his guidance and support throughout my graduate life at McGill, it has been and will always be a matter of great pride, pleasure to work for him, his perpetual energy and enthusiasm has motivated all his advisees including me.

I would also like to thank Dr. Valerie Orsat for serving as my advisor and the guidance she provided with the technical problems that I faced during my doctorate program. Special thanks to Mr. Yvan Gariepy for his patience, knowledge and his willingness to help me with all technical problems that I faced during my doctorate program.

I would also like to thank the faculty and staff in the Department of Bioresource Engineering, especially Ms. Susan Gregus, Ms. Abida Subhan and Ms. Patricia Singleton for their help in administrative affairs and Dr. Darwin Lyew for patiently helping me out with queries on grant applications. I am also appreciative of the help and support provided by Dr. F.C. Lai, Dr. Venkatesh Meda and Dr. Chithra Karunakaran during my internship at University of Oklahoma, University of Saskatchewan and Canadian Light Source respectively.

Special thanks to Dr. Rachid Lahlali for teaching me the Fourier Transform Infrared Spectroscopy technique data analysis (PCA, Curve Fitting) and for being a great mentor. I deeply value your guidance and mentorship.

I would like to express my appreciation to my friends Gopu, Jiby, Sai Kranthi Kumar, Abid, Ting Ting, Pansa, Tarun Khatri, Jamshid, Nandkishor for their moral support and motivation. Thanks to all my other friends here, there, and everywhere.

I gratefully acknowledge Natural Sciences and Engineering Research Council of Canada (NSERC), Fonds québécois de la recherche sur la nature et les technologies (FQRNT) and CALCUL Canada for the financial and supercomputing support throughout my thesis work.

Lastly, I would like to acknowledge my parents Mr. Yadubansh Narayan Singh and Mrs. Pushpa Singh for the struggle and hardship they have faced in raising me and making me what I am now. I thank my brother Mr. Thakur Anshuman Singh, my sister in-law Mrs. Ankita Divya, my cute niece Annapurna, my sister Priyanka and love of my life Shireen for all their love and support. This thesis is dedicated to you all.

Thesis Format

This thesis is submitted in the format of papers suitable for journal publication. This thesis format has been approved by the Faculty of Graduate and Postdoctoral Studies, McGill University, and follows the conditions outlined in the Guidelines: Concerning Thesis Preparation, which are as follows:

"As an alternative to the traditional thesis format, the dissertation can consist of a collection of papers of which the student is an author or co-author. These papers must have a cohesive, unitary character making them a report of a single program of research. The structure for the manuscript-based thesis must conform to the following:

1. Candidates have the option of including, as part of the thesis, the text of one or more papers submitted, or to be submitted, for publication, or the clearly duplicated text (not the reprints) of one or more published papers. These texts must conform to the "Guidelines for Thesis Preparation" with respect to font size, line spacing and margin sizes and must be bound together as an integral part of the thesis. (Reprints of published papers can be included in the appendices at the end of the thesis).
2. The thesis must be more than a collection of manuscripts. All components must be integrated into a cohesive unit with a logical progression from one chapter to the next. In order to ensure that the thesis has continuity, connecting texts that provide logical bridges between the different papers are mandatory.
3. The thesis must conform to all other requirements of the "Guidelines for Thesis Preparation" in addition to the manuscripts.

The thesis must include the following

(a) A table of contents;

(b) An abstract in English and French;

(c) An introduction which clearly states the rational and objectives of the research;

(d) A comprehensive review of the literature (in addition to that covered in the introduction to each paper);

(e) A final conclusion and summary;

4. As manuscripts for publication are frequently very concise documents, where appropriate, additional material must be provided (e.g., in appendices) in sufficient detail to allow a clear and precise judgment to be made of the importance and originality of the research reported in the thesis.

5. In general, when co-authored papers are included in a thesis the candidate must have made a substantial contribution to all papers included in the thesis. In addition, the candidate is required to make an explicit statement in the thesis as to who contributed to such work and to what extent. This statement should appear in a single section entitled "Contributions of Authors" as a preface to the thesis. The supervisor must attest to the accuracy of this statement at the doctoral oral defense. Since the task of the examiners is made more difficult in these cases, it is in the candidate's interest to clearly specify the responsibilities of all the authors of the co-authored papers".

Contribution of Authors

The following are the manuscripts prepared for publication.

1. **Singh, Ashutosh**; Orsat, Valérie; Raghavan, Vijaya. 2012 "A comprehensive review on electrohydrodynamic drying and high voltage electric field in the context of food and bioprocessing" Drying Technology 30, 1812–1820.
2. **Singh, Ashutosh**; Nair, Gopu; Rahimi, Jamshid; Gariepy, Yvan; Raghavan, G.S.V. 2013. "Effect of static high electric field pre-treatment on microwave-assisted drying of potato slices." Drying Technology 31, 1960-1968.
3. **Singh, Ashutosh**; Orsat, Valérie; Raghavan, Vijaya. 2013. "Soybean Hydrophobic Protein Response to External Electric Field: A Molecular Modeling Approach." Biomolecules 3, no. 1: 168-179.
4. **Singh, Ashutosh**; Munshi, Shirin; Raghavan, G.S.V. 2013. "Effect of external electric field stress on gliadin protein conformation" Proteomes 1, no. 2: 25-39.
5. **Singh, Ashutosh**; Rachid Lahlali; Sai Kranthi Kumar Vanga; Chithra Karunakarn; Valerie Orsat; Raghavan, Vijaya. 2014. "Effect of high electric field on secondary structure of wheat gluten" Journal of Cereal Science. (Submitted)
6. **Singh, Ashutosh**; Sai Kranthi Kumar Vanga; Gopu Raveendran Nair; Yvan Gariepy; Valerie Orsat; Raghavan, Vijaya. 2014.. "Electrohydrodynamic Drying of Sand." Journal of Electrostatics. (Submitted)
7. **Singh, Ashutosh**; Sai Kranthi Kumar Vanga; Gopu Raveendran Nair; Yvan Gariepy; Valerie Orsat; Raghavan, Vijaya. 2014.. "Electrohydrodynamic Drying of Wheat and its Effect on Wheat Protein Conformation." (To be Submitted)

The research work reported here was performed and completed by the candidate Ashutosh Singh. He was responsible for the experimental setup, design of experiment, analytical work in the laboratory, data analysis, modeling and preparing the manuscripts and thesis. Professor G. S. Vijaya Raghavan is the thesis supervisor, providing scientific advice and technical supervision. He was also directly associated with editing and reviewing the manuscripts. Dr. Valerie Orsat is the Professor and Chair of Department of Bioresource Engineering. She provided the scientific advice and guidance throughout the thesis work.

Dr. Rachid Lahlali (Research Associate) and Dr. Chithra Karunakarn (Beamline scientist) at Canadian Light Source significantly contributed in the analysis of FT-IR data for wheat gluten.

Mr. Yvan Gariepy is an academic associate in the Department of Bioresource Engineering, McGill University, Canada. He was actively involved in providing the research facilities for conducting the experiments. Ms. Shirin Munshi, M.Sc. School of Dietetics and Human Nutrition; Mr Gopu Raveendran Nair, Mr. Jamshid Rahimi PhD candidates in Bioresource Engineering Department, and Mr. Sai Kranthi Kumar Vanga M.Sc. Candidate in Bioresource Engineering Department, McGill University, Canada contributed with technical support for the research and helped in editing.

Table of Content

ABSTRACT ..... **ii**

RESUME ..... **iv**

ACKNOWLEDGEMENTS ..... **vi**

THESIS FORMAT ..... **vii**

CONTRIBUTION OF AUTHORS ..... **viii**

LIST OF TABLES ..... **xv**

LIST OF FIGURES ..... **xviii**

NOMENCLATURE ..... **xxiv**

CHAPTER 1. INTRODUCTION **1**

1.1. Hypothesis 4
1.2. Objectives 4
1.2.1. Overall objective 4
1.2.2. Specific objectives 4

CHAPTER 2. PART 1: A COMPREHENSIVE REVIEW ON ELECTROHYDRODYNAMIC DRYING AND HIGH VOLTAGE ELECTRIC FIELD IN THE CONTEXT OF FOOD AND BIOPROCESSING **6**

2.1. Abstract 6
2.2. Introduction 7
2.3. Electrohydrodynamic (EHD) drying mechanism 8
2.3.1. Electro-kinetic property of corona wind 10
2.3.2. EHD drying system 12
2.3.3. EHD efficiency 13
2.4. Drying of agricultural products 17
2.4.1. EHD application in drying of food products 18
2.4.2. Application in post-harvest storage 21
2.5. Conclusion 22

CONNECTING STATEMENT **24**

CHAPTER 3. EFFECT OF HIGH ELECTRIC FIELD PRE-TREATMENT ON MICROWAVE-ASSISTED DRYING OF POTATO SLICES 25

3.1. Abstract 25
3.2. Introduction 25
3.3. Experimental Section 27
3.3.1. Materials and Methods 27
3.3.2. Static High Electric Field Pre-Treatment 27
3.3.3. Microwave-Convective Drying 28
3.3.4. Hot-Air Drying 28
3.3.5. Experimental Design 29
3.3.6. Mathematical Modeling 29
3.3.7. Effective Diffusion Coefficient 30
3.3.8. Color Measurement 31
3.3.9. Texture Analysis 31
3.3.10. Statistical Analysis 32
3.4. Results and Discussion 32
3.4.1. Drying Kinetics 32
3.4.2. Effective Moisture Diffusion 37
3.4.3. Texture Analysis 37
3.4.4. Color Analysis 38
3.5. Conclusion 40

CONNECTING STATEMENT 41

CHAPTER 4. ELECTROHYDRODYNAMIC DRYING (EHD) OF SAND 42

4.1. Abstract 42
4.2. Introduction 42
4.3. Materials and Methods 44
4.3.1. Test Sample Preparation 44
4.3.2. Experimental Setup 44
4.3.3. Experimental Design 45
4.3.4. Mathematical Modeling 47
4.3.5. Determination of Specific Energy Consumption 49
4.3.6. Statistical Analysis 49
4.4. Results and Discussion 50
4.4.1. Current-Voltage Relationship 50
4.4.2. Drying Kinetics 51
4.4.3. Response Surface Analysis 52
4.5. Conclusion 60

CONNECTING STATEMENT 61

CHAPTER 5. ELECTROHYDRODYNAMIC DRYING (EHD) OF WHEAT AND ITS AEFFECT ON WHEAT PROTEIN CONFORMATION 62

5.1. Abstract 62
5.2. Introduction 63
5.3. Materials and Methods 65
5.3.1. Sample Preparation 65
5.3.2. Experimental Setup 65
5.3.3. Drying Experiment 66
5.3.4. Mathematical Modeling 66
5.3.5. Determination of Specific Energy Consumption 68
5.3.6. FT-IR Spectroscopy 68
5.3.7. Differential Scanning Calorimetry 69
5.3.8. Statistical Analysis 69
5.4. Results and Discussion 69
5.4.1. Current-Voltage Relationship 69
5.4.2. Drying Kinetics and Specific Energy Consumed 70
5.4.3. Effect of EHD Drying on Wheat Protein 73
5.4.4. Thermal Properties of EHD dried Wheat 81
5.5. Conclusion 83

CONNECTING STATEMENT 84

CHAPTER 6. PART II – THEORETICAL ASPECTS OF MOLECULAR DYNAMICS (MD) INCLUDING ITS APPLICATION THROUGH SIMULATION OF PROTEIN'S STRUCTURE UNDER VARYING EXTERNAL STRESSES 85

6.1. Abstract 85
6.2. Introduction 86
6.3. Molecular Modeling of Proteins 91
6.3.1. Molecular Dynamics 92
6.3.2. Simulation Methodologies and Stages 97
6.4. Application of MD in Studying Food Proteins 99
6.4.1. Hydration of Proteins 101
6.4.2. Thermal Treatment of Protein 102
6.4.3. Electrical Treatment of Protein 104
6.5. Conclusion 105

CONNECTING STATEMENT 106

CHAPTER 7. SOYBEAN HYDROPHOBIC PROTEIN RESPONSE TO EXTERNAL ELECTRIC FIELD: A MOLECULAR MODELING APPROACH 107

7.1. Abstract 107
7.2. Introduction 107
7.3. Experimental Section 108

7.4. Results and Discussion 110
7.4.1. Secondary Structure Analysis 110
7.4.2. Dipole Moment Distribution 111
7.4.3. Root Mean Square Deviation (RMSD) 115
7.4.4. Radius of Gyration 115
7.4.5. Solvent Accessible Surface Area (SASA) 117
7.5. Conclusion 118
CONNECTING STATEMENT 119

CHAPTER 8. EFFECT OF EXTERNAL ELECTRIC FIELD STRESS ON GLIADIN PROTEIN CONFORMATION 120
8.1. Abstract 120
8.2. Introduction 120
8.3. Experimental Section 121
8.4. Results and Discussion 122
8.4.1. Secondary Structure Analysis 122
8.4.2. Dipole Moment Distribution 125
8.4.3. Root Mean Square Deviation (RMSD) 127
8.4.4. Radius of Gyration 131
8.4.5. Solvent Accessible Surface Area (SASA) 131
8.5. Conclusion 135
CONNECTING STATEMENT 136

CHAPTER 9. EFFECT OF HIGH ELECTRIC FIELD ON THE SECONDARY STRUCTURE OF WHEAT GLUTEN 137
9.1. Abstract 137
9.2. Introduction 138
9.3. Materials and Methods 140
9.3.1. Gluten Protein Sample 140
9.3.2. Electric Field Treatment 141
9.3.3. FT-IR Spectroscopy 142
9.3.4. Principal Component Analysis 142
9.4. Results and Discussion 142
9.4.1. FT-IR Analysis of Conformational Changes in Gluten Protein 142
9.4.2. PCA Analysis 151
9.5. Conclusion 152

CHAPTER 10. SUMMARY, CONCLUSION, CONTRIBUTION TO KNOWLEDGE AND FUTURE WORK 153
10.1. Summary 153
10.2. Conclusion 156
10.3. Contribution to Knowledge 159

10.4. Future Work 160

BIBLIOGRAPHY.....161

List of Tables

Table 2.1 Comparison of electrode configuration and amount of specific energy consumed 16

Table 2.2 Specific energy consumption for several food products using spouted bed dryer 18

Table 2.3 EHD and high voltage application in food industry 22

Table 3.1 Various mathematical models used for predicting drying kinetics of potato slices 29

Table 3.2 Estimated statistical values, *RMSE* and R^2 values obtained for different drying models. 36

Table 3.3 Effective moisture diffusion coefficient of potato slices. Column –wise values followed by the same letter are not significantly different. Test used: Duncan's Multiple Range test ($p \leq 0.05$) 37

Table 3.4 Color properties of fresh and dried potato slices. Column –wise values followed by the same letter are not significantly different. Test used: Duncan's Multiple Range test ($p \leq 0.05$) 39

Table 4.1 Coded (individually for each experimental factor) and corresponding actual values of all independent variables. 46

Table 4.2 The Central Composite Design for response surface analysis of the interaction between independent variables (factors) and their effect on dependent variables (responses).....46

Table 4.3 Mathematical models to fit drying kinetics 47

Table 4.4 Best fitted drying models and their corresponding statistical values of RMSE, R^2 and SSE for different experimental conditions 52

Table 4.5 ANOVA analysis for the effect of process parameters, air speed (A), electrode gap (G_e) and applied voltage (V) on percentage water removed 55

Table 4.6 ANOVA analysis for the effect of process parameters, air speed (A), electrode gap (G_e) and applied voltage (V) on Sherwood's number 56

Table 4.7 ANOVA analysis for the effect of process parameters, air speed (A), electrode gap (G_e) and applied voltage (V) on EHD number 57

Table 4.8 Regression Equations established between process parameters, air velocity (A), electrode gap (G_e) and applied voltage (V) and dependent variables (water removed (%), Sherwood and EHD Numbers and Specific energy consumed (kJ/kg).....59

Table 5.1 Mathematical models used to predict EHD drying kinetics of wheat. 67

Table 5.2 Estimated statistical values, RMSE, R^2 and SSE values obtained for various drying models..... 72

Table 5.3 Amide I band frequencies and assignments to protein secondary structure in H_2O media 74

Table 5.4 Positions, width and areas of the bands fitted to the normalized FT-IR spectra of wheat protein (1720 cm^{-1} – 1580 cm^{-1}) subjected to different electric field intensities and treatment time.....80

Table 6.1 Functional properties of food proteins 87

Table 6.2 Effect of food processing techniques on amino acids and proteins 89

Table 6.3 Health-functional properties of proteins 90

Table 7.1 Summary of parameters used in the MD simulated systems 110

Table 7.2 RMSD, Radius of Gyration and Total Dipole moment of the SHP protein Backbone, averaged over 1ns of simulation time..... 112

Table 8.1 Primary sequence of α-β gliadin [Chain C of protein database bank (PDB): 2NNA]. 122

Table 8.2 Backbone Root Mean Square Deviation (RMSD), radius of gyration and total dipole moment, averaged over 10 ns of simulation time. 126

Table 8.3 Hydrogen bond formation between donor and acceptor amino acids and their occupancy (over 2%) during the course of simulation under external electric field stress. 131

Table 9.1 Infrared absorption bands of peptide linkages 140

Table 9.2 Amide I band frequencies and assignment to protein secondary structure in H_2O media 143

Table 9.3 Positions, width and areas of the bands fitted to the normalized FT-IR spectra of hydrated gluten protein (1720 cm^{-1} – 1580 cm^{-1}) subjected to different electric field intensities and treatment time. 149

List of Figures

Figure 2.1 Schematic of the system used by Goodenough et al. for their experimental study of a corona wind blower 11

Figure 2.2 Schematic of electrohydrodynamic drying (EHD) system 12

Figure 2.3 *V-I* curves for needle electrode configuration with electrode spacing of 1.27cm and 2.54 cm 14

Figure 2.4 Performance for negative and positive corona discharges for 3 mm glass beads 15

Figure 2.5 Performance for negative and positive corona discharges for 6 mm glass beads. 15

Figure 2.6 Specific energy consumption (kJ/kg water) at various voltages for different electrode configurations 16

Figure 3.1 Schematic of high voltage electric field setup: 1, voltage regulator; 2, AC step up transformer; 3, Aluminum plate; 4, potato slices; 5, grounded aluminum plate; 6, ground; 7, supporting insulator; 8, 110 V alternating current source. 27

Figure 3.2 Schematic of microwave-convective drying apparatus. 28

Figure 3.3 Instron Universal testing machine schematic equipped with Kramer sheer press 32

Figure 3.4 (a) Moisture content and (b) moisture ratio variation with change in time for potato slices dried in hot-air (HA) alone and pretreated with high electric field (HA-HEF) 33

Figure 3.5 (a) Moisture content and (b) moisture ratio variation with change in time for potato slices dried in microwave-convective dryer (MW) and pretreated with high electric field (MW-HEF). HEF pretreatment had no significant effect and hence the data obtained overlapped. 33

Figure 3.6 Drying kinetic model fitting to the drying curve for (a) hot-air (HA) and (b) high electric field pretreated samples (HA+HEF).....35

Figure 3.7 Drying kinetic model fitting to the drying curve for (a) microwave convective (MW) and (b) high electric field pretreated samples (MW+HEF).....35

Figure 3.8 Force required to crush the fresh and dried potato slices with and without pretreatment.....38

Figure 3.9 Energy required to crush the fresh and dried potato slices with and without pretreatment 38

Figure 3.10 Curling of potato slices dried under hot air and microwave convective dryer 39

Figure 3.11 No Curling was observed in HEF pretreated potato slices dried under hot air and microwave-convective dryer 39

Figure 4.1 Schematic of the EHD experimental setup 45

Figure 4.2 Current-Voltage relationship with respect to electrode gap.....50

Figure 4.3 Drying curve for saturated sand sample under all experimental conditions.....51

Figure 4.4 Tukey's HSD (honest significant difference) test on effect of different experimental conditions (coded) and percentage of water removed 53

Figure 4.5 Response surface plot of the effect of process parameters on percentage of water removed. 54

Figure 4.6 Summary Response surface plot of the effect of process parameters on Sherwood number. 56

Figure 4.7 Response surface plot of the effect of process parameters on EHD number. 57

Figure 4.8 Response surface plot of the effect of process parameters on specific energy consumed (kJ/kg). 58

Figure 5.1 Backbone Schematic of the EHD experimental setup. 66

Figure 5.2 Current-Voltage relationship with respect to electrode gap 70

Figure 5.3 Drying curve for conditioned wheat (20% d.b.) sample under all experimental conditions. 72

Figure 5.4 Typical FT-IR scan of conditioned wheat (20 % d.b.) and EHD dried wheat (air velocity 2m/s; applied voltage 15 kV)..... 75

Figure 5.5 FT-IR second-derivative spectra for conditioned wheat (Control) and EHD dried wheat (air velocity 2 m/s; applied voltage 15 kV). 76

Figure 5.6 Normalized FT-IR spectra of the Amide I region of EHD dried wheat and control samples. 77

Figure 5.7 Second-derivative of normalized spectra showing the valleys and peaks for all EHD dried wheat samples and control (conditioned wheat). Note: Experimental conditions of air velocity 1-1.5-2 m/s; applied voltage 0 kV had similar second derivative as conditioned wheat (CW). 77

Figure 5.8 DSC thermograms for all experimental conditions and control..... 82

Figure 6.1 (a) FASTA sequence of soybean hydrophobic protein (SHP) (PDB Accession Code: 1HYP) (Primary structure) (b) Tertiary structure of soybean hydrophobic protein (SHP) representing 3 α-helical and a 3/10 helical substructures (Secondary structure) (Singh et al., 2013c) 86

Figure 6.2 A typical cubic simulation box with protein in the center, surrounded by explicit solvent atoms (water). 96

Figure 6.3 Three-dimensional illustration of periodic boundary conditions. The protein is represented in green in the center. The box in the center is the main simulation box. 97

Figure 6.4 Outline of the simulation stages commonly followed while using GROMACS MD simulation package. 98

Figure 7.1 FASTA sequence of SPH protein, four disulphide bonds between Cys8-Cys43, Cys14-Cys28, Cys45-Cys77 and Cys29-Cys67 (PDB accession code 1HYP). ..110

Figure 7.2 STRIDE showing evolution of secondary structure of soybean hydrophobic protein (SHP) (a) without electric field (b) 0.002 V/nm (c) 0.004 V/nm and (d) 3 V/nm external electric field. 111

Figure 7.3 Total dipole moment of SHP under the influence of an external electric field. 113

Figure 7.4 SHP protein under no external electric field. 113

Figure 7.5 SHP protein snapshot at the end of the MD simulation under the influence of 0.002 V/nm and 0.004 V/nm. 114

Figure 7.6 SHP protein snapshot at the end of the MD simulation under the influence of 0.002 V/nm and 0.004 V/nm. 115

Figure 7.7 RMSD of SHP backbone under the effect of external electric field. 116

Figure 7.8 SHP radius of gyration (Rg) in the absence and presence of various external electric fields. 116

Figure 7.9 Solvent accessible surface area (nm^2) under the influence of an external electric field. 117

Figure 7.10 SHP snapshot of surface properties at the beginning and end of the MD simulation under electric field intensity of 3V/nm.. 118

Figure 8.1 Stride evolution of secondary structures of gliadin protein under an external electric field (a) Without external electric field; (b) Under electric field strength 0.001V/nm; (c) Under electric field strength 0.002 V/nm (Color code: Cyan denotes turn). 124

Figure 8.2 Evolution of the hydrogen bonds during the course of simulation under the influence of an applied external electric field.....126

Figure 8.3 Total dipole moment of gliadin protein under the influence of an applied external electric field. 127

Figure 8.4 RMSD of the gliadin protein backbone under the influence of an external electric field.....129

Figure 8.5 RMSD evolution with respect to number of hydrogen bonds; (a) without electric field (b) 0.001V/nm; (c) 0.002 V/nm. 130

Figure 8.6 Radius of gyration (Rg) of gliadin protein under the stress of an external electric field.....132

Figure 8.7 Radius of gyration evolution with respect to number of hydrogen bonds; (a) without electric field (b) 0.001V/nm; (c) 0.002 V/nm. 134

Figure 8.8 Changes in solvent accessible surface area [SASA (nm^2)] under the influence of an external electric field.. 134

Figure 8.9 Snapshots of gliadin protein surface at the (a) beginning; and (b) end of simulation under external electric field strength of 0.002 V/nm. 135

Figure 9.1 Schematic of the static high electric field treatment system. 141

Figure 9.2 Typical FTIR spectra of hydrated wheat gluten protein.....144

Figure 9.3 FT-IR spectra of hydrated (H) gluten proteins treated with high electric field intensities (0, 3.5 and 7 kV/cm) for set times (30, 60 and 90 minutes) 144

Figure 9.4 Normalized spectra of the Amide I region of hydrated gluten protein.....145

Figure 9.5 Normalized Amide I band of hydrated gluten protein subjected to control conditions of 0kV electric field intensity for 30 minutes fitted with sums of Gaussian bands. 146

Figure 9.6 Second derivative of normalized spectra showing the valleys and peaks associated with specific secondary structures for all experimental conditions.....147

Figure 9.7 Variations in relative areas of the bands fitted to the normalized FT-IT spectra of Amide I region (1720 cm^{-1} – 1580 cm^{-1}) of gluten protein. 151

Figure 9.8 PCA loadings plots of the FT-IR spectra in the 1720-1580 cm-1 Amide I region.....152

Nomenclature

EHD	Electrohydrodynamic drying
F_V	volume force (N)
q_e	charge density of ions ($C*m^{-3}$)
ρ_m	mass density of air ($kg*m^{-3}$)
e_0	permittivity of the medium ($F*m^{-1}$)
∇	vector gradient operator.
ν	velocity ($m\ s^{-1}$)
x, y and *z*	dimensional variables in the horizontal, longitudinal and vertical directions respectively;
d	electrode spacing (cm)
E	electric field strength ($V\ m^{-1}$)
B	represents ion mobility ($m^2\ V^{-1}\ s^{-1}$)
V	applied voltage (kV)
i/I	current (μA)
ε_0	electrical permittivity of air ($F\ m^{-1}$)
V_i	initiation voltage of the corona wind (kV)
Se	specific energy consumed (kJ/kg)
HEF	high electric field
MW	microwave
M.C.	moisture content
M_w	mass of water in the sample (g)
M_s	mass of the solid in the sample (g)
w.b.	wet basis
d.b.	dry basis
MR	moisture ratio

k	drying rate constant (min^{-1})
n, a, b and c	drying coefficients (unitless) which have values depending on the drying curve and equation
t	is the time (min)
$RMSE$	room mean square error
χ^2	Chi-squared
MR_i^{pred}	predicted MR at time t_i
$MR_i^{\exp}$	measured value of MR at time t_i
R^2	coefficient of determination
$\overline{MR}^{\exp}$	mean experimentally measured value of MR
SSE	reduced sum of square error
D_{eff}	effective coefficient of moisture diffusivity (m^2/s)
L	half-thickness of the potato slices
L*	whiteness or brightness/darkness
a*	redness/greenness
b*	yellowness/blueness
ΔE	color change
CCD	central composite design
RSM	response surface method
$(X_i,X_j,X_k....)$	independent variables/ process parameters/ factors
Y	response variable
Sh	Sherwood number
h_m	mass transfer coefficient (m/s)
d	diameter of the emitting wire electrode (m)
D	mass diffusivity (m^2/s)
$\dot{m}$	rate of mass transfer (kg/s)

A_c	sample surface area exposed to the corona wind (m^2)
Δc	water vapor concentration difference between the sample surface and ambient air (kg/m^3).
N_{EHD}	EHD number
M	mass of water removed (kg)
G_e	electrode gap (cm)
FT-IR	Fourier Transform Infrared Spectroscopy
H	Hamiltonian
$K(p)$	kinetic energy as a function of momenta
$V(q)$	potential energy as the function of generalized coordinates
F_i	total force experienced by an atom i in the direction r,
m_i	mass of the atom
r_i	position of the atom i
$r(t)$	current position
$a(t)$	acceleration
$r(t - \delta t)$	position of the atom from previous step
NAMD	Not Another Molecular Dynamics
VMD	Visual Molecular Dynamics
RMSD	Root mean square displacement/deviation (nm)
Rg	Radius of Gyration (nm)
SASA	Solvent accessible surface area (nm^2)
NPT	Constant number of particles, pressure, and temperature
NVT	Constant number of particles, volume, and temperature

Chapter 1

Introduction

This thesis is written in two parts, the first part of the thesis deals with the design and development of an electrohydrodynamic drying system and its applications in drying of food products. Drying is one of the most important and most commonly used unit operation in food industries to dehydrate food products in order to preserve and increase their shelf life. Conventional drying techniques involve the application of heat using conductive, convective and radiative sources alone or in combination to enhance mass transfer in food products (Bajgai et al., 2006b). These thermal processing techniques reduce the moisture content of these food materials in order to make them less susceptible to microbial activity and chemical deterioration. Drying is an energy intensive process and it accounts for about 10 % of the total energy required in food processing industries (Li et al., 2006).

Application of high drying temperatures adversely affects the nutritional and organoleptic properties of the food products (Raghavan et al., 2005a; Sunjka et al., 2004). Recent changes in consumer demand for products with superior organoleptic and nutritional properties and fresh like feel has forced food processors to look for alternate drying and processing techniques. This has led to the application of novel techniques such as freeze drying, microwave, radio-frequency and superheated steam either alone or in combination with conventional drying methods to produce dehydrated food products of higher quality. Freeze drying produces a product with excellent sensory and rehydration properties but it is extremely difficult and expensive to implement on an industrial scale (Raghavan et al., 2005a). Application of microwave and radio-frequency has led to decreased drying times and improved energy efficiencies of the process but problems associated with scale up has posed serious implementation issues.

Increasing global population and changes in world economy are placing severe pressure on utilization of natural resources for energy production. Emission of greenhouse gases (GHG) from conventional dryers utilizing fossil fuels for operation in food industries has raised concerns at both consumer and environmental levels. Resolution of these issues requires

innovative measures and practices for the development of alternative drying methods, which have minimal, or no effect on the food quality and also answer the environmental concerns associated with the drying process (Chen et al., 1994).

Electrohydrodynamic drying (EHD) is one of the important non-thermal food processing methods that has been receiving considerable attention lately. In EHD, when high voltage is applied to an electrode of small radius of curvature a corona wind is generated. This corona wind disturbs the boundary layer developed over the sample surface hence enhancing the mass transfer between the biological surface and the ambient air (Barthakur, 1990). It has several advantages over conventional drying techniques namely, it has a simplistic design with no movable parts, consumes less energy as compared to conventional drying techniques and can dry samples under ambient conditions (Lai, 2010).

Several studies have shown that electric field can be used to significantly enhance the drying rate and within the last few decades the use of electric field for the enhancement of heat and mass transfer processes has garnered great interest (Bajgai and Hashinaga, 2001a, b; Cao et al., 2004a; Cao et al., 2004b); for example studies on tomato slices (Esehaghbeygi and Basiry, 2011), apple slices (Atungulu et al., 2004; Hashinaga et al., 1999), potato slab (Chen et al., 1994), wheat (Cao et al., 2004a), rice (Cao et al., 2004b), scallop (Yaxiang et al., 2009), Japanese radish (Bajgai and Hashinaga, 2001b), okara (Li et al., 2006, 2005) are available in published journals. As most of these studies evaluate the application of EHD in drying of food products, hardly any of them discuss the effect of processing parameters including electrode gap, electrode geometry, applied voltage, and discharge polarity. It is important to analyze how these parameters interact with each other and affect the efficiency and applicability of the EHD process.

In the second part of the thesis exploration is made to understand the behavior of food proteins under an external electric field stress. Proteins are one of the most fundamental and integral food components. They act as a source of energy and the amino acids are essential for growth and maintenance of the human body. Proteins are not only vital nutritionally but also possess specific biological properties, which make them an essential functional food component. At present it is well demonstrated that physical methods such as application of heat and alkali or chemical modifications brought by phosphorylation, acylation and deamidation can be used to

modify the functional properties of food proteins by bringing out changes in protein structure (Sorgentini et al., 1995). Novel technologies such as high pressure processing (Ahmed et al., 2007) and pulsed electric field (Xiang et al., 2011) have also been used to modify food proteins such as whey and soy proteins. Pulsed electric field utilizes short electric pulses, which leads to structural modification in food proteins and reduces or improves their functional properties. In another study conducted by Han et al. in 2009 on the effect of pulsed electric field treatment on the properties of cornstarch, they demonstrated that application of electric field strength of 50 $kVcm^{-1}$ resulted in reduction of gelatinization temperatures and enthalpy. The shape of the cornstarch and crystallinity degree were affected significantly and it lost its granule shape and its crystallinity decreased. The rheological properties of cornstarch was also affected, the peak breakdown and final viscosity decreased with increase in electric field intensity (Han et al., 2009). To our knowledge no literature is available demonstrating the effect of EHD on the structural and functional properties of proteins and starch.

The field of molecular dynamics (MD) modeling is concerned with the atomic and molecular interactions that take place within the physical system that governs its microscopic and macroscopic behaviors. It was developed as a tool to numerically simulate simplistic models in statistical mechanics (Alder and Wainwright, 1959a), but advancement in computer technology paved the path for the development of MD modeling techniques to understand the structural and dynamic properties of biomolecules. The technique has been widely used in the field of molecular biology and pharmaceutical sciences, and it has led to the development of a wide range of efficient and accurate drug systems based on the structural and dynamic data obtained from the simulation. However, its use in food process engineering has been negligible; its development and application to modern sophisticated unit operations in food manufacturing is essential to evaluate the changes in the organoleptic and nutritional quality of the final food product. Current consumer preference is for high nutritional food products, manufactured through the application of energy efficient processes, which has challenged industries and researchers to develop and utilize newer techniques such as microwave or pulsed electric field and radio frequency, alone or in combination with traditional unit operations (Dev et al., 2008a). The development and optimization of food processes depends on mechanical limitations and the needs stated by the consumers in terms of the final product. In general, the quality of the final

product is estimated by quantifying its components such as proteins, starch, mineral, vitamins and other constituents. However, the quality of the constituents themselves is rarely considered as a parameter for the optimization process. Application of unit operations such as drying, freezing, filtration, *etc*. not only negatively impacts the quantity of the food constituents but also has a significant effect on their quality (Dutta et al., 2012).

1.1 Hypothesis

Application of EHD in the drying of food products requires a thorough understanding of the mechanism involved in generation of corona wind and removal of moisture from biological samples. Very few studies have studied the interaction between the process parameters and their effect on drying efficiency. For Part I of this study, the hypothesis is that the process parameters such as applied voltage, electrode gap and air cross-flow will affect the drying condition depending on their interaction with each other and it is important to understand this interaction to design, develop and optimize an EHD drying system.

For Part II of the thesis, since food contains several macromolecular constituents such as starch and proteins, the electric field used in EHD or even in other high voltage techniques like PEF will interact with the macromolecules. This interaction needs to be studied not only at the macro level but also at the molecular level. The hypothesis of this study is that an electric field can induce conformational changes and molecular dynamic simulation technique can be used to validate and visualize this change and help in the designing and optimization of food processes.

1.2 Objectives

1.2.1 Overall objective:

The overall objective of this study is to develop a new electrohydrodynamic drying method and elucidate its mechanisms and also examine its effect on the structural and chemical properties of wheat proteins.

1.2.2 Specific objectives:

The specific objectives of this study are as follows:

1. To evaluate the theoretical and numerical aspect of the principle of an EHD system.
2. To investigate the effect of process parameters such as electrode configuration, polarity,

applied voltage and electrode gap on EHD efficiency.

3. To investigate the effect of EHD drying of wheat on the structural conformation of wheat protein using Fourier transform infrared spectroscopy (FTIR) technique.
4. To evaluate the applicability of molecular dynamic simulation for studying the effect of processing on food proteins.
5. To investigate and confirm the structural modification of wheat protein under the influence of an electric field by using molecular dynamic modeling tools.

PART I

Chapter 2

Electrohydrodynamic Review:

A Comprehensive Review on Electrohydrodynamic Drying and High-Voltage Electric Field in the Context of Food and Bioprocessing

2.1 Abstract

Increasing global energy demand and application of more energy consuming processes has forced food industries to investigate into alternative processes. This chapter pertains to one such novel and promising alternative drying process "electrohydrodynamic (EHD) drying". EHD is a method of inducing electric wind that is generated by gaseous ions under the influence of a high-voltage electric field. This paper evaluates the available literature and discusses the experimental investigations carried out to explain the effect of operating parameters on the drying rate and specific energy consumption (kJ/kg water) of the EHD process. Through the review it was established that corona current increased linearly with an increase in applied voltage (kV) for both positive and negative polarities; and the negative corona discharge produced a larger corona current as compared to a positive corona discharge. It was also revealed that the specific energy consumption increased with an increase in applied voltage for both polarities but was lower when compared to conventional drying processes such as fluidized bed drying, but it was observed that the specific energy consumed by the EHD process was lower than that of the latent heat of vaporization, indicating the removal of water from the surface of sample by other means in addition to

evaporation. Electrode configuration plays an important role in determining the efficiency of the EHD process; the multiple needle electrode configurations had better efficiency than the wire and single electrode configuration. Recent and past studies on application of EHD in post-harvest and food processing were also reviewed and the benefit of using EHD for food and bioprocessing due to its unique properties supported the feasibility and applicability of EHD as a suitable alternative for processing thermally sensitive biological materials.

2.2 Introduction

Electrohydrodynamic (EHD) drying is one of the important non-thermal food processing methods that has been receiving considerable attention lately. It complies well with both drying issues, namely high product quality and low energy consumption (Bajgai et al., 2006b). The primary mechanism involved in EHD is the production of an electric wind also termed as corona wind by applying high voltage to an electrode with a small radius of curvature. This corona wind disturbs the boundary layer developed from the grounded surface on which the biological material is placed hence enhancing the mass transfer between the biological surface and the ambient air (Bracken, 1987). Since application of EHD takes place at ambient temperature and pressure conditions, it is vastly considered as a suitable alternative to conventional processes where we use a vast amount of airflow at elevated temperatures. The advantages of EHD are its design simplicity with no movable parts and no wear and tear; it also consumes less energy as compared to conventional drying techniques (Bai et al., 2011; Lai and Wong, 2003).

Scientists and engineers have worked on the application of high-voltage electric field in food processing for decades. In 1976, Asakawa reported a pioneering work on the effect of an electric field on heat transfer. His study revealed that under the influence of an electric field, vaporization of water could be enhanced by up to 40-50 times at 12 °C and the rate of heat transfer can be increased by 1.5 times for gas, 2 times for liquids and 1.6 times for solids depending on the position of the electrode (Asakawa, 1976). Since then, several researchers have reported their studies on new applications of high-voltage electric field in several sectors including bio-meteorological, food processing and biomedical engineering. In 1968, Hart and Bachman investigated the application of an ionic wind for a drying application, where they looked at evaporation of various liquid substances such as n-heptane, ethyl

alcohol and saline solution (Hart and Bachman, 1968). In 1989, an EHD technique based on the application of electric wind caused by ionic drag was developed for removal of moisture from soil samples (Barthakur and Al-Kanani, 1989). Chen and Barthakur worked on one of the very first applications of EHD in the field of food drying in 1994. They investigated drying of potato (*Solanum tuberosum* L.) slab exposed to high fluxes of unipolar air ions produced by corona discharge (Chen et al., 1994). Since then, application of EHD in the field of food processing has received major attention and several research groups are studying the principle aspects of EHD and the process parameters involved in its application to the field.

This review presents a concise but in-depth introduction to the mechanisms and applications of EHD in the field of food processing.

2.3 Electrohydrodynamic (EHD) drying mechanism

EHD is considered as a branch of fluid mechanics that is concerned with the effect of electrical forces on fluid movement. In EHD, both motion of the fluid and electric field influence each other (Kharel and Hashinaga, 1996). It has wide industrial applications such as in arc welding, hard coating deposition and convective mass transfer in bread and cookie baking (Wangnipparnto et al., 2002). In spite of its numerous applications in diverse fields, its application in drying of heat-sensitive material has begun only recently.

EHD applications depend on the corona wind that is generated by gaseous ions that accelerate under the influence of a high electric field. These charged ions collide with non-charged molecules and transfer their momentum, which results in an ion-drag phenomenon commonly known as ionic wind. The corona wind produced impinges on the moist biological material and disturbs the saturated air layer, leading to evaporation enhancement. The water molecules within the material orient themselves in the direction of the electric field, which leads to lowering of entropy as observed during this process, which results in lowering of the temperature of the biological material being dried (Hashinaga et al., 1999). Thus EHD can be classified as a non-thermal process and a novel alternative that can be used to dry heat-sensitive materials.

Detailed mathematical description of EHD is complex due to the interaction of charges under the influence of a strong electric field with gas, liquid water and dry matter of the food,

which all have different dielectric properties (Davidson and Shaughnessy, 1986). Hence it becomes difficult to keep track of the electrostatic coulomb forces existing amongst all charges. To simplify this complexity, the concept of volume force was introduced in which the volume force expression F_v (Panofsky and Phillips, 1962) is given as force per unit volume:

$$F_v = q_e E - 1/2\, E^2 \nabla e_0 + 1/2\, \nabla [E^2 \rho_m (de_0 / d\rho_m)] \quad (2.1)$$

Where E = electric field strength ($V*m^{-1}$), q_e = charge density of ions ($C*m^{-3}$), ρ_m = mass density of air ($kg*m^{-3}$), e_0 = permittivity of the medium ($F*m^{-1}$) and ∇ = vector gradient operator.

In Equation 2.1, the first term on the right represents the Coulomb force acting on the charged particles. The second term results from the force produced by the spatial change of electrical permittivity. The last term deals with an electrostrictive phenomenon which is caused by the inhomogeneity of the electric field strength. Coulomb force is the main force that is responsible for the acceleration of the ions and generation of the electric wind (Hashinaga et al., 1999), which disturbs the thermal boundary layer of saturated air layer over the surface. EHD operates on the basis of this Coulomb force producing the ion drag phenomenon (Stuetzer, 1959, 1960).

The EHD depends on the strength of the electric wind generated which results in enhancement of mass transfer rates of the liquid and volatile matters inside the biological medium. The velocity (ν ($m\ s^{-1}$)) of the generated electrical wind, when air is used as the working fluid, can be estimated by Equation 2.2.

$$\nu = (e_0/\rho_m)^{1/2} E \quad (2.2)$$

The generated electric wind velocity has a limitation, it cannot be increased infinitely with an increase in electric field (E) beyond the breakdown voltage which is 1.2 to 3.0×10^6 $V\ m^{-1}$. Equation 2.2 is obtained by combining the conservation of energy and Gauss' law and by integrating in one dimension (Barthakur, 1989). This equation is valid for inertial flow, which is most commonly encountered in industrial processes. In this type of flow the acceleration term of the fluid is comparable to the electrical force, i.e. electrical energy is converted to kinetic energy of the fluid. Equation 2.2 is obtained under certain assumptions; the dominant electrical body force is Coulomb force, while the force due to gradient of dielectric constant and the electro-restrictive force are negligible. To simplify the calculation

it is also assumed that the ionic wind flow is laminar and the turbulence caused due to viscosity of the medium is negligible. If we consider the flow of ions in a viscous medium we have to consider the resistance and the viscosity of the fluid medium for calculation of the ionic wind velocity. In this case the ionic velocity becomes inversely proportional to the fluid viscosity.

We can observe that EHD is a result of conversion of electrical energy into mechanical energy of ions and is convective in nature (Chen and Barthakur, 1991). The reason behind this enhancement of mass transfer is not well understood. Some researchers postulate that the interaction of charged molecules with the biological material generates a vortex like motion leading to movement which forces water molecules and other components out of the biological matrix (Chen et al., 1994).

2.3.1 Electro-kinetic property of corona wind

From Equations 2.1 and 2.2 we can infer that the electrical and kinetic property of corona wind will depend directly on the applied electric field (E) and the ionic wind velocity (ν) (Basiry and Esehaghbeygi, 2010; Roupassov et al., 2009). In 2007, Goodenough et al. conducted a study to theoretically explain the efficiency of a corona wind blower and compare it with the experimental data (Figure 2.1). To explain the electrical property of the corona wind they expanded the field power dissipation equation using Gauss's law to produce the definition of current drawn for a given voltage (Goodenough et al., 2007).

$$Vi = xyb\varepsilon_0 E \int_0^d (\nabla . E) E \, dz \tag{2.3}$$

Where, x, y and z are dimensional variables in the horizontal, longitudinal and vertical directions respectively; d = electrode spacing; E = Electric field strength (V m^{-1}); b = represents ion mobility (m^2 V^{-1} s^{-1}), V = applied voltage, i = current and ε_0 = electrical permittivity of air (F m^{-1}). Integration of Equation 2.3 with an assumption that $E = V/d$ gave Equations 2.4, 2.5 and 2.6 (Goodenough et al., 2007):

$$i = \frac{xyb\varepsilon_0}{2d^3} V^2 \tag{2.4}$$

$$d = (xyb\varepsilon_0)^{1/3} \frac{V^{\frac{2}{3}}}{i^{\frac{1}{3}} 2^{\frac{1}{3}}} \tag{2.5}$$

$$i = \frac{xyb\varepsilon_0}{2d^3}(V - V_i)^2 \tag{2.6}$$

Where, V_i is the initiation voltage of the corona wind. They observed a good correlation between the mathematical values obtained using Equation 2.6 with the data obtained during the experiment using the hot wire anemometer technique (Goodenough et al., 2007).

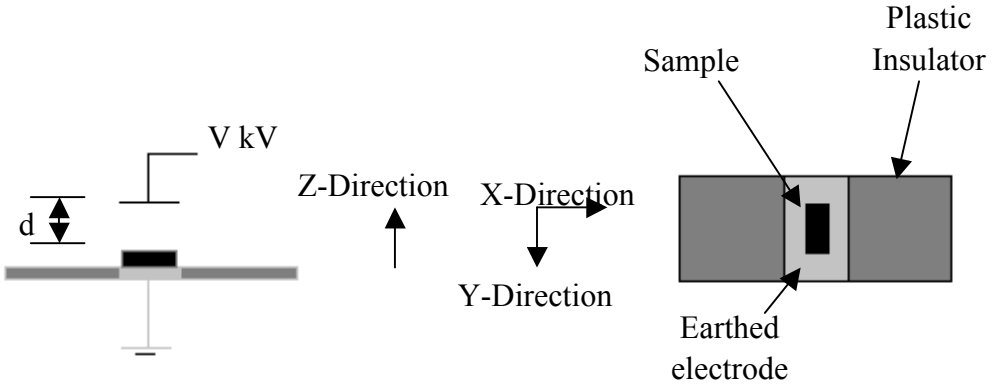

Figure 2.1: Schematic of the system used by Goodenough et al. for their experimental study of a corona wind blower (Adapted from (Goodenough et al., 2007)).

They also estimated the kinetic property of the corona wind and represented the relation between electrical power consumption (P) (Equation 2.8) and ionic wind velocity (ν) by substituting d from Equation 2.5 in Equation 2.7:

$$v = \sqrt{\frac{\varepsilon_0}{\rho_g}} E = \sqrt{\frac{\varepsilon_0}{\rho_g}} \frac{V}{d} \tag{2.7}$$

$$v = \frac{2^{1/3} \varepsilon_0^{1/6}}{\rho_g^{1/2} (xyb)^{1/3}} P^{1/3} \tag{2.8}$$

Equation 2.8 allows researchers to make generic calculations that are not dependent on the geometry of the apparatus used. They also quantified the electro-kinetic efficiency as a ratio of kinetic power and electrical power. Using Equations 2.2 and 2.5 the efficiency in air can be calculated as shown in Equation 2.9 (Goodenough et al., 2007):

$$Efficiency\ in\ air = \frac{\varepsilon_0^{1/2}}{b} \tag{2.9}$$

For Equation 2.9, the authors assumed the electric field to be parallel and uniform in the Z-direction. But they observed that the discharge wires (Figure 2.1) used for the experiment by the authors produced significantly higher electric field strength around the wire resulting in higher ionic wind velocity and efficiency (Goodenough et al., 2007).

2.3.2 EHD drying system

A typical EHD system is shown in Figure (2.2), and is similar to the electrostatic precipitator commonly used for particle removal from power plant flue gases. The EHD system consists of a vertically mounted electrode with multiple pointed needles projected to a fixed horizontal grounded metallic plate on which the food material to be dried is placed. The distance between the high voltage electrodes and grounded electrode can be adjusted by moving the sharp point electrode. The sharp point electrode is connected to an AC or a DC high voltage source. Depending on the need for polarity, the DC high-voltage is chosen to supply either a positive or a negative voltage. To set the desired high voltage parameters for EHD, the power source is connected to a voltage regulator, with a set range of adjustable voltage (Hashinaga et al., 1999).

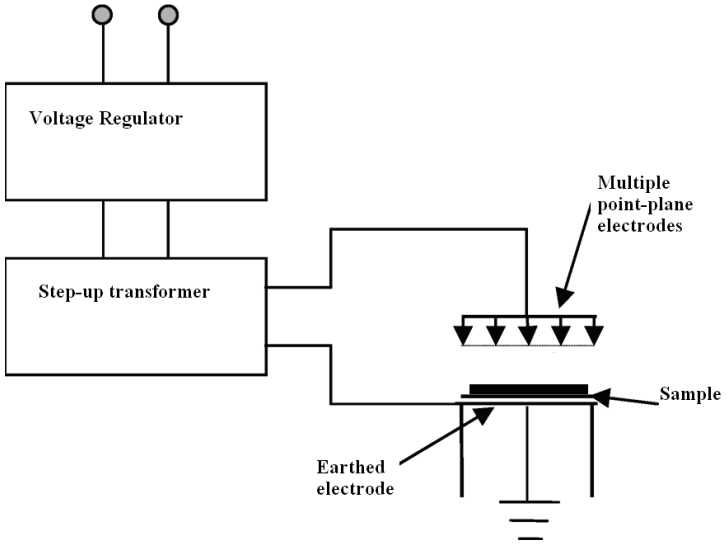

Figure 2.2: Schematic of electrohydrodynamic drying (EHD) system [Adapted from [(Bajgai et al., 2006b)].

2.3.3 EHD efficiency

Several studies have been conducted to examine the application of EHD in enhancement of evaporation process, most of them have focused on the feasibility of the technique in drying, (Basiry and Esehaghbeygi, 2010; Chen et al., 1994; Hashinaga et al., 1999; Ogata and Yabe, 1993; Paschkewitz and Pratt, 2000; Yamashita et al., 1991). Lai et al. (Alem-Rajabi and Lai, 2005; Balcer and Lai, 2004; Lai and Lai, 2002; Lai and Sharma, 2005) conducted a series of experiments to investigate the effect of corona discharge on the overall drying rate and to optimize drying as a function of the electric field parameter such as the electrode geometry (wire, single needle and multiple needle), discharge polarity, and electrode spacing. They conducted their experiments in a wind tunnel using uniform glass beads (with diameter of 3 mm or 6 mm) saturated with water. Two experimental runs were carried simultaneously, one in the ambient condition and one with the electric field in the wind tunnel with the blower being turned on and off. The blower introduced a uniform airflow over the sample surface. The applied voltage was increased at an increment of 1kV till spark-over occurred. In their study on EHD enhanced drying with needle electrode the authors investigated the effect of negative and positive corona discharge at two separate electrode spacing of 1.27 cm and 2.54 cm. Figure 2.3 represents the relation between applied voltage (V) and current (I (μA)). They observed that corona current increased linearly with an increase in applied voltage for both polarities. As the electrode spacing is reduced, spark-over occurs at lower voltage and it can also be observed that the negative corona produces a larger corona current as compared to positive corona (Lai and Wong, 2003).

During the study with single needle electrode the authors also estimated the performance of positive and negative corona and expressed their data in terms of mass of moisture removed per unit of electrical energy consumed. In this review we analyzed the performance results obtained by Lai et al. and represented it as the amount of specific energy consumed (kJ) to evaporate a kg of water. From Figure 2.4-2.6 it can be assessed that the energy required to evaporate a kg of water increases with an increase in applied voltage and the best performance can be achieved at lower applied voltage. It also suggests that the positive corona discharge has slightly better performance at lower applied voltage compared to negative corona discharge. Lai et al. concluded that drying rate was highest when the electrode spacing was the lowest and still below the threshold voltage after which arcs were

observed (Jafar Dalvand et al., 2013; Lai and Wong, 2003). We can also observe from Figure 2.6 that performance of the needle electrode is better as compared to wire electrode for a voltage range between 15 kV – 20 kV and as the applied voltage is increased the amount of energy consumed by wire electrode increases. For drying of 3mm glass beads the amount of energy consumed by needle electrode and multiple needle electrode was similar to each other.

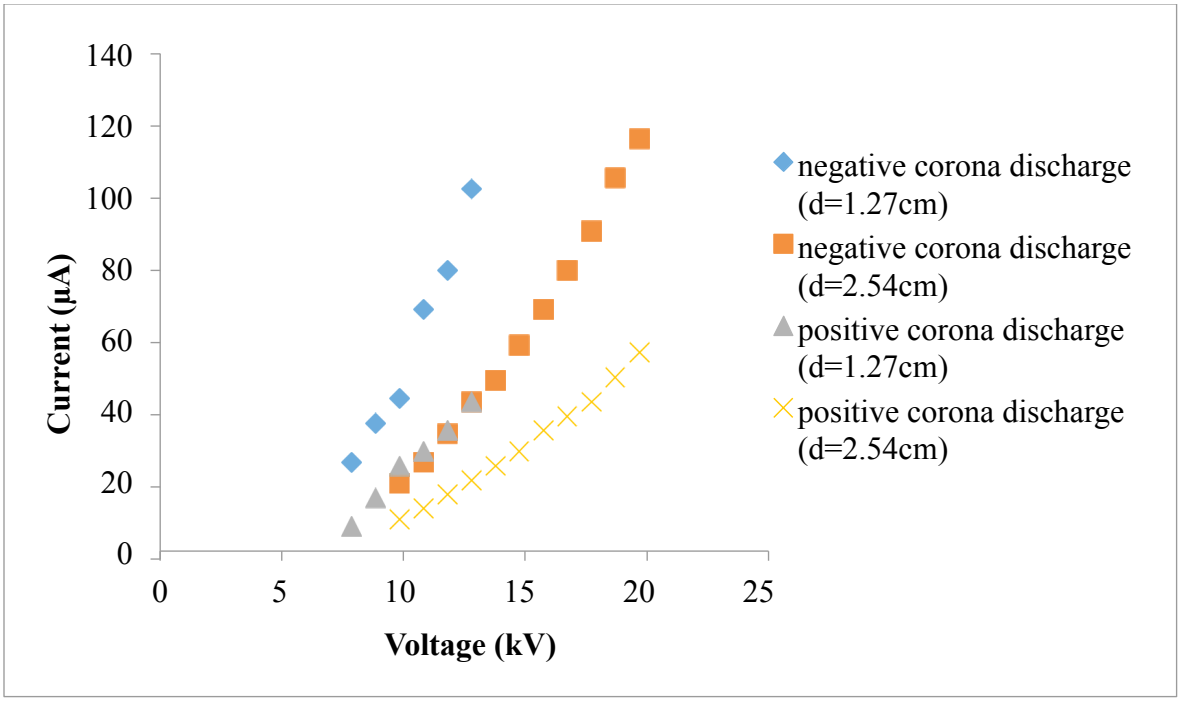

Figure 2.3: *V-I* curves for needle electrode configuration with electrode spacing of 1.27cm and 2.54 cm [Adapted from (Lai and Wong, 2003)].

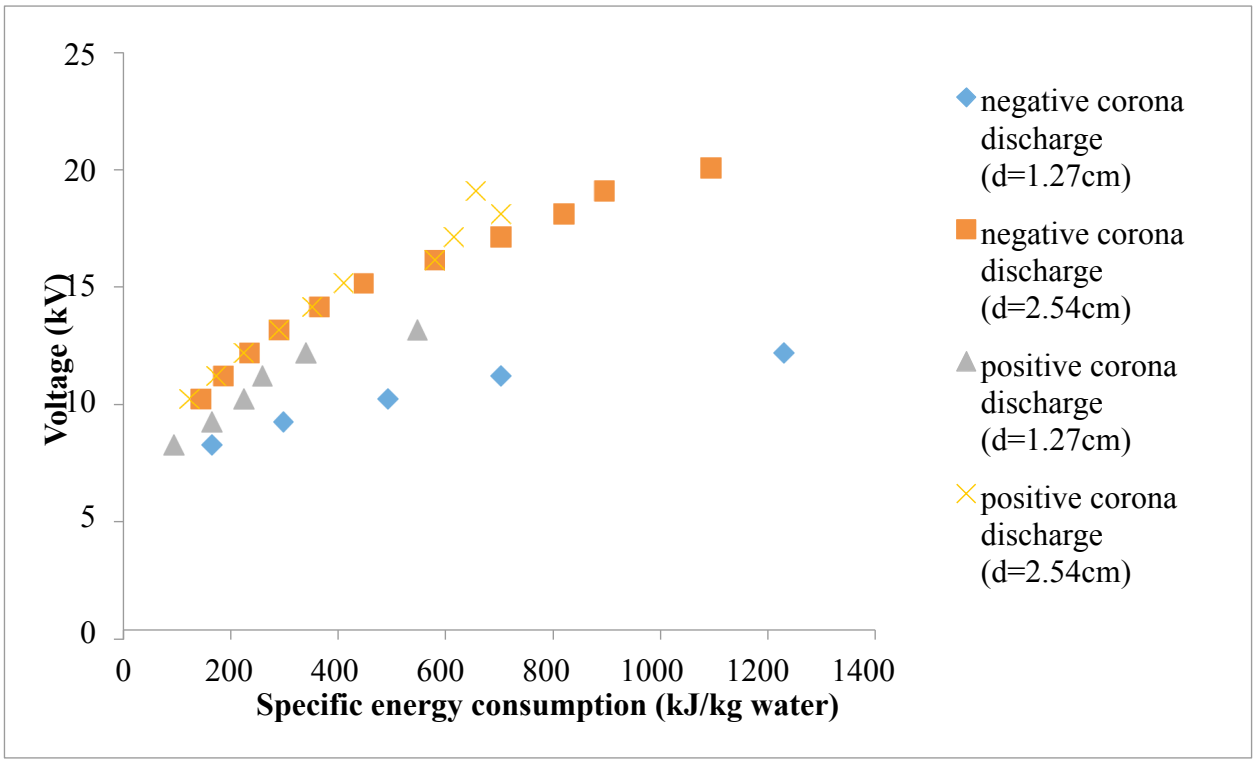

Figure 2.4: Performance for negative and positive corona discharges for 3 mm glass beads.

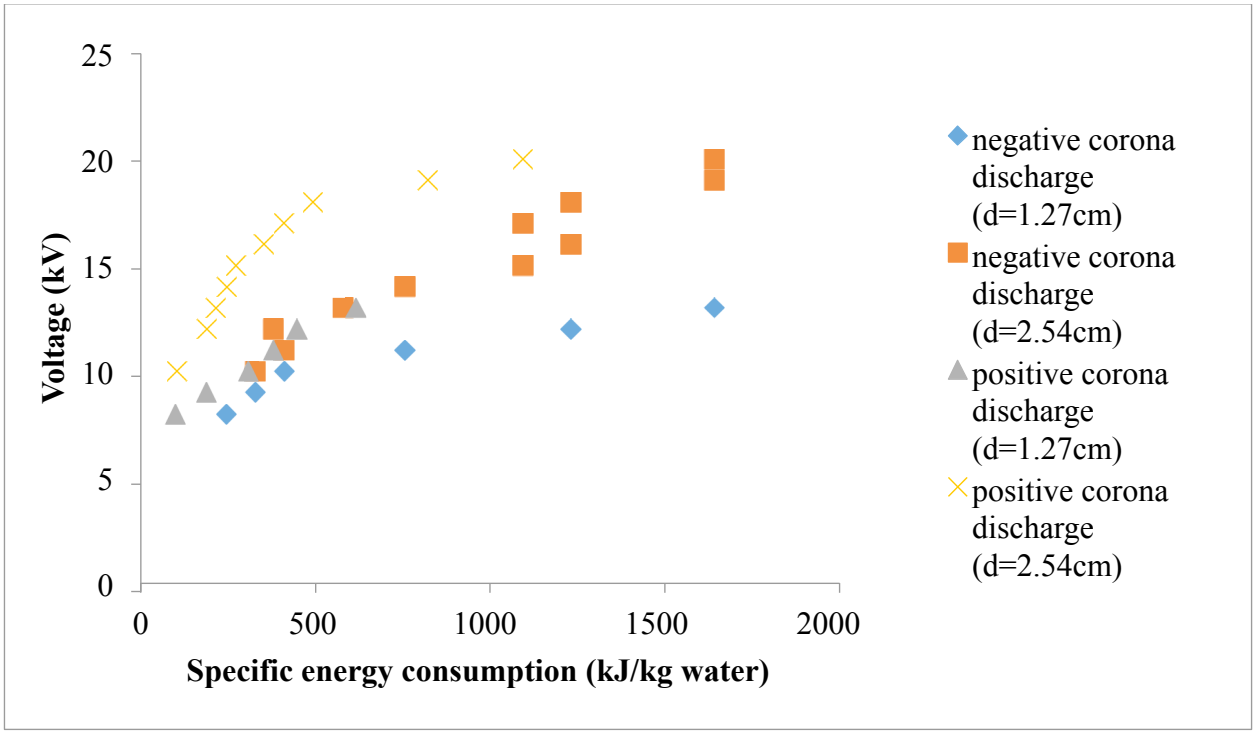

Figure 2.5: Performance for negative and positive corona discharges for 6 mm glass beads.

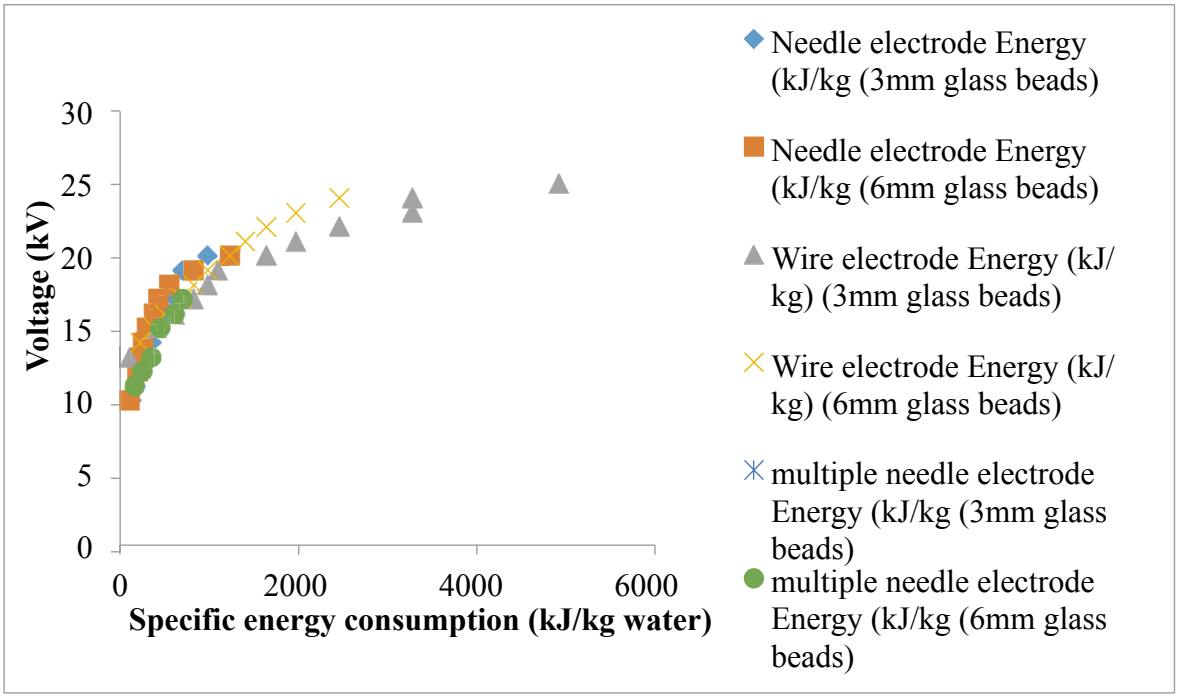

Figure 2.6: Specific energy consumption (kJ/kg water) at various voltages for different electrode configurations.

These observations are similar to those obtained by Zheng et al. in 2011 (Zheng et al., 2011). Using the data, a common prediction equation was obtained to predict the amount of voltage (V) (kV) required to estimate the amount of specific energy (Se) required for the drying process (Equation 2.10).

$$V = +\ 13.129 + 0.005 \times (Se) - 5\times10^{-7}\times (Se)^2 \qquad R^2 = 0.98 \qquad (2.10)$$

Investigating the performance data presented by Lai et al. and Zheng et al. (Lai and Sharma, 2005; Zheng et al., 2011) we can conclude that performance of multiple needle electrode was better in comparison to wire and single electrode configurations (Table 2.1).

Table 2.1: Comparison of electrode configuration and amount of specific energy consumed.

Electrode configuration	Energy consumed (kJ/kg)
Single needle	100 kJ - 1250 kJ
Multiple needle	100 kJ - 800 kJ
Wire electrode	200 kJ - 5000 kJ

The specific energy consumption values obtained in studies conducted by Lai et al. were a

lot lower in comparison to the theoretical value of approximately 2700 kJ required to evaporate a kg of water (latent heat of vaporization). To estimate the feasibility of EHD application in food industry, it is necessary to study the efficiency of EHD in drying of food as the water is present in a bound state and thermodynamically the amount of energy required to change the phase of bound water to gas would be more than the theoretical value. Several other researchers have recently estimated the EHD efficiency in drying of food and food products (Basiry and Esehaghbeygi, 2010; Cao et al., 2004a; Esehaghbeygi and Basiry, 2011; Yaxiang et al., 2009) and concluded it to be better than other conventional drying processes. One possible explanation to this lower energy consumption can be that the surface water was removed by the cross-flow of air over the sample surface used during the experiments conducted by the researchers, this is still a grey area which requires an extensive study to estimate the EHD efficiency accurately.

2.4 Drying of agricultural products

The selection of a process for drying of agricultural products is determined not only by their chemical composition and physical properties but also based on their probable use after processing. Fruits and vegetables have high moisture content and drying is applied to preserve them and increase their shelf life. Similarly grains and cereals are also dried to increase their storability and shelf life. But while using conventional drying methods such as fluidized bed or spouted bed drying the operational parameters plays a major role in determining the quality and quantity of the dried product. Parameters such as flow rate and temperature have to be optimized to suit the needs of the product being dried. In case of seeds the drying temperature has to be maintained at a lower level to maintain their viability and this lowers the drying rate. When we want to estimate the efficiency of a drying method, we have to consider several factors such as specific energy consumption for the product, the total energy required for the drying process which includes the energy required by the main and auxiliary heating sources and time required for drying. Table 2.2 summarizes the values obtained for specific energy consumption (kJ/kg water) in a spouted bed dryer, which is widely used in drying of several agricultural products (Elizabeth et al., 2006).

Table 2.2: Specific energy consumption for several food products using spouted bed dryer.

Sample	Specific energy consumption (kJ/kg)
Wheat	3360-7683
Corn	3290-3535
Paprika	4091-6158
Potato pulp	3025
Brewery yeast	3000-3500

If we compare the values of specific energy consumed by different EHD electrode configurations (Table 2.1) with spouted bed drying (Table 2.2), we observe that the values obtained in EHD are lower as it uses very small electric power as compared to conventional drying methods. But still a lot of research is required to realize its implementation in industries. Lai in 2010 designed a prototype of an EHD-enhanced drying system. The designed prototype had similar drying enhancement as demonstrated in the lab scale. But the design of an industrially implementable system has to depend a lot on the optimization of the process parameters and the type of food product being dried.

2.4.1 EHD application in drying of food products

Enhancement of heat and mass transfer in drying of agricultural products by application of electric field has been extensively studied. Table 2.3 summarizes most of the research conducted on the application of EHD and high voltage in food industries. EHD application in augmenting convective mass transfer in bread and cookies was studied by Kulacki in 1978 (Kulacki and Daumenmier, 1978) while the drying of potato slabs was studied by Chen and Bathakur in 1994 (Chen et al., 1994) using a single point-plane electrode establishing EHD process as an alternative for treatment of heat sensitive food and food products. In the same year another investigation was carried out on radish (*Raphanus sativus* L.) and shiitake mushroom under EHD corona discharge (Xue et al., 1994) and it was reported that the drying rate of radish was 1.5 times faster compared to control and drying time for shiitake mushroom was 2 hours shorter than the control.

Hashinaga et al. (Hashinaga et al., 1999) used multiple point-plane electrode with AC high voltage to dry apple slices. They concluded that application of EHD accelerated the initial drying rate by 4.5 times over the control (ambient air drying). They also investigated

the effect of the electric field strength, size of point electrode and electrode gap on the drying rate. Since during the process of corona discharge, ozone and nitrous oxide are produced, they also made an attempt to detect any formation of extraneous compounds in the drying of apple slices. The HPLC analysis concluded that no extraneous harmful compounds were produced during the EHD process.

In 2001, Bajgai and Hashinaga (Bajgai and Hashinaga, 2001a, b) dried radish (*Raphanus sativus* L.) and spinach (*Spinacia oleracea* L.) using EHD process with an objective of studying the effectiveness of multiple needle electrode, and the effect of high electric field on color, chlorophyll, organic acid and sugar content of the dried food product. Throughout the experiment, they maintained an electric field of 4.30 kV/cm. They observed that after drying for 7 hrs under EHD process, they were able to remove 80.1% of total moisture as compared to 79.8% and 19.3% under hot air oven (60 °C) and ambient air (25 °C). They also concluded that chlorophyll content in EHD dried spinach was significantly higher than the oven-dried samples. This is because EHD process is conducted under ambient conditions and is classified as non-thermal despite there being a slight increase in temperature of the samples. Storage studies conducted on the dried spinach revealed that after six weeks the ascorbic acid content in EHD dried spinach was higher than oven-dried sample. In a separate study, the same authors conducted another set of EHD experiments on Japanese radish (*Raphanus sativus* L.) to investigate its effect on the quality parameters such as shrinkage, color and rehydration ratio. The researchers used a multiple point-plane electrode with a grounded copper mesh electrode. They observed that the average drying rate of EHD process was 0.0012 g/min higher than oven drying and EHD-dried radish, which exhibited less shrinkage, better rehydration ratio and better color retention than oven dried samples (Bajgai and Hashinaga, 2001b).

In 2004, Cao et al. (Cao et al., 2004b) undertook a study in which they investigated the effect of EHD or high voltage electric field (HVEF) on the drying rate of rough rice, and also evaluated its effect on the rice fissuring and germination rate. The authors used a multiple point-plane electrode and subjected the sample to high voltage values of 10, 20 and 30 kV. The results were compared to those obtained under ambient air conditions without electric field. The results obtained revealed that HVEF treatment significantly enhanced the drying rate and followed an exponential model. HVEF treatment had no significant effect on the fissuring and germination rate (Cao et al., 2004b). In another study the same authors

investigated the effect of EHD on drying characteristics of wheat (Cao et al., 2004a). They reported that EHD treatment improved the average drying rate by 2.1, 2.0 and 1.7 times for electric field strengths of 10, 7.5 and 5 kV/cm respectively. The total power consumption for the EHD process was very small with the current of a few microamperes (Cao et al., 2004a).

Li et al. (Li et al., 2005) studied the effect of EHD drying techniques on appearance of okara cake. The authors used DC- polarity of 20 kV for their study. In their experiment, the number of needles in the point-plane electrodes was 1 and 3, while the electrode gaps were 35, 50 and 65 mm. The results indicated that the application of EHD contributes towards a decrease of the drying time by 15-40 % compared to control to reach the final moisture content of 10% (wet basis). One of the reasons for the enhanced drying rate was that the diffusion rate of moisture from the interior of the okara cake increased with EHD treatment. EHD also had a significant effect in maintaining quality attributes of the okara cake. They observed that the dried cake retained its shape and no cracks were observed on the surface as compared to control where some cracks were visible. The only disadvantage of EHD application was that the EHD-dried okara cakes had browner appearance as compared to control especially the part just under the needle electrode (Li et al., 2005). This can be attributed to the fact that the maximum ionic wind flux is observed just below the tip of the needle and the moisture within the biological material is further reduced at this point (Chen et al., 1994).

Preservation of marine products using conventional drying techniques has been a major concern with producers and processors. Conventional drying processes cause heat damage and adversely affect the texture, flavor, color and nutritional qualities of dried products. Application of non-thermal EHD process is not limited to only agricultural and food products, its application in preservation of marine products such as kelp, shrimps fish and scallop has also been widely investigated (Bai and Sun, 2011; Ya-xiang et al., 2008; Yaxiang et al., 2009)[39, 47, 48]. Ya-xiang et al. (Ya-xiang et al., 2008) in 2008 dried kelp under multiple needle point-plane electrodes using DC high voltage ranging from 5 kV - 55 kV. Their result indicated that EHD treatment significantly enhanced the drying rate of kelp. The authors also reported that at 45 kV, they were able to evaporate 42 % of total moisture from kelp within an hour. Drying in hot air oven at 60 °C removed 65.3 % of the total moisture content within an hour but significantly damaged the quality parameters of kelp. EHD dried kelp had better rehydration capacity and superior sensory qualities than oven

dried samples. In 2009, another group of investigators (Yaxiang et al., 2009) also studied the effect of EHD process on sensory qualities of scallop muscle. Their observation was in accordance with the study conducted by Ya-xing et al. on kelp (Ya-xiang et al., 2008). The authors also observed EHD drying process leading to energy saving of 93% compared to the oven drying method.

More recently in 2011, Bai and Sun (Bai and Sun, 2011) investigated the feasibility of EHD process for shrimps. They used a multiple needle point-plane electrode connected to a DC high-voltage power source that supplied positive high voltage. In their study they investigated the effect of EHD on shrinkage rate, water absorption, rehydration ratio, solid loss and sensory attributes such as color and texture of shrimps. The results indicated that EHD process significantly improved the drying rate and provided better sensory properties than conventionally dried shrimps.

2.4.2 Application in post-harvest storage

Numerous applications of EHD have been developed in the field of food dehydration and storage but very few studies are available on the effect of EHD on the shelf life of food materials. In 1990, Toda conducted a series of experiment on lettuce (*Lactuca sativa* L.), spinach and *komatsuna,* Japanese mustard spinach (*Brassica rapa var. perviridis* L.H. Bailey) and reported that the product's respiration rate was reduced following EHD treatment (Toda, 1990). In another study, Kharel et al. (Kharel and Hashinaga, 1996; Kharel et al., 1996) noted a reduction in respiration rates of pear (*Pyrus communis* L.), plum (*Prunus domestica* var. *domestica* L.) and banana (*Musa sapientum* L.) during climacteric period. Several other shelf life studies have been conducted on *Satsuma* mandarin (*Citrus reticulate* Blanco) (Han and Fumio, 1997), apple (*Malus domestica* L.) (Atungulu et al., 2004) and emblic (*Phyllanthus emblica* L.) fruit (Bajgai et al., 2006a).

More recently in 2009, Palanimuthu et al. investigated the effect of EHD treatment of cranberries (*Vaccinium macrocarpon* Aiton*)* on their respiration, color, total soluble solid content and texture (Palanimuthu et al., 2009). The authors treated cranberries with high voltage electric field of 2, 5 and 8 kV/ cm in a parallel plate electrode system for 30, 60 and 120 minutes. Treated fruit was stored under ambient conditions (23 °C and 65 % RH) for three weeks. They reported the respiration rate of EHD treated cranberries to be significantly

lowered than the control; no significant difference was observed in color and total soluble solid content between EHD treated and control samples. These observations showed the potential of EHD as a postharvest treatment for increasing the shelf life of perishable fruits and vegetables.

Table 2.3 EHD and high voltage application in food industry.

Reported Literature	Sample	Electrode configuration	Voltage (kV)	Specific energy consumed (kJ/kg water)
(Alem-Rajabi and Lai, 2005)	Glass Beads	Wire Electrode	19-20	2727
(Esehaghbeygi and Basiry, 2011)	Tomato slices	Multiple needle	6-10	4400-16500
(Hashinaga et al., 1999)	Apple slices	Multiple needle	5	N.A.
(Chen et al., 1994)	Potato slab	Single needle	5	N.A.
(Cao et al., 2004a)	Wheat	Multiple needle	5-10	N.A.
(Li et al., 2005)	Okara	Multiple needle	20	N.A.
(Bajgai and Hashinaga, 2001a)	Spinach	Multiple needle	4.3	N.A.
(Xue et al., 1999)	Whey Protein	Single needle	5.2	N.A.
(Cao et al., 2004b)	Rough rice	Multiple needle	10-30	N.A.
(Yaxiang et al., 2009)	Scallop	Multiple needle	5-50	N.A.
(Yaxiang et al., 2010)	Tofu	Wire Electrode	5-50	N.A.
(Bajgai et al., 2006a)	Emblic Fruit	Parallel plate Electrode	4.3	N.A.
(Bajgai and Hashinaga, 2001b)	Japanese radish	Multiple needle	4.3	N.A.

2.5 Conclusion

Drying of agricultural and food products by conventional drying methods not only deteriorates the organoleptic qualities but also the nutritional properties. These concerns have forced researchers and industries to look for alternative technologies to dry heat sensitive foods and food products and the unique advantages of EHD make it as one of the most suitable candidate.

The understanding of the mechanisms involved in the EHD drying process and its interaction with biological systems has been limited to the removal of water from the matrix; its interaction with biochemical components such as proteins, phenolic compounds, starch and

other components of the food matrix is still unclear. Most of the researchers who have applied EHD drying process have used either multiple needle point-plane electrode or single needle point-plane electrodes; application of parallel plate electrode has been limited to shelf life studies and the mechanisms involved in the generation of an electric wind still needs better investigation. Still under development, the EHD process has a huge potential as an alternative for conventional drying processes. Low cost involved in its implementation and maintenance makes it an ideal process for industries but still a successful EHD continuous processing system has yet to be designed, built and tested for a complex biological matrix. Design of a continuous EHD system will require extensive understanding of the mechanisms involved, and the study of the cost and the energy required for the implementation of the process at an industrial level. To achieve this, a life cycle assessment of the EHD process has to be carried out including inputs from all the stakeholders including ones in the social, industrial and environmental domains. A successful assessment of these attributes demands considerable research to be done in this area as it has immense potential to be used in multi-disciplinary fields. Several industries including mechanical, chemical, pharmaceutical and food can provide R&D possibilities for applying EHD in key sections of the processing cycle to answer the economical and environmental concerns related to conventional methods of drying.

Connecting Statement

After a review of the literatures on electrohydrodynamic drying mechanism and its application in food and bioprocessing, it is crucial to gain experience in high electric field processing and integrate the knowledge obtained from review of literatures to experimental results. The following study was conducted to evaluate the effect of high electric field pre-treatment on microwave-assisted drying kinetics of potato slices. For this study we designed and developed a parallel plate electrode and used it for pre-treatment of potato slices. The results obtained from this study were further useful to set the objective of future studies.

Chapter 3

High Electric Field Pretreatment:

Effect of High Electric Field Pre-Treatment on Microwave-Assisted Drying of Potato Slices

3.1 Abstract

Dehydration of fruits and vegetables affect their physical, biochemical and organoleptic properties. In the present study, effect of static high electric field intensity of 4 kV/cm on drying kinetics of microwave-convective and hot air drying systems was evaluated. The studied electric field intensity had minimal to no effect on the drying kinetics of the potato slices. Less to no curling was observed for high electric field pretreated samples compared to non-treated microwave-convective and hot air dried samples. This characteristic was attributed to the membrane permeabilization induced by application of a high electric field.

3.2 Introduction

For over a century potato chips have been one of the most popular snacks. The unique desirable texture and flavor of the potato chips is due to its high oil content, which ranges from 35-45 g/100g (wet basis) (Garayo and Moreira, 2002; Pedreschi and Moyano, 2005). Established health concerns over consumption of deep fried food products and increased consumer awareness on nutritional aspects of food has initiated research in the development of lower fat food products. Various approaches such as vacuum frying (Garayo and Moreira, 2002), pre-drying using hot-air treatment or microwaves have resulted in significant reduction in oil absorption during frying. It has been reported that blanching of potato slices prior to frying (Califano and Calvelo, 1987) or as a pretreatment to drying can reduce oil

uptake by gelatinization of surface starch and it also helps in improving the texture and color by inactivating enzymes which lead to major quality degradation of dried and fried potato chips (Leeratanarak et al., 2006; Senadeera et al., 2000). Various factors such as frying temperature, composition, time and shape of the product affect the amount of oil absorbed during the process of deep fat frying (Debnath et al., 2003; Pravisani and Calvelo, 1986). Initial solid content of the product is also one of the most critical factors that influence the oil uptake and also the frying time. Thus drying of the food products prior to frying will reduce the oil uptake and frying time. Drying of high sugar content food products might lead to degradation of organoleptic and nutritional properties of the food product. Conventional convective drying requires longer drying time and also leads to degradation of textural and nutritional quality of potato chips (Leeratanarak et al., 2006). Pretreatments prior to drying such as pulsed electric field, conventional hot air, microwave or osmotic dehydration have shown to be effective in decreasing the drying time and retaining the texture and nutritional characteristics of the food products (Ade-Omowaye et al., 2003). Novel processes such as pulsed electric field effect involve subjection of the biological material to pulsed high voltage field for a short period of time, inducing pore formation leading to permeabilization of cell membrane. Formation of pores helps in movement of cell constituents outside the cell membrane enhancing the extraction or dewatering processes (Fincan and Dejmek, 2003; Fincan et al., 2004). Formation of pores can be reversible or permanent depending on the field intensity, several researchers have suggested that for an effective plant tissue disintegration using PEF requires an high electric field of 10-20 kV/cm or a moderate electric field of 200/1000 V/cm (Angersbach et al., 2000; Lebovka et al., 2000). Pulsed electric field is a novel and promising technique but due to high instrumentation cost and technical operation, its usage in industry has been limited (Ade-Omowaye et al., 2003). It is expected that application of static electric field will follow a similar mechanism of pore formation but it is still a grey area and requires more research to reach an actual conclusion (Singh et al., 2012). Application of static high electric field (HEF) as a drying method or as a pretreatment is a new area of study and researchers have shown that HEF complies with major issues like lower energy consumption, simple instrumentation and high product quality (Bajgai et al., 2006b).

The present study was aimed at studying the effect of high electric field pretreatment, drying methods (hot-air and combined hot-air and microwave) on the drying kinetics and

quality of potato chips in terms of texture and color.

3.3 Experimental Section

3.3.1 Materials and Methods

Fresh potatoes (cv. Russet Burbank) were obtained from a local supermarket and stored at 4 ˚C. Prior to the experiment the potatoes were washed, peeled and sliced into chips of 3.2 ± 0.5 mm thickness and with a diameter of 37 ± 2 mm. The initial moisture content of the potato slices on wet basis (w.b.) was estimated by drying 25 g of sample at 105 ˚C for 24 hours (AACC 1986)(Granda et al., 2004). Moisture content (M.C.) of potato slices was calculated using Equation 3.1.

$$M.C.(w.b.) = \frac{M_w}{M_w + M_s} \tag{3.1}$$

Where, M_w is the mass of water in the sample (g); M_s is the mass of the solid in the sample (g).

3.3.2 Static High Electric Field Pre-Treatment

The apparatus utilized to apply the pre-treatment consisted of two parallel aluminum plate-electrodes connected to a General Electric Ignition Transformer and a Superior Electric Co. Powerstat adjustable transformer (Figure 3.1). The Powerstat transformer was used to modulate the input AC voltage of the ignition transformer in order to obtain the required electric field strength of 4 kV/cm between the plates. The pre-treatment consisted of placing the potato slices between the electrodes and applying the prescribed electric field strength for 1 hour. The slices were then removed and dried under different conditions.

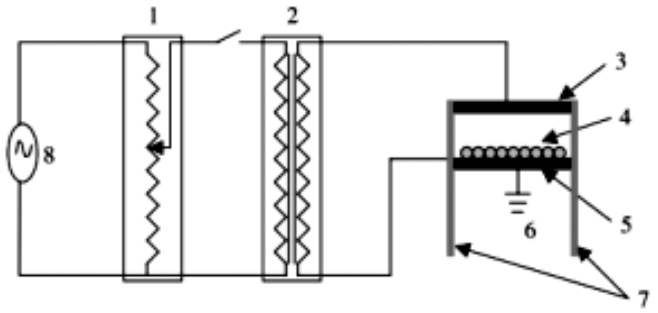

Figure 3.1: Schematic of high voltage electric field setup: 1, voltage regulator; 2, AC step up transformer; 3, Aluminum plate; 4, potato slices; 5, grounded aluminum plate; 6, ground; 7, supporting insulator; 8, 110 V alternating current source.

3.3.3 Microwave-Convective Drying

Sample of 100 ± 5 g of potato slices were subjected to microwave assisted hot air drying (Figure 3.2). The microwave generator was operating at 2450 MHz with a power density set at 1.00 W/g of initial sample mass. The modulation of the microwave generator was controlled by the sample temperature and the set point was 50˚C. Hot air was delivered to the sample at a constant temperature of 50 ± 1 ˚C with a superficial velocity of 1.4 m/s. Air inlet and outlet temperatures were monitored using type-T thermocouples while the product temperature was monitored using an Neoptix optic fiber probe. Mass of potato slices was recorded at 30 s interval with a load cell. Throughout the drying experiment the microwave reflectance was controlled manually with tuners. The drying was terminated when the potato slice moisture content reached ~20% (w. b.).

3.3.4 Hot-Air Drying

The sample of 100 ± 5 g was dried in the same drying chamber but without applied microwave power. The air temperature was set at 50 ± 1 ˚C with a superficial velocity of 1.4 m/s. Here also, the mass of the sample was recorded with a load cell at 30 s intervals. The drying process was ended when the moisture content of the potato slices reached ~20% (w. b.)

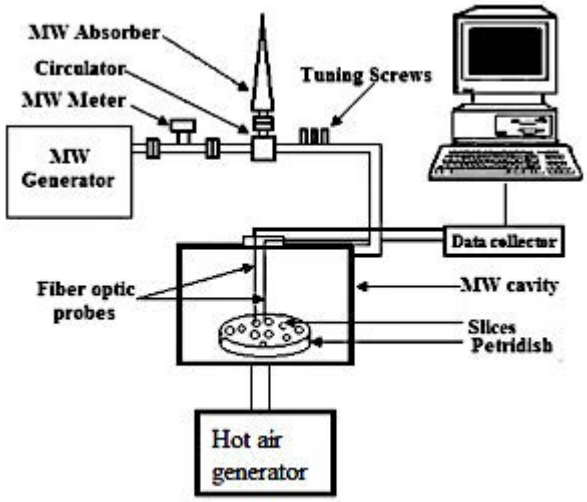

Figure 3.2: Schematic of microwave-convective drying apparatus.

3.3.5 Experimental Design

Untreated and HEF treated potato slices were dried by either microwave assisted hot-air drying method or a hot-air drying method, each operating at 50˚C. The given temperature was selected after preliminary drying experiments were conducted to obtain an optimized temperature, microwave power with respect to color and textural properties of potato chips. For the current study, drying characteristics were recorded and analyzed. All the experiments were conducted in triplicates. Color and texture of the dried potato slices were measured and analyzed.

3.3.6 Mathematical Modeling

The effect of the parameters on the drying kinetics was evaluated on the basis of mathematical models of thin layer drying including Newton, Page, Henderson & Pabis, Modified Page and Wang and Singh (Table 3.1).

Table 3.1: Various mathematical models used for predicting drying kinetics of potato slices (Nair et al., 2011).

Model Name	Equation	Equation No.
Newton	$MR = e^{-kt}$	3.2
Page	$MR = e^{-kt^n}$	3.3
Henderson & Pabis	$MR = a\, e^{-kt}$	3.4
Modified Page	$MR = e^{(-kt)^n}$	3.5
Wang and Singh	$MR=1+at+bt^2$	3.6

Where, k is the drying rate constant (min^{-1}); n, a, b and c are drying coefficients (dimensionless) which have values depending on the drying curve and equation; t is the time (min); and MR is the moisture ratio (Equation 3.7).

$$MR = \frac{M_i - M_e}{M_0 - M_e} \tag{3.7}$$

Where, M_0, M_i and M_e are initial moisture content, moisture content at time t_i and equilibrium moisture content respectively. Since the equilibrium moisture content is

negligible in case of microwave and convective drying, the Equation 3.7 reduces to:

$$MR = \frac{M_i}{M_0} \tag{3.8}$$

Parameters such as root mean square error (*RMSE*) (Equation 3.9), Chi-square (Equation 3.10) and coefficient of determination R^2 (Equation 3.11) are used to estimate the closeness of fit of model curves (Nair et al., 2011). In our study we estimated the *RMSE* and Chi-square values for the drying models.

$$RMSE = \sqrt{\frac{1}{n}\sum_{i=1}^{i=n}(MR_i^{pred} - MR_i^{\exp})} \tag{3.9}$$

Where, n is the number of observations, MR_i^{pred} is the predicted *MR* at time t_i and $MR_i^{\exp}$ is the measured value of *MR* at time t_i .

$$\chi^2 = \sum_{i=1}^{i=n}\frac{(MR_i^{\Pr ed} - MR_i^{\exp})^2}{n-m} \tag{3.10}$$

Where, χ^2 is the Chi-squared statistic, and *m* is defined as the number of constants in the selected drying model.

The coefficient of determination R^2 is calculated using Equation 3.11.

$$R^2 = 1 - \frac{\sum_{i=1}^{i=n}(MR_i^{\exp} - MR_i^{\Pr ed})^2}{\sum_{i=1}^{i=n}(MR_i^{\exp} - \overline{MR}^{\exp})^2} \tag{3.11}$$

Where, $\overline{MR}^{\exp}$ represents the mean experimentally measured value of *MR*. In addition to the coefficient of determination R^2, another statistical parameter such as reduced sum square error (*SSE*) was also determined using Equation 3.12 as the criteria for goodness of fit.

$$SSE = \frac{1}{n}\left(\sum_{i=1}^{i=n}(MR_i^{pred} - MR_i^{\exp})^2\right) \tag{3.12}$$

3.3.7 Effective Diffusion Coefficient

Effective diffusion coefficient was estimated using one of the simplifications of Fick's second law of diffusion by Crank in 1975 (Equation 3.13) (Crank, 1975).

$$MR = \frac{8}{\pi^2}\sum_{n=0}^{\infty}\frac{1}{(2n+1)^2}\exp\left[-(2n+1)^2\frac{\pi^2 D_{eff} t_i}{L^2}\right] \quad (3.13)$$

Where, $MR = \frac{M_i - M_e}{M_0 - M_e}$ and D_{eff} is the effective coefficient of moisture diffusivity (m^2/s) and L is the half-thickness of the potato slices. Equation 3.13 can be further approximated to a one term exponential model commonly used to estimate effective diffusivity of food samples (Equation 3.14) (Arevalo et al., 2004; Caixeta et al., 2002).

$$MR = \frac{8}{\pi^2}\exp\left[-\frac{\pi^2 D_{eff} t_i}{L^2}\right] \quad (3.14)$$

Equation 3.14 was used to determine effective moisture diffusivity of potato slices dried under aforementioned experimental conditions.

3.3.8 Color Measurement

Color measurements were carried out directly on the surface of fresh and dried potato slices using a chromameter (Model CR-300X, with d/0 (diffuse illumination/ 0° viewing system, Minolta Co. Ltd., Japan). The chromameter illuminates the sample from all directions at a constant luminance and only the light, which is reflected perpendicular to the sample surface is accepted for measurement. The CIE 1976 (L*, a*, b*) color space was used to define the color of the samples. Color values expressed as L* (whiteness or brightness/darkness), a* (redness/greenness) and b* (yellowness/blueness) were determined for all samples. Three replicates of each sample were measured. Reference values for the fresh samples (L_f, a_f, b_f) and color values from dried samples (L_d, a_d, b_d) were used to calculate the color change (ΔE) as defined by:

$$\Delta E = \sqrt{(L_f - L_d)^2 + (a_f - a_d)^2 + (b_f - b_d)^2} \quad (3.15)$$

3.3.9 Texture Analysis

Texture of the fresh and dried potato slices was measured with an Instron-4502 Universal Testing Machine (Instron Corporation, USA) equipped with a Kramer sheer press, controlled

by computer software (Instron series IX, version 8.25). The samples were placed inside the sheer press apparatus and crushed at a speed of 25 mm/min. Parameter recorded included maximum forces and energy (Figure 3.3).

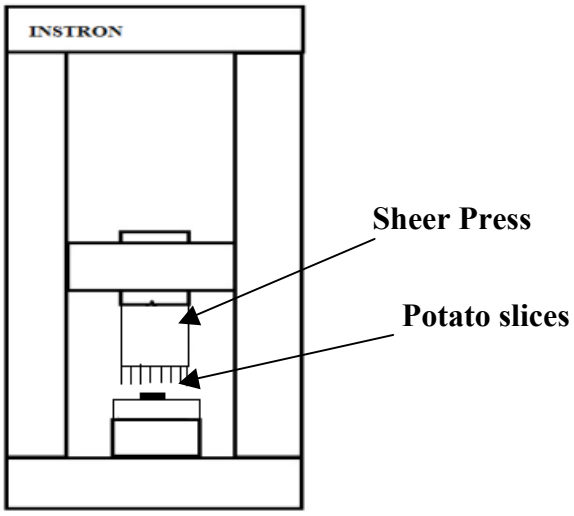

Figure 3.3: Instron Universal testing machine schematic equipped with Kramer sheer press.

3.3.10 Statistical Analysis

The analysis of variance (ANOVA) of the sample Duncan's Multiple Range test were performed using Statistical Analysis Software (SAS 9.2, SAS Institute Inc., Cary, NC, USA) at 95% confidence ($p \leq 0.05$) level, Lavene test was used to check the homogeneity of variance across samples. The drying kinetics for control and pretreated samples was determined using MATLAB R2009b. (Mathworks Inc.).

3.4 Results and Discussion

3.4.1 Drying Kinetics

Drying of control and pretreated potato slices revealed that, the drying was slower when potato slices were dried with hot air alone, it took approximately 167 minutes to reach the required moisture content of ~20% (w.b.). HEF pre-treatment of potato slices didn't have any significant effect on the drying time (Figure 3.4). Microwave convective drying had the highest drying rate and the required moisture content was reached only in only 47 minutes. This was a reduction of 72% when compared to hot air alone. In microwave convective drying, HEF pre-treatment of potato samples had no effect on the drying time (Figure 3.5).

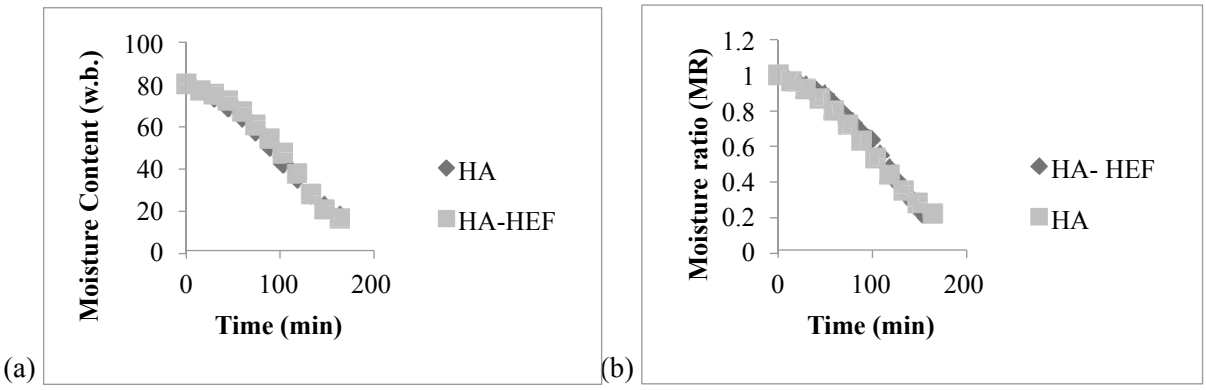

Figure 3.4: (a) Moisture content and (b) moisture ratio variation with change in time for potato slices dried in hot-air (HA) alone and pretreated with high electric field (HA-HEF)

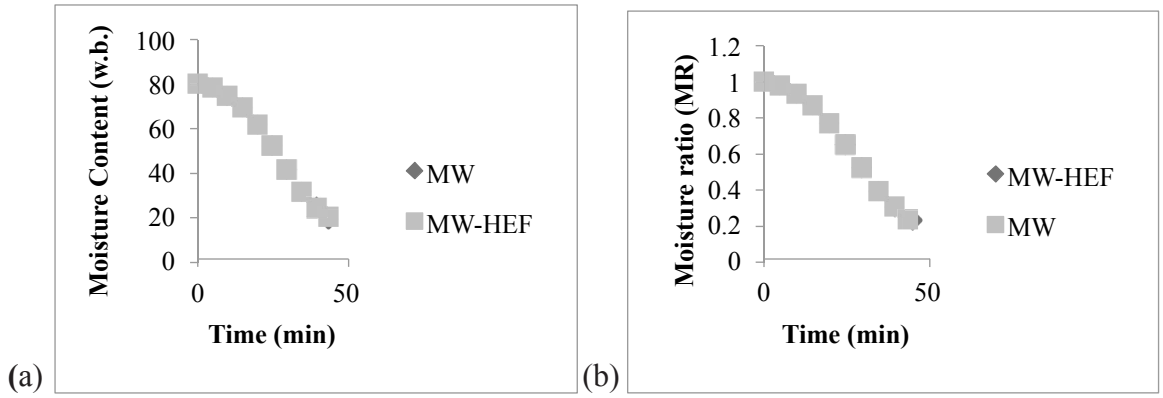

Figure 3.5: (a) Moisture content and (b) moisture ratio variation with change in time for potato slices dried in microwave-convective dryer (MW) and pretreated with high electric field (MW-HEF). HEF pretreatment had no significant effect and hence the data obtained overlapped.

Mathematical models from Table 3.1 (Equations 3.2-3.6) were fitted to the potato slices drying curves and statistical values used to define the accuracy of the model to fit and predict the drying kinetics were calculated (Table 3.2). Criterion for selection of the best model describing the drying kinetics for HA, HA-HEF, MW and MW-HEF drying conditions were according to the highest R^2 average values, and lowest *RMSE, SSE* and χ^2. From Table 3.2 it can be observed that for HA drying; Page and Modified Page models fitted the drying data well with *RMSE* value of 0.0117 and 0.0115, χ^2 value of 0.000135 and 0.000133, lowest *SSE* of 0.044 and 0.043 and R^2 of 0.998 and 0.996 respectively. For pretreated potato slices dried under HA, Page and Modified Page were the best mathematical models to fit the drying

curve with *RMSE* value of 0.0189 and 0.019 and χ^2 of 0.0009 and 0.0004, lowest *SSE* of 0.1109 and 0.1109 and R^2 of 0.994 and 0.994 respectively (Figure 3.6). For MW treatment the *RMSE* value of 0.0094, χ^2 of 0.00009, *SSE* of 0.0077 and R^2 of 0.9987 suggested Page model to be appropriate to estimate the drying kinetics. For MW-HEF treatment the Page model also had the least *RMSE* of 0.0103, χ^2 of 0.000105, *SSE* of 0.0097 and R^2 of 0.9985 suggesting it to be the perfect drying model (Figure 3.7).

Since no significant difference was observed in the drying time of control and pretreated samples, it was assessed that the pretreatment with high-electric field intensity of 4 kV/cm had no significant effect on the drying conditions, but it was observed that the potato slices pretreated with high electric field were less curled and had better texture compared to non-treated samples. Our observations were in accordance with the results obtained by Bouraoui et al. in 1994 (Bouraoui et al., 1994). They reported that results of microwave drying were very similar to those of combined microwave and convective drying and the time duration was 1/60 of that in convective drying (hot air). They also reported that less shrinkage was observed in case of microwave drying compared to convective drying. Lebovka et al. evaluated effect of application of pulsed electric field as a pretreatment to convective drying in 2007 (Lebovka et al., 2001). They reported that application of pulsed electric field pretreatment before drying and during the course of drying enhanced the moisture's effective diffusion coefficient. Since in our study we applied static electric field at low electric field intensity of 4 kV/cm, minimal to no effect was observed on drying time. Pulsed electric field involves placement of the sample between the electrode where short pulses of high electric voltage are passed through the sample, but in the present study the samples were placed between the electrode with a gap of 1cm from top electrode and there was no contact between the samples and electrodes, hence chances of occurrence of ohmic heating was negligible as observed in pulsed electric field. Ohmic heating during pulsed electric field treatment leads to enhanced permeabilization of cell membranes and in turn improve the increases in moisture diffusivity (Lebovka et al., 2005; Lebovka et al., 2007).

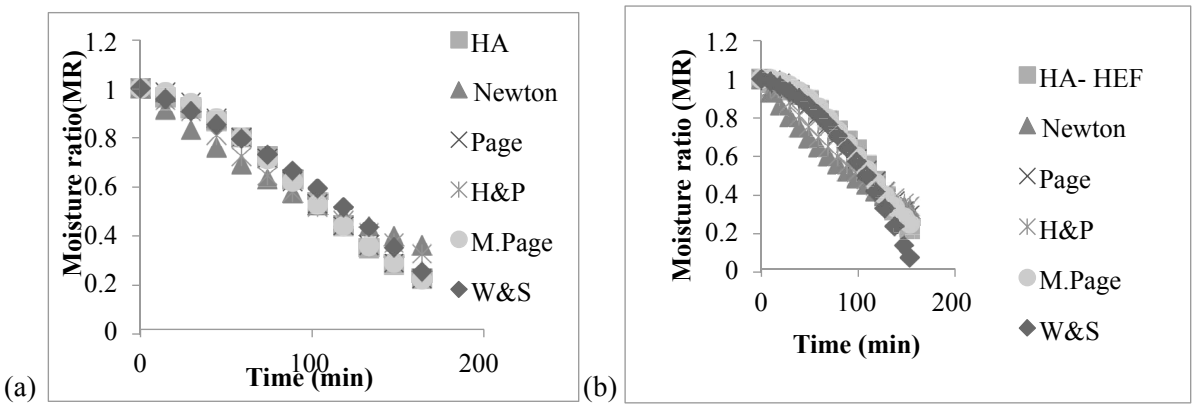

Note: HA: hot-air; HA-HEF: high electric field pretreated samples drying under hot air; H&P: Henderson and Pabis ; M.Page: Modified Page model; W&S: Wang and Singh drying kinetic model.

Figure 3.6: Drying kinetic model fitting to the drying curve for (a) hot-air (HA) and (b) high electric field pretreated samples (HA+HEF).

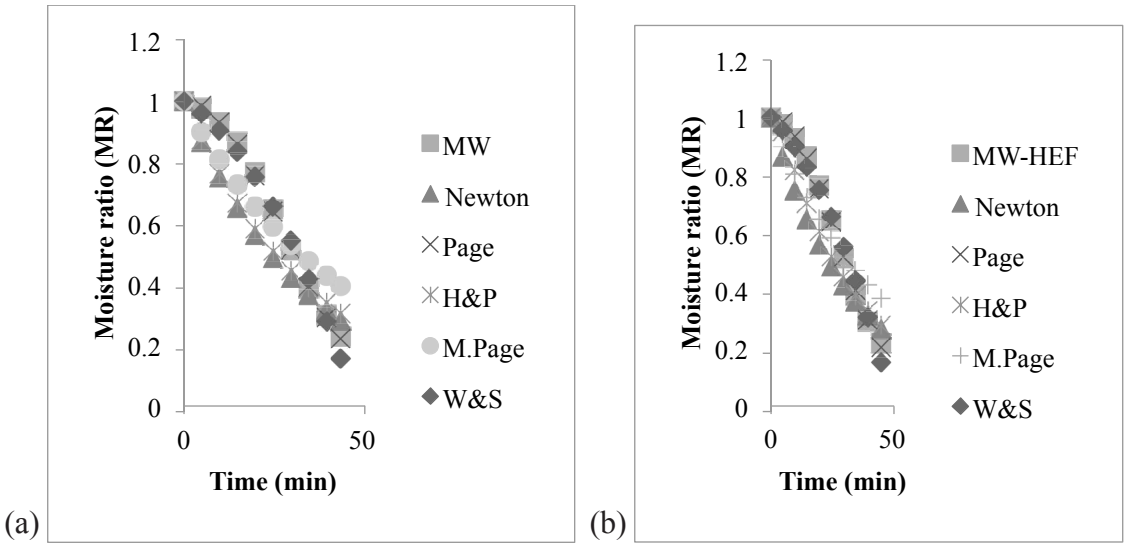

Note: MW: microwave convective; MW-HEF: high electric field pretreated samples drying under microwave convective process; H&P: Henderson and Pabis ; M.Page: Modified Page model; W&S: Wang and Singh drying kinetic model.

Figure 3.7: Drying kinetic model fitting to the drying curve for (a) microwave convective (MW) and (b) high electric field pretreated samples (MW+HEF)

Table 3.2: Estimated statistical values, *RMSE* and R^2 values obtained for different drying models.

Methods	Statitstics/ Coefficient	Models				
		Newtons	Page	Henderson & Pabis	Modified Page	Wang &Singh
		k	k / n	a / k	k / n	a / b
HA	Coefficient	0.006	0.000099/1.890	1.1398/0.00774	0.00763/1.890	−0.00291/-0.00001..
	χ2	0.002	0.0001	0.00442	0.0001	0.0022
	RMSE	0.04	0.0117	0.0665	0.0115	0.021
	SSE	2.515	0.044	1.477	0.043	0.145
	R^2	0.884	0.998	0.932	0.996	0.993
HA-HEF	Coefficient	0.0055	0.00250 /2.0584	1.1429 / 0.00705	0.00752/ 2.2462	−0.00135 / −0.00003
	χ2	0.0009	0.0009	0.0096	0.0004	0.5312
	RMSE	0.1000	0.0189	0.081	0.019	0.0531
	SSE	3.148	0.1109	2.0459	0.1109	0.011
	R^2	0.830	0.994	0.8897	0.994	0.965
MW	Coefficient	0.0213	0.000461/2.1395	1.1591/ 0.0272	1.487/0.0143	−0.00686 / −0.00028
	χ2	0.019	0.00009	0.0154	0.0100	0.0008
	RMSE	0.1008	0.0094	0.0768	0.1014	0.0284
	SSE	0.8950	0.0077	0.5125	0.8950	0.0703
	R^2	0.8465	0.9987	0.9111	0.8448	0.9879
MW-HEF	Coefficient	0.0216	0.000514/2.1047	1.1629/ 0.0275	0.4785/0.0451	−0.00771/ −0.00024
	χ2	0.0135	0.0001	0.0098	0.0100	0.001
	RMSE	0.1015	0.0103	0.07676	0.102	0.0322
	SSE	0.9369	0.0097	0.5303	0.9369	0.0936
	R^2	0.8516	0.9985	0.9160	0.8516	0.9850

3.4.2 Effective Moisture Diffusion

Analysis of the effective moisture diffusion coefficient (D_{eff}) revealed that potato slices subjected to MW and MW- HEF drying had a significant increase in D_{eff} compared to HA and HA- HEF. No significant difference was observed between MW and MW-HEF or HA and HA- HEF (Table 3.3). This can be attributed to the fact the electric field intensity used for the study was not important enough to induce any effective change in the cell structure of the potato slices. More intensive study is required to understand the interaction of electric field generated by parallel plate electrodes with biological materials (Singh et al., 2012).

Table 3.3: Effective moisture diffusion coefficient of potato slices. Column –wise values followed by the same letter are not significantly different. Test used: Duncan's Multiple Range test ($p \leq 0.05$)

Samples	**Effective moisture diffusion coefficient (D_{eff} × E+09)**
HA	1.376 ± 0.12^{a}
HA+HEF	1.283 ± 0.09^{a}
MW	5.115 ± 0.07^{b}
MW+HEF	5.063 ± 0.02^{b}

3.4.3 Texture Analysis

Textural analysis of dried and fresh potato slices using the Instron reveled that lower force and energy was required to crush the fresh potato slices then the dried samples. From Figures 3.8-3.9 it can be observed that HA dried potato slices required less force and energy in comparison to MW and HEF pre-treated samples. Figures 3.10 and 3.11 revealed that curling (drying shrinkage) of potato slices was observed in HA and MW dried samples but no curling was observed in potato slices pretreated with high electric field. This characteristic can be attributed to the effect of high electric field; under the influence of the electric field the cell membranes may have permeabilized and water got evenly distributed throughout the sample and lead to a uniform drying leading to less curling, this notion still needs to be validated and an intensive study is required to explain how moisture diffusion takes place in a food matrix under the influence of an applied electric field. This uniformity can also be a reason for why the energy required to crush the pre-treated samples was higher compared to fresh, HA and MW dried samples.

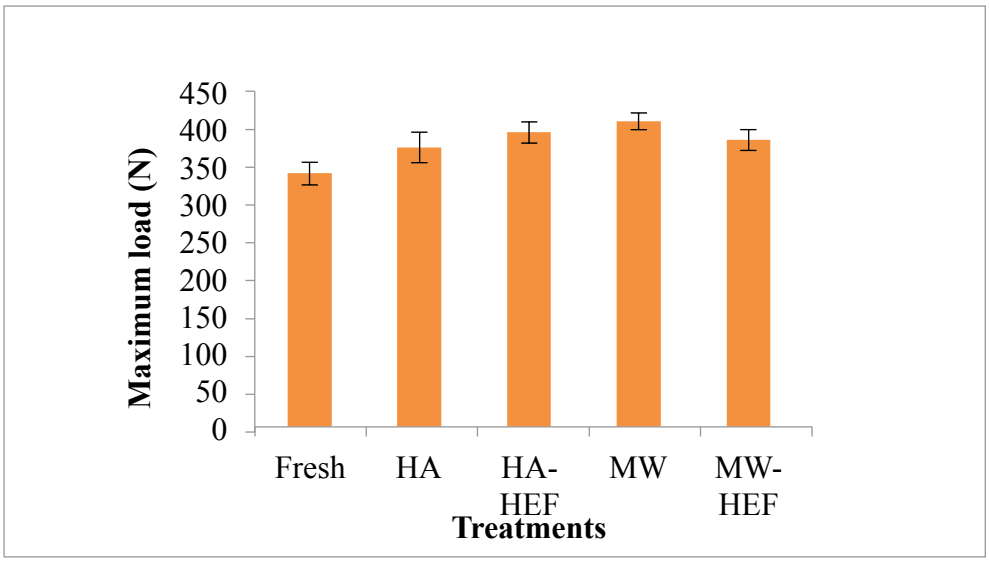

Figure 3.8: Force required to crush the fresh and dried potato slices with and without pretreatment.

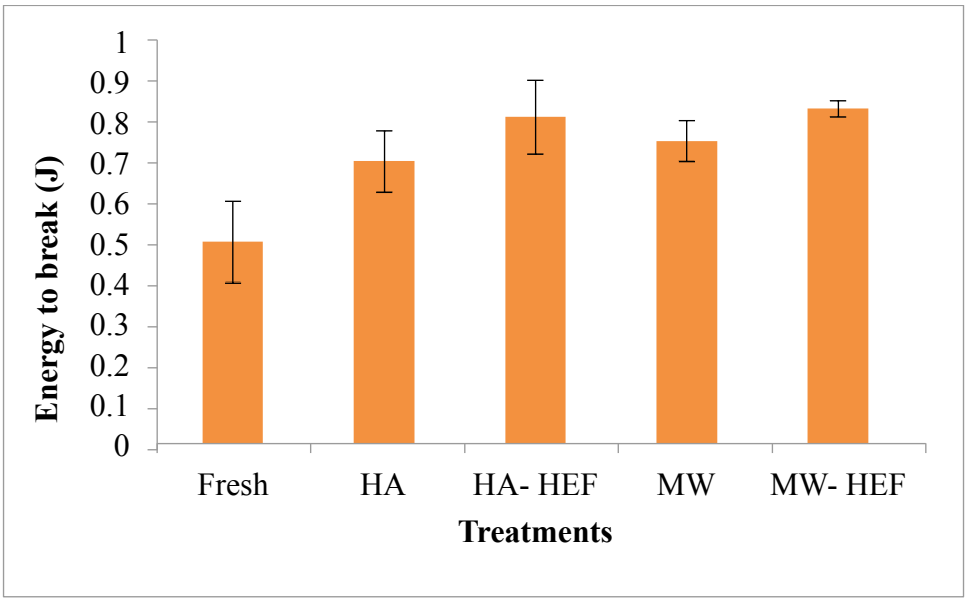

Figure 3.9: Energy required to crush the fresh and dried potato slices with and without pretreatment.

3.4.4 Color Analysis

It was observed that drying conditions affected the final color of the dried samples. Potato slices dried in hot air alone with no pre-treatment had lower L* values when compared to fresh and HEF treated potato slices. MW and HA-HEF dried potato samples had similar final color. HEF pre-treated microwave convective dried potato slices had an *L** value closer to the fresh sample. The a* and b* values of the samples also showed a similar trend (Table 3.4).

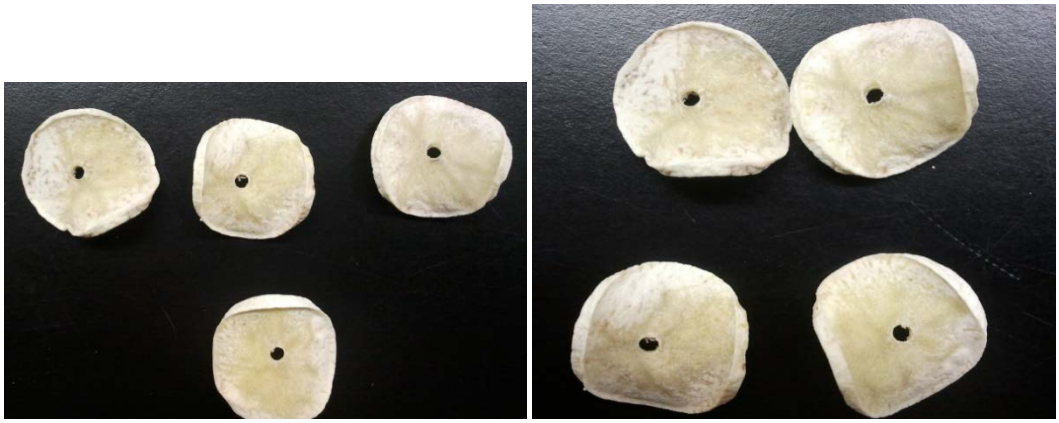

Figure 3.10: Curling of potato slices dried under hot air and microwave convective dryer.

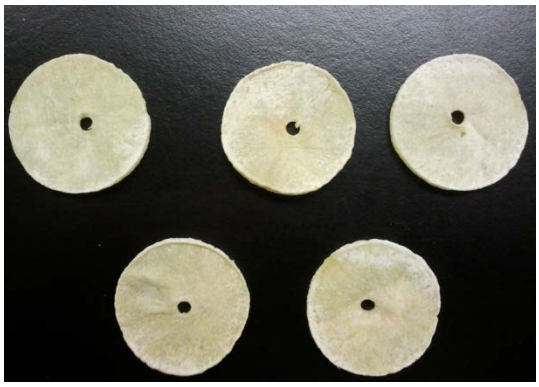

Figure 3.11: No Curling was observed in HEF pretreated potato slices dried under hot air and microwave-convective dryer.

Table 3.4: Color properties of fresh and dried potato slices. Column –wise values followed by the same letter are not significantly different. Test used: Duncan's Multiple Range test ($p \leq 0.05$)

Samples	**L***	**a***	**b***	**ΔE**
Fresh	73.16 ± 1.6^{a}	-5.45 ± 1.20^{a}	27.81 ± 1.20^{a}	
HA	62.86 ± 0.8^{c}	-0.56 ± 0.56^{c}	20.61 ± 0.83^{c}	13.50 ± 0.11^{a}
MW	67.68 ± 2.1^{b}	-1.65 ± 0.21^{b}	23.17 ± 0.95^{b}	8.12 ± 0.38^{b}
HA-HEF	68.37 ± 0.5^{b}	-1.13 ± 0.50^{b}	22.03 ± 1.67^{b}	8.65 ± 0.84^{b}
MW-HEF	71.77 ± 0.2^{a}	-2.06 ± 0.92^{b}	23.58 ± 0.82^{b}	5.59 ± 0.26^{c}

3.5 Conclusion

Our investigation in the application of a high electric field pre-treatment prior to drying had minimal effect on the drying kinetics, effective moisture diffusivity and quality of potato slices. Microwave-convective drying and hot air drying had significant effect on the color characteristics of potato slices. Moreover the pretreated potato slices were less curled and had uniform distribution of moisture within the potato slices. Our investigation suggests that more intensive study is required to explain the uniform distribution of water within the potato slices and higher electric field intensities should be tested to check their impact on drying kinetics and quality characteristics of potato slices.

Connecting Statement

From the previous study on high electric field pretreatment of potato slices using a parallel plate electrode, we observed that electric field pre-treatment had a significant effect on distribution of water in potato slices; this observation raised further questions on the effect of electric field on other components of potato slices including carbohydrates, proteins, sugar, salt etc., We also realized that the parallel plate electrode provides a uniform electric field but no corona discharge or ionic wind as corona discharge takes place in the narrow region of highly curved charged electrodes like the tip of a needle or a thin wire. During this time an opportunity was offered to visit the University of Oklahoma, where under the supervision of Dr. F.C. Lai, I got introduced to the design and fabrication of EHD systems based on wire electrodes. Hence once I returned I designed and developed an EHD system with a wire electrode and studied the effect of process parameters on drying kinetics of sand. Sand was used as the test sample to study the efficiency of an EHD system for the removal of loosely bound surface moisture.

Chapter 4

Electrohydrodynamic Drying (EHD) of Sand

4.1 Abstract

The effect of process parameters on drying kinetics and dependent variables was investigated using a central composite design and response surface methodology. Maximum drying was obtained at air velocity of 2 m/s, electrode gap of 1.5 cm and applied voltage of 15 kV. Air velocity and electric field intensity had significant effects on percentage water removed (%) and Sherwood number but in the case of EHD number and specific energy consumed, all process parameters had significant effect. This study also suggested that the EHD drying process in combination with cross-flow will lead to higher drying rate and lower energy consumption under ambient conditions.

4.2 Introduction

Drying is one of the most important unit operations used to separate moisture or other volatile substances trapped within the microstructure of a solid material (Singh et al., 2013b). Conventional drying systems involve application of convective, conductive and radiative heat sources in combination or alone for enhancement of heat and mass transfer (Singh et al., 2012). Since the drying material only absorbs a fraction of the energy conveyed from these sources, a major part of the energy is lost, making these techniques highly inefficient in terms of energy conservation (Lai and Lai, 2002). Increasing global concerns over climate change, which is often attributed to emission of greenhouse gases (GHG's) from industrial and domestic sources, have led to the search and development of novel energy sources and techniques that are highly efficient in energy utilization. The food industries emission of GHG's from conventional dryers utilizing fossil fuels for operation have risen serious environmental and consumer concerns (Singh et al., 2012). To combat these issues,

innovative drying techniques are being developed. Electrohydrodynamic (EHD) drying is one such method that utilizes the energy produced from a corona discharge that occurs in the narrow region close to a highly curved charged electrode (such as the tip of a needle or a small diameter wire) and the gas molecules surrounding the electrode. The electrons emitted from the charged electrode transfer their energy to the gas molecules, which get ionized by the high electric field. These charged molecules then migrate towards the ground electrode and during the process, transfer their momentum to neutral molecules via collision. This generates an ion bulk, which is termed as ionic wind or corona wind (Chen et al., 1994; Hashinaga et al., 1999; Lai and Lai, 2002; Lai and Sharma, 2005; Singh et al., 2012). EHD techniques provide several advantages over conventional drying techniques. Firstly, it requires no movable parts to convert electric energy into kinetic energy; therefore design, fabrication and maintenance of an EHD applicator require less monetary investments. Secondly, the amount of power consumed for generation of the corona wind is usually very small, which makes this technique quite attractive from an energy point of view as compared to conventional drying techniques. The only disadvantage of the EHD process is generation of ozone that might pose health risks, but ozone generation can be effectively monitored, controlled and even eradicated (Bajgai et al., 2006b; Singh et al., 2012).

Several studies have shown that electric field can be used to significantly enhance the drying rate and within the last few decades the use of electric field for enhancement of heat and mass transfer processes has garnered great interest (Bajgai and Hashinaga, 2001a, b; Cao et al., 2004a; Cao et al., 2004b); for example studies on tomato slices (Esehaghbeygi and Basiry, 2011), apple slices (Atungulu et al., 2004; Hashinaga et al., 1999), potato slab (Chen et al., 1994), wheat (Cao et al., 2004a), rice (Cao et al., 2004b), scallop (Yaxiang et al., 2009), Japanese radish (Bajgai and Hashinaga, 2001b), okara (Li et al., 2006, 2005) are available in published journals. As most of these studies evaluate the application of EHD in drying of food products, hardly any of them discuss the effect of processing parameters including electrode gap, electrode geometry, applied voltage, and discharge polarity. Only Lai et al. (Alem-Rajabi and Lai, 2005; Balcer and Lai, 2004; Lai, 2010; Lai and Lai, 2002) have conducted a series of studies to evaluate the effect of corona discharge on overall drying rate and optimization of the drying process as a function of the aforementioned processing parameters. In their comprehensive review on application of EHD and high-electric field for food and bioprocessing Singh et al. (Singh et al., 2012) showed that the

specific energy consumed, which is defined as the amount of energy (kJ) consumed to evaporate one kilogram of water is much lower for an EHD drying process as compared to the theoretical value of latent heat of vaporization (2,700 kJ/kg), which makes EHD a highly energy efficient process for drying. However this also generates several questions on how and in which form is the water removed during EHD drying process. As a possible explanation they suggested that the lower specific energy consumption during EHD process might be because of the presence of cross-flow of air over the sample surfaces used in the studies evaluated by them. Hence, this study was carried out to understand the interaction between cross-flow of air over sample surface and electrical parameters including applied voltage and electrode gap on drying enhancement using a single wire electrode system.

4.3 Materials and Methods

4.3.1 Test Sample Preparation

The test sample consisted of Ottawa Sand Standard (20-30 Mesh) saturated with water. Sand samples were bone dried in an oven for 12 hours and left to cool down to ambient temperature before every experiment, later a pre-determined amount of water was added to the sand sample to ensure it was completely saturated.

4.3.2 Experimental Setup

Figure 4.1 shows the schematic diagram of the EHD setup used for the present study. It consisted of a sample compartment made of Plexiglas of the following dimensions; 281 mm long, 110 mm wide and 80 mm high. It was connected to a blower at one end, which forced the air into the compartment at different velocities (1 m/s, 1.5 m/s and 2 m/s) set manually before the start of the experiment. The sample container was also made of Plexiglas of dimensions; 100 mm long, 25 mm wide and 25 mm deep. The base of the sample container was made of aluminum, which acted as the ground electrode. The sample compartment also enclosed a vertically mounted emitting electrode (copper wire of 0.5 mm in diameter), which was suspended above the sample box. The gap between the emitting electrode and sample surface was varied between 1.5 cm and 2.5 cm. A direct current at high voltage (positive polarity) was applied to the emitting electrode from a power supply unit, which had the

maximum voltage output of 30 kV. The temperature and the relative humidity of the ambient air and the loss of water was recorded by a data logger every 10 s. The drying experiment was conducted for at least 5 h and during all the experiments the ambient temperature remained fairly constant, as the lab temperature was controlled but during some experiments the relative humidity showed substantial changes, this change might have contributed to the variability in the data that will be discussed in the following sections.

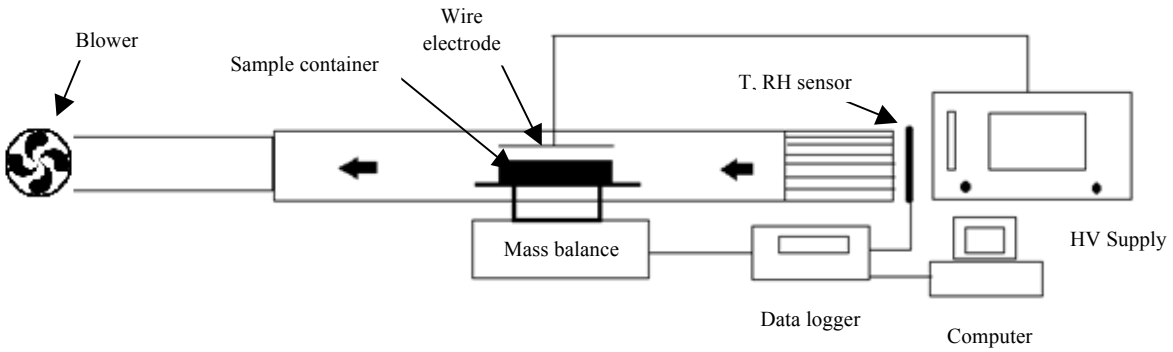

Figure 4.1: Schematic of the EHD experimental setup

Note: T: Temperature; RH: Relative Humidity; HV: High Voltage

4.3.3 Experimental Design

The experiment consisted of three factors (air velocity, applied voltage and electrode gap (distance between the emitting electrode and sample surface)) with 3 levels each, which were used to generate a face centered Central Composite Design (CCD). The experimental design was developed using JMP software (ver. 10, SAS Institute Inc., Cary, NC, USA) to determine the effect of the process parameters (variables), each at three equidistant levels (-1, 0, +1) or (a, 0, A) (Tables 4.1- 4.2) and their interaction on the response variables, such as percentage water removed, Sherwood number, EHD number and specific energy consumed (kJ/kg). The CCD consisted of 20 experimental combinations of factors including six central point combinations, six axial combinations and eight factorial combinations. All the factorial and axial experimental combinations were replicated thrice and the data were analyzed using Response Surface Methodology (RSM). Results from the three replicates of control samples (only air cross-flow) were used as reference to evaluate the drying enhancement with electric field.

Table 4.1: Coded (individually for each experimental factor) and corresponding actual values of all independent variables.

Code	Air Velocity (m/s)	Electrode Gap (cm)	Applied Voltage (kV)
-1 / a	1	1.5	10
0	1.5	2	12.5
+1 / A	2	2.5	15

Table 4.2: The Central Composite Design for response surface analysis of the interaction between independent variables (factors) and their effect on dependent variables (responses).

Coded	Air Velocity (m/s)	Electrode gap (cm)	Applied Voltage (kV)	Water removed (%)	Sherwood No.	EHD No.	Specific Energy Consumed (kJ/kg)
a00	1	2	12.5	19.32±0.1	0.17±*0.02*	1.44±*0.2*	1590.91±*6.1*
−++	1	2.5	15	18.65±*0.8*	0.16±*0.01*	1.95±*0.0*	3031.13±*2.3*
−−−	1	1.5	10	20.1*0*±*0.6*	0.17±*0.05*	0.95±*0.2*	550.22±*3*.0
−−+	1	1.5	15	20.97±0.5	0.21±*0.02*	2.04±*0.2*	3306.74±8.2
−+−	1	2.5	10	19.6*0*±*0.2*	0.18±*0.01*	0.90±*0.0*	347.83±*1.2*
0a0	1.5	1.5	12.5	23.04±*0.2*	0.20±*0.01*	0.96±*0.1*	1405.17±*9.1*
000	1.5	2	12.5	21.96±*0.4*	0.19±*0.03*	0.96±*0.3*	1386.14±*2.1*
00a	1.5	2	10	26.61±*1.1*	0.23±*0.08*	0.62±*0.1*	373.87±*6.2*
000	1.5	2	12.5	21.86±*0.5*	0.19±*0.01*	0.96±*0.3*	1391.65±*5.2*
000	1.5	2	12.5	20.42±*0.2*	0.2*0*±*0.01*	0.96±*0.2*	1486.36±*4.4*
000	1.5	2	12.5	*22.25±02*	0.21±*0.01*	0.96±*0.1*	1367.19±*2*
000	1.5	2	12.5	21.15±*0.3*	0.2*0*±*0.05*	0.96±*0.1*	1439.44±*0.6*
0A0	1.5	2.5	12.5	23.77±*0.3*	0.12±*0.08*	0.97±*0.1*	1114.47±*4.8*
000	1.5	2	12.5	24.5*0*±*0.2*	0.18±*0.01*	0.96±*0.1*	1243.34±*5.6*
00A	1.5	2	15	27.98±*1.4*	0.24±*0.05*	1.34±*0.1*	2386.34±*7.2*
+−+	2	1.5	15	38.1*0*±*0.7*	0.33±*0.01*	1.02±*0.1*	2058.04±*1.2*
+++	2	2.5	15	19.62±*0.9*	0.17±*0.07*	0.98±*0.1*	2481.08±*8.1*
A00	2	2	12.5	23.26±*0.3*	0.20±*0.09*	0.72±*0.1*	1333.33±*4.1*
++−	2	2.5	10	26.03±*0.2*	0.22±*0.01*	0.44±*0.3*	275.86±*2.8*
+−−	2	1.5	10	26.42±*0.2*	0.23±*0.06*	0.47±*0.4*	420.00±*8.5*

The CCD uses least-square regression to fit the data obtained from the experiment to a quadratic model (Singh et al., 2011). The quadratic model is used to describe the relationship between response *(Y)* and the independent variables, also termed as factors or process parameters (X_i,X_j,X_k….). This relationship can be represented by the following equation:

$$Y = \beta_0 + \sum_{i=1}^{i=n} \beta_i X_i + \sum_{i=1}^{i=n} \beta_{ii} X_i^2 + \sum_{i=1}^{i=n} \sum_{j=1}^{j=n} \beta_{ij} X_i X_j \ldots\ldots\ldots \quad (4.1)$$

Where, β_0 is the constant coefficient, β_i is the linear coefficient, β_{ii} is the quadratic coefficient for main process parameters and β_{ij} is the second order interaction coefficient of variables *i* and *j*, respectively.

4.3.4 Mathematical Modeling

The effect of the process parameters on the drying kinetics was evaluated using mathematical models including Newton, Page, Modified Page, Henderson and Pabis and Wang and Singh (Table 4.3).

Table 4.3: Mathematical models to fit drying kinetics

Model Name	Equation	Equation No.
Newton	$MR = e^{-kt}$	4.2
Page	$MR = e^{-kt^n}$	4.3
Henderson and Pabis	$MR = a\, e^{-kt}$	4.4
Modified Page	$MR = e^{(-kt)^n}$	4.5
Wang and Singh	$MR = a + at + bt^2$	4.6

Note: Where, *k* is the drying rate constant (min^{-1}); n, a, b and c are drying coefficients (dimension less) which have values depending on the drying curve and equation; *t* is the time (min); and *MR* is the moisture ratio (Equation 4.8) (Singh et al., 2013b).

The bone-dried sand of mass 100 g ± 1.3 g was used for all the experiments and a known mass of water was added to it. The initial moisture content of the saturated sand sample for all experimental runs on dry basis (d.b.) was estimated to be (23 ± 0.3 %).

$$M.C.(d.b.) = \frac{M_w}{M_s} \quad (4.7)$$

Where, M_w is the mass of water in the sample (g); M_s is the mass of the solid in the sample (g).

$$MR = \frac{M_i - M_e}{M_0 - M_e} \quad (4.8)$$

Where, M_0, M_i and M_e are initial moisture content, moisture content at time t_i and equilibrium moisture content respectively. The value of equilibrium moisture content was relatively small compared to M_0 and M_i, hence the error involved in simplification was negligible, and so the Equation 4.8 reduces to (here, we can also state moisture ratio as moisture relative value) (Aghbashlo et al. 2008):

$$MR = \frac{M_i}{M_0} \tag{4.9}$$

Parameters such as root mean square error (*RMSE*) (Equation 4.10), coefficient of determination R^2 (Equation 4.11) and sum square error (SSE) were used to estimate the goodness of fit of the model curves.

$$RMSE = \sqrt{\frac{1}{n}\sum_{i=1}^{i=n}(MR_i^{pred} - MR_i^{\exp})} \tag{4.10}$$

Where, n is the number of observations, MR_i^{pred} is the predicted *MR* at time t_i and $MR_i^{\exp}$ is the measured value of *MR* at time t_i.

The coefficient of determination R^2 is calculated using Equation 4.11.

$$R^2 = 1 - \frac{\sum_{i=1}^{i=n}(MR_i^{\exp} - MR_i^{\Pr ed})^2}{\sum_{i=1}^{i=n}(MR_i^{\exp} - \overline{MR}^{\exp})^2} \tag{4.11}$$

Where, $\overline{MR}^{\exp}$ represents the mean experimentally measured value of *MR*. The sum square error (*SSE*) was also determined using Equation 4.12 as the criteria for goodness of fit (Singh et al., 2013b).

$$SSE = \frac{1}{n}\left(\sum_{i=1}^{i=n}(MR_i^{pred} - MR_i^{\exp})^2\right) \tag{4.12}$$

Lai et al. (Alem-Rajabi and Lai, 2005; Lai and Sharma, 2005), represented the enhanced drying rate from the applied electric field under cross-flow conditions as a function of Sherwood number and EHD number. Hence, these two variables were also estimated in the present study to evaluate the effect of different experimental conditions on them.

Sherwood number was expressed as below (Lai and Sharma, 2005):

$$Sh = \frac{h_m d}{D} = \left[\frac{\dot{m}}{A_c \Delta c}\right]\frac{d}{D} \tag{4.13}$$

Where, *Sh* is the Sherwood number; h_m is the mass transfer coefficient (m/s); *d* is the diameter of the emitting wire electrode (m); *D* is the mass diffusivity (m^2/s); $\dot{m}$ is defined as rate of mass transfer (kg/s); A_c is the sample surface area exposed to the corona wind (m^2); Δc is the water vapor concentration difference between the sample surface and ambient air (kg/m^3). The Sherwood number is the measure of the ratio of convective mass transfer, i.e. it is the ratio of mass transfer coefficient to molecular diffusion, which is commonly represented by diffusivity.

EHD number (N_{EHD}) (Equation 4.14) is defined as the ratio of corona wind velocity and air velocity (cross-flow) (Lai and Sharma, 2005).

$$N_{EHD} = \frac{u_e}{u_i} \tag{4.14}$$

Where, u_e is the corona wind velocity (m/s) and u_i is the air velocity (m/s). The corona wind velocity was estimated using the equation suggested by Lai et al. (Lai et al., 1995).

4.3.5 Determination of Specific Energy Consumption

The applied power (*P*) and the energy (*E*) for the EHD drying process were estimated by Equation 4.15- 4.16.

$$P = I \times V \tag{4.15}$$

$$E = P \times t \tag{4.16}$$

Where, *I* is the current (A); *V* is the applied voltage and t is the drying time. The specific energy consumed (*SEC*) was determined using Equation 4.17.

$$SEC = \frac{E}{M} \tag{4.17}$$

Where, *E* (kJ) is the energy consumed and *M* (kg) is the mass of water removed.

4.3.6 Statistical Analysis

All statistical analyses were carried out using JMP software (ver. 10, SAS Institute Inc., Cary, NC, USA). The fitness of the model for CCD was determined by evaluating the Fisher Test value (F-Value), and the coefficient of determination (R^2) as obtained from the analysis of variance (ANOVA) at 95% confidence ($p \leq 0.05$) level. Duncan Multiple Range test was

performed using Statistical Analysis Software (SAS 9.2, SAS institute Inc., Cary, NC, USA). The drying kinetics for the samples were determined using MATLAB R2009b (Mathworks Inc. MA, USA).

4.4 Results and Discussion

4.4.1 Current-Voltage Relationship

Before the start of the experiment, the relation between the current and voltage was determined by increasing the positive applied voltage in the range of 7-25 kV and the corona current (μA) was measured. To estimate the effect of electrode gap on the current-voltage relationship, the aforementioned steps were repeated for each electrode distances (1.5, 2 and 2.5 cm). The resulting relationship is shown in Figure 4.2.

It can be observed that the corona current increased with an increase in applied voltage but as the difference between electrode gap was not significant, no conclusive difference in the corona current values were observed among different electrode gaps. As the voltage was increased, spark over was observed beyond 20 kV for an electrode gap of 1.5 cm, hence, for the present study applied voltage values were set at 10, 12.5 and 15 kV. The electrode gap was not reduced further below 1.5 cm as the high voltage system became unstable and system interruptions were occurring.

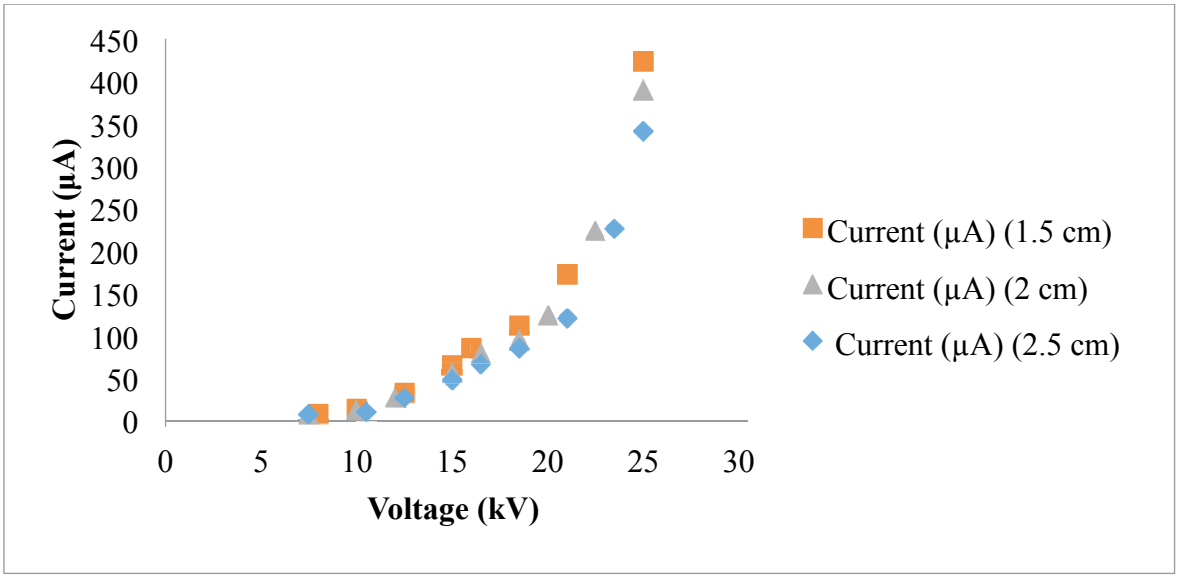

Figure 4.2: Current-Voltage relationship with respect to electrode gap.

4.4.2 Drying Kinetics

The drying curves for EHD dried saturated sand samples under different experimental conditions are shown in Figure 4.3. From the figure it can be observed that the sand sample exposed to the experimental condition of 2 (air velocity, m/s); 1.5 (electrode gap, cm) and 15 (applied voltage, kV) dried faster than all other experimental conditions and control.

Considering the drying kinetics it can also be observed that for almost all the experimental conditions and control, a constant-rate drying period was observed, which was in accordance with the findings of Lai et al. (Lai and Lai, 2002; Lai and Sharma, 2005). For only the experiments conducted at 1.5 (air velocity, m/s), 2 (electrode gap, cm) and 10 (applied voltage, kV) a variation was observed that can be attributed to the changes in the ambient relative humidity. Mathematical models presented in Table 4.3 (Equations 4.2 to 4.6) were fitted to the drying curves and statistical values used to define the goodness of model fitness were calculated (Table 4.4).

Only the best-fitted models for each experimental condition are presented in Table 4.4. The criteria for selection were according to highest R^2 average values, and lowest RMSE and SSE values. From Table 4.4, it can be observed that Page model can be used to fit all the experimental conditions except for 1.5 (air velocity, m/s), 2 (electrode gap, cm) and 10 (applied voltage, kV), which was affected by the change in relative humidity during the experiment.

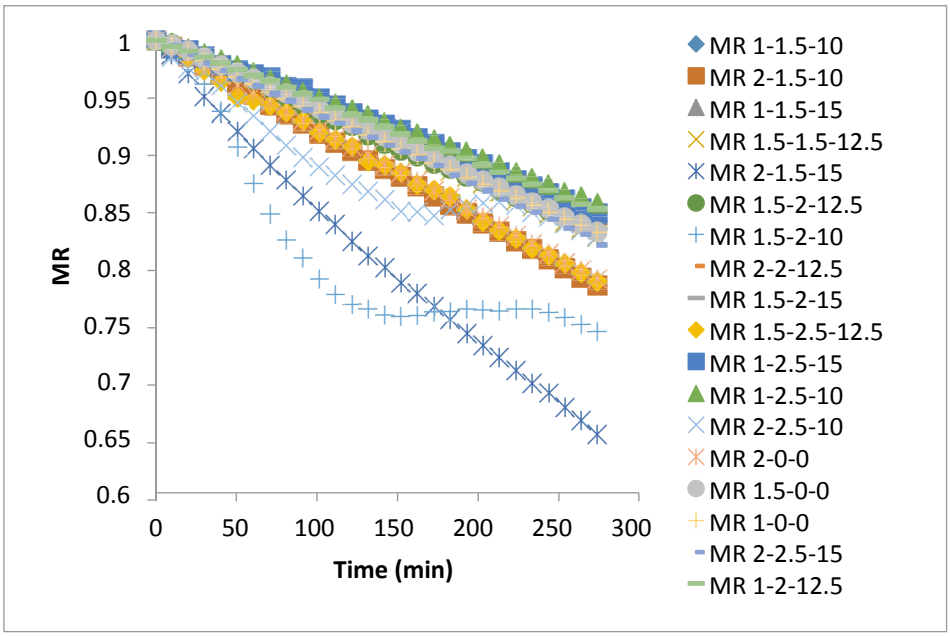

Note: Experimental conditions are represented in the format "air velocity – electrode gap – applied voltage"

Figure 4.3: Drying curve for saturated sand sample under all experimental conditions.

Table 4.4: Best fitted drying models and their corresponding statistical values of RMSE, R^2 and SSE for different experimental conditions.

Air velocity (m/s)	Electrode gap (cm)	Applied voltage (V)	Best fitted model	SSE	R^2	RMSE
2	1.5	10	Page	0.01748	0.998	0.003084
1	1.5	10	Page	0.003473	0.9992	0.001383
1	1.5	15	Page	0.005652	0.9986	0.001752
1.5	1.5	12.5	Page	0.01805	0.9968	0.003145
2	1.5	15	Page	0.009902	0.9995	0.002339
1.5	2	10	Wang & Singh	0.6526	0.9435	0.01906
1.5	2	12.5	Page	0.01298	0.9984	0.002668
1.5	2	15	Page	0.01583	0.998	0.002966
2	2	12.5	Page	0.03901	0.9917	0.004652
1.5	2.5	12.5	Page	0.001143	0.9998	0.0007934
1	2.5	15	Page	0.004864	0.9989	0.001636
1	2.5	10	Page	0.02346	0.9943	0.003563
2	2.5	10	Page	0.2873	0.9358	0.01272
2	0	0	Page	0.01682	0.9978	0.003057
1.5	0	0	Page	0.000628	0.9999	0.000587
1	0	0	Page	0.001013	0.9998	0.0007496
2	2.5	15	Page	0.003282	0.9994	0.00135
1	2	12.5	Page	0.001819	0.9995	0.001004

4.4.3 Response Surface Analysis

The results of the CCD experimental design are reported in Table 4.4. From the table it can be observed that maximum water removal (38.1%) took place when the applied voltage was set to 15 kV, electrode gap at 1.5 cm and air velocity at 2 m/s and the minimum (19.32 %) occurred when applied voltage was set to 12.5 kV, electrode gap at 2 cm and air velocity at 1 m/s. The ANOVA analysis for the effect of process parameters on percentage water removed (Table 4.5) revealed that air velocity (m/s) and electrode gap (cm) had a significant influence ($p \leq 0.0021$ and $p \leq 0.0325$, respectively). Whereas, applied voltage had no significant effect ($p > 0.05$). Out of all the cross terms, only the cross term between applied voltage and electrode gap had a significant effect on the amount of water removed, which was obvious as this cross term refers to the electric field intensity (applied voltage/electrode gap). Several studies have suggested that the higher the electric field intensity, the higher is the drying rate (Bajgai and Hashinaga, 2001a, b; Lai and Lai, 2002). At lower electric field intensity, i.e. when the applied voltage is low or the electrode gap is increased, cross flow can suppress the

corona wind effect and could produce an adverse effect on drying. This phenomenon can be attributed for lower water removal percentage for experiments conducted at higher air velocity in combination with lower applied voltage and higher electrode gap. Figure 4.4 presents the results of the Tukey's HSD (honest significant difference) test, where it can be observed that most of the experimental conditions except for (+-+: air velocity of 2 m/s, electrode gap of 1.5 cm and applied voltage of 15 kV and 00A: air velocity of 1.5 m/s, electrode gap of 2 cm and applied voltage of 15 kV)) had a significant effect on the percentage of moisture removed. The interaction among the process parameters was analyzed using a three-dimensional response surface graph (Figure 4.5). From the figure, it can be inferred that air velocity and electric field intensity, which is the ratio of applied voltage and electrode gap, had a significant effect on the amount of moisture removed. When the applied voltage and electrode gap were set at the lowest value of 10 kV and 1.5 cm, an increase in air velocity led to an increase in amount of water removed and as the voltage was increased at any given air velocity, similar results were obtained, indicating an increase in amount of water removed.

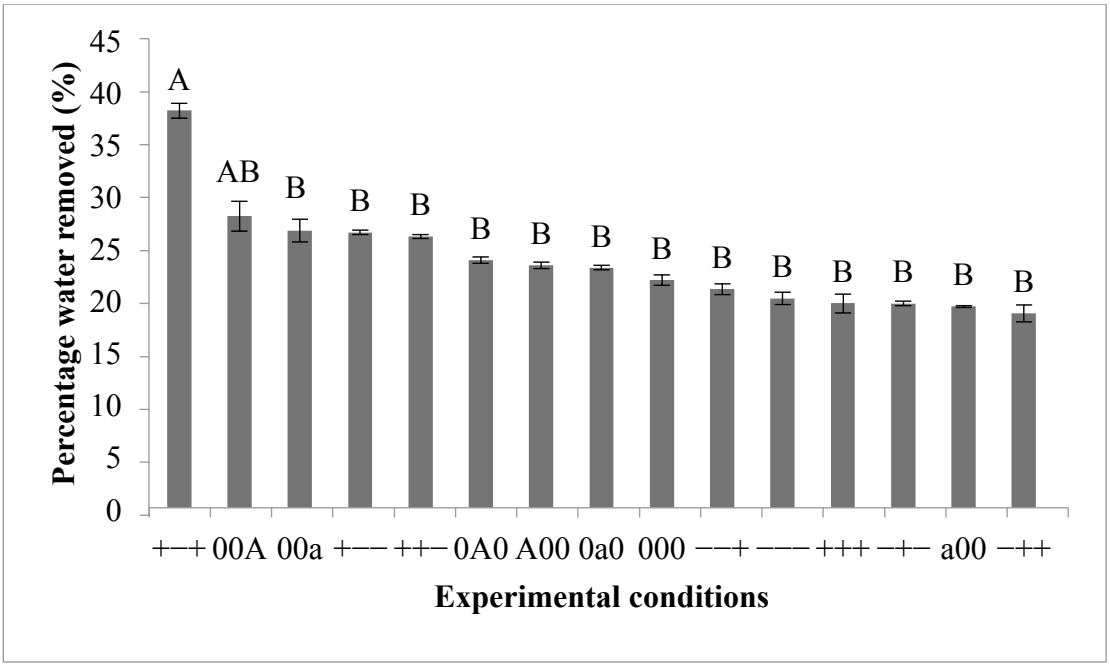

Figure 4.4: Tukey's HSD (honest significant difference) test on effect of different experimental conditions (coded) and percentage of water removed.

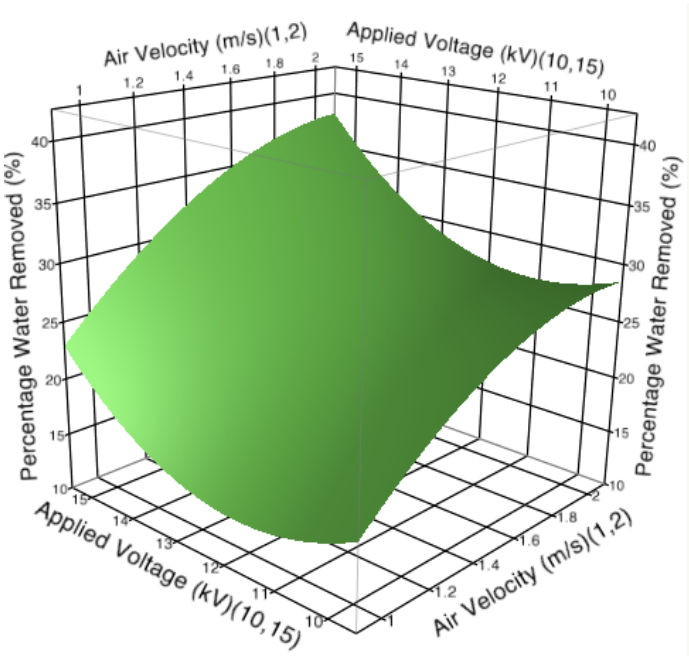

Figure 4.5: Response surface plot of the effect of process parameters on percentage of water removed.

As suggested by Lai et al. (Balcer and Lai, 2004; Lai and Lai, 2002), the Sherwood and EHD numbers were also estimated to predict the interactions between the process parameters and their effect on them. Lai et al. (Lai and Sharma, 2005) expressed the enhanced drying rate by EHD as a function of Sherwood's number and EHD's number (in the presence of cross-flow). In this study it was observed that process parameters such as air speed and electrode gap had significant effect on drying rate, while applied voltage alone had no significant effect. The interaction between electrode gap and applied voltage i.e. the applied electric field intensity had a significant effect on the Sherwood number and so did their individual quadratic terms (Table 4.6, Figure 4.6). It was also interesting to note that the Sherwood number was affected by the interaction between air velocity and electrode gap (suggesting the effect of electric field intensity), but as concluded by scores of researchers that cross-flow can suppress the EHD drying, in the present study it was observed that cross-flow in combination with high electric field intensity actually enhances the drying rate. Only for cases where the applied voltage was low and electrode gap was higher (low electric field intensity), cross-flow suppressed the drying enhancement from the applied electric field.

Table 4.5: ANOVA analysis for the effect of process parameters, air speed (A), electrode gap (G_e) and applied voltage (V) on percentage water removed.

Source	Sum of Squares	Degree of freedom	F Ratio	*p-value*
Model	297.67843	9	4.6335	0.0126
A (m/s)	121.03441	1	16.9557	0.0021
G_e (cm)	43.93216	1	6.1545	0.0325
V (kV)	4.30336	1	0.6029	0.4555
A× G_e	32.20031	1	4.5109	0.0596
A×V	3.57781	1	0.5012	0.4951
G_e ×V	49.55101	1	6.9416	0.0250
A^2	14.31271	1	2.0051	0.1872
G_e^2	0.07611	1	0.0107	0.9198
V^2	38.13004	1	5.3416	0.0434

With respect to the EHD number which is defined as the ratio of ion velocity or drag to inertial force or air velocity (Sadek and Hurwitz, 1972), it was observed that all process parameters; air velocity, electrode gap and applied voltage had a significant effect on the EHD number (Table 4.7, Figure 4.7). This observation was not a surprise because, as per the definition, the calculation of EHD number includes electric field intensity that governs the ion drag and air speed. From Equation 4.14 it can be understood that a higher EHD number suggests that ion drag or the corona wind prevails over the air velocity and vice versa. Hence looking at the experimental data obtained in Table 4.2, for a given air velocity and electrode gap, if the applied voltage is increased from 10 kV to 15 kV, the percentage water removed increases and so does the EHD number. This observation was in accordance with Lai and Lai (Lai and Lai, 2002), who suggested that an increase in EHD number will improve the rate of drying but as the air velocity is increased and electric field intensity reduced, air velocity or inertial force will prevail over ion drag (Wolny, 1992; Wolny and Kaniuk, 1996).

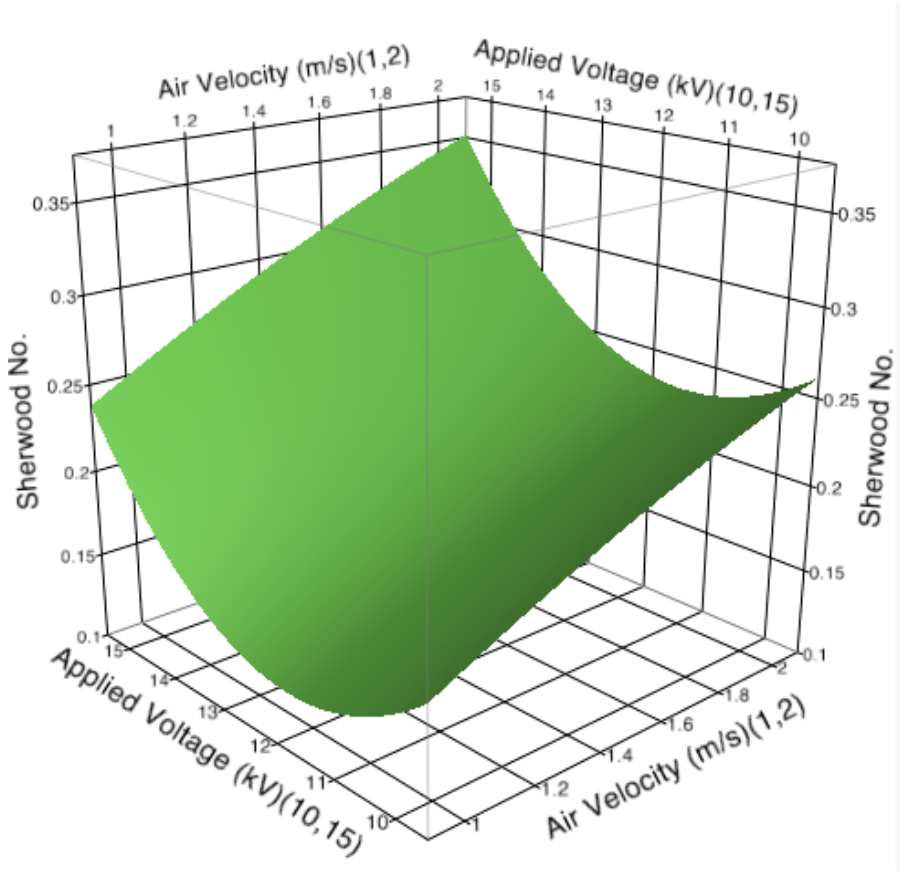

Figure 4.6: Response surface plot of the effect of process parameters on Sherwood number.

Table 4.6: ANOVA analysis for the effect of process parameters, air speed (A), electrode gap (G_e) and applied voltage (V) on Sherwood's number.

Source	Sum of Squares	Degree of freedom	F Ratio	*p-value*
Model	0.02932923	9	12.6478	0.0002
A (m/s)	0.00718240	1	27.8758	0.0004
G_e (cm)	0.00806560	1	31.3036	0.0002
V (kV)	0.00067240	1	2.6097	0.1373
A× G_e	0.00195313	1	7.5803	0.0204
A×V	0.00012012	1	0.4662	0.5102
G_e ×V	0.00475313	1	18.4475	0.0016
A^2	0.00005020	1	0.1949	0.6683
$G_e{}^2$	0.00204545	1	7.9387	0.9198
V^2	0.00600445	1	23.3041	0.0182

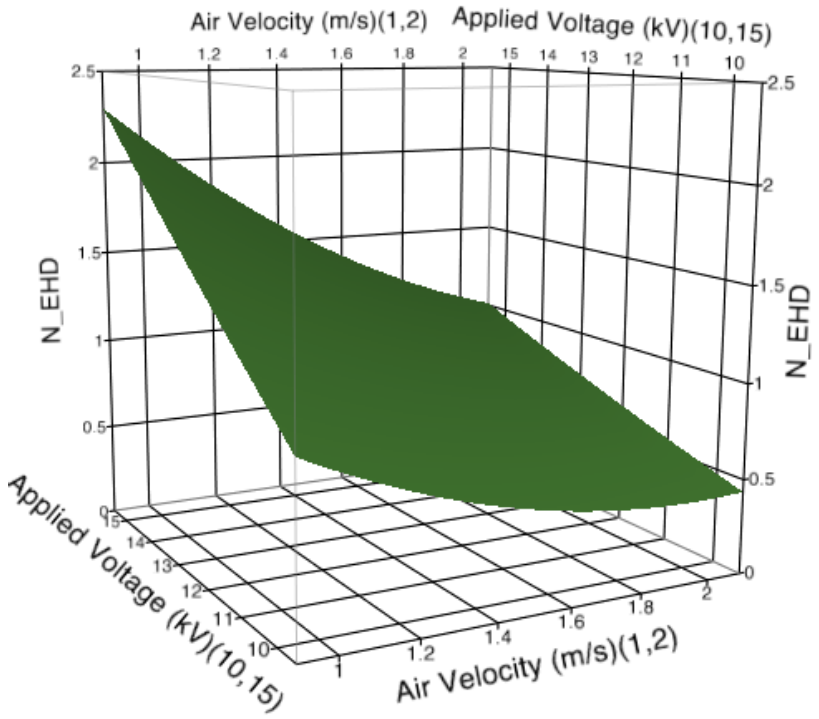

Figure 4.7: Response surface plot of the effect of process parameters on EHD number.

Table 4.7: ANOVA analysis for the effect of process parameters, air speed (A), electrode gap (G_e) and applied voltage (V) on EHD number.

Source	Sum of Squares	Degree of freedom	F Ratio	*p-value*
Model	3.1200264	9	613.8423	0.0001
A (m/s)	1.3195056	1	2336.427	<0.0001
G_e (cm)	0.0048974	1	8.6717	0.0147
V (kV)	1.5721225	1	2783.732	<0.0001
A× G_e	0.0007801	1	1.3814	0.2671
A×V	0.1460701	1	258.6440	<0.0001
G_e ×V	0.0003125	1	0.5533	0.4741
A^2	0.0365155	1	64.6575	<0.0001
G_e^2	3.72784 E^{-7}	1	0.0007	0.9800
V^2	0.0004998	1	0.8851	0.3690

In the case of specific energy consumed, it was observed that as the applied voltage increased, the amount of specific energy consumed increased. The ANOVA analysis suggested that all given process parameters including air velocity, electrode gap and applied voltage had a significant effect on the specific energy consumed during the EHD process. The three-dimensional response plot of the effect of process parameters on specific energy consumed (Figure 4.8) at a set electrode gap of 1.5 cm revealed that the amount of specific energy consumed increased with an increase in applied voltage but an increase in air velocity at a given voltage reduced the amount of energy consumed because of its significant effect on the overall drying rate. For the present study, the values of specific energy consumed values ranged between 420-3306 kJ/kg, which was in accordance with data presented by Singh et al. (Singh et al., 2012). When compared to conventional drying processes such as spouted bed drying the values obtained for specific energy consumption for EHD drying are on the lower side, which proves and supports the objective of this study that application of electric field in combination with cross flow can enhance the drying rate and that cross-flow has a significant effect on the amount of water removed during the drying process. Table 4.8 presents the regression expressions showing the relation of process parameters; air speed (A), electrode gap (G_e) and applied voltage (V) on dependent variables including percentage water removed, Sherwood number, EHD number and specific energy consumed (kJ/kg).

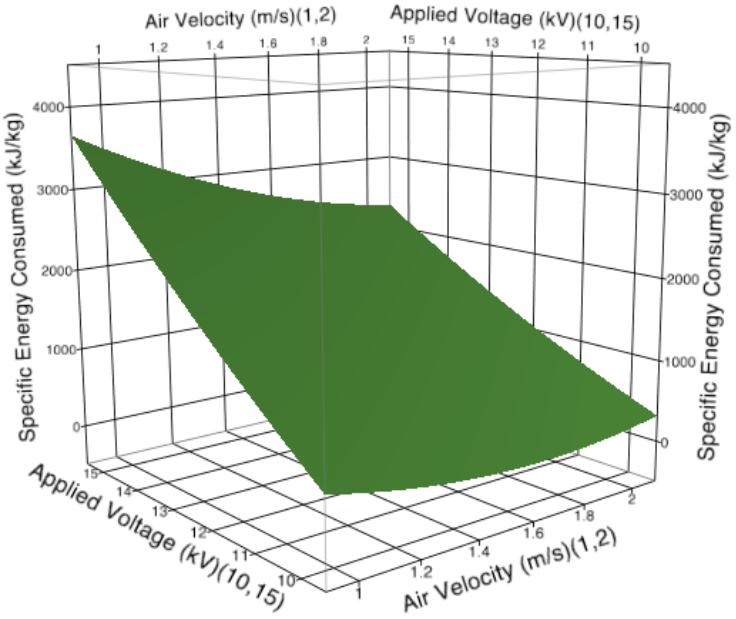

Figure 4.8: Response surface plot of the effect of process parameters on specific energy consumed (kJ/kg).

Table 4.8: Regression Equations established between process parameters, air velocity (A), electrode gap (G_e) and applied voltage (V) and dependent variables (water removed (%), Sherwood and EHD Numbers and Specific energy consumed (kJ/kg).

Dependent Variables	**Regression Equation**	
Percentage of water removed (%)	$22.643 + 3.479(A) - 2.096(G_E) + 0.656(V) - 2.488(G_E \times V) + 3.72(V^2)$	$R^2 = 0.81$ ($p<0.0126$)
Sherwood Number	$0.194 + 0.0268(A) - 0.0284(G_E) + 0.008(V) - 0.0156(G_E \times A) - 0.0244(G_E \times V) - 0.0272\ (G_E^2) + 0.0467(V^2)$	$R^2 = 0.92$ ($p<0.0002$)
EHD number	$0.965 - 0.363(A) - 0.0221(G_E) + 0.396(V) - 0.135(A \times V) + 0.115(A^2)$	$R^2 = 0.99$ ($p<0.0001$)
Specific Energy Consumed (kJ/kg)	$1352.49 - 225.851(A) - 48.980(G_E) + 1129.555(V) - 199.570(\ A \times V)$	$R^2 = 0.92$ ($p<0.0002$)

4.5 Conclusion

This study thoroughly examines the effect of process parameters such as air velocity, electrode gap and applied voltage for EHD drying using a wire electrode. The percentage of water removed was shown to be dependent on the strength of the applied electric field (i.e. electric field intensity) and air velocity. It was also observed that the amount of energy (kJ) consumed to dry a kg of water increased linearly with an increase in applied voltage but decreased when air speed was increased, suggesting that EHD drying in combination with a cross flow consumes less energy and provides better drying efficiency. The most significant outcome of this study is also the fact that all these experiments were conducted at ambient condition as compared to other conventional drying techniques. Further studies need to be conducted to explain the relation between the process parameters and removal of bound moisture as in this study the sample moisture available for removal was surficial or loosely packed between the pores of the sand particles and these studies will also be able to define the capabilities and limitations of the EHD drying process as compared to a conventional drying process.

Connecting Statement

In the previous chapter, the design aspect of EHD and its performance was evaluated for non-hygroscopic material (sand). In the next chapter the system will be evaluated for hygroscopic material such as wheat. Also to understand the effect of high voltage on protein-conformation, which could help find applications of EHD in evaluating beyond drying of biological matrix.

Chapter 5

Electrohydrodynamic Drying (EHD) of Wheat and its Effect on Wheat Protein Conformation

5.1 Abstract

This study investigates the electrohydrodynamic drying characteristics of wheat and its effect on the conformation of wheat protein using Fourier Transform Infrared Spectroscopy (FTIR). It was observed that the drying rate of EHD dried wheat was significantly higher than that of the control. A single wire electrode EHD system was used with a set electrode gap of 1.5 cm, applied voltages of 10 kV, 12.5 kV and 15 kV in combination with air cross-flow of velocities 1m/s, 1.5 m/s and 2m/s. It was observed that the drying rate of wheat sample was significantly affected by applied voltage and air velocity. The drying rate increased with an increase in air velocity and applied voltage. The exponential equation showed good agreement with the EHD drying kinetics of wheat. This study also showed that wheat protein conformation was significantly affected by EHD drying. In the analysis of the Amide I region (1720-1580 cm^{-1}) of wheat protein, FT-IR spectra showed distinct valleys at 1682 - 1686 cm^{-1} (β-sheets), 1674 cm^{-1} (β-sheets), 1664 -1667 cm^{-1} (turns), 1654 - 1657 cm^{-1} (α-helices), 1651 cm^{-1} (α-helices), 1645 - 1647 cm^{-1} (Random coils) and 1633 - 1634 cm^{-1} (β-sheets). Peak fitting using Gaussian band shapes suggested that exposure to electric field influenced the hydrogen bonding pattern of wheat protein resulting in shifts between low and high frequency bands which further supported these results. Thermal analysis of EHD dried wheat samples did not provide any conclusive results. The significance of these results was further discussed in relevance to protein structural changes.

5.2 Introduction

Drying is an important unit operation in the food industry primarily used for reducing the moisture content of the food. Reduction in moisture improves the shelf life and also moderates the transportation costs of food products (Singh et al., 2012). Traditionally, drying is conducted by exposing the food to high temperatures and this exposure results in various compositional/structural changes, both desirable and undesirable (Bajgai et al., 2006c; Singh et al., 2012; Sunjka et al., 2004). Moreover, conventional drying techniques use large quantities of fossil fuels to generate the required thermal energy, which also has a negative environmental impact (Raghavan et al., 2005b; Sagar and Kumar, 2010). Growing concerns over recent climatic changes and environmental impacts of application of fossil fuels has instigated the demand from both the public and the government agencies for development of green processing techniques in all industrial sectors (Bajgai et al., 2006c; Raghavan et al., 2005b). For food industries meeting the environmental impact guidelines and consumer demand for foods with better nutritional and sensory characteristics and has led to the acceleration in the development of novel processing techniques (Singh et al., 2012) which can be classified into two categories, electro technologies and non-thermal processing methods (Joyce and Rajamohamed, 2009; Pereira and Vicente, 2010; Richardson, 2001).

Electrohydrodynamic (EHD) drying is one of the non-thermal, novel processing techniques with a lot of potential for wide applications in the food industry. This process involves the use of corona wind, which is generated when a high voltage is applied to an electrode of very small radius of curvature (Singh et al., 2012). The ions produced around the electrode have either excess or deficiency of electrons and are bound with the coulomb forces acting between them. These ions when emitted from the charged electrode collide with neutral air molecules, which get charged due to the high electric field and migrate towards the ground/neutral electrode causing an ionic wind also termed as ’corona wind’. This corona wind enhances the mass transfer by disrupting the saturated vapor layer over the food surface paving a path for the moisture to escape (Singh et al., 2012).

The characteristic physico-chemical properties of all proteins are dependent on their structural conformation (Arntfield and Murray, 1981; Gu and Bourne, 2009; Singh et al., 2013a). Amino acids are the building blocks of a protein; they form a peptide bond with each other by giving out a water molecule and this linear arrangement gives a protein its ‘primary

structure'(Fruton, 1972; Sanger, 1952) which is the first of the four levels of structure. Depending on the amino acids forming the linear structure, the protein folds into helices, β-sheet and turns which are defined as the 'secondary structures' (Goormaghtigh et al., 1994; Pelton and McLean, 2000; Surewicz et al., 1993). The 'tertiary structure' is formed because of various bonds between the amino acid chains including the hydrogen bonds and di-sulphide bonds giving the protein a three dimensional structure. The 'quaternary structure' is observed in large protein molecules that are formed when multiple protein subunits come together to form a large three-dimensional structure. The destruction of these protein structures is known as protein denaturation. When food proteins are subjected to an external stress including thermal, electrical, chemical, pressure etc., they undergo conformational changes that lead to variation in their functional properties (Arntfield and Murray, 1981; Singh et al., 2013a).

In this study, the effect of electrohydrodynamic drying on wheat proteins has been evaluated using a Fourier Transform Infrared Spectrometer (FT-IR) and Differential Scanning Calorimeter (DSC). FT-IR spectroscopy is widely employed to study protein structures. Several researchers have conducted FT-IR analysis on various food proteins including the wheat protein (Belton, 1999; Belton et al., 1995; Georget and Belton, 2006b; Wang et al., 2001). The protein sample absorbs the infrared radiation at specific intensity and wavelength, which when measured gives the structural data of the polypeptide secondary structures of the protein. And when the Fourier transform in used to convert this raw data obtained into a proper spectral data, it is called an FT-IR spectrum (Haris and Severcan, 1999; Jackson and Mantsch, 1995). The structural units present in the protein give rise to a total of 9 distinct regions which are named Amide A, B and I-VII (Kong and Yu, 2007). The secondary structures of the proteins can be analyzed using the Amide I region (1720 cm^{-1} - 1580 cm^{-1}) which is responsible for the vibrations of the C=O stretch in peptide linkages and also is the most prominent of all the amide regions (Haris and Severcan, 1999; Mangavel et al., 2001). Amide II region of the spectra is caused due to the vibration in the C-N bond stretching and the N-H bond bending in the protein structure (Georget and Belton, 2006b).

The use of DSC to study thermal properties of proteins is not new (Delben and Crescenzi, 1969; Privalov and Khechinashvili, 1974). It is a thermo-analytical technique, which monitors the changes in the physical or chemical properties of a material as a function of temperature by monitoring the heat flow changes associated with these processes (Delben

and Crescenzi, 1969). This change in heat flow is recorded as a peak and the area under the peak is directly proportional to enthalpy of the process. Study of protein structural changes during thermal denaturation is complex as it undergoes a reversible thermal denaturation, provided it is studied under a condition, which inhibits this reversibility (Arntfield and Murray, 1981). The objective of this study was to investigate the effect of EHD on drying characteristics of wheat and evaluate its effect on the conformation of wheat protein using FT-IR and analyze the effect of change in conformation on thermal properties of wheat protein using DSC.

5.3 Materials and Methods

5.3.1 Sample Preparation

Wheat sample at moisture content around 8 % dry basis (d.b.) was procured from the local market. The wheat was cleaned and later conditioned by addition of water to increase its initial moisture content to 20% d.b. This sample was then stored in the refrigerator at 4 °C.

5.3.2 Experimental Setup

The schematic diagram of the EHD setup used for the present study is shown in Figure 5.1. The setup consisted of a sample compartment made of Plexiglas of the following dimensions; 28.1 cm long, 11 cm wide and 8 cm high. It was connected to a blower at one end, which forced the air into the compartment at different velocities (1 m/s, 1.5 m/s and 2 m/s) set manually before the start of the experiment. The sample container was also made of Plexiglas of dimensions; 10 cm long, 2.5 cm wide and 2.5 cm deep. The base of the sample container was made of aluminum, which acted as the ground electrode. The sample compartment also enclosed a vertically mounted emitting electrode (copper wire of 0.5 mm diameter), which was suspended above the sample box. The gap between the emitting electrode and sample surface was fixed at 1.5 cm. A direct current at high voltage (positive polarity) was applied to the emitting electrode from a power supply unit, which could provide a maximum voltage output of 30 kV. A data logger recorded the temperature, relative humidity of the ambient air and the change in mass of wheat every minute. The drying experiment was conducted till the moisture content of the sample reduced to 15 %

d.b. and during all the experiments the ambient temperature remained fairly constant, as the lab temperature was controlled but during some experiments the relative humidity showed substantial changes, this change might have contributed to the variability in the data that will be discussed in the following sections.

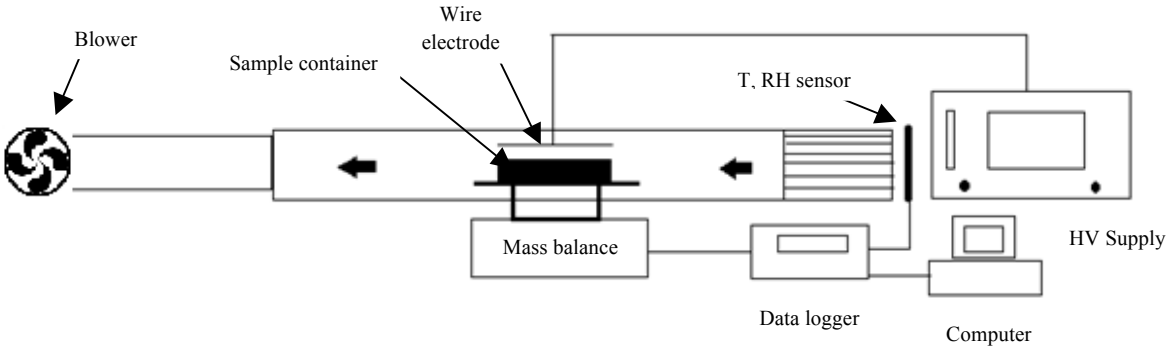

Figure 5.1: Schematic of the EHD experimental setup.

Note: T: Temperature; RH: Relative Humidity; HV: High Voltage

5.3.3 Drying Experiment

The wheat samples were removed from the refrigerator and kept at ambient temperature till they reached the ambient conditions. About 40 g of wheat samples was used for EHD drying. The drying experiment consisted of 2 factors (air velocity and applied voltage) with 3 levels each (air velocity: 1, 1.5, 2 m/s; applied voltage: 10, 12.5, 15 kV), which were used to generate a full factorial experimental design. The experimental design was developed using JMP software (ver. 10, SAS Institute Inc., Cary, NC, USA). All the experiments were replicated thrice and the data were analyzed. Results from three replicates of the control samples (only air cross-flow) were used as reference to evaluate the drying enhancement with the applied electric field.

5.3.4 Mathematical Modeling

The effect of the process parameters on the EHD drying kinetics of wheat was evaluated using mathematical models including Newton, Page, Modified Page, Henderson and Pabis and Exponential (Cao et al., 2004a) (Table 5.1).

A wheat sample size of 40 g ± 0.7 g was used for all the experiments. The initial moisture content (20% d.b.) of the wheat sample for all experimental runs on a dry basis (d.b.) was estimated by the official method 925.10 of AOAC (2000) using Equation 5.6.

Table 5.1: Mathematical models used to predict EHD drying kinetics of wheat.

Model Name	Equation	Equation No.
Newton	$MR = e^{-kt}$	5.1
Page	$MR = e^{-kt^n}$	5.2
Henderson and Pabis	$MR = a\, e^{-kt}$	5.3
Modified Page	$MR = e^{(-kt)^n}$	5.4
Exponential (Cao et al., 2004a)	$MR = ae^{-kt^n}$	5.5

Note: Where, k is the drying rate constant (min^{-1}); n & a are drying coefficients (unitless) which have values depending on the drying curve and equation; t is the time (min); and MR is the moisture ratio (Equation 5.7) (Singh et al., 2013b).

$$M.C.(d.b.) = \frac{M_w}{M_s} \tag{5.6}$$

Where, M_w is the mass of water in the sample (g); M_s is the mass of the solid in the sample (g). The moisture ratio of the sample was determined using Equation 5.7.

$$MR = \frac{M_i - M_e}{M_0 - M_e} \tag{5.7}$$

Where, M_0, M_i and M_e are initial moisture content, moisture content at time t_i and equilibrium moisture content respectively. The value of equilibrium moisture content was relatively small compared to M_0 and M_i, hence the error involved in simplification was negligible, and so the Equation 5.7 reduces to (here, we can also state moisture ratio as moisture relative value) (Aghbashlo et al. 2008):

$$MR = \frac{M_i}{M_0} \tag{5.8}$$

Statistical parameters including root mean square error (*RMSE*) (Equation 5.9), coefficient of

determination R^2 (Equation 5.10) and sum square error (SSE) (Equation 5.11) were used to estimate the goodness of fit of all drying model curves.

$$RMSE = \sqrt{\frac{1}{n}\sum_{i=1}^{i=n}(MR_i^{pred} - MR_i^{\exp})} \tag{5.9}$$

Where, n is the number of observations, MR_i^{pred} is the predicted *MR* at time t_i and $MR_i^{\exp}$ is the measured value of *MR* at time t_i.

The coefficient of determination R^2 is calculated using Equation 5.10.

$$R^2 = 1 - \frac{\sum_{i=1}^{i=n}(MR_i^{\exp} - MR_i^{Pred})^2}{\sum_{i=1}^{i=n}(MR_i^{\exp} - \overline{MR}^{\exp})^2} \tag{5.10}$$

Where, $\overline{MR}^{\exp}$ represents the mean experimentally measured value of *MR*. The sum square error (*SSE*) was also determined using Equation 5.11 as the criteria for goodness of fit (Singh et al., 2013b).

$$SSE = \frac{1}{n}\left(\sum_{i=1}^{i=n}(MR_i^{pred} - MR_i^{\exp})^2\right) \tag{5.11}$$

5.3.5 Determination of Specific Energy Consumption

The applied power (*P*) and the energy (*E*) for the EHD drying process were estimated using Equations 5.12-5.13.

$$P = I \times V \tag{5.12}$$

$$E = P \times t \tag{5.13}$$

Where, I is the current (A); V is the applied voltage and t is the drying time. The specific energy consumed (*SEC*) was determined using Equation 5.14.

$$SEC = \frac{E}{M} \tag{5.14}$$

Where, *E* (kJ) is the energy consumed and *M* (kg) is the mass of water removed.

5.3.6 FT-IR Spectroscopy

FT-IR spectral analysis of EHD dried wheat samples was conducted using a Nicolet iS5

ATR-FT-IR spectrometer. Dried wheat was ground into fine powder and later this powder was used as the sample for FT-IR analysis. Samples were directly applied to the single-reflection diamond ATR (attenuated total reflectance) and pressed down to ensure good contact with the ATR diamond. For each sample, 32 spectra at 4 cm^{-1} resolutions were averaged and the spectra for empty ATR diamond acted as the reference. The spectra were analyzed using the OMNIC software (version 8, Thermo Nicolet Instrument Corp., Madison, WI) and Origin Pro (Version 9, OriginLab Corporation, Northampton, MA, USA).

5.3.7 Differential Scanning Calorimetry (DSC)

The thermal properties of wheat protein were examined using a Differential Scanning Calorimeter (DSC Q100, TA Instruments, Wilmington, DE, USA). The DSC was calibrated using pure indium standard. About 9.5 ± 0.2 mg of wheat sample was carefully placed at the center of a pre-weighed aluminum pan. The pans were later hermetically sealed with TA sample encapsulating press. The sample pans were placed in the sample cells while an empty pan was placed in the reference cell of the DSC. Later the samples were heated from 20 °C to 200 °C at a rate of 5 °C/min. DSC thermograms obtained were later analyzed using available TA instrument software.

5.3.8 Statistical Analysis

All statistical analyses were carried out using JMP software (ver. 10, SAS Institute Inc., Cary, NC, USA). Duncan Multiple Range test was performed using Statistical Analysis Software (SAS 9.2, SAS institute Inc., Cary, NC, USA). The drying kinetics for the samples were determined using MATLAB R2012b (Mathworks Inc. MA, USA).

5.4 Results and Discussion

5.4.1 Current-Voltage Relationship

Before the start of the experiment, the relation between the current and voltage was determined by increasing the positive applied voltage in the range of 7-25 kV and the corona current (μA) was measured. In our previous studies we have estimated the effect of the

electrode gap on the current-voltage relationship, and the relationship obtained is shown in Figure 5.2. It was observed that the corona current increased with an increase in applied voltage while there was no significant difference in the corona current values were observed between different electrode gaps. For the present study the electrode gap was set at 1.5 cm because it was the lowest value of electrode gap that could be reached with the present design and equipment stability constraints. With electrode gaps below 1.5 cm the high voltage system became unstable and system interruptions were occurring.

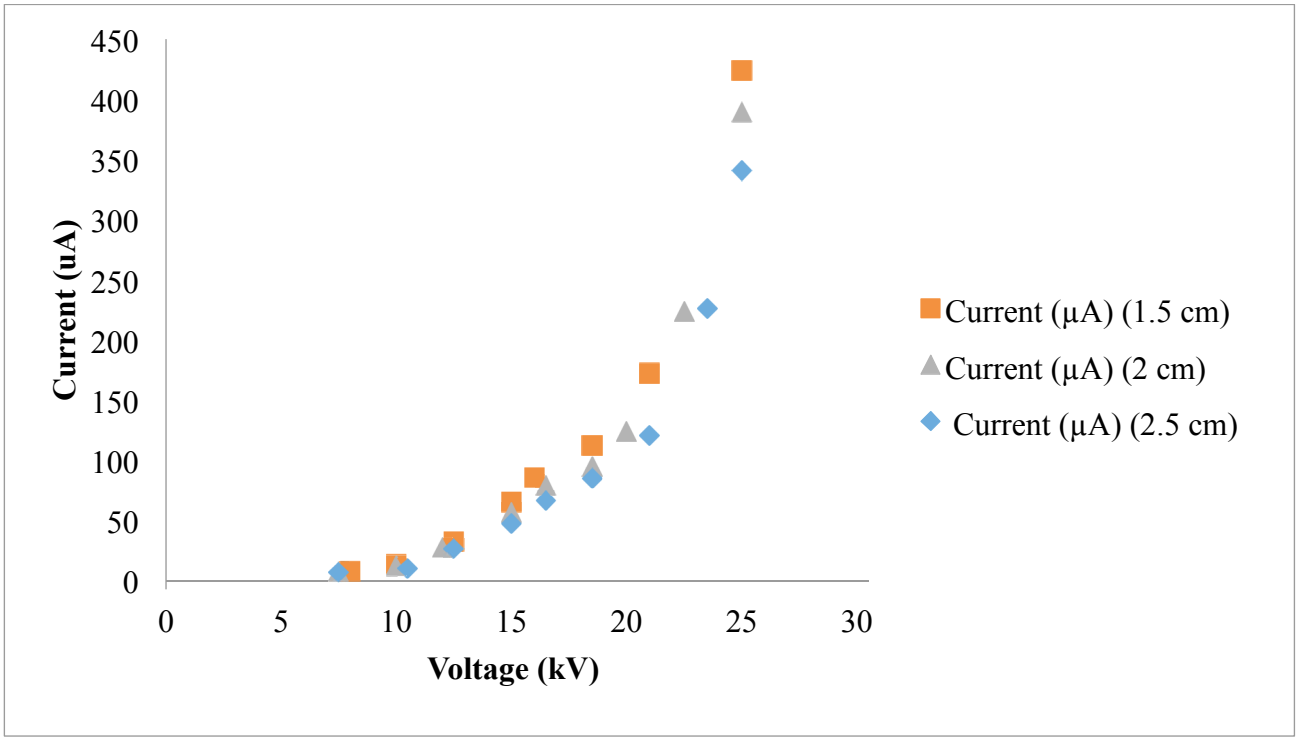

Figure 5.2: Current-Voltage relationship with respect to electrode gap

5.4.2 Drying Kinetics and Specific Energy Consumed

The drying curves for wheat samples dried under different air cross-flow with and without electric field are shown in Figure 5.3. From the figure it can be observed that the wheat sample subjected to high voltage drying in combination with cross flow dried much faster than the control (only cross flow). The highest drying rate was obtained when the wheat sample was subjected to an applied voltage of 15 kV with an air cross-flow of 2 m/s. In their study on EHD drying of wheat under different electric field intensities and temperature, Cao et al. (Cao et al., 2004a) observed that the drying rate increased with an increase in temperature and the application of an electric field significantly enhanced the drying rate at

20 °C. They stated that as the electric field intensity was increased the drying rate also increased, they attributed this to the ionic wind generated during the EHD process. In this study the temperature of the experimental room was controlled at 20 °C but a significant change in relative humidity was observed which lead to a variable drying rate observed at different air velocities and applied voltage, and similar observations were made by Lai et al. (Balcer and Lai, 2004; Lai and Lai, 2002). The obtained drying curves (Figure 5.3) were further fitted with the drying models presented in Table 5.1. From Table 5.2 it can be concluded that the exponential model suggested by Cao et al. (Cao et al., 2004a) had the best fit for all the experimental conditions and even for the control conditions. To estimate the EHD drying efficiency, specific energy consumed during the EHD drying process was also estimated. The lowest specific energy consumption of 893.61 kJ/kg was obtained for the experimental combination of air velocity of 1.5 m/s and applied voltage of 10 kV and maximum value of 11175.94 kJ/kg was obtained for air velocity of 1.5 m/s and applied voltage of 15 kV. The extent of this difference in the amount of specific energy consumed can be attributed to the longer drying time taken by the later experimental combination under a high relative humidity condition. For the experimental combination of air velocity 2 m/s and applied voltage 15 kV, which had the lowest drying time, the total specific energy consumed was estimated to be 8175 kJ/kg. These values followed a common trend, where the total specific energy consumed during the EHD process, increased with an increase in applied voltage, but the results obtained in this study have higher specific energy consumption values as compared to the ones reported by Singh et al., (Singh et al., 2012). They stated that the specific energy consumed by an EHD process using a wire electrode ranged between 200-5000 kJ/kg, while it is interesting to note that the values they have reported were for water present on the surface of glass beads and between the pores but not within, i.e. there was no bound moisture, but in this study, the wheat sample has both surface and bound moisture and it is obvious that the amount of energy required to release the surface moisture would be less than for the bound moisture.

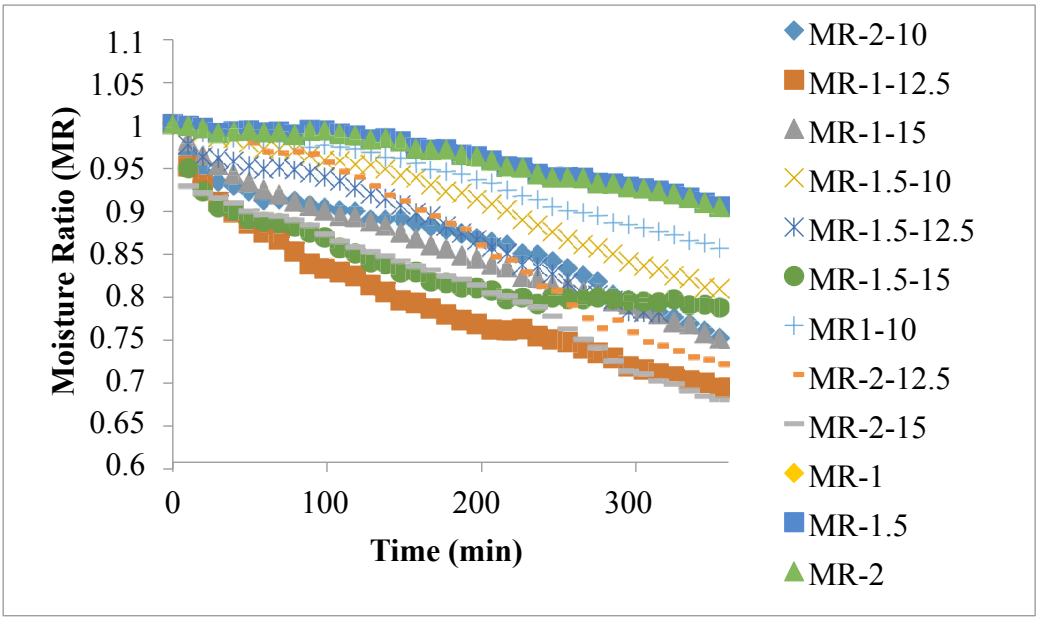

Figure 5.3: Drying curve for conditioned wheat (20% d.b.) sample under all experimental conditions. Note: Experimental conditions are represented in the format "air velocity – applied voltage"

Table 5.2: Estimated statistical values, RMSE, R^2 and SSE values obtained for various drying models.

Experimental Condition	**Models**	**Statistical Parameters**					
		SSE	**R^2**	**RMSD**	**k**	**a**	**n**
1-10	Newton	0.2443	0.9865	0.01581	0.000688		
	Page	0.2423	0.9866	0.01576	0.0007602		0.9845
	H&P	0.2014	0.9889	0.01436	0.0006611	0.9846	
	Modified Page	0.2443	0.9865	0.01582	0.04404		0.01562
	Exponential (Cao et al., 2004a)	0.000647	0.9962	0.003835	0.001021	0.9972	1.402
1-12.5	Newton	1.778	0.8174	0.04521	0.0008034		
	Page	0.03748	0.9962	0.006568	0.01011		0.5987
	H&P	0.1822	0.9813	0.01448	0.0005987	0.9009	
	Modified Page	1.778	0.8174	0.04521	0.001173		0.6846
	Exponential (Cao et al., 2004a)	0.02462	0.9975	0.005326	0.005962	0.9705	0.6707
1-15	Newton	0.1843	0.9808	0.01498	0.0006592		
	Page	0.03622	0.9962	0.006646	0.001799		0.8405
	H&P	0.02548	0.9973	0.005574	0.0005949	0.9686	
	Modified Page	0.1843	0.9808	0.01498	0.02826		0.02332
	Exponential (Cao et al., 2004a)	0.02038	0.9979	0.004988	0.0009248	0.9783	0.9352
1.5-10	Newton	0.2344	0.981	0.01638	0.0005305		
	Page	0.08224	0.9933	0.009706	0.000158		1.19
	H&P	0.1064	0.9914	0.0104	0.0005805	1.027	
	Modified Page	0.2344	0.981	0.01638	0.05347		0.009922
	Exponential (Cao et al., 2004a)	0.07699	0.9937	0.009397	0.0002248	1.009	1.139

Table 5.2 continued

1.5-12.5	Newton	0.046	0.9722	0.01083	0.0006489		
	Page	0.04028	0.9757	0.01015	0.0003767		1.097
	H&P	0.04521	0.9727	0.01075	0.0006369	0.997	
	Modified Page	0.046	0.9722	0.01085	0.002733		0.2374
	Exponential (Cao et al., 2004a)	0.009986	0.994	0.00506	3.19E-05	0.9715	1.5
1.5-15	Newton	0.5017	0.5066	0.03295	0.0005887		
	Page	0.04215	0.9585	0.009563	0.01222		0.4712
	H&P	0.1402	0.8621	0.01744	0.0003807	0.9407	
	Modified Page	0.5017	0.5066	0.03295	0.0184		0.03199
	Exponential (Cao et al., 2004a)	0.03471	0.9659	0.008686	0.02845	1.041	0.3589
2-10	Newton	0.07923	0.9158	0.01186	0.0002072		
	Page	0.008809	0.9906	0.003959	5.39E-06		1.607
	H&P	0.02846	0.9697	0.007116	0.0002597	1.02	
	Modified Page	0.07923	0.9158	0.01186	0.0002808		0.7381
	Exponential (Cao et al., 2004a)	0.007756	0.9918	0.003718	1.05E-05	1.004	1.504
2-12.5	Newton	0.3882	0.9819	0.01977	0.0006996		
	Page	0.3751	0.9825	0.01945	0.0008765		0.9651
	H&P	0.3776	0.9824	0.01951	0.000713	1.008	
	Modified Page	0.3882	0.9819	0.01977	0.05116		0.01367
	Exponential (Cao et al., 2004a)	0.2503	0.9884	0.01589	0.002564	1.053	0.8172
2-15	Newton	0.05636	0.9783	0.01138	0.0006967		
	Page	0.04407	0.9831	0.1008	0.0003603		1.115
	H&P	0.05626	0.9784	0.01139	0.0007004	1.001	
	Modified Page	0.05636	0.9783	0.0114	0.001595		0.4368
	Exponential (Cao et al., 2004a)	0.01708	0.9934	0.006281	4.93E-05	0.9728	1.435
1-0	Newton	0.0051	0.9314	0.0107	0.0002647		
	Page	0.00068181	0.9909	0.0039	0.00001325		1.517
	H&P	0.0026	0.9648	0.0077	0.0003145	1.015	
	Modified Page	0.0051	0.9314	0.0108	0.0005185		0.5101
	Exponential (Cao et al., 2004a)	0.00068095	0.9909	0.0040	0.00001247	0.9996	1.526
1.5-0	Newton	0.0051	0.9319	0.0106	0.0002651		
	Page	0.0006823	0.9909	0.003989	0.0004401		1.514
	H&P	0.002634	0.9648	0.007737	0.003146	1.015	
	Modified Page	0.0005102	0.9319	0.01077	0.004299		0.6165
	Exponential (Cao et al., 2004a)	0.000681	0.9909	0.00398	0.0004193	0.9996	1.526
2-0	Newton	0.0051	0.9319	0.0106	0.0002651		
	Page	0.0006827	0.9909	0.003939	0.0004425		1.513
	H&P	0.002633	0.9648	0.007735	0.003146	1.015	
	Modified Page	0.005085	0.9321	0.01075	0.004486		0.5912
	Exponential (Cao et al., 2004a)	0.0006811	0.9909	0.00398	0.0004202	0.9995	1.526

5.4.3 Effect of EHD Drying on Wheat Protein

Fourier transform infrared spectroscopy was used to study the effect of EHD drying of wheat on the wheat protein conformation. The rational for this study lies in the increasing cases of

gluten protein intolerances and allergies across the developed nations (Ortolani and Pastorello, 2006). Gluten protein allergy can be defined as an adverse response of the immune system of an individual in the form of IgE-mediated reactions to the protein, on the other hand intolerance can be defined as the non-immunological response towards gluten protein (Eigenmann, 2009). Gluten protein is a storage protein complex found in wheat and is an important component involved in determining the bread-formation and its quality. This protein regulates several physico-chemical properties of dough including its viscosity, cohesivity, water absorption and elasticity. The gluten protein can be divided into two major components, gliadin and glutenin (Singh et al., 2013a). Gliadin is the soluble fraction and governs the viscous flow behavior of the dough and glutenin is the insoluble fraction, which determines the elasticity of the dough. Both of these subunits of gluten protein not only define the physical properties of wheat-based products but also play an important role in the pathophysiology of an autoimmune disorder called *Coeliac* disease (Singh et al., 2013a). In this study, Amide I region of the wheat protein was studied as it is one of the most sensitive and most useful for elucidation of secondary structures of a protein (Kong and Yu, 2007). Figure 5.4 presents a typical FT-IR spectrum (4000 cm^{-1} - 500 cm^{-1}) of wheat flour. The Amide I band (1720 cm^{-1} - 1580 cm^{-1}) (Figure 5.4) is the sum of overlapping components bands. These component bands include α-helices, β-sheets, β-turns and randomly coiled conformations because they are mainly related to the C=O stretching vibrations coupled with the in-plane NH bending (Ahmed et al., 2007; Kong and Yu, 2007). The determination of secondary structures backbone conformation and hydrogen bonding patterns in this region depends on the nature of the hydrogen bond formed between C=O and NH moieties. In this study the Amide I band assignments were based on previous works by Georget and Belton, 2006; Goormaghtigh et al., 1994 and Kong and Yu, 2007 (Table 5.3).

Table 5.3: Amide I band frequencies and assignments to protein secondary structure in H_2O media (Adapted from(Georget and Belton, 2006a; Goormaghtigh et al., 1994; Kong and Yu, 2007).

Secondary structure	Frequencies (cm^{-1})	Average
α helix	1660-1648	1654
α helix turns	1630	1630
3_{10} Helix	1665-1663	1664
β sheets	1641-1612	1625
	1640-1626	1633
	1697-1670	1682
turns	1684-1662	1673
Random coils	1650-1640	1645

The analysis of the normalized spectra of dried wheat flour samples revealed that EHD drying led to changes in the secondary structures (Figures 5.5-5.6). In the Amide I region of the protein, distinct valleys were observed at 1682 - 1686 cm^{-1} (β-sheets), 1674 cm^{-1} (β-sheets), 1664 -1667 cm^{-1} (turns), 1654 - 1657 cm^{-1} (α-helices), 1651 cm^{-1} (α-helices), 1645 - 1647 cm^{-1} (Random coils) and 1633 - 1634 cm^{-1} (β-sheets). It is well known that full assignment of bands in the Amide I region is difficult because bands such as low-frequency bands can represent strongly hydrogen bonded peptide groups of β-sheets or intermolecular β-sheets or even extended structures (Georget and Belton, 2006a; Micard and Guilbert, 2000; Sourice et al., 2003). In this study we have ignored some of the bands such as 1610 cm^{-1}, 1669 cm^{-1}, and 1595 cm^{-1}, from our analysis because as stated by several researchers the band at 1669 cm^{-1} is assigned to β-turns which are involved in the formation of repetitive domains in the high molecular weight glutenins, but these are also found in gliadins (Mangavel et al., 2001; Popineau et al., 1994; Subirade et al., 1998; Van Velzen et al., 2003). The band at 1650 cm^{-1} is neglected since with random coils and α-helices and it is very difficult to differentiate which of the secondary structures are responsible for absorbance at this band. Glutamine has been shown to have two contributions one at 1658 cm^{-1} and the other at 1605 cm^{-1} but their absorbance band is typically at 1595 cm^{-1}, hence to improve the clarity of our study these bands were ignored from the analysis.

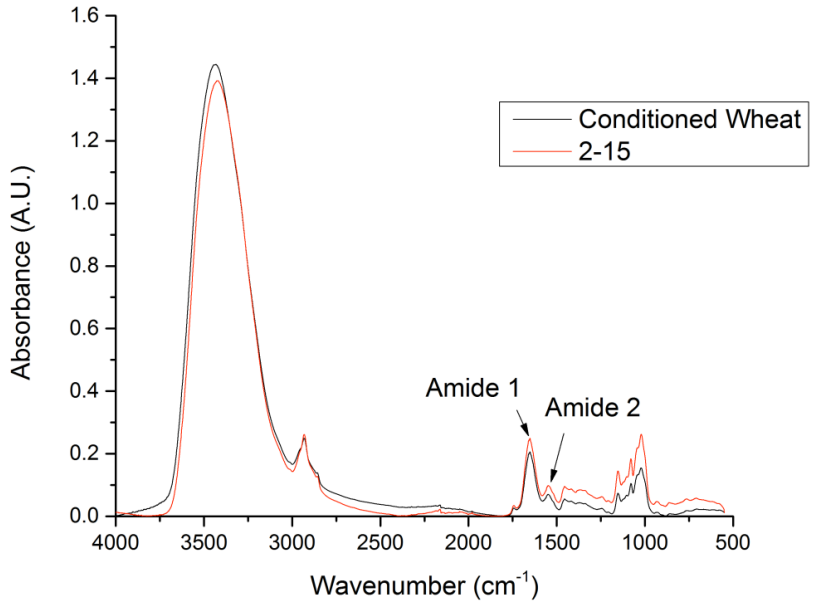

Figure 5.4: Typical FT-IR scan of conditioned wheat (20 % d.b.) and EHD dried wheat (air velocity 2m/s; applied voltage 15 kV).

Figures 5.6 and 5.7 show the normalized and second derivative spectra of EHD dried wheat samples. From the Figures (5.6-5.7) it was observed that maximum structural conversion and reorganization took place in wheat samples which were subjected to longer drying time as in the case of experimental conditions of air velocity 2 m/s and applied voltage of 12.5 kV and air velocity 1.5 m/s and applied voltage of 12.5 kV. Both of these aforementioned experimental conditions were affected by change in the relative humidity during the drying process and this led to longer drying time or electric field exposure time. No significant variations in the absorbance values were observed for experimental conditions of air velocity 1 m/s and 1.5 m/s with applied voltage of 10 kV and 15 kV. For samples dried under cross-flow alone, the absorbance values were similar to that obtained for conditioned wheat. From the analysis of the spectral patterns it was also concluded that as the electric field intensity increased variations in the secondary structure were observed. Major variations were observed for wheat samples dried under air velocity of 2 m/s and applied voltage of 12.5 kV, followed by applied voltage of 15 kV and 10 kV. We could attribute this variation to the loss of moisture during the drying process, which would lead to variations in the protein structural conformations and also to the influence of the electric field on the kinetics of folding and unfolding of the wheat protein.

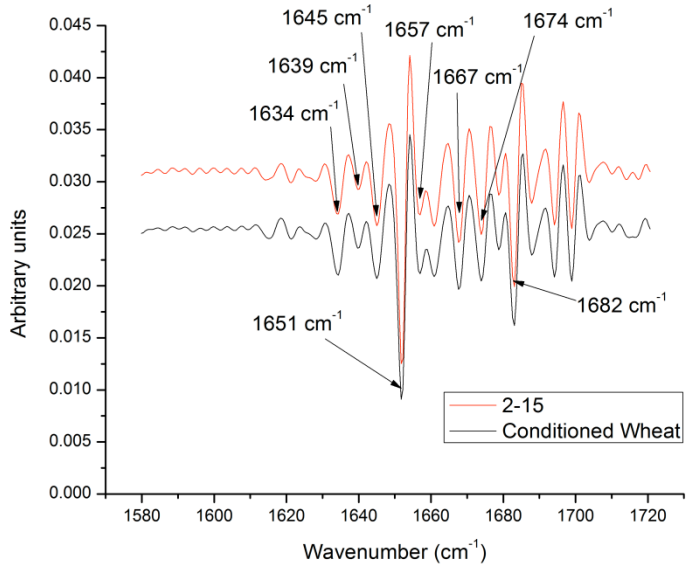

Figure 5.5: FT-IR second-derivative spectra for conditioned wheat (Control) and EHD dried wheat (air velocity 2 m/s; applied voltage 15 kV).

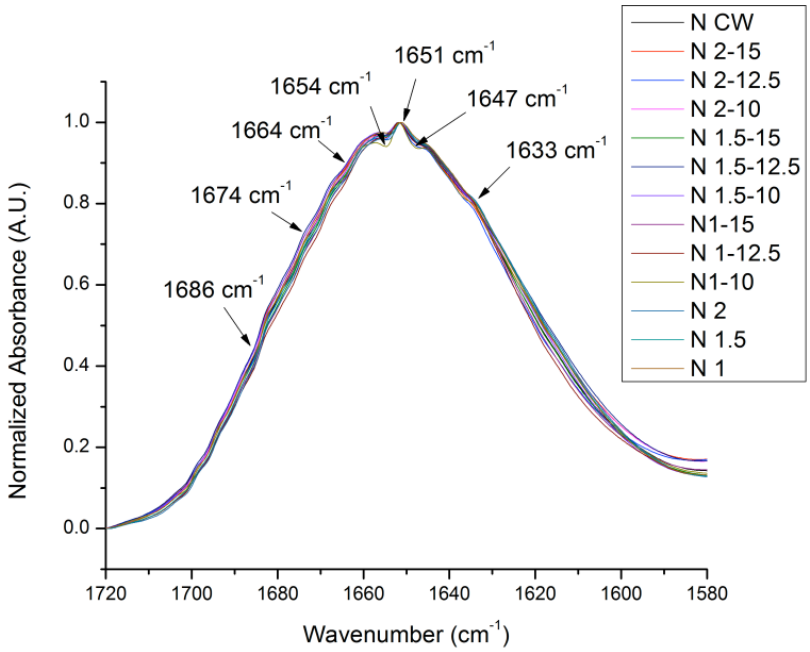

Figure 5.6: Normalized FT-IR spectra of the Amide I region of EHD dried wheat and control samples.

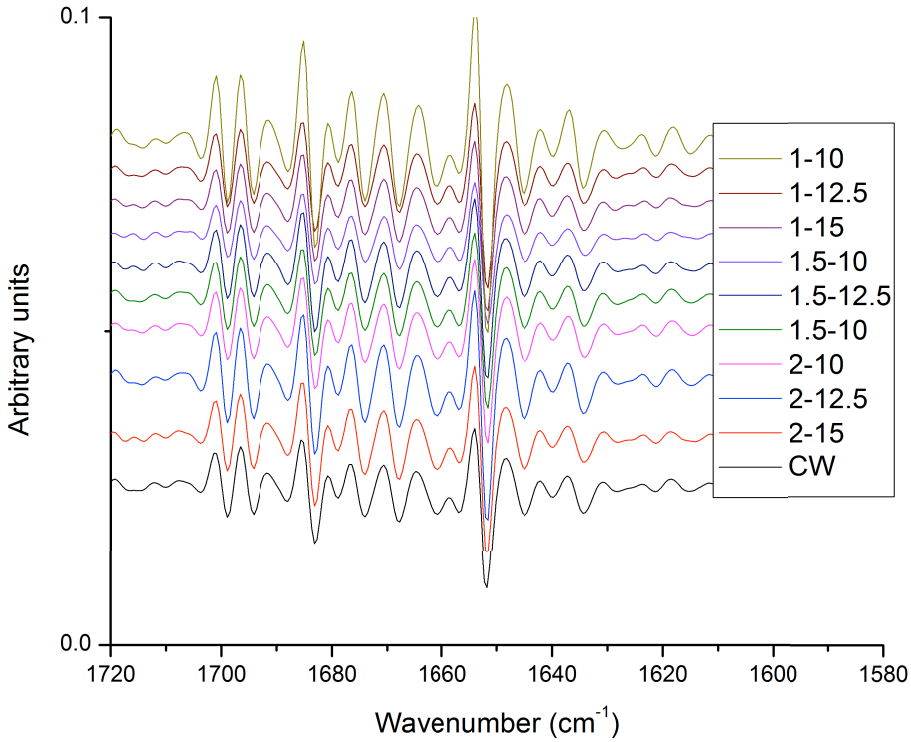

Figure 5.7: Second-derivative of normalized spectra showing the valleys and peaks for all EHD dried wheat samples and control (conditioned wheat). Note: Experimental conditions of air velocity 1-1.5-2 m/s; applied voltage 0 kV had similar second derivative as conditioned wheat (CW).

The bands at 1631 - 1634 cm^{-1}/1682 - 1656 cm^{-1} and 1654 - 1657 cm^{-1} are assigned to β-sheets and α-helices respectively. From Figure 5.7 we can observe shifts of intensity (increase in depth of valleys) between high frequency bands (1682 - 1656 cm^{-1}) and low frequency bands (1631 - 1634 cm^{-1}), which can be attributed to changes in the hydrogen bonding patterns due to application of an electric field and removal of moisture during EHD drying. Similar observations were made by Georget and Belton (Georget and Belton, 2006a) who evaluated the effect of temperature on hydrated gluten protein. They suggested that the shift towards low frequency from high frequency is due to weakening of hydrogen bond strength. In the present study the shift may also have been caused due to the influence of electric field, because in the molecular modeling study conducted by Singh et al. (Singh et al., 2013a) on the effect of a static external electric field on gliadin protein conformation, it was observed that the external electric field influenced the hydrogen bonding pattern of the gliadin protein. In order to quantify these shifts and understand the effect of EHD drying on wheat protein conformation, a curve fitting procedure was applied using Origin Pro (Version 9, OriginLab Corporation, Northampton, MA, USA). The multi-peak curve fitting is based on the least-squares minimization procedure, where the software attempts to minimize the sum of squares of the differences between the experimental spectra and the computed spectra, which is created by the summation of the component curves. The second-derivative spectra (Figures 5.5 and 5.7) were used to identify the component bands and the result was reported in terms of peak area and width (Table 5.4).

Table 5.4 shows the position, relative area and width of the bands fitted to the normalized FT-IR spectra of EHD treated wheat sample. From the Table 5.4 it can be observed that β-sheets and β-turns/turns were the major secondary structures representing approximately 30-37% and 35-40% of the total protein secondary structures respectively; α-helices represented 10-15 % and random coils represented the rest. As mentioned earlier the shift between the low frequency and high frequency bands were clearly visible in the data obtained from the Gaussian fitting. For the EHD control samples (air velocity 1-1.5-2 m/s; applied voltage 0 kV) it was observed that as the air velocity increased an increase was observed in the total area for the band at 1628 cm^{-1} representing β-sheets and an opposite phenomenon was observed for the band at 1634 cm^{-1}. As we follow the Table 5.4 for control samples from top to bottom with respect to increase in frequency, it was observed that there is an increase in the area for random coils (1644 cm^{-1}) from 11.34 % for drying under air

velocity of 1m/s to 18% at 2 m/s. A reduction in the total area of β-turns/turns was also observed. These shifts can be attributed to the variability in the moisture content of the sample dried under different air velocities. Removal of water will lead to change in the hydrogen-bonding pattern of the protein. As the electric field was introduced for enhancement of drying, shifts between high frequency band regions and low frequency band regions were more concentrated on increase and decrease in area (%) of turns and random coils. For the band area and width of the wheat samples dried under EHD conditions of air velocity 1m/s and applied voltage of 10-12.5-15 kV, it was observed that area (%) of β-sheets (1641 cm^{-1}) increased with increase in applied voltage and at the expense of random coils at 1645 cm^{-1}. A decrease in the band area of random coils also led to an increase in band area of 1651 cm^{-1} associated with α-helices. At an air velocity of 1.5 m/s an increase in applied voltage led to an increase in area of β-sheets at the expense of random structures and turns. For experiments conducted at air velocity of 2 m/s and with an increase in applied voltage it was observed that when the wheat samples were dried under applied voltage of 12.5 kV, the longer drying time caused by the humidity led to an increase in area of β-sheets at the expense of α-helices suggesting an effect of the electric field on the protein hydrogen bonding patterns. It is important to note here that the complexity of wheat protein makes it very difficult to decipher a clear-cut pattern in its behavior under external electric field or any form of external stresses. The structural riddle of wheat protein is yet to be solved and since gluten protein, which is the major wheat protein, responsible for the food intolerance and allergies of wheat based products, an intensive study to understand the structural changes in gluten protein under various external stresses including electrical and thermal becomes a necessity.

Table 5.4: Positions, width and areas of the bands fitted to the normalized FT-IR spectra of wheat protein (1720 cm^{-1} – 1580 cm^{-1}) subjected to different electric field intensities and treatment time.

Experimental conditions								
1-0			**1.5-0**			**2-0**		
Pos (cm^{-1})	**Area (%)**	**Width (cm^{-1})**	**Pos (cm^{-1})**	**Area (%)**	**Width (cm^{-1})**	**Pos (cm^{-1})**	**Area (%)**	**Width (cm^{-1})**
1619	17.36	31.85	1618	17.74	31.89	1617	16.70	31.22
1628	0.68	49.18	1628	5.60	18.19	1627	6.61	17.91
1634	12.08	19.44	1634	3.72	12.62	1634	3.95	11.80
1637	6.75	33.93	1639	9.42	28.84	1638	8.65	25.57
1644	11.34	14.45	1644	14.56	15.02	1646	18.08	15.54
1650	3.34	10.25	1651	1.38	8.25	1651	0.42	3.73
1656	11.89	13.91	1656	12.35	14.41	1657	11.73	12.38
1667	12.02	15.97	1667	10.95	16.72	1668	11.34	13.67
1674	10.50	18.76	1673	13.83	20.75	1674	12.35	17.60
1684	13.99	25.76	1685	10.99	24.45	1686	10.12	22.55
1-10			**1-12.5**			**1-15**		
Pos (cm^{-1})	**Area (%)**	**Width (cm^{-1})**	**Pos (cm^{-1})**	**Area (%)**	**Width (cm^{-1})**	**Pos (cm^{-1})**	**Area (%)**	**Width (cm^{-1})**
1618	17.42	32.02	1618	14.91	33.27	1618	14.65	32.11
1627	7.01	16.79	1628	7.93	19.18	1628	6.75	14.50
1634	5.40	11.82	1636	4.65	11.43	1635	3.57	11.14
1641	1.08	10.33	1638	9.12	25.12	1640	11.23	33.57
1645	21.88	15.01	1645	13.24	12.27	1645	10.83	14.79
1651	0.82	4.45	1651	2.02	6.67	1651	6.98	6.29
1656	9.65	10.73	1656	11.98	11.66	1656	9.54	11.46
1667	11.90	13.34	1668	12.62	14.48	1667	12.25	14.39
1674	12.09	18.15	1674	11.34	18.44	1674	12.36	18.67
1685	12.75	25.32	1685	12.13	24.65	1685	11.79	24.17
1.5-10			**1.5-12.5**			**1.5-15**		
Pos (cm^{-1})	**Area (%)**	**Width (cm^{-1})**	**Pos (cm^{-1})**	**Area (%)**	**Width (cm^{-1})**	**Pos (cm^{-1})**	**Area (%)**	**Width (cm^{-1})**
1619	17.10	31.81	1617	15.19	30.66	1618	15.11	33.43
1629	2.00	16.30	1628	5.99	17.90	1628	1.18	15.21
1634	10.85	21.64	1636	6.00	13.25	1634	10.65	19.43
1640	6.75	39.38	1640	11.35	32.64	1640	16.43	32.48
1645	11.65	16.51	1647	13.50	13.73	1645	7.17	12.65
1652	3.70	12.84	1651	0.36	3.79	1651	2.13	9.04
1657	11.98	15.95	1657	11.00	12.53	1657	12.77	15.91
1668	10.65	16.51	1668	10.75	14.52	1668	11.45	19.25
1674	12.49	19.98	1674	11.61	19.53	1674	12.15	21.41
1685	12.79	25.45	1684	14.21	27.34	1685	10.96	25.14

Table 5.4 Continued

2-10			2-12.5			2-15		
Pos (cm^{-1})	**Area (%)**	**Width (cm^{-1})**	**Pos (cm^{-1})**	**Area (%)**	**Width (cm^{-1})**	**Pos (cm^{-1})**	**Area (%)**	**Width (cm^{-1})**
1617	14.89	31.04	1618	13.45	30.67	1618	15.60	30.57
1628	6.18	18.41	1629	3.55	16.26	1628	6.97	18.52
1635	3.68	11.98	1634	1.62	9.63	1636	3.47	11.31
1639	11.71	28.27	1640	20.28	30.50	1638	9.73	20.82
1646	14.01	14.62	1646	13.42	15.57	1646	13.30	12.68
1651	0.29	3.44	1651	0.37	3.43	1651	1.36	5.95
1656	11.39	13.65	1656	8.81	13.05	1657	10.50	11.27
1667	12.57	16.16	1667	12.77	16.23	1667	12.23	14.58
1674	12.94	20.52	1674	12.43	20.59	1674	13.80	20.19
1685	12.28	25.73	1685	13.25	26.87	1685	13.04	26.47

Control		
Pos (cm^{-1})	**Area (%)**	**Width (cm^{-1})**
1618	16.16	32.30
1628	8.41	19.20
1634	1.81	10.02
1639	9.71	19.40
1645	11.37	13.09
1651	2.60	8.43
1656	11.94	12.84
1668	11.57	15.86
1674	14.70	22.58
1685	11.73	27.91

5.4.4 Thermal Properties of EHD dried Wheat

Wheat protein functionality is closely related to its structure, which in turn is influenced by processing conditions (Leon et al., 2003; Singh et al., 2013a). This study investigated the effect of EHD drying on the conformation of wheat proteins to verify its effect on the thermal properties of the wheat. Since temperature is one of the most important process parameter during bread making, it is important to see how a structural change in wheat protein conformation (minor or major) would affect its thermal properties. Figure 5.8 shows the DSC thermograms obtained for all experimental conditions except for samples dried under cross-flow alone as their thermograms were overlapping that of the conditioned wheat. According to the available literature very few studies have been reported on the thermal characteristics of wheat proteins (Eliasson and Hegg, 1980; Harwalkar and Ma, 1987; Leon et al., 2003). This is because the major wheat protein; gluten with its two subunits gliadin

and glutenin show little to no calorimetric response (Ma, 1990). Even in our study we didn't observe any exothermic peak for gluten denaturation. This lack of peak can be attributed to the cancellation of energy released during the breaking of the hydrogen bond of the protein by the energy gained from disruption of the hydrophobic interactions caused by removal of moisture (Arntfield and Murray, 1981). From Figure 5.8 the minimum heat flow was observed for the experimental condition of air velocity 2 m/s and applied voltage of 15 kV and rest of experimental conditions had mostly an overlapping thermogram. From these observation we conclude that the water content of the sample might have influenced the thermal behavior of the wheat protein and this observation can be supported by findings of several researchers (Leon et al., 2003; Micard and Guilbert, 2000), who have reported that if the water content is not the limiting factor, we will observe characteristic thermal properties of the wheat protein. Since the main objective of this study was to understand the effect of EHD drying on wheat protein conformation, removal of water by freeze drying or other methods to prepare a dry sample for DSC measurement might have further influenced the conformational changes in the wheat protein; and the study is not able to differentiate the effect of EHD on wheat protein conformation rather it represents a culmination of all effects including EHD, freeze drying or any other sample preparation step.

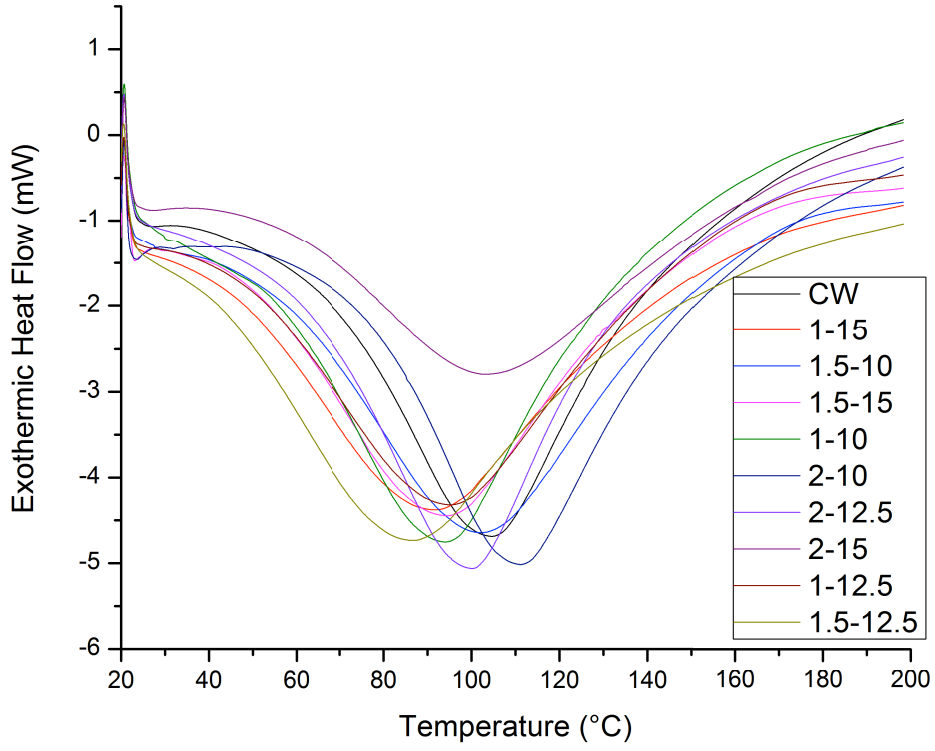

Figure 5.8: DSC thermograms for all experimental conditions and control.

5.5 Conclusion

This study presents the experimental results for electrohydrodynamic drying of wheat and its effect on the conformation of wheat protein. The wheat sample was dried using a single wire electrode system and it was observed that the drying rate of wheat sample was significantly affected by the applied voltage and air velocity. The drying rate increased with an increase in air velocity and applied voltage. The exponential equation showed good agreement with the EHD drying kinetics of wheat. This study also showed that wheat protein conformation was significantly affected by EHD drying. Analysis of Amide I region of wheat protein from the FT-IR spectra suggested that exposure to electric field influenced the hydrogen bonding pattern resulting in shifts between low and high frequency bands. Peak fitting using Gaussian band shapes further supported these results. Thermal analysis of EHD dried wheat sample didn’t provide any conclusive result for the effect of EHD on wheat protein conformation and its effect on thermal properties. However, it doesn't show differences in heat flow for change in voltage conditions.

Connecting Statement

The next part of the thesis deals with application of molecular dynamic (MD) simulation technique to study the effect of external electric field stress on the conformation and surface properties of proteins. Since protein's functional properties are dependent on its structure, the effect of an external electric field using MD on soybean hydrophobic protein and wheat gliadin protein could help understand the implications. The results obtained for MD simulation of wheat gliadin could help in validating the results of FT-IR study on the effect of electric field on wheat gluten.

PART II

Chapter 6

Theoretical Aspects of Molecular Dynamics (MD) including its application through simulation of Protein's structure under varying external stresses.

6.1 Abstract

This review presents an overview of the application of molecular dynamic simulation to study food proteins. Food proteins are a part of a multicomponent, non-ideal complex system. Processing of food using thermal, chemical, radiation, electromagnetic and mechanical techniques subject its macromolecular bio-components such as carbohydrates and proteins to extreme heat, ionic strength, pH and mechanical deformation. These processing factors affect protein's functional properties such as emulsification, dough formation, gelation, etc. which are associated with changes in their structure. It is difficult to study the structural changes of protein during processing using standard methods and hence in this chapter application of molecular dynamic, simulation to visualize and analyze the protein dynamics during processing has been evaluated. Effect of external stresses such as hydration, temperature and electric field, on protein structure have been analyzed and related mechanisms are explained. The response of food proteins to these stresses demonstrated that it is necessary to gain insight into protein dynamics to be able to develop novel and/or modify existing food processing techniques to improve the overall nutritional and organoleptic qualities of processed food products.

6.2 Introduction

Proteins are an essential component of diet. They play a central role in determining the overall nutritional and organoleptic quality of the food. In addition to their nutritional and sensorial role, proteins also impart the structural basis of various functional properties of foods. Their functional role in food is not contributed only by virtue of its physico-chemical properties; rather it is attributable trough it's complex interactions of several intrinsic and extrinsic properties. These properties of proteins are based on their structure (Singh et al., 2013c), which is classified as primary structure referring to the linear sequence of amino acid polypeptide chain; secondary, which are the highly regular local substructures such as α-helix, β-sheet conceived due to formation of hydrogen bonds between main-chain peptide groups; tertiary structure referring to the three-dimensional form of a single protein; and quaternary referring to the complex three-dimensional structure of multi-subunit protein (Figure 6.1).

(a)

(b)

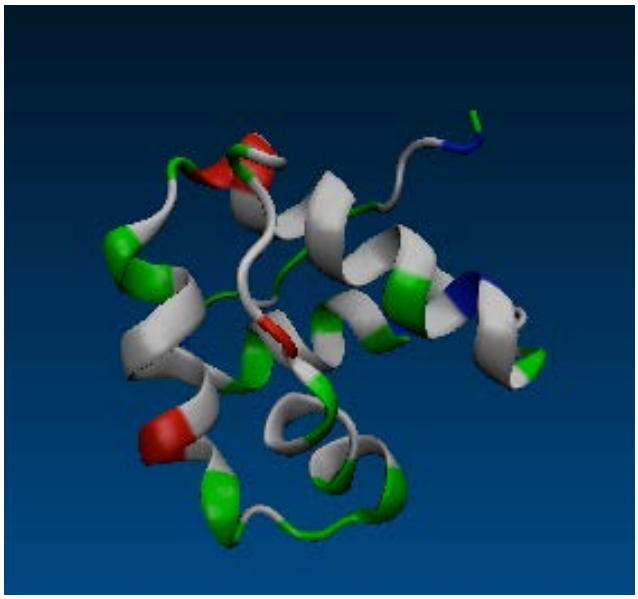

Figure 6.1: (a) FASTA sequence of soybean hydrophobic protein (SHP) (PDB Accession Code: 1HYP) (Primary structure) (b) Tertiary structure of soybean hydrophobic protein (SHP) representing 3 α-helical and a 3/10 helical substructures (Secondary structure) (Singh et al., 2013c).

The functional properties of proteins are related to their physicochemical and structural properties such as shape, size, amino acid sequence, hydrophobicity, hydrophilicity, charge and ability of the protein structure to change in a given environment (Table 6.1).

Table 6.1: Functional properties of food proteins (Adapted from (Damodaran, 1994))

Function	**Mechanism**	**Food system**	**Common protein source**
Solubility	Hydrophilicity	Beverages	Whey proteins
Viscosity	Hydrodynamic properties (molecular volume, size, axial ratio, shape)	Soups, salad dressing and desserts	Gelatin
Water binding	Hydrogen bonding, ionic hydration	Meat sausages, cakes, breads	Muscle and egg proteins
Gelation	Water entrapment and immobilization, network formation	Meats, gels, cakes, cheese	Muscle proteins, egg and milk proteins
Cohesion/Adhesion	Hydrophobic, ionic, hydrogen bonding	Meat, sausages, pasta, baked goods	Muscle, egg and whey protein
Elasticity	Hydrophobic bonding, disulfide cross-links	Meats, bakery	Muscle and cereal proteins
Emulsification	Adsorption and film formation at interfaces	Sausages, bologna, soup, cakes, dressing	Muscle, egg and milk proteins
Foaming	Interfacial adsorption and film formation	Whipped toppings, ice cream, cakes, desserts	Egg and milk proteins
Fat and flavor binding	Hydrophobic bonding, entrapment	Low-fat bakery products, doughnuts	Milk, egg and cereal proteins

The primary structure of the protein, i.e. the amino acid sequence governs the final three-dimensional structure of the protein, its thermodynamic stability and the distribution of hydrophilic and hydrophobic patches on the surface of the protein. The folding of the protein

is dictated by the need of reaching a thermodynamically stable state, in order to do so the hydrophobic groups are buried inside and the hydrophilic and charged residues are on the surface, but in several food proteins the presence of hydrophobic groups on the surface, due to structural constraints, influences the functional properties such as solubility of the protein. Many proteins such as casein and gelatin have high proline (amino acid) content, which results in the high flexibility of these proteins which exhibit important functional properties such as gelation, emulsification and foaming properties (Damodaran, 1994). Processing of foods and food products using conventional and novel techniques to improve their quality and shelf life, subjects' food proteins to varied physical and chemical environment and these bring changes in their functional properties. Physical treatments such as addition of heat or milling; chemical treatments such as addition of acids, alkalis, enzymes and fermentation can unfold or even break the polypeptide chain into smaller fragments impacting the protein's functional properties. Sometimes these changes are desirable, such as improvement in the digestibility of food proteins but in most cases they are negative and are undesirable.

Major protein modification during processing occurs due to proteolysis, protein crosslinking, reaction induced due to high temperature and pressure and protein interaction with polyphenols (Meade et al., 2005). Proteolysis is the process of breaking down polypeptide into smaller peptide fragments. It is achieved by adding specific enzymes during processing of the food. Proteolysis releases bioactive compounds and peptides, which may have beneficial nutritional effect or sometimes even detrimental, as in the case of the Maillard reaction, where a chemical reaction between amino acids and reducing sugars leads to the formation of bioactive, and carcinogenic compounds like acrylamide (Ames, 1998). Crosslinking of protein during processing under the influence of high temperature, extreme pH and presence of oxidizing agents results in reduction in their digestibility due to structural modifications and proteins cannot bind to the enzymes active site for hydrolysis. Crosslinking is important for some food products such as milk where it brings out the gelling of milk proteins (Singh, 1991). Oxidative reactions lead to modification of amino acids including methionine, cysteine, tryptophan and lysine resulting into crosslinking of proteins, affecting their functional properties. Application of heat and high pressure denatures the protein molecules improving their digestibility but also makes them susceptible to chemical reactions such as the Maillard reaction. Table 6.2 presents some of the impacts of processing on proteins.

Table 6.2: Effect of food processing techniques on amino acids and proteins (Adapted from (Damodaran and Paraf, 1997))

Processing conditions	Phenomenon	Nutritional effects
Heat treatment	Protein denaturation	Improvement in intrinsic digestibility
	Heat-sensitive amino acids	Different residues exposed
	Intramolecular reaction	Destruction
	Reaction with sugars	Crosslink formation
	Racemization	Maillard reaction
		Destruction of lysine
		Bioavailability
High pressure	Protein denaturation	Improvement in intrinsic digestibility
		Different residues exposed
	Solubilization	Improvement of solubility
pH change	Acid/alkaline hydrolysis	Unspecific peptide bond breakage
	pH-sensitive amino acids	Destruction
		Crosslink formation
		Racemization
Enzymatic reaction	Proteases	Oxidation of amino acids through lipid or polyphenol oxidation
	Oxygenases	
Modifications to improve food properties	Structural modifications	Reductive alkylation, acylation
	Enzymatic modifications	Proteolysis, cross-linkages, loss of amino acids, less allergenic, amino acid fortification
	Maillard reaction	
	Proteolytic enzymes	
	Covalent fixation of amino acids	

From a nutritional and clinical point of view, proteins are vital for human growth. They are considered as one of the building blocks of the body and act as a source of energy, producing 4 kcal/g just like carbohydrates and lipids. Table 6.3 presents some of the health-functional properties of proteins. The structure of the protein plays a pivotal role in defining their role in maintenance of human health. Proteins are also responsible for certain allergenic diseases. Most of the food allergens are proteins and some of the most commonly reported are related to peanuts, cow's milk, hen eggs, fish and wheat. Many of the known food allergens can be grouped into cupin and prolamin families, which are storage proteins in seeds and cereals. It is important to note that many factors play a role in determining whether a protein can trigger allergic reactions, some of these factors are primary, secondary and tertiary structure of proteins, food processing methods, their quantity in food and their ability to resist gastric digestion (Breiteneder and Radauer, 2004).

Table 6.3: Health-functional properties of proteins (Damodaran and Paraf, 1997)

Function	Mechanism
Antibiotic	Specialized protein with ability to attach to foreign particles such as bacteria. Their attachment depends on the surface topography of the protein. This is governed by the distribution of hydrophilic and hydrophobic residues on the surface of the protein.
Hormone	Small peptides, which regulate many biochemical functions within the body. Their ability to interact with other cellular components depending on their surficial properties.
Structural	Collagen, keratin, elastin are involved in formation of structures such as skin and exoskeleton. Ability to make networks helps in providing the structural stability
Energy storage	Egg ovalbumin, milk casein and almost all other protein can be easily digested and used as energy source.

It is therefore important for food engineers to understand how the proteins behave during processing and how their structural modification leads to changes in their functional properties. Techniques such as nuclear magnetic resonance (NMR) and X-ray diffraction have been widely used to understand protein structure and relation to its functionality. But in order to gain insight into the mechanism of the interactions between processing conditions and proteins, it is necessary to investigate and understand the influence at molecular or even atomistic level (Singh et al., 2013c).

The field of molecular dynamic (MD) modeling studies the atomic and molecular

interactions that take place within a physical system and how it governs its microscopic and macroscopic behavior (Singh et al., 2013c). The technique has been widely used to develop novel drug systems in the field of pharmaceutical sciences. However its application in food process engineering has been negligible (Singh et al., 2013c). Only a handful of articles in the literature are available on the application of MD modeling of food proteins. This review presents a concise but in-depth introduction to molecular dynamic modeling and how it can be applied to define the structural and functional dynamics of food proteins under thermal and electrical processing conditions.

6.3 Molecular Modeling of Proteins

For decades scientists have been interested in deciphering the connection between structure and function of proteins. In early 1951, Linus Pauling and Robert Corey proposed the two main structural features of the protein: α-helix and β-sheet, which now are known to be the building blocks for tens of thousands of proteins (Eisenberg, 2003); these structures were deduced from the structural data obtained from x-ray diffraction and Pauling's resonance theory of chemical bonding, which predicted the planar peptide groups. Later in 1953, Linus Pauling and Robert Corey introduced the scale models representing the molecules of amino acids and related compounds (Corey and Pauling, 1953), which was improved by Walter L. Koltun in 1965 and since then it has been widely used to study and make accurate structural measurements of proteins (Koltun, 1965). This traditional method provides only the ensemble-averaged information, i.e. it can only define the mean of a physical quantity as a function of the micro-state of a system. With the advent of supercomputer based simulation techniques, it has been possible to overcome the limitation of traditional method by visualizing the atomistic details of the system.

The computer simulation process can be organized into five broad categories including *Ab-initio,* which calculates properties of the system like proteins by numerically solving Schrödinger's equations. In this method the interaction between atoms is determined by their electronic configuration and position in the system. The second method is the *semi-empirical method,* which simplifies the calculations of the *ab-initio* method and can be used to study large systems. The *Molecular mechanics* method is widely used to study larger systems using *Born-Oppenheimer approximation* in which the state of the system can be determined using the positions and velocities of the atoms. *Molecular mechanics* method is typically used to

study systems with thousands of molecules like proteins and carbohydrates and is widely used to study the thermodynamic and interaction of molecules. In this method the interactions between each atom are estimated using interatomic potentials derived from the *ab-initio* method and the two methods implemented in these systems are Monte-Carlo and molecular dynamics (Rohs et al., 1999).

6.3.1 Molecular Dynamics

The basis of molecular dynamics lies in the heart of the molecular mechanics method, which uses *Born-Oppenheimer approximation*. By virtue of the approximation theory, only the positions and velocities of the atoms are required to describe the microscopic state of the system, in our case a protein. Equation 6.1 is used to express the Hamiltonian of the system as a function of nuclear variables (Leimkuhler, 1994).

$$H(q,p) = K(p) + V(q) \tag{6.1}$$

Where, H is the Hamiltonian, $K(p)$ is the kinetic energy as a function of momenta i.e. it contains the momenta of each atom, and $V(q)$ is the potential energy as the function of generalized coordinates i.e. it contains the details of the interatomic interactions. For better understanding, it helps in understanding what exactly molecular mechanics does. Molecular mechanics considers the atomic composition of a molecule such as a protein to be a collection of masses that are interacting with each other though harmonic forces. Further simplification suggests that in molecular mechanics the atoms are considered as balls and the bonds between them are considered as springs. Now to visualize and study the dynamics of this system we need to apply a force. It is possible to generate an equation of motion in Newtonian form using the Hamiltonian (Equation 6.2) (Leimkuhler, 1994).

$$\frac{d^2 r_i}{dt^2} = \frac{F_i}{m_i} \tag{6.2}$$

Where, F_i is defined as the total force experienced by an atom i in the direction r, m_i is the mass of the atom and r_i is the position of the atom i. So if we consider that we have the position and velocity of the atom i at a given time t, then the position and velocity at time $t + \delta t$, where δt is the time interval between two simulation snapshots, can be estimated by solving Equation 6.2 using an integration scheme. The most commonly used scheme is the Verlet algorithm (Adcock and McCammon, 2006; Alder and Wainwright, 1959b; Van Der Spoel et al., 2005b). For the Verlet algorithm we require the values for the current position,

r(t); acceleration, *a(t)*; and position of the atom from previous step, *r(t - δt)*. The position and velocities of the atom *i* for the next step can then be found using equations 6.3 and 6.4 respectively (Grubmüller et al., 1991; van der Spoel et al., 2008).

$$r(t+\delta t) = 2r(t) - r(t-\delta t) + \delta t^2 a(t) \tag{6.3}$$

$$v(t) = \frac{r(t+\delta t) - r(t-\delta t)}{2\delta t} \tag{6.4}$$

The equations 6.3 and 6.4 are the basic form of Verlet algorithm and are prone to truncation error of the order of δt^4 for position and δt^2 for the velocities. Estimation of velocities is important as it is used to compute the kinetic energy; computation of kinetic energy is required to test the conservation of total energy. This test is one of the most important step during MD simulation as it verifies the stability and correctness of the MD simulation. To combat the problem of truncation errors that are associated with the basic form of the Verlet algorithm, several variants of the Verlet algorithm have been developed. One of the most notable and commonly used variant is the Velocity Verlet algorithm. In this the position and velocities of the atom are estimated using a modified form of the Verlet algorithm (Equations 6.5-6.6) (Grubmüller et al., 1991).

$$r(t+\delta t) = r(t) + v(t)\delta t + \frac{1}{2}\delta t^2 a(t) \tag{6.5}$$

$$v(t+\delta t) = v(t+\frac{\delta t}{2}) + \frac{1}{2}a(t+\delta t)\delta t \tag{6.6}$$

In molecular mechanics the forces acting on the atom *i* can arise from both internal and external sources. The internal sources are basically the interaction forces acting between bonded and non-bonded atoms. The external sources can be environmental stresses including electric field, heat and pressure, which are imposed on the system externally. To determine the forces, it is important to obtain the potential energy of the system that can be expressed as a sum of bonded, non-bonded and cross-term interactions. The derivatives of the potential energy function are known as forcefields (Equation 6.7) (van der Spoel et al., 2008).

$$E_{total} = E_{bonded} + E_{non\text{-}bonded} + E_{cross\text{-}term} \tag{6.7}$$

Bonded interaction are also termed as valence interactions and incorporate diagonal terms such as bond-stretching, angle-bending, dihedral-angle torsion, inversion or out of plane interactions. Since in molecular mechanics it is assumed that the interactions are through harmonic forces, the potential energy associated with bond-stretching can be represented as:

$$E_{stretching} = \frac{1}{2} k_b (b - b_0)^2 \tag{6.8}$$

Where, k_b is force constant for the bond length, b_0 is the equilibrium bond length and b is the actual bond length. Similarly for angle bending, the simple harmonic expression would be:

$$E_{angle-bending} = \frac{1}{2} k_\theta (\theta - \theta_0)^2 \tag{6.9}$$

Where, k_θ is the force constant for bond angles, θ_0 is the equilibrium bond angle and θ is the actual bond angle. The dihedral-angle torsion potential energy is represented as a cosine expression (Equation 6.10).

$$E_{torsion} = \frac{1}{2} k_\phi (1 + \cos(n\phi - \phi_0)) \tag{6.10}$$

Where, k_ϕ is the force constant for the dihedral angle, ϕ_0 is the reference torsion angle and ϕ is the actual torsion angle. All the aforementioned potential energy functions belong to *Class I* force-fields, which only incorporate diagonal terms and non-bonded interactions (Karplus and McCammon, 2002). This class of force-field is widely used to simulate complicated systems such as proteins, as one has to consider different degree of freedoms associated with it. Some of the widely used force-fields of *Class I* are CHARMM, AMBER and GROMOS (Brooks et al., 1983; Case et al., 2005; Christen et al., 2005). The non-bonded interactions defined in this class of force-fields include electrostatic and van der Waals interactions. The electrostatic interactions can be described as an interaction between two charged particles and is expressed with a Coulombic potential function (Equation 6.11).

$$E_{electrostatic} = \sum_{ij} \frac{q_i q_j}{4\pi D r_{ij}} \tag{6.11}$$

Where, q is the charge of the particle, D is the dielectric constant of the material, r_{ij} is the distance between the centers of the particles i and j.

The van der Waals interaction between non-bonded atoms can be accounted for using the Lennard-Jones potential (Karplus and McCammon, 2002). In molecular mechanics the simplest potential energy function is the hard sphere potential. This assumes that the particles would travel in a straight line until hitting another particle, which will lead to elastic scattering. This potential doesn't include the attractive and repulsive component, which make it inappropriate for the study of huge systems such as proteins. The Lennard-Jones potential included both attractive and repulsive components and can be expressed using Equation 6.12.

$$E = 4\varepsilon\left[\left(\frac{\sigma}{r}\right)^{12} - \left(\frac{\sigma}{r}\right)^{6}\right] \tag{6.12}$$

Where, ε is the depth of the potential well, r is the distance between the particles and σ is the distance at which the inter-particle potential is zero. This potential function is also called as 12-6 potential, which represents the exponent terms for repulsive and attractive components respectively (Sagui and Darden, 1999). Using Equation 6.12, the van der Waals interaction between non-bonded particles can be presented as:

$$E_{vdw} = \sum_{ij} \varepsilon_{ij}\left[\left(\frac{R_{\min,ij}}{r_{ij}}\right)^{12} - 2\left(\frac{R_{\min,ij}}{r_{ij}}\right)^{6}\right] \tag{6.13}$$

Where, r_{ij} is the distance between the particles, ε_{ij} is the minimum value for van der Waals term and R_{min} is the radius where the van der Waals term is minimum (Sagui and Darden, 1999).

Some modern force-fields including CFF, MM3 and MMFF94 also include another class of force-fields, *Class II*, which incorporates the cross-term interaction between the particles. These cross-terms are required to reproduce the experimental vibrational frequencies of molecules and include the bond-bond, angle-angle, bond-angle, bond-dihedrals, angles-angles-dihedrals and bond-bond-dihedrals (van der Spoel et al., 2008). All these terms account for effects such as distortion of bond angles due to stretching of the bonds or changes in bond length due to changes in the other in an opposite direction. The purpose of these force-fields is to describe the complete potential energy surface of the molecule as accurately as possible. If we want to study the effect of external stresses on a molecule, we can look at the changes in the potential energy functions and determine how they are affected by stress (Alder and Wainwright, 1959a).

All of the aforementioned force-fields are used in molecular modeling of proteins to provide the parameters of mathematical functions used to describe the potential energy of all the atoms of the protein system (Karplus and McCammon, 2002). In molecular dynamics, proteins are studied in an aqueous environment and to simulate these systems it is necessary to understand the interaction between the particles at the surface and the particles within. Figure 6.2 presents a protein in an aqueous environment system (Bekker et al., 1995). The forces experienced by the particles on the surface are transcended across the system and this influences the forces experienced by the particles within the system. If we consider a system,

which has small number of water molecules surrounding the protein, the surface to volume ratio of this system will be large and so will be the surface effect (Bekker et al., 1995). The surface effect, include the imbalance of forces between the solvent and the vacuum surrounding the solution droplet. Water molecules in a simulation system behave just like a real solution and would try to escape into the surrounding vacuum i.e. evaporate and this will change the dynamics of the system and make it difficult to accurately study the system. Hence, when simulating a bulk system like protein in an aqueous environment it is important to minimize or completely eliminate the surface effect. Application of periodic boundary conditions (PBC) helps in completely eliminating the surface effect (Karplus and McCammon, 2002). In PBC, the simulation box, i.e protein with the water molecules surrounding it (Figure 6.2) is replicated in three dimensions to form an infinite lattice, i.e. exact images of the box (system = protein + water molecules) are stacked over each other in all directions, such that there are no surface to the solution. This helps in eliminating any surface tension effect and if a water molecule leaves the simulation box the net effect is such that a copy of the same molecule enters the box, this way the water molecules never escape (van der Spoel et al., 2008). Figure 6.3 presents a three dimensional PBC.

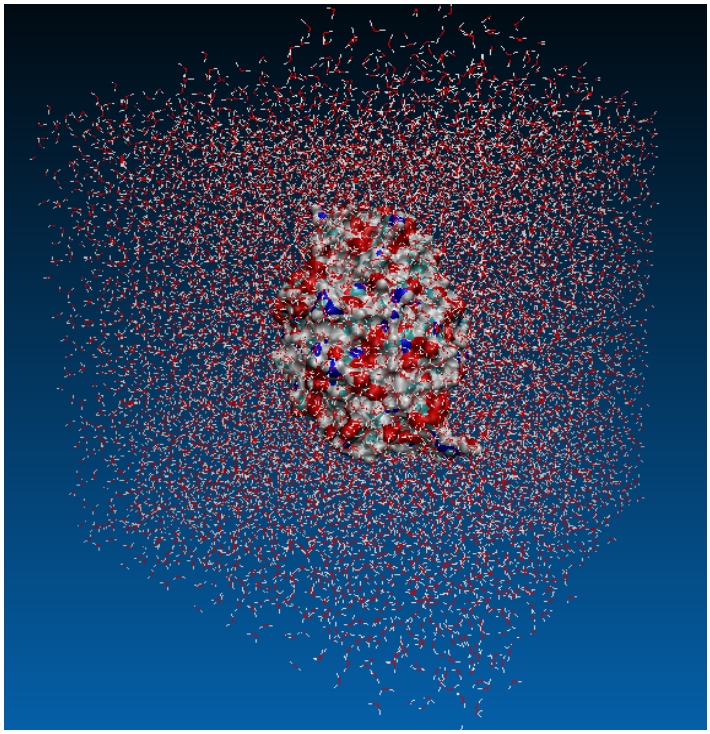

Figure 6.2: A typical cubic simulation box with protein in the center, surrounded by explicit solvent atoms (water).

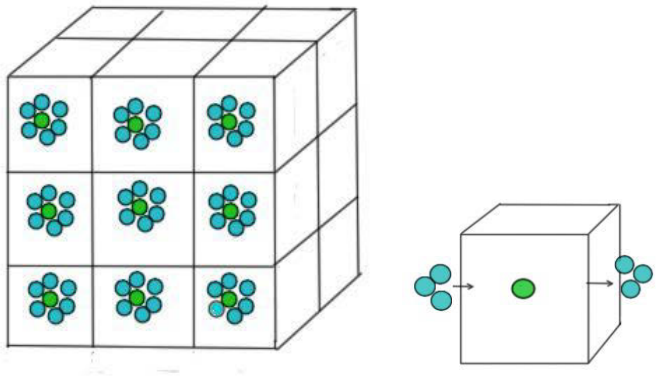

Figure 6.3: Three-dimensional illustration of periodic boundary conditions. The protein is represented in green in the center. The box in the center is the main simulation box.

6.3.2 Simulation Methodologies and Stages

Molecular dynamics (MD) is routinely applied for the investigation of dynamic properties and processes in the field of structural biochemistry, molecular biology, pharmaceutical science and biotechnology. This tool helps researchers to generate a trajectory of macromolecules such as protein, i.e. it generates a progress of simulated structure with respect to time. The most common methodologies incorporated in the study of food proteins include classical molecular dynamics, which is implemented into various software packages such as Groningen Machine for Chemical Simulations (GROMACS) (Van Der Spoel et al., 2005a), Not just Another Molecular Dynamics program (NAMD)(Kalé et al., 1999), Assisted Model Building with Energy Refinement (AMBER)(Case et al., 2005) and Chemistry at Harvard Macromolecular Mechanics (CHARMM)(Brooks et al., 1983). Various experimental conditions can be simulated using MD. In earlier protein studies conducted using MD, it was common to consider the protein molecule as isolated entities present in a vacuum. Slowly, with advancement in MD techniques simulations, it included explicit water and neighboring protein molecules as in a crystal environment (Karplus and McCammon, 2002). This is why we use the periodic boundary conditions as discussed in the previous section. Typically, a periodic boundary condition is implemented on a cubic system; however it is not necessary and several other geometries including rhombic, dodecahedron and truncated octahedron can be used (Bekker et al., 1995). These geometries significantly reduce the number of solvent atoms required in the system, which in turn reduces the computational time.

The length of the simulation is determined by various factors, including the number of interactions that needs to be evaluated at each time step and number of time steps and degrees of freedom that need to be produced. Hence to improve the simulation and computational efficiency, several algorithms are used including the Verlet integration algorithms discussed in the previous section. Other algorithms such as SHAKE, RATTLE and LINCS are commonly implemented to improve the MD efficiency by increasing the time-step without compromising the accuracy of the simulation (Budi et al., 2004).

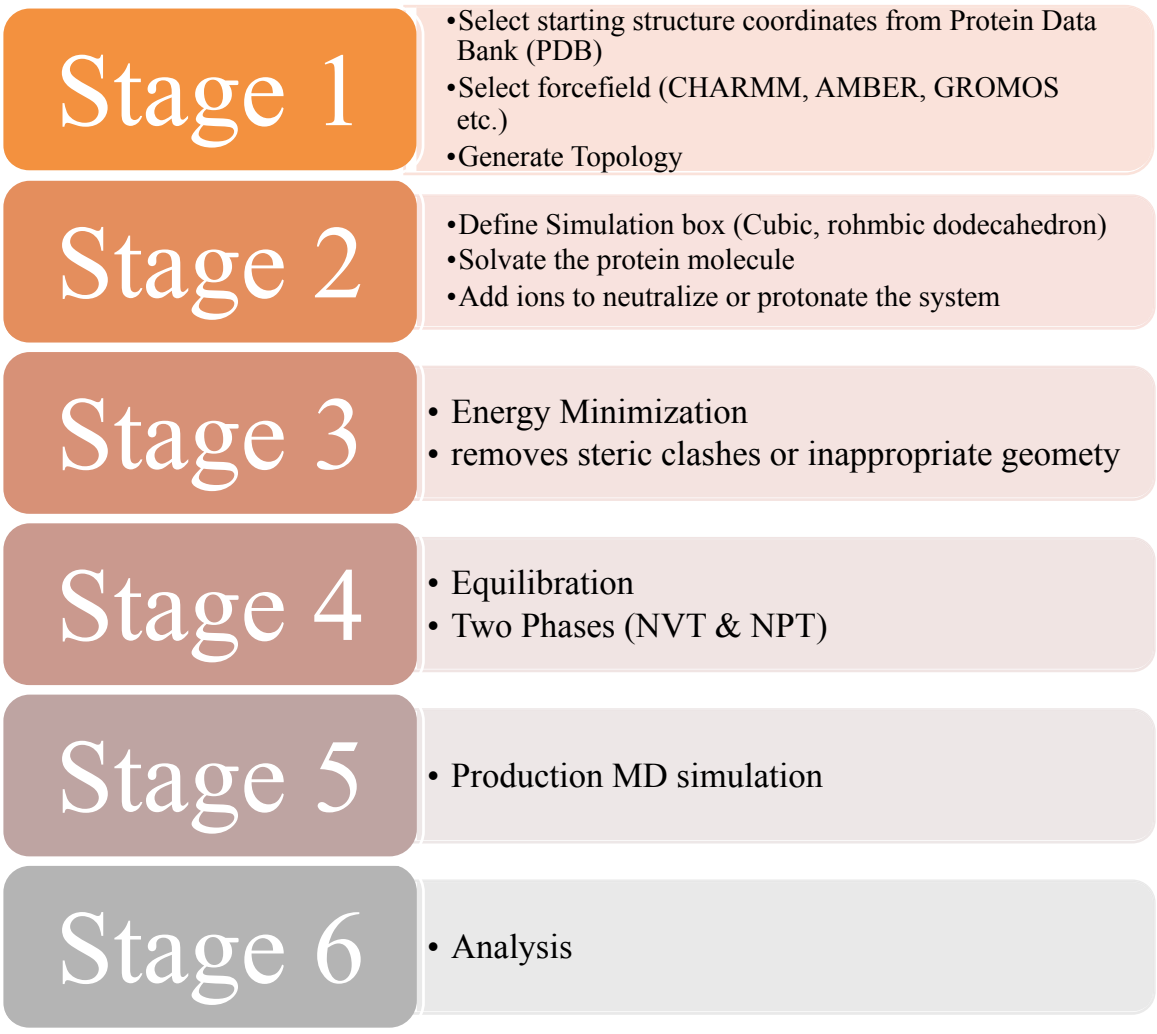

Figure 6.4: Outline of the simulation stages commonly followed while using GROMACS MD simulation package.

Typically in a MD simulation, it is important to accurately replicate the experimental conditions. To obtain the starting structure coordinates of the protein of interest, researchers search the Protein Data Bank (PDB) (Astrakas et al., 2011b). The structures available in the

PDB were obtained by using x-ray diffraction and nuclear magnetic resonance techniques. In GROMACS (Figure 6.4) it is necessary to generate a topology file, which contains all the information including bonded and non-bonded parameters required to define the molecule within the simulation (van der Spoel et al., 2008). Once the required force-fields are selected, the protein structure is put into a simulation box and immersed in water. It is important to note that in nature most proteins are at least partially within an aqueous environment, hence it is justifiable to immerse a protein structure into water containing an ion or without. Ions are added to the system (protein + water) to neutralize or protonate the system. Solvent effects on the simulation results are important as they contribute to specific interactions necessary to mediate protein structure or function. Some of the explicit water models commonly used in the simulation of food proteins are TIP3P, TIP4P, TIP5P, SPC and SPC/E (Lindahl et al., 2001). For the simulation, the parameters of the water models are so adjusted that they reproduce the enthalpy of vaporization and density of water during the simulation. The dipole moment of the aforementioned water models is about 2.8 D instead of 1.85, which is the experimental gas–phase value (van der Spoel et al., 2008). One of the demerits of these models is with respect to the temperature dependence of density of water; except for TIP5P none of the models define this dependence accurately. Once the system has been neutralized, the solvated electro-neutral system is relaxed to ensure that it has no steric clashes or inappropriate geometry. After minimization, the system undergoes NVT (fixed number of atoms, N, fixed volume, V, and fixed temperature, T) and NPT (fixed number of atoms, N, fixed pressure, P, and fixed temperature, T) equilibration. At this point the system is called as an ensemble, which is defined as a collection of all possible systems that have varied microscopic state, but have a single thermodynamic state. Physical experiments are mostly carried out at constant temperature and pressure or constant temperature and volume, hence it is desirable to conduct simulation at the two aforementioned states. These states are also called as canonical ensemble (NVT) and isobaric-isothermal ensemble (NPT). Once the system has been equilibrated, MD simulations are carried out with or without the presence of an external stress (van der Spoel et al., 2008).

6.4 Application of MD in Studying Food Proteins

As mentioned earlier the forces involved in the stability of the protein structure are quite complex and can be grouped into two categories: (a) intramolecular interactions involving

forces intrinsic to the protein molecule (steric strains and van der Waals interaction), and (b) the intramolecular interactions involving the surrounding environment including the solvent and other food components (hydrogen bonds, electrostatic interactions, hydrophobic interactions and disulfide bonds) (Dunker et al., 2002). All the aforementioned intramolecular interactions and intermolecular interactions can be studied using molecular dynamics. In food, which is a complex blend of major and minor components, the native structure of the protein is the net result of the various attractive and repulsive forces emanating from the inter- and intramolecular interactions. Changes in the environment such as pH, surrounding solvent ionic strength, solvent composition, temperature and so forth can alter proteins (Meade et al., 2005). When the protein surrounding is changed, the protein undergoes a conformational adaptability stage, where it acquires a molecular conformation that doesn't alter its molecular architecture, but when external stresses such as thermal, chemical and electrical are involved in changing the surrounding major changes in the secondary, tertiary and quaternary structures takes place without cleavage of any backbone peptide bonds, this is termed as denaturation (Meade et al., 2005). Physical agents such as temperature induce denaturation of food proteins to varying degrees during processing. The mechanism involved is destabilization of hydrogen bonds and electrostatic interactions, which are exothermic in nature. Increase in temperature stabilizes the endothermic processes including hydrophobic interactions. The amino acid composition of protein also influences its thermal stability. The presence of hydrophobic amino acid residues greatly increases proteins thermal stability, and it is mainly due to the formation of salt bridges and hydrogen bonds between non-polar residues buried deep inside the protein structure (Ma, 1990). Hydration simply classified as presence of water greatly facilitates protein denaturation. Dry protein powders are extremely stable to thermal denaturation and as the water content increases thermal stability decreases. This is because in a dry state proteins have static state and as the water content increases the hydration and penetration of water into surface cavities of proteins; hence their backbone mobility and flexibility increases and when this structure is subjected to high temperature, it ends up in a denaturation state (Halle, 2004). Other external stress which too can affect protein structural stability includes hydrostatic pressure, presence of chemical agents that alter the pH of the surrounding solvent, presence of detergents and chaotropic salts (Balasubramaniam and Farkas, 2008). For this review we will evaluate the applicability of MD studies in understanding the dynamics of food protein hydration and the effect of thermal

and electrical stresses.

6.4.1 Hydration of Proteins

Several rheological and textural properties of food depend on the interaction of the food macromolecules and water. Functional properties such as swelling, solubility, viscosity, gelation, emulsification etc. depend on the modification of physico-chemical properties of food proteins caused by water-protein and protein-protein interactions. For several food products such as bread and other bakery products, balance between these interactions is key for their acceptability by consumers. The water binding capacity, commonly known as the hydration capacity of protein, depends largely on its amino acid composition (Rupley and Careri, 1991). When a protein molecule is hydrated, the primary interaction is between the water and the surface of the protein. Since proteins are a defined three dimensional arrangement of several secondary structures, the interactions with water or any other solvent is based on the surface property of that particular secondary structure of the protein, which is facing the water or other solvent molecules (Halle, 2004).

In general, water plays a pivotal role in maintaining the surface properties of the protein due to the availability of hydrophobic and hydrophilic binding sites (Levy and Onuchic, 2004). As mentioned earlier the amount of hydration over the surface of the protein is an important factor in stabilizing the protein and also any variation in the amount of hydration can lead to change in the functional properties of the protein (Ansari et al., 1992; Fenimore et al., 2002; Levy and Onuchic, 2004). Several researchers have studied experimentally the effect of hydration on the structure of the protein and in turn the changes in its biological functions (Colombo et al., 1992; Rupley and Careri, 1991).

In a study on soy protein, Were *et al*. (Were et al., 1997) evaluated various modification treatments and found out that the alkali treatment increases the hydration capacity of the protein by 20 times. They proposed that this rise in hydration capacity of the protein molecule is due to changes in its quaternary structure. If, we applied MD simulation for this study we would be able to visualize the conformational changes in real time and also obtain an insight into the dynamics involved. Apart from acting as a visual aid molecular dynamic simulation can also provide statistical information's such as hydration energy, efficiency and even the involved kinetics. For example, in 2009 Mobley et al. (Mobley et al., 2009) conducted a MD study to estimate the hydration free energy of 504 organic compounds

in explicit TIP3P water. They reported a very good correlation between their simulated data and experimental data. We can employ a similar method to study the hydration energies of food proteins where the hydration energy can be defined as the quantification of the effect of hydration on solvent free energies and the protein – water inter molecular interactions evaluated using both the attractive forces and the repulsive forces (Karino and Matubayasi, 2011; Roy and Bagchi, 2012).

Another probable application of hydration studies using MD modeling technique is for estimation of efficiency of various solvent extraction techniques. It is well known that the solvent extraction efficiency depends largely on the interaction between the desired compound and the solvent in question; and if the desired compound is a protein it would be wise to understand the relation between a chosen solvent and the protein molecule before using the solvent for extraction. Hence, understanding the dynamics of a protein's interaction with various solvents can provide beneficial information and hints on the efficiency of an extraction process. For example, Micaelo and Sores (Micaêlo and Soares, 2007) performed an MD simulation study on the hydration mechanism of the enzyme serine protease cutinase in non-aqueous media. In their study, they differentiated the solvents into three different classes: polar organic solvents (Hexane, diisopropyl ether and 3-pentanone), non-polar organic solvents (Ethanol and Acetonitrile) and water. They evaluated the dynamics and structure of the enzyme used in the simulation at different hydration levels and concluded that the water stripping capacity of a solvent is directly dependent on the nature of the solvent and that the protein undergoes structural modifications due to variations in its hydration capacities and inter molecular interaction between solvent molecules and protein side chains. Hence, an understanding of protein interaction with water or any given solvent at molecular level can help the researchers at least predict the behavior of the process flow including efficiency of extraction or how protein will behave structurally or functionally.

6.4.2 Thermal Treatment of Protein

Several food processing techniques such as pasteurization, sterilization, boiling etc. require subjecting protein to thermal stresses. Thermal stress is associated with an increase heat or thermal energy, which forces proteins to adopt conformational phases or stages that are irreversible. Changes in conformation of protein affect their functional properties; this phenomenon makes an interesting subject of investigation at both macro and molecular level.

At the macro level, when a protein is subjected to an increase in temperature beyond a threshold value represented as the transition temperature, it undergoes a transition from its native state to its denaturation state. The primary mechanism involved in this is the effect of temperature on the noncovalent interactions i.e. an increase in hydrophobic interactions and destabilization of hydrogen bonding and electrostatic interactions are observed. The net stability of a protein at a given temperature is defined as the total sum of all of these interactions. But not all proteins are affected at high temperature, some food proteins such as lysozyme, denature at cold temperature and its stability increases with an increase in temperature. Hence, a question arises on how does lysozyme protein behave under the influence of thermal stress? This is an important question because in today's era, the commercially sold eggs are normally treated to high temperature to extend their shelf-life by disinfecting any surface pathogens present on the egg shell (Froning and Producers, 2002). Various methods of thermal treatment of eggs require exposing the egg to a certain temperature for a predetermined period of time to destroy the pathogens over the shell. But, due to the exposure to high temperatures, and other forms of stress, there can be changes that take place to the various properties of the egg that are later consumed (Denmat et al., 1999; Min et al., 2005). Furthermore, the pasteurization might also involve exposing eggs to various electromagnetic radiations including microwave (Dev et al., 2008b) and radio waves (Ball Jr et al., 1997). Also, apart from pasteurization, eggs are processed in various ways, which can all affect the functional properties of the egg; all of these changes can be attributed to the structural change in the egg proteins.

Several researchers have made an effort in studying the effect of temperature on the structural and functional properties of the egg protein. For example, Gilquin *et al*. (Gilquin et al., 2000) conducted an MD simulation study on the role the inter-domain interactions in the secondary structure play in the unfolding path followed by the hen egg lysozyme at 300K. They conducted the simulations for 1.2 ns and used PEDC (Path Exploration with Distance Constraints) to find out the least energy structures as a function of the RMSD in the simulation. They concluded that the results obtained from the simulations were completely in accordance with experimental results obtained from fluorescence spectroscopy. They stated that the loss of stability was caused by changes in the hydrophobicity of the protein core due to conformational changes of the protein structure.

In another work Mark and Van Gunsteren (Mark and Van Gunsteren, 1992) studied the

thermal denaturation of the hen egg lysozyme in water under wide range of temperatures using the MD simulation technique. They analyzed the unfolding (conformational change) of the hen egg lysozyme as a function of the radius of gyration, RMSD and hydrogen bonding pattern during the period of simulation. They came to similar conclusion as those of Gilquin *et al*. (Gilquin et al., 2000). Similarly as we can answer the effect of thermal stress on lysozyme protein, we may also be able to answer the same question on the dynamics of folding and unfolding of other food proteins using MD technique, but all within the limitations of MD.

6.4.3 Electrical Treatment of Protein

As mentioned before, traditional thermal processing methods can lead to deterioration of food components, such as proteins, starch and vitamins, resulting into possible changes in its nutritional and organoleptic properties. In recent years, several non-thermal processing methods such as pulsed electric field processing (PEF), high voltage processing (HVP), ultrasonication etc. have garnered huge attention by virtue of their advantages over conventional thermal processing methods. PEF has been widely investigated for its ability to kill microorganisms while maintaining the original nutritional and organoleptic properties. In PEF processing, application of high electric field pulses inactivates microorganisms and several enzymes responsible for deterioration of food, but its effect on the structural modification of proteins, enzyme and other food components has not been widely studied. For example Xiang et al. (2011) studied the effect of pulsed electric field on structural conformation of whey and soy protein isolates using fluorescence spectroscopy. They reported the structural modification as a function of changes in the surface hydrophobicity of the protein. For whey protein isolate, they stated that application of electric field intensities of 12, 16 and 20 kV/cm and number of pulses (10, 20 and 30) resulted in an increase in the intrinsic tryptophan fluorescence intensity indicating shift in the polarity of the tryptophan residues micro-environment from less polar to a more polar environment. Since the hydration and several functional properties of the protein depend on the surface properties of the protein which in turn are governed by their structural conformation, we can conclude that application of electric field will certainly have to have an effect on the structural conformation of the protein to bring about changes (folding or unfolding) in its micro-environment. Xiang et al. (2011) reported similar observations for soy protein isolate. Since these changes are intrinsic

and can be visualized, it is difficult to study these changes at a molecular level without using expensive experimental setups such as X-ray diffraction or NMR. It is here, where Molecular Dynamic Simulation can be used to evaluate the effect of external stresses such as static or oscillating electric field. Singh et al. (Singh et al., 2013c) studied the effect of static external electric field on the conformation of soybean hydrophobic protein. In their MD simulations study they subjected the soybean hydrophobic protein to three electric field intensities 0.002 V/nm, 0.004 V/nm and 3 V/nm. They observed that when nominal electric field intensities (0.002-0.004 V/nm) were applied no major effect on the structural and surficial properties of the protein was observed, but when the field strength was increased to 3 V/nm, which at present is practically impossible to obtain at an industrial scale, the protein underwent unfolding and significant changes in the surface properties were observed. Their study was one of the few, which actually targeted application of MD simulation for the study of food proteins. Singh *et al.* (Singh et al., 2013a) also studied the effect of an electric field on conformation of gliadin protein conformation, which is an important component of wheat gluten protein and they reported that application of an electric field actually varied the hydrogen-bonding pattern of the protein and that the intensity of the field plays an important role. Both of the studies conducted by Singh et al. (2013) suggest that the electric field has an influence on protein conformation and may impact its functional properties. Since application of MD simulation for study of food proteins is still in its novice state and prone to limitations such as the availability of defined crystalline structure of food proteins, which are big and hard to crystallize, but still it can be a beneficial tool to study the molecular configuration of food protein interactions with other food components and also how they actually contribute to the organoleptic and nutritional properties of a food.

6.5 Conclusion

This overview has presented the details about the effect of various food processing condition and their associated effects in protein structure and functional properties. The relation between structure-function of a protein was also elucidated and so was the molecular dynamic simulation methodology. The probable applications of MD simulation in studying food protein were also discussed.

Connecting Statement

The overview on molecular dynamic (MD) simulation provided an understanding of the methods used to estimate and study the dynamics of protein. Since the primary objective of the thesis was to develop and design an electrohydrodynamic system for drying of wheat and study its importance in understanding how electric field will interact with its constituents, especially proteins, two simulation studies using MD simulation technique on soybean protein isolate and gliadin protein were considered. Soybean protein was selected for the next study because in past several researchers have shown that the application of pulsed electric field affects the surface properties of the protein and hence by studying soybean protein under external electric field stress using MD technique leads to understanding of the behavior at the molecular level. GROMACS molecular modeling software was used for this study as it was freely available and necessary modification to the code to implement static electric field used in this chapter was achieved.

Chapter 7

Soybean Simulation:
Soybean Hydrophobic Protein Response to External Electric Field: A Molecular Modeling Approach

7.1 Abstract

The molecular dynamic (MD) modeling approach was applied to evaluate the effect of an external electric field on soybean hydrophobic protein and its surface properties. Nominal electric field strengths of 0.002 V/nm and 0.004 V/nm had no major effect on the structure and surface properties of the protein isolate but the higher electric field strength of 3 V/nm significantly affected the protein conformation and solvent accessible surface area. The response of protein isolate to various external field stresses demonstrated that it is necessary to gain insight into protein dynamics under electromagnetic fields in order to be able to better their utilization in food processing and other biological applications.

7.2 Introduction

Proteins play a fundamental role for humans and are an important constituent of foods. Processing methods and parameters have diverse effects on protein quality and quantity. Protein functions depend on its structure and any change due to the presence of external stresses such as heat, pH, chemicals and electromagnetic field, which can lead to its denaturation leading to nonfunctional characteristics. The effect of an electromagnetic field on protein conformation has been extensively studied (De Pomerai et al., 2003; Fernandez-Diaz et al., 2000; Laurence et al., 2000; Xiang et al., 2011), but it is challenging to quantify

the effect, as the alteration to conformation takes place in a very short time span (nanoscale) (Astrakas et al., 2011a). It is our understanding that in order to gain the insight into the mechanism of the interaction between electromagnetic fields and food constituents, it is necessary to understand the influence at the atomistic and molecular level.

A MD modeling approach to analyze the effect of a high electric field on the conformation of soybean hydrophobic protein (SHP), which is part of the soybean protein isolate has been used. Soybean protein (SP) is one of the most extensively studied food proteins. Protein isolates from soybean are prepared from defatted soybean flour using a water extraction process under mild alkaline conditions (Xiang et al., 2011). SP has excellent functional and nutritional properties (Puppo et al., 2004; Sorgentini et al., 1995), but conventional thermal treatment processes used in food industries have undesirable effects on their solubility and water absorption characteristics (Kinsella, 1979). Several novel processing techniques apply electromagnetic waves such as microwave and radio frequency or high electric field to achieve superior food quality (Singh et al., 2012). In 2011, Xiang et al. studied the structural modification induced by the application of PEF on soybean protein isolate. They reported that the application of an electric field intensity of 20–25 kV/cm and pulse number varying from 30–120 induced changes in the microenvironment of the soy protein's tryptophan residues from a less polar to a more polar environment. They indicated that these changes in the polarity were brought by partial denaturation of the protein under PEF treatment.

Hence in this study, emphasis has been put on quantification of conformational changes using root mean square deviation, radius of gyration and total dipole moment data and its effect on surface hydrophobicity and hydrophilicity of SHP.

7.3 Experimental Section

MD simulation on SHP was performed using a classical MD algorithm as implemented in Groningen machine for chemical simulations (GROMACS) software package, version 4.5.5 from the Stockholm Center for Biomembrane Research, Stockholm, Sweden (Van Der Spoel et al., 2005b). SHP consists of 75 amino acid residues, where more than 50% of the secondary structure consists mainly of helices (4 helices; 3 - α helix (Val25-Gly33, Asp37-Leu51 and Leu56-Ser66) and 1–3/10 helix (Ser12-Gly19) (Figure 7.1) (PDB sequence detail). The SHP molecule surface contains 70% apolar atoms and the four disulphide bonds

found in SHP provide stability to the protein (Figure 7.1). SHP starting configuration (PDB accession code 1HYP) was used for our study. All atom CHARMM27 force field was used to describe the potential energy and provide functions and parameters for every type of atom in the system (Astrakas et al., 2011a). The SHP configuration was enclosed in a periodic cubic water box at a distance of 10 Å from the edge of the box to satisfy the minimum image convention. The water model used was TIP3P (Astrakas et al., 2011a) and one sodium ion was added to neutralize the system. The neutral solvated protein system was first energy minimized using steepest descent for 20000 steps and equilibrated at constant volume (NVT) and temperature (NPT) for 200 ps. Due to limited computing power available, the MD simulation was run for 1000 ps with temperature maintained at 300° K and using Berendsen thermostat and pressure was maintained at 1 bar. The constant temperature and pressure coupling was 0.1 ps and 2 ps respectively. To limit the short-range nonbonded interactions, van der Waals interactions and long-range electrostatic interactions, a cut-off of 1 nm was used. PME algorithm was used with grid spacing of 0.16 nm and the time step during the simulation was 2 fs (Petersen, 1995). MD simulations were run under constant electric field of 0.002 V/nm, 0.004 V/nm and 3 V/nm (Table 7.1). One MD simulation was run without electric field as a reference. The values of electric field chosen cover the achievable range of 20–40 kV/cm (0.002 V/nm and 0.004 V/nm) used commonly for pulsed electric field and electrohydrodynamic processing of food products (Singh et al., 2012). The highest value of 3 V/nm corresponds to the values where other researchers observed structural changes in other proteins such as Chignolin (Astrakas et al., 2011a). All the electric fields were applied in the *x*-axis to the equilibrated solvated protein system.

Root mean square deviation (RMSD) and radius of gyration (Rg) of the backbone atoms were calculated to represent any conformational changes in the protein. Surface hydrophobicity and hydrophylicity of the system were also estimated to evaluate the effect of electric field on the electrical and surface properties. Changes in these parameters were used as an index of protein conformational alteration and studied using GROMACS analyzing tools. The effect of external electric field on secondary structure of the protein was characterized using STRIDE algorithm implemented in visual molecular dynamics (VMD) (Humphrey et al., 1996). The snapshots of protein conformational change were taken using PyMOL Molecular Graphics System, Version 1.5.0.4 Schrödinger, LLC.

Table 7.1. Summary of parameters used in the MD simulated systems.

Protein System	Electric field strength (V/nm)	Temperature (K) and Pressure (bar)	Simulation length (ns)
SHP (1HYP)	0.002	300 K, 1 bar	1
SHP (1HYP)	0.004	300 K, 1 bar	1
SHP (1HYP)	3	300 K, 1 bar	1

Figure 7.1: FASTA sequence of SPH protein, four disulphide bonds between Cys8-Cys43, Cys14-Cys28, Cys45-Cys77 and Cys29-Cys67 (PDB accession code 1HYP).

7.4 Results and Discussion

7.4.1 Secondary Structure Analysis

The effect of an external electric field on secondary structures of SHP was evaluated using the STRIDE algorithm. Figure 7.2 demonstrates that application of electric field strengths 0.002 V/nm and 0.004 V/nm had no major effect on the helical region of SHP, but minor changes can be observed on turns and coils, as compared to no electric field. Application of a 3V/nm electric field severely disrupts the helical region of the protein, as compared to 0.002 and 0.004 V/nm. It is interesting to observe that the application of 3V/nm led to a transition between α- helix and π-helix, and similar transitions were observed by Budi et al., (2005) (Budi et al., 2005) in their study on the effect of an electric field on Insulin protein Chain-B conformation. They stated that this transition is an integral part of protein's dynamic property and plays an important role in defining its function (Budi et al., 2005).

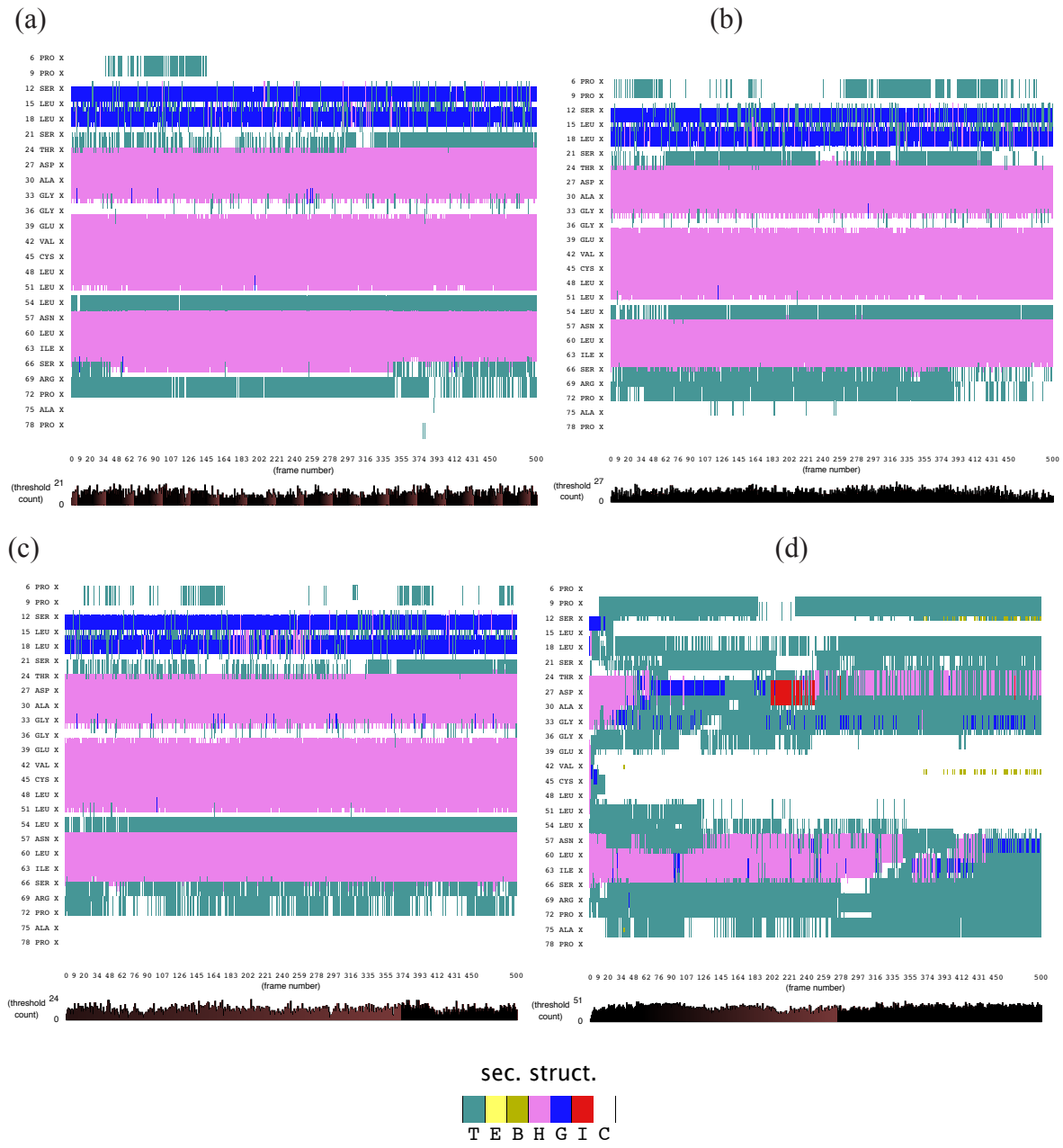

Figure 7.2: STRIDE showing evolution of secondary structure of soybean hydrophobic protein (SHP) (a) without electric field (b) 0.002 V/nm (c) 0.004 V/nm and (d) 3 V/nm external electric field. Note: Color code: Magneta denotes α- helix, red denotes π-helix, cyan denotes turn, blue denotes 3–10 helix and white denotes coil

7.4.2 Dipole Moment Distribution

Proteins, due to their secondary structure conformations such as helices, sheets, turns, coils, *etc*. possess electric dipole moment and the application of a external electric field induces an alignment change in their organization with respect to the direction of the applied field (Budi et al., 2007). The electric dipole of a protein is represented as:

$$\vec{d} = \sum_{i=1}^{N} q_i(i)\vec{r_i} \tag{7.1}$$

Where $\vec{d}$ is the dipole, q_i is the charge of the atom *i*, $\vec{r_i}$ is the directional vector of each atom and *N* is the number of atoms. When an external electric field *E* is applied the protein orients itself in the direction of the field and in our study, the electric field was applied in the *x-axis*. Depending on the strength of the applied field, unfolding or re-orientation of protein is observed. From Figure 7.3 and Table 7.2 it can be noted that the application of an external electric field changed the total dipole moment of SHP under MD simulation. The total dipole moment, for an applied field strength of 3V/nm increased until 1000 Debye in approximately 200 ps and remained constant thereafter because the protein completely unfolded and all the major secondary structures were lost (Figure 7.6). From Figures 7.4 and 7.5 it can also be observed that at the end of the simulation, the helices of SPI were realigned in the direction of the applied electric field, but no preferential alignment of helices was observed in the control reference (no field), confirming that under an external electric field, proteins orient themselves in the direction of the field (Astrakas et al., 2012; Astrakas et al., 2011a; Budi et al., 2005).

Table 7.2. RMSD, Radius of Gyration and Total Dipole moment of the SHP protein Backbone, averaged over 1ns of simulation time.

Molecule	**Electric field strength (V/nm)**	**RMSD average (nm)**	**Rg average (nm)**	**Total Dipole moment (Debye)**
SHP (1HYP)	0	0.122 ± 0.022	1.150 ± 0.024	−121 ± 45.311
SHP (1HYP)	0.002	0.114 ± 0.016	1.163 ± 0.037	27 ± 31.444
SHP (1HYP)	0.004	0.119 ± 0.021	1.150 ± 0.021	38 ± 42.460
SHP (1HYP)	3	0.803 ± 0.060	1.435 ± 0.043	971 ± 102.666

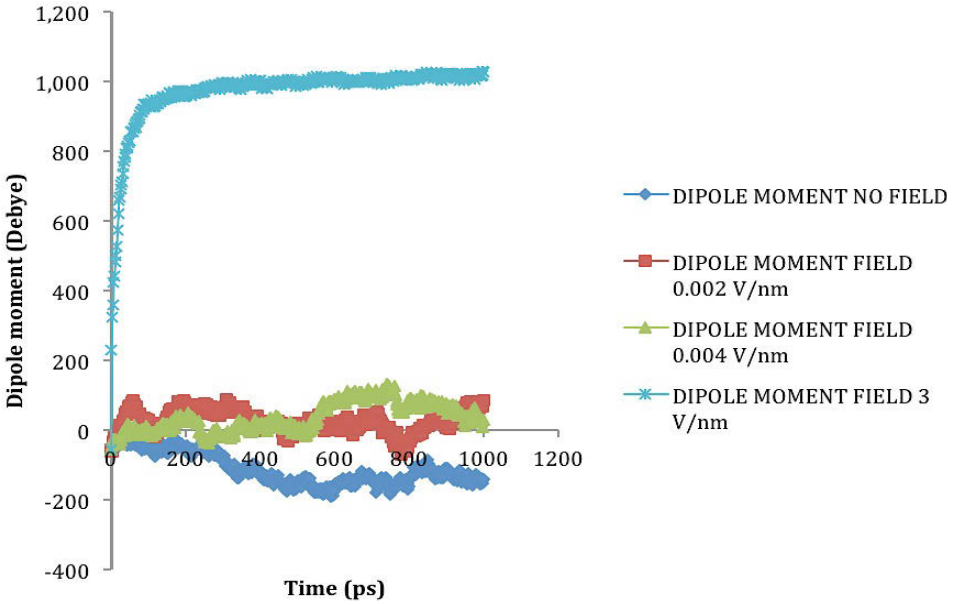

Figure 7.3: Total dipole moment of SHP under the influence of an external electric field.

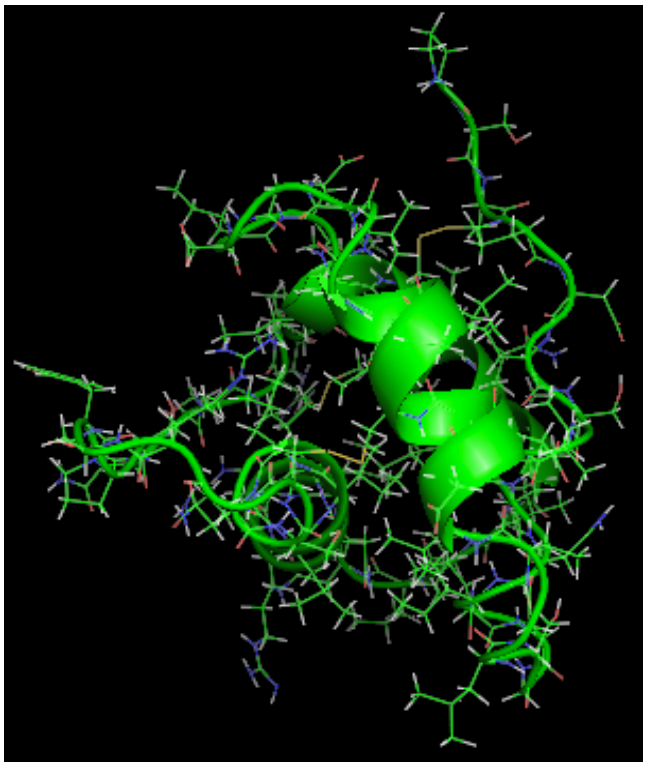

Figure 7.4: SHP protein under no external electric field.

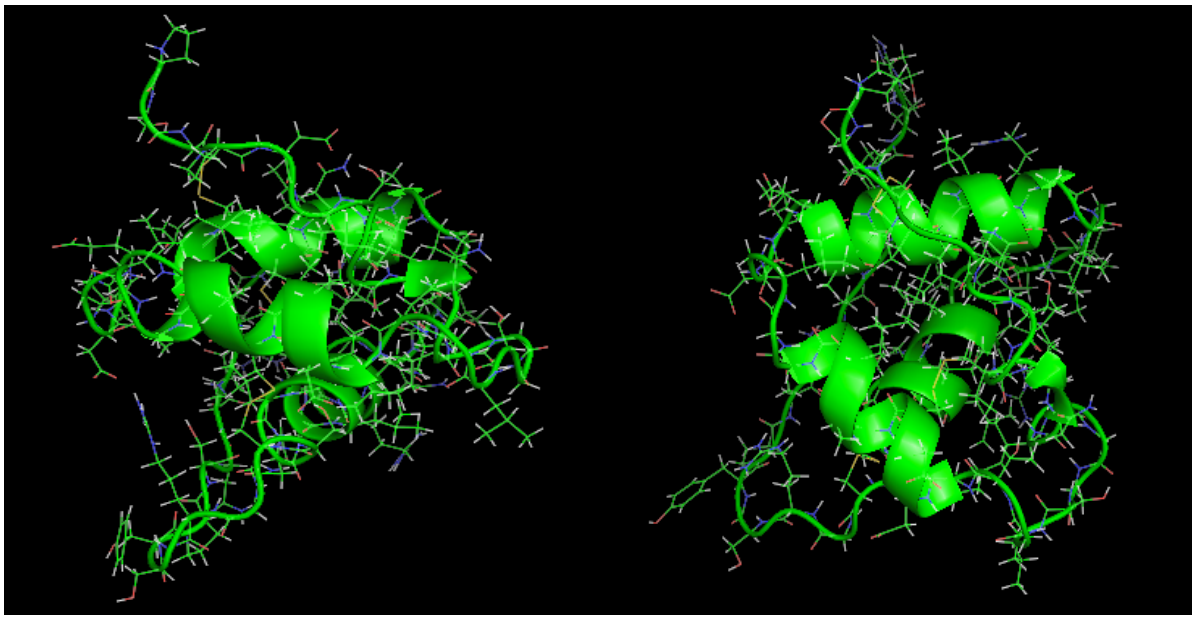

Figure 7.5: SHP protein snapshot at the end of the MD simulation under the influence of 0.002 V/nm and 0.004 V/nm.

(a) (b)

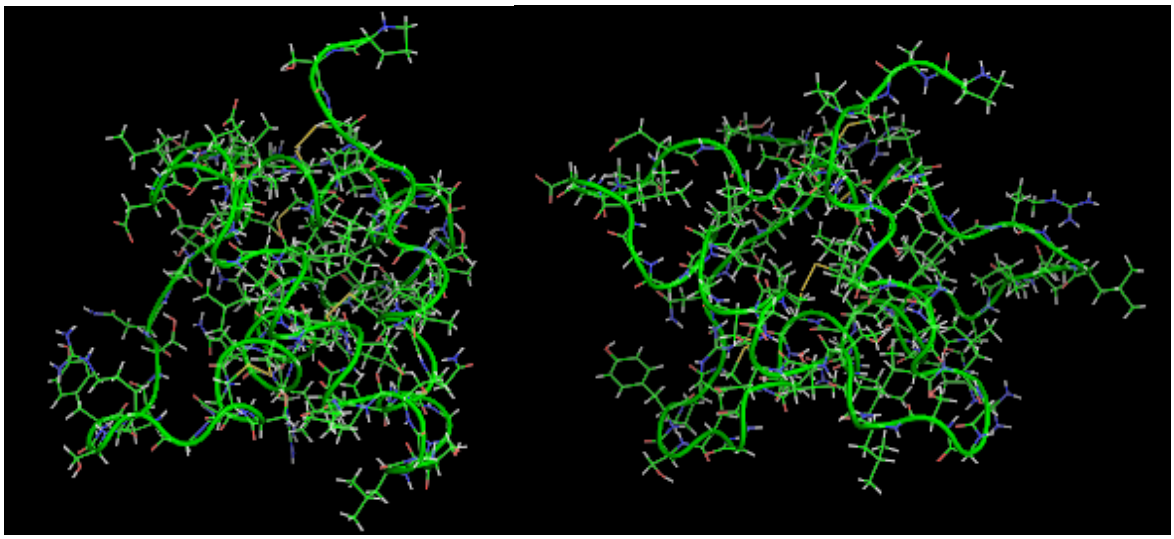

(c) (d)

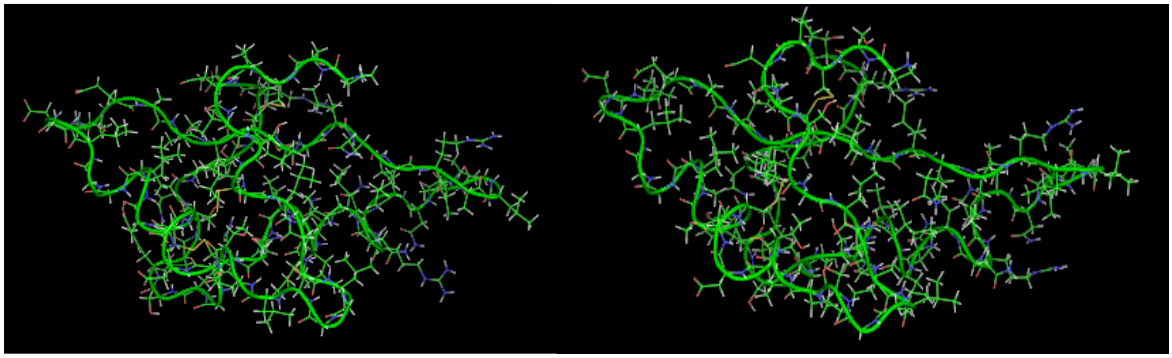

(e)

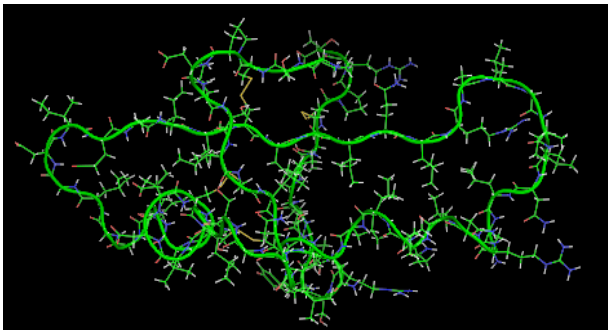

Figure 7.6: SHP snapshots at the beginning (a) and at different time spans (b), (c), (d) and at the end of the MD simulation (e) with an applied electric field of 3 V/nm.

7.4.3 Root Mean Square Deviation (RMSD)

The RMSD of a protein during simulation provides a quantitative measure of any structural variation. RMSD is calculated by comparing the structure of simulated protein during simulation with the reference (Budi et al., 2004). RMSD of a protein is represented as:

$$RMSD = \sqrt{\frac{1}{N}.\sum_{i=1}^{N}\left|r_{final}(i) - r_{initial}(i)\right|^2} \tag{7.2}$$

Where $r_{final}(i)$ is the final coordinates of an atom *i*, and $r_{initial}(i)$ is the initial coordinate of the atom *i*, and *N* is the number of atoms.

The average value of RMSD for 1ns simulation is shown in Table 7.2. It can be assessed from Table 7.2 and Figure 7.7, that the application of an electric field strength of 0.002 V/nm and 0.004 V/nm had no major effect on the stability of the SPI structure as their RMSD value were similar to the reference (no applied electric field), but at 3V/nm the partial and complete loss of the helical secondary structures produced a higher RMSD value.

7.4.4 Radius of Gyration (Rg)

The Rg of the protein quantifies the distribution of the atoms in the space relative to their center of mass; it provides an understanding of the changes in shape and size of the protein under the influence of external stresses such as an electric field (Budi et al., 2008). It can be calculated using Equation 7.3.

$$Rg = \sqrt{\frac{1}{N}.\sum_{i=1}^{N}\left|r(i) - r_{center}\right|^2} \tag{7.3}$$

Where $r(i)$ is the coordinates of an atom i and r_{center} is the coordinates of the protein's center of mass, N is the number of atoms.

The radius of gyration (Rg) values for SHP under the influence of electric field strength 0.002 V/nm and 0.004 V/nm did not vary much with respect to the control/reference, because no significant change to the structure was observed, but when the electric field of 3 V/nm was applied the Rg value obtained was higher compared to the reference and other applied intensities because of the loss of secondary structures and resulting protein unfolding (Figure 7.8).

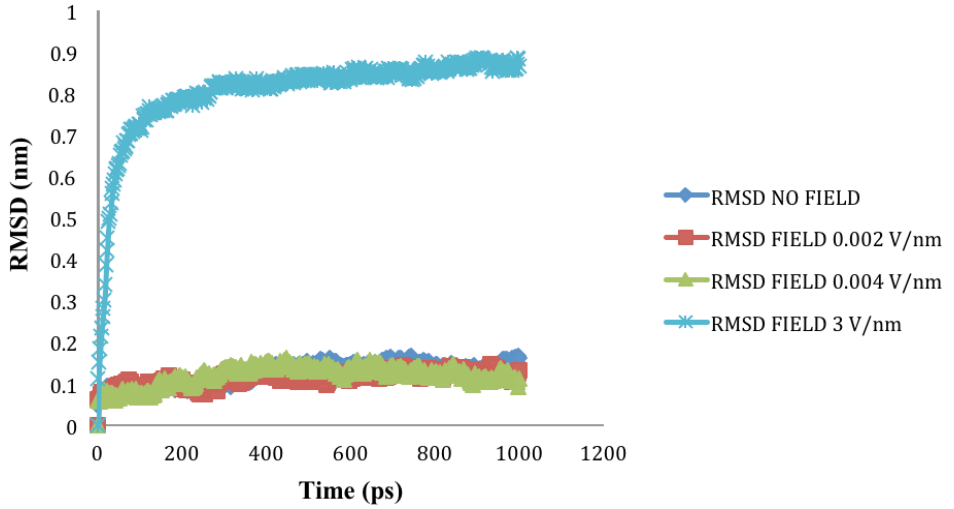

Figure 7.7: RMSD of SHP backbone under the effect of external electric field.

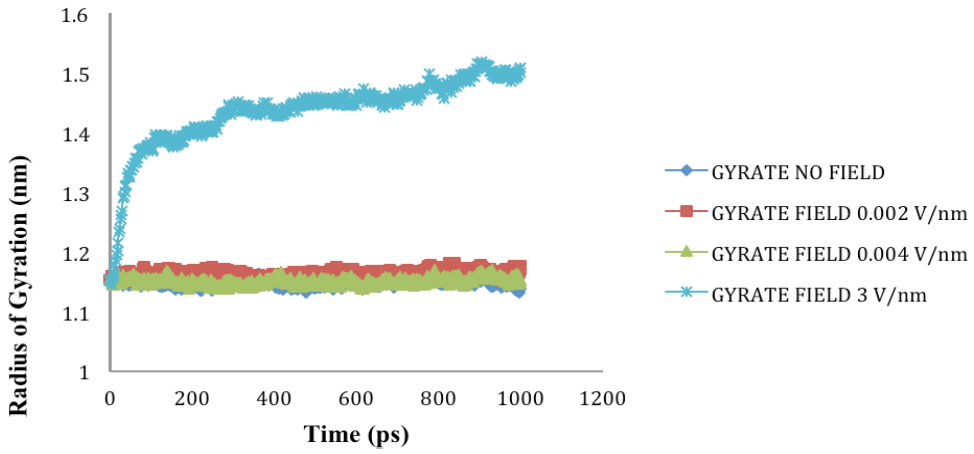

Figure 7.8: SHP radius of gyration (Rg) in the absence and presence of various external electric fields.

7.4.5 Solvent Accessible Surface Area (SASA)

SASA denotes the area that is available on the protein surface for interaction with solvents and other molecules of similar sizes. Under cellular conditions, the hydrophobic residues of a protein are arranged in a manner to minimize exposure to solvents. However, when a protein is subjected to external stress such as thermal and high electric field, it undergoes conformational changes, which lead to increase in exposure of hydrophobic residues to water and other solvents. In our study, application of electric field stresses of 0.002 V/nm and 0.004 V/nm had no noticeable change on SASA until the electric field intensity of 3 V/nm was applied. Due to unfolding of SPI under this extreme stress, the hydrophobic and hydrophilic residues were exposed thus increasing the SASA (Figure 7.9-7.10).

In 2011, Xiang et al. reported that the application of pulsed electric field treatment of 25 kV/cm and 120 pulses on soybean protein isolate (SPI) showed an 18% increase in surface hydrophobicity. They attributed these changes to denaturation of the proteins (Xiang et al., 2011). In the present study, the protein was subjected to an external electric field in an aqueous system at neutral pH and the simulation was conducted at constant temperature and pH. Application of pulsed electric field or static high electric field to a protein in an aqueous environment would lead to the generation of ohmic heating, in the study conducted by Xiang et al., the effect of temperature was considered to be minimal.

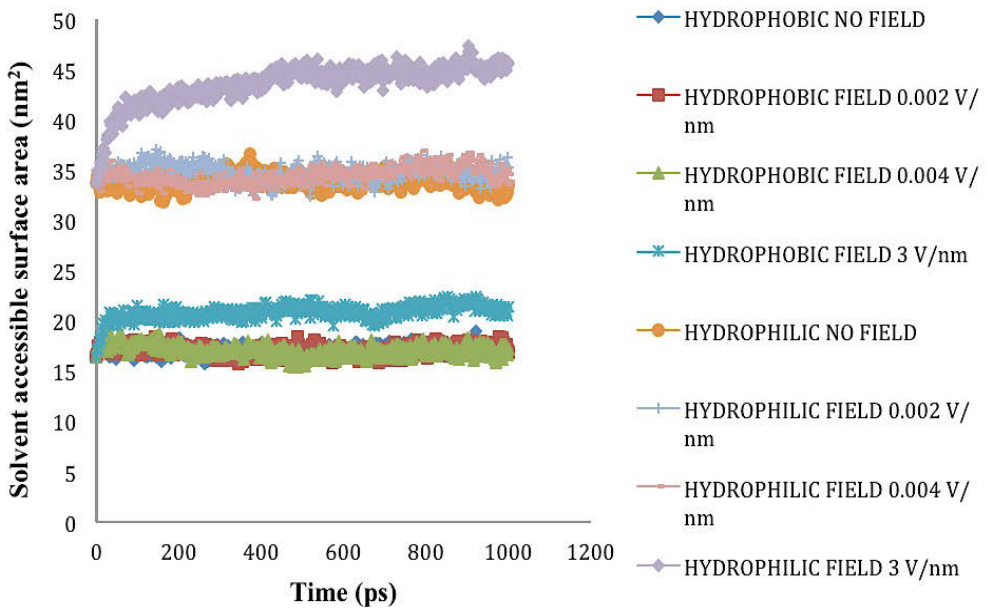

Figure 7.9: Solvent accessible surface area (nm^2) under the influence of an external electric field.

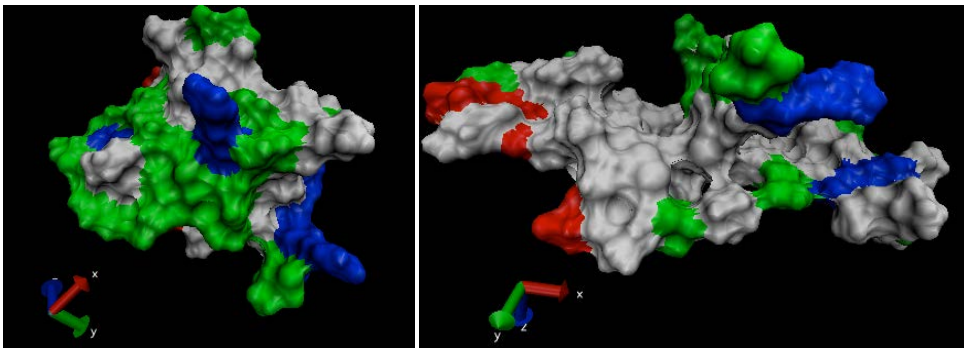

Figure 7.10: SHP snapshot of surface properties at the beginning and end of the MD simulation under electric field intensity of 3V/nm. Note: non-polar residues (white), basic (blue), acidic (red) and polar residues (green).

The findings of the present study were in accordance with several studies conducted on molecular dynamic simulation of proteins under externally applied electric fields (Astrakas et al., 2011a; Budi et al., 2007, 2005). It is important to note that the results obtained are under the assumptions applicable for MD simulation and more analysis is required to evaluate the interaction of an external field with each and every atom under the accepted force fields. Nonetheless, the MD simulation conducted for the present study does provide information about the direct influence of an external electric field on the SPH.

7.5 Conclusion

In this work, by means of MD simulation, we explored the effect of externally applied static electric fields of 0.002 V/nm, 0.004 V/nm and 3V/nm strength on the structural stability of soybean protein isolate. Our observation indicates that under the effect of lower intensity electric field, SHP protein reorients itself in the direction of the electric field and no major effect was observed on the secondary structure of the protein, but under 3V/nm, the protein unfolded and almost all the helical structures were lost as shown during the simulation. It can also be concluded that more work with oscillating electric field at different frequencies is required in order to better understand the effect on proteins' structural and functional properties. Knowledge gained through MD simulation under external electric field will be useful to explain the effect of novel food processing techniques such as microwave, radiofrequency, pulsed electric field and electrohydrodynamics on the biochemical composition of food products.

Connecting Statement

After validating the application of static electric field through GROMACS and its effect on the conformational and surface properties of soybean hydrophobic protein, implementation of the technique to study the effect of static electric field of strength 0.001 and 0.002 V/nm, on gliadin protein, which is a major subunit of wheat gluten protein was carried out in the next chapter. Gliadin protein for this study was selected because there was no crystal structure available for wheat gluten. This decision is in accordance to the literature results obtained earlier.

Chapter 8

Gliadin Simulation:

Effect of External Electric Field Stress on Gliadin Protein Conformation

8.1 Abstract

A molecular dynamic (MD) modeling approach was applied to evaluate the effect of an external applied electric field on gliadin protein structure and surface properties. Static electric field strengths of 0.001 V/nm and 0.002 V/nm induced conformational changes in the protein but had no significant effect on its surface properties. The study of hydrogen bond evolution during the course of simulation revealed that the root mean square deviation, radius of gyration and secondary structure formation, all depend significantly on the number of hydrogen bonds formed. This study demonstrated that it is necessary to gain insight into protein dynamics under external electric field stress, in order to develop the novel food processing techniques that can be potentially used to reduce or eradicate food allergens.

8.2 Introduction

Gluten is a storage protein found in wheat, it plays an important role in regulating its baking quality governing the viscosity, cohesivity, water absorption and elasticity of the dough (Bekes et al., 1998). Gluten protein found in wheat can be divided into two major fractions based on their solubility in aqueous alcohol; gliadin (soluble) and glutenin (insoluble). They both are characterized by their high content of glutamine and proline amino acids (Bekes et al., 1998). The presence of these amino acids not only determine the physical property of wheat-based products but also plays an important role in the patho-physiology of the autoimmune disorder called *coeliac* disease.

Coeliac disease can be defined as a permanent intolerance to certain cereal proteins such as gluten in wheat, hordeins in barley and secalins in rye. These proteins contain high percentage of proline and glutamine residues, but their content varies widely between cereals and so is their toxicity level. Uncontaminated oat is considered to be a safer cereal for coeliac patients due to lower content of proline residue in its protein avenin (Vader et al., 2003). Several attempts have been made to determine the role of cereal proteins in coeliac disease while currently for patients suffering from this disease a strict gluten-free diet is often the recommended treatment (Chand and Mihas, 2006; Stoven et al., 2012).

The complexity of a gluten-free diet has led food industries to look for alternatives and develop technologies to reduce or completely remove the effect of gluten protein on human health. This study puts emphasis on the effect of an external electric field on the conformation of gliadin protein. Results obtained from the study provide an insight into what we can expect to happen, and since this study is the authors' first attempt to check the viability and applicability of a novel food processing techniques using molecular dynamic simulation, only changes in conformation have been the focal point. Future work will explore deeper into the mechanisms and changes in activity of gliadin protein.

8.3 Experimental Section

Molecular dynamic (MD) simulation of Gliadin protein was performed using molecular dynamic algorithm implements in the Groningen machine for chemical structure (GROMACS) software package (version 4.5.4, Stockholm Center for Biomembrane Research, Stockholm, Sweden) (Van Der Spoel et al., 2005b). Gliadin protein starting sequence configuration was obtained from Chain C of protein database bank (PDB) accession code 2NNA, which represents the structure of the MHC class II molecule HLA-DQ8 bound with a deamidated gluten peptide. The α-β gliadin peptide Chain C sequence (QQYPSGEGSFQPSQENPQ) (Table 8.1) had minimal to no defined secondary structures other than turns. All atoms CHARMM27 (Chemistry at Harvard Macromolecular Mechanics) force field was used in this study to provide the parameters and mathematical functions to describe the potential energy of all the atoms in the system. The protein configuration was enclosed in the center of a periodic cubic 3-Point (TIP3P) water box size 10.3 × 10.3 × 10.3 nm containing 33,832 water molecules to satisfy the minimum image convention. Two sodium ions were added to the system to neutralize it and later the solvated neutral system

was energy minimized using steepest descent for 50,000 steps and equilibrated at constant temperature (NPT) and pressure (NPT) for 200 ps. MD simulation was carried out for 10 ns at constant temperature of 300 K and pressure of 1 bar maintained using Berendsen thermostat and barostat respectively (Berendsen et al., 1984). For the temperature and pressure coupling was 0.1 ps and 2 ps respectively. A cut of 1 nm was used to limit the short-range non-bonded interactions, van der Waals interactions and long-range electrostatic interactions. PME algorithm was used with a grid spacing of 0.16 nm and time step during the simulation was set to 2 fs (Astrakas et al., 2011a). During the simulation the protein configuration was subjected to static electric field strength of 0.001 V/nm and 0.002 V/nm (Table 8.1). One MD simulation was run without electric field as a control/reference.

Table 8.1. Primary sequence of α-β gliadin [Chain C of protein database bank (PDB): 2NNA].

	1	**2**	**3**	**4**	**5**	**6**	**7**	**8**	**9**
0	GLN	GLN	TYR	PRO	SER	GLY	GLU	GLY	SER
10	PHE	GLN	PRO	SER	GLN	GLU	ASN	PRO	GLN

Note: GLY: glycine; GLU: glutamic acid; GLN: glutamine; PRO: proline; ASN: asparagine; SER: serine; TYR: tyrosine; PHE: phenylalanine.

The conformational changes of the protein were represented using root mean square deviation (RMSD) and radius of gyration. The solvent accessible surface area of the protein was also analyzed to represent the changes in surface properties under the influence of the external electric field. Influence on hydrogen bonds evolution during the simulation was also analyzed, as they are needed for protein folding, binding to other proteins or enzymes and other processes. The STRIDE algorithm implemented in the visual molecular dynamics (VMD) software package was used to study the changes in the secondary structures of the protein (Humphrey et al., 1996).

8.4 Results and Discussion

8.4.1 Secondary Structure Analysis

Gluten protein comprises of about 50 protein components that can be classified into two

major groups: monomeric gliadin and polymeric glutenin (Wellner et al., 2005). One subgroup of glutenin also called as high molecular weight (HMW) subunits of glutenin comprises approximately of 650–820 amino acid residues containing an extensive repetitive domain (480–680 residues) conferring a β-spiral (β-reverse turns) in a solution (Wellner et al., 2005). These subunits account for 8%–10% of the gluten protein, the rest consists of light molecular weight (LMW) subunits and α, β and γ gliadins (Purcell et al., 1988). The effect of the external electric field on the secondary structure of the gliadin protein was estimated using STRIDE algorithm implemented in VMD software package. The STRIDE algorithm (Heinig and Frishman, 2004), implemented in VMD helps to simplify the analysis of tertiary conformational changes of a protein by assigning secondary structure type to each residues based on knowledge-based algorithm, which takes into account hydrogen bond energy and statistically derived backbone torsional angle information. The protein conformation obtained from ChainC (PDB accession code: 2NNA) was subjected to external electric field strength of 0.001 V/nm and 0.002 V/nm. The protein sequence obtained had no distinct secondary structures defined such as alpha helices and beta sheets, and the only structure that were visible and analyzed were the turns (Figure 8.1).

(a.)

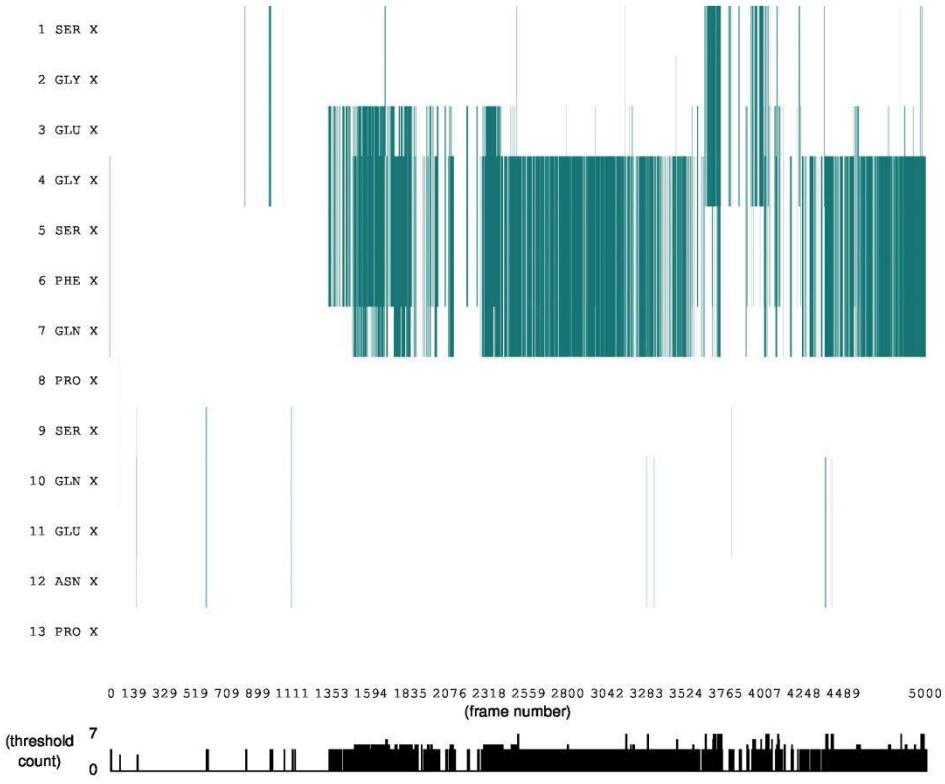

Figure 8.1. *Cont.*

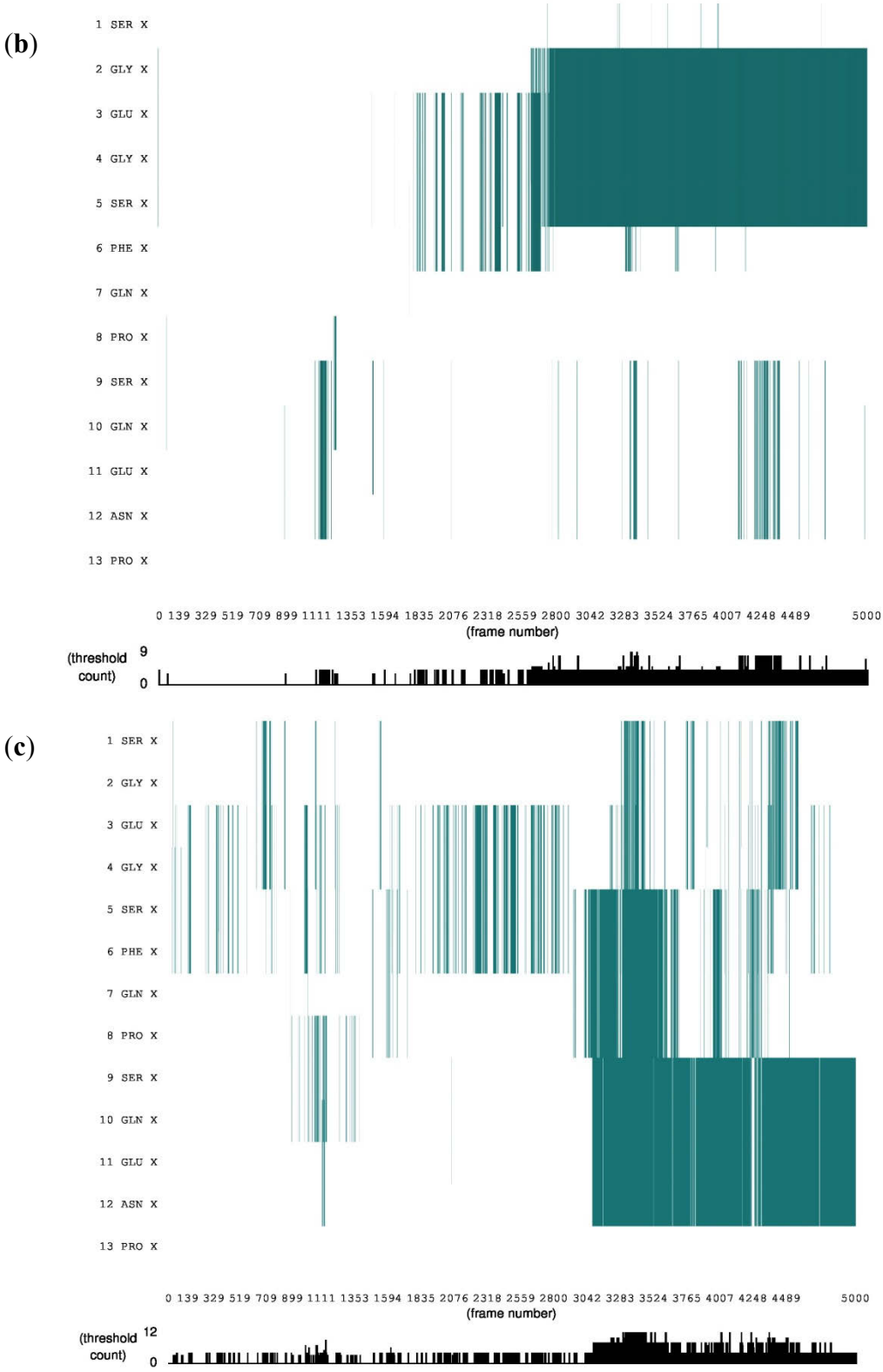

Figure 8.1: Stride evolution of secondary structures of gliadin protein under an external electric field (a) Without external electric field; (b) Under electric field strength 0.001 V/nm; (c) Under electric field strength 0.002 V/nm (Color code: Cyan denotes turn).

There has been relatively little study of the conformational structure of gliadin protein. In 1988, Purcell et al. conducted a Fourier transform infrared spectroscopy (FTIR) study on secondary structures of wheat α- and ω-gliadin protein, and they showed that the α-helical structure may make a significant contribution to the secondary structure of α-gliadin, but they also suggested that the absorption spectrum which they observed near 1,654 cm^{-1} confirming the presence of α-helical structure may be due to the presence of β-turns which have an absorption at 1,658 cm^{-1}. They concluded that gliadin protein includes a significant proportion of β-turn structures. These observations made by Purcell et al. (Purcell et al., 1988) support our finding of no other secondary structure other than turns. Analysis of Figure 8.1 shows that as the protein configuration was subjected to an electric field, the number of protein amino acids involved in formation of the turn increased. This behavior can be attributed to glycine and proline residues present in the gliadin sequence. From Figure 8.2 we can suggest that during the course of the simulation both the number of hydrogen bonds and number of turns increased with time.

8.4.2 Dipole Moment Distribution

In general, proteins possess an electric dipole moment by virtue of their secondary structure conformations such as helices, sheets, turns, coils, *etc.* When an external electric field is applied, it induces an alignment change with respect to the direction of the applied field. The electric dipole moment of a protein is represented as (Budi et al., 2005):

$$\vec{d} = \sum_{i=1}^{N} q_i(i)\vec{r}_i \tag{8.1}$$

where $\vec{d}$ is the dipole, q_i is the charge of the atom *i*, $\vec{r}_i$ is the directional vector of each atom and *N* is the number of atoms. In our study, the electric field was applied in the *z-axis*. Depending on the strength of the applied field, a change in the total dipole moment of the gliadin protein was observed (Figure 8.3).

Table 8.2. Backbone Root Mean Square Deviation (RMSD), radius of gyration and total dipole moment, averaged over 10 ns of simulation time.

Molecule	Electric field strength (V/nm)	RMSD average (nm)	Rg average (nm)	Total Dipole moment (Debye)
Gliadin protein	0	0.536 ± 0.131	0.942 ± 0.095	59.8 ± 38.66
Gliadin protein	0.001	0.461 ± 0.102	1.030 ± 0.065	33.3 ± 78.48
Gliadin protein	0.002	0.617 ± 0.137	0.911 ± 0.094	26.9 ± 53.41

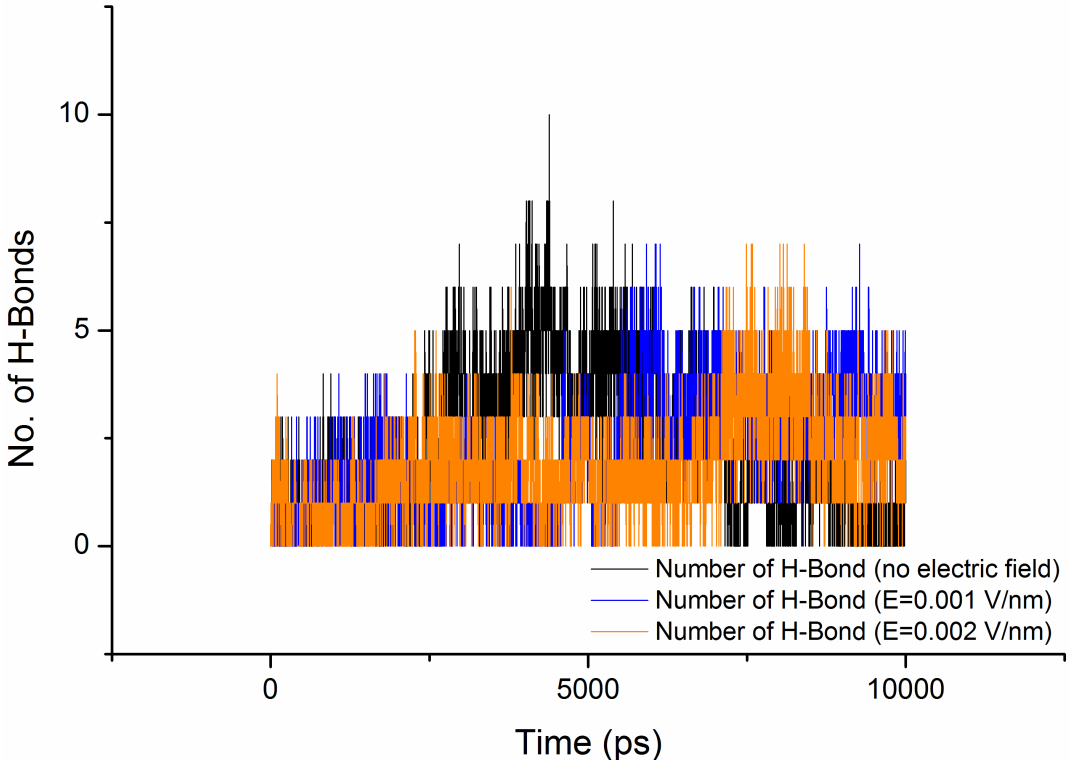

Figure 8.2: Evolution of the hydrogen bonds during the course of simulation under the influence of an applied external electric field.

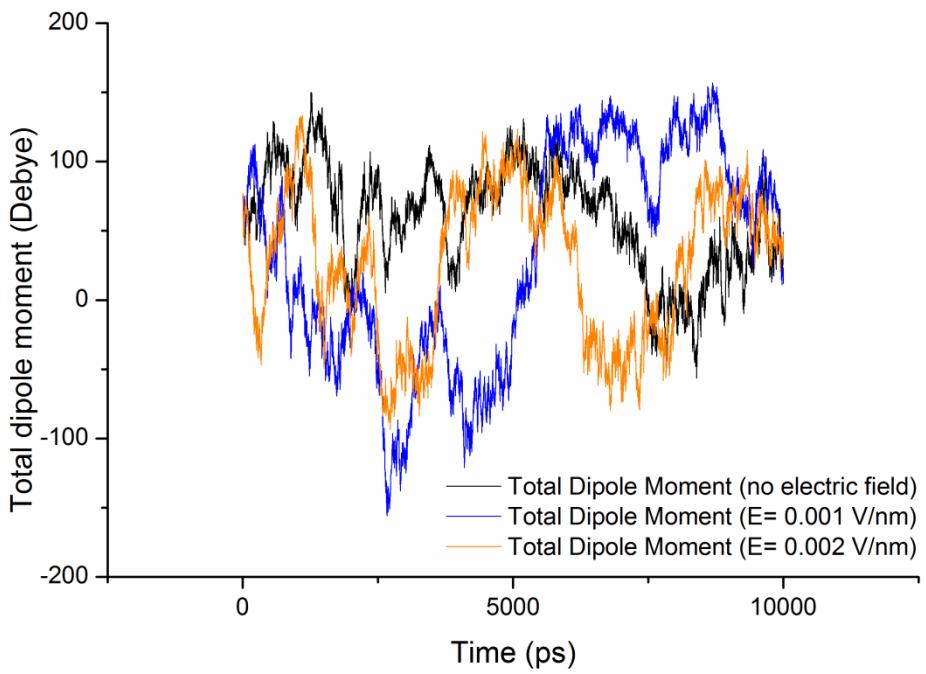

Figure 8.3: Total dipole moment of gliadin protein under the influence of an applied external electric field.

From Figure 8.3 it can be observed that the total dipole moment of gliadin protein under the stress of an applied external electric field varied significantly (Table 8.2). It is important to note that under the influence of an electric field the protein structure tries to reorients itself in the direction of the field, but in the case of gliadin protein, the absence of any distinct secondary structures such as helices and beta-sheets, should have shown similar dipole moment as the control/reference (without electric field). However sharp changes in the total dipole moment were observed, which can be attributed to the electrical properties of the constituent amino acids trying to orient themselves in the direction of the field. For a protein with defined secondary structures such as helices, their dipole moment contributes to the binding of charged substrates or coenzymes at the termini and can also enhance the reaction rates (Budi et al., 2008).

8.4.3 Root Mean Square Deviation (RMSD)

Changes in the conformation of protein can be quantitatively measured by determining the RMSD of a protein. RMSD is estimated by comparing the structure of simulated protein during simulation with the reference. RMSD of a protein is represented as (Budi et al., 2005):

$$RMSD = \sqrt{\frac{1}{N}.\sum_{i=1}^{N}\left|r_{final}(i) - r_{initial}(i)\right|^2} \tag{8.2}$$

where $r_{final}(i)$ is the final coordinates of an atom *i*, and $r_{initial}(i)$ is the initial coordinate of the atom *i*, and *N* is the number of atoms.

The average value of RMSD obtained for the 10 ns simulation is shown in Table 8.2. It can be observed that varied deviation can be observed in the RMSD of the protein under the influence of electric field. RMSD of the protein under a field strength of 0.001 V/nm was lower compared to the control/reference and for a field strength of 0.002 V/nm (Figure 8.4). This variation in the protein RMSD can be attributed to the change in the orientation of the protein and involvement of amino acids in the formation of turns via hydrogen bonds as observed in Figure 8.5. The trend analysis revealed that for reference simulation the RMSD value decreased with increase in number of hydrogen bonds (Figure 8.5). A similar trend was observed for simulation performed under electric field strength of 0.001 V/nm, but for electric field strength of 0.002 V/nm the increase in number of hydrogen bond had no significant effect on the RMSD value.

Hydrogen bonds play a significant role in stabilizing the secondary structures of proteins. The loss of internal hydrogen bonds between amino acids due to applied stress can cause destabilization of the secondary structures and lead to protein unfolding (Kortemme et al., 2003). Table 8.3 presents information on the number of hydrogen bonds (hbonds) formed during the course of the simulation as a function of time under external applied electric field stress (Fabiola et al., 2002; Mata et al., 2009). In this study, in order to be classified as a hydrogen bond, the donor-acceptor atom separation was set to be no more than 3.5 Å. From Table 8.3 it can be observed that glutamine (GLN) and glutamic acid (GLU) were among the major donor and acceptor of hbonds. In this study we analyzed the effect of the external electric field stress on deamidated gliadin peptide. Deamidated gliadin peptide is produced by enzymatic action of tissue transglutaminase, which converts excess glutamines to glutamic acid and it is well known that cellular immunity to a deamidated α-β-gliadin is more severe than normal α-β-gliadin. Extensive immunological studies have been carried out on deamidated gliadins (Henderson et al., 2007; Maiuri et al., 2003).

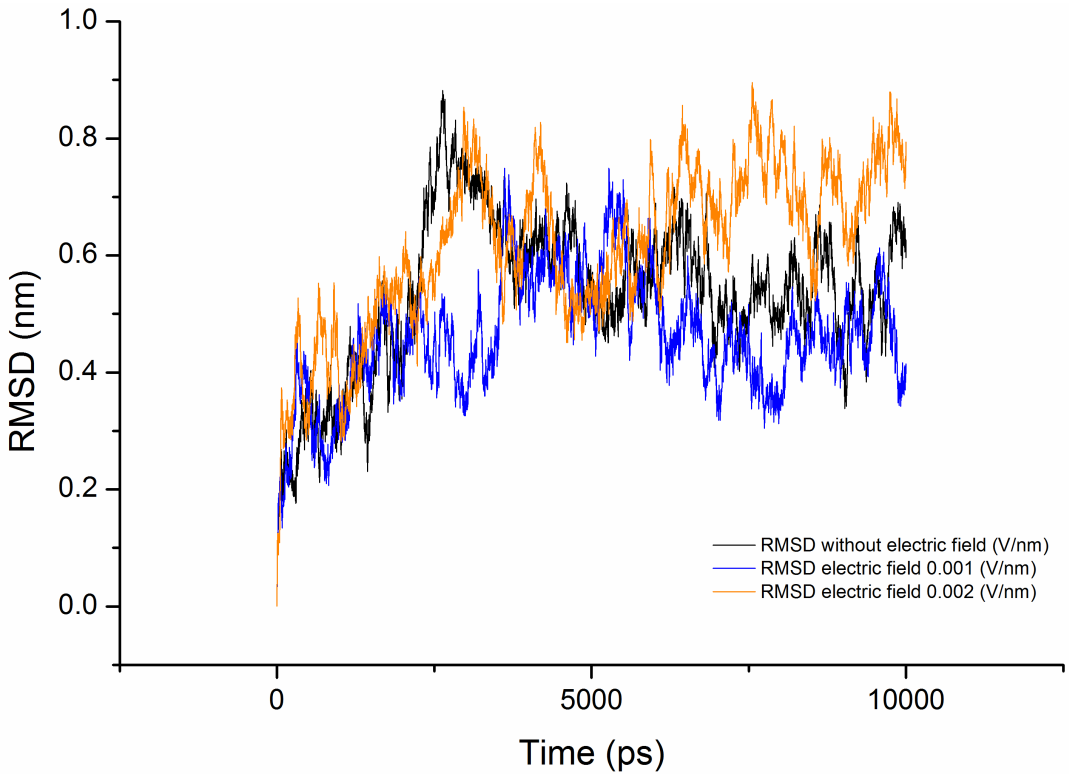

Figure 8.4: RMSD of the gliadin protein backbone under the influence of an external electric field.

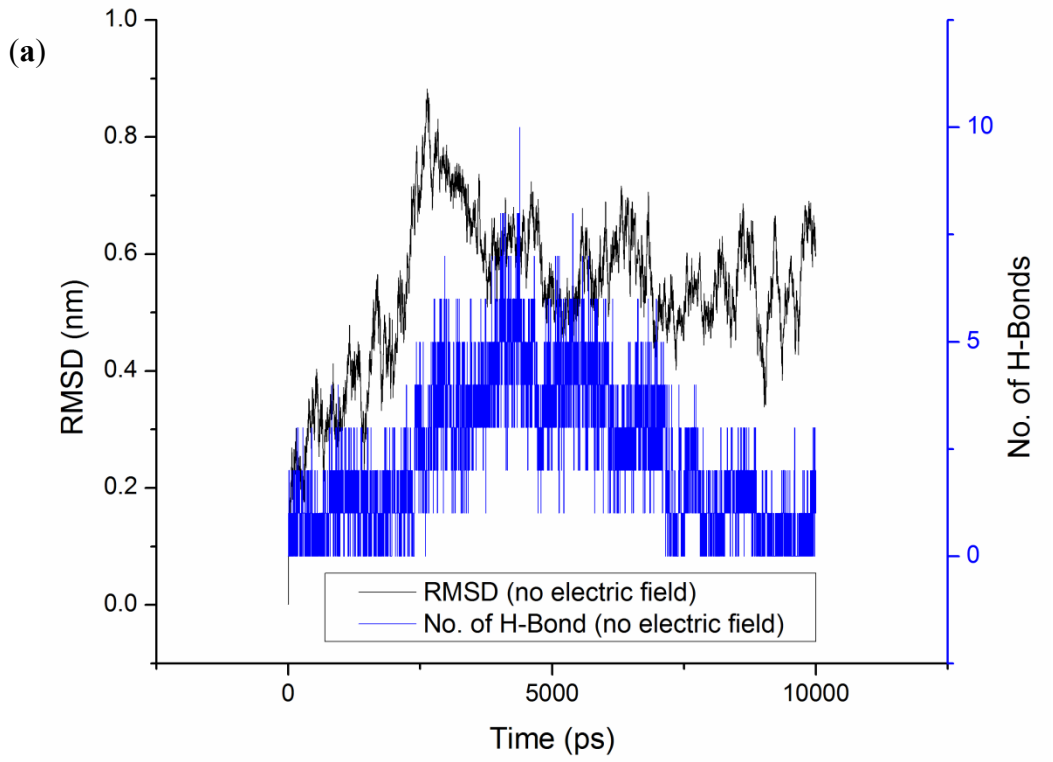

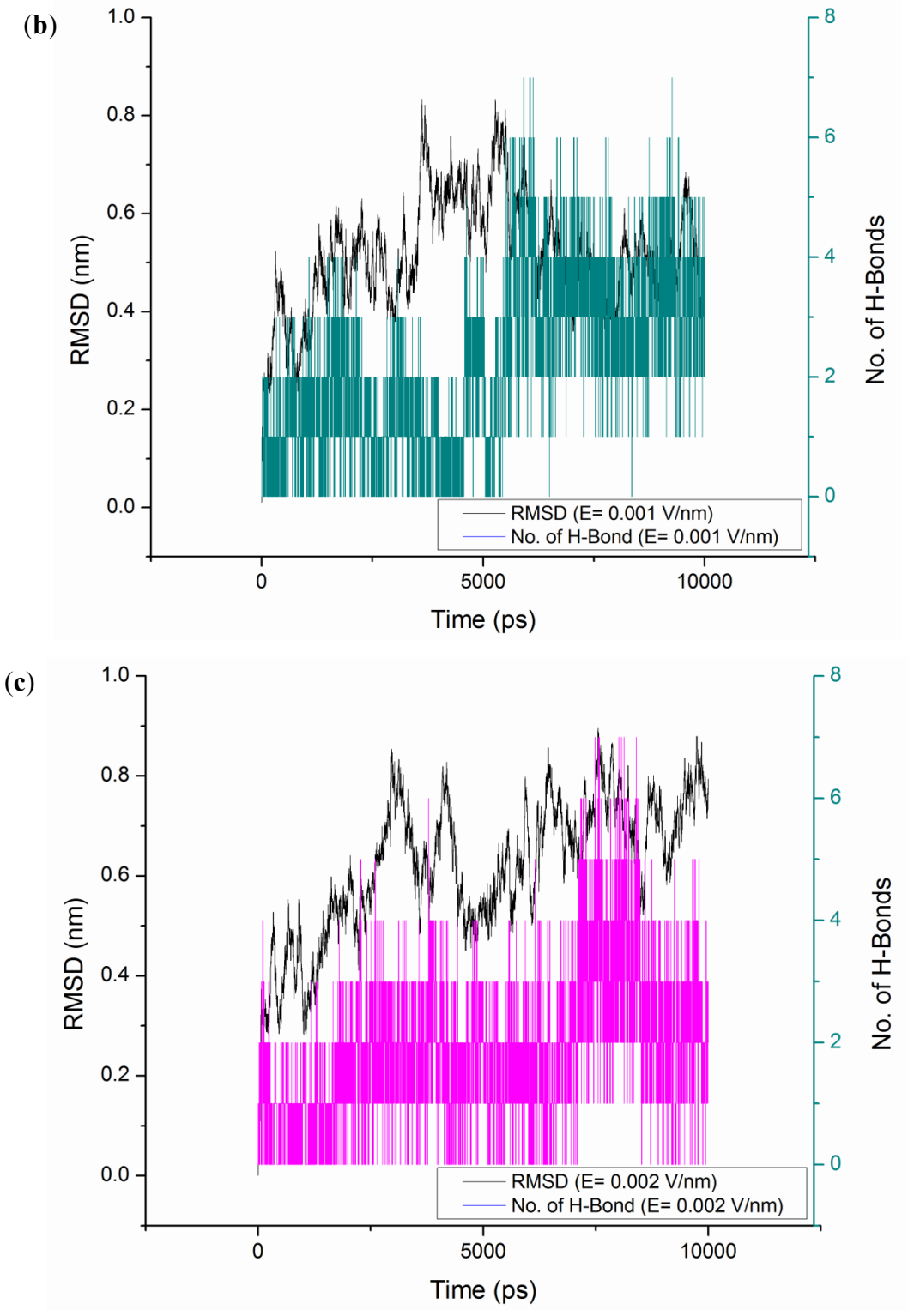

Figure 8.5: RMSD evolution with respect to number of hydrogen bonds; (a) without electric field (b) 0.001V/nm; (c) 0.002 V/nm.

Table 8.3. Hydrogen bond formation between donor and acceptor amino acids and their occupancy (over 2%) during the course of simulation under external electric field stress.

Without electric field (52 hbonds)			**E = 0.001 V/nm (50 hbonds)**			**E = 0.002 V/nm (54 hbonds)**		
Donor	Acceptor	Occupancy	Donor	Acceptor	Occupancy	Donor	Acceptor	Occupancy
GLY	GLU	5.14%	GLY	GLU	3.12%	GLY	GLU	11.86%
GLN	PRO	2.12%	GLN	PRO	8.08%	SER	GLU	21.30%
ASN	GLN	5.54%	GLU	SER	25.13%	GLN	PRO	3.10%
GLU	SER	9.50%	SER	GLU	40.05%	GLN	SER	24.04%
GLN-	SER	3.24%	GLU	GLU	6.08%	GLN	ASN	2.92%
GLN	ASN	3.44%	SER	GLY	2.02%	SER	ASN	2.38%
SER	GLU	22.00%	SER	GLY	8.26%	GLU	SER	2.02%
GLN	GLU	4.46%				SER	ASN	4.50%
SER	GLU	25.39%				GLU	SER	5.22%
GLU	GLU	9.78%						
SER	GLN	2.06%						

8.4.4 Radius of Gyration (Rg)

Another property that quantifies any change in the structure of protein is Rg. The Rg of the protein basically quantifies the distribution of the atoms in the space relative to their center of mass. It can be determined using Equation (8.3) (Budi et al., 2005).

$$Rg = \sqrt{\frac{1}{N}.\sum_{i=1}^{N}\left|r(i) - r_{center}\right|^2} \tag{8.3}$$

where $r(i)$ is the coordinates of an atom *i* and r_{center} is the coordinates of the protein's center of mass, *N* is the number of atoms.

The radius of gyration (Rg) values for gliadin protein under the influence of electric field strengths of 0.001 V/nm and 0.002 V/nm were lower with respect to the control/reference (Table 8.2) (Figure 8.6), because under the influence of an electric field it can be observed from Figure 8.7, that during the course of the simulation the protein tended to compact itself by forming turns via hydrogen bonds. For all the simulation conditions, a common trend of decrease in radius of gyration was observed with an increase in the number of hydrogen bonds.

8.4.5 Solvent Accessible Surface Area (SASA)

Protein activity widely depends on its surface properties, which in turn depend on the structure of the protein (primary and secondary structures). Analysis of SASA provides

information about proteins ability to interact with solvents and other molecules such as other proteins and enzymes (Budi et al., 2008). It is known that when a protein is subjected to external stresses such as thermal, electrical or chemical stresses, changes in structural configuration leads to varied surface properties (Budi et al., 2005). In our study, no significant changes were observed in the solvent accessible surface area (Figures 8.8 and 8.9). Several researchers have observed changes in SASA over the period of the simulation under applied external electric field stress (Budi et al., 2004; Budi et al., 2007); in our study, no variation was observed because the protein studied was too small with no defined significant secondary structure. Since α-β gliadin residues form mostly β-turns they become essential in enabling the gluten protein to fold and form compact tertiary structures, and these structures minimize the proteins SASA. It is well known that turns are significant in governing the flexibility of regions in protein structure, which in turn affect its activity. Our results on RMSD and Rg of gliadin protein under the influence of high electric field suggest that a decrease in their value leads to compactness of the gliadin protein structure, which may directly affect the overall tertiary structure of the gluten protein and its SASA. This would be interesting to investigate and hence further studies are required to prove this hypothesis.

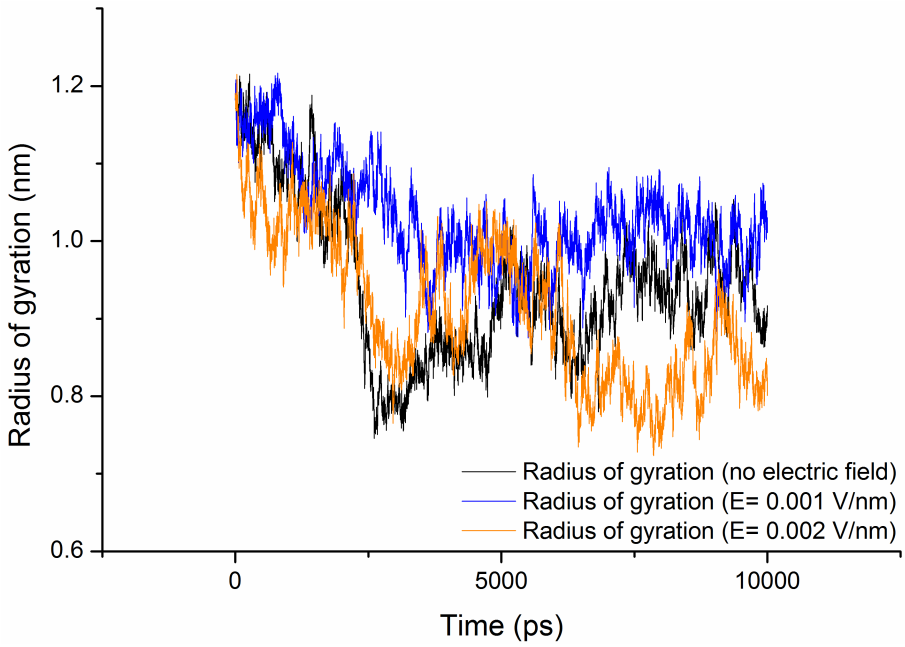

Figure 8.6: Radius of gyration (Rg) of gliadin protein under the stress of an external electric field.

(a)

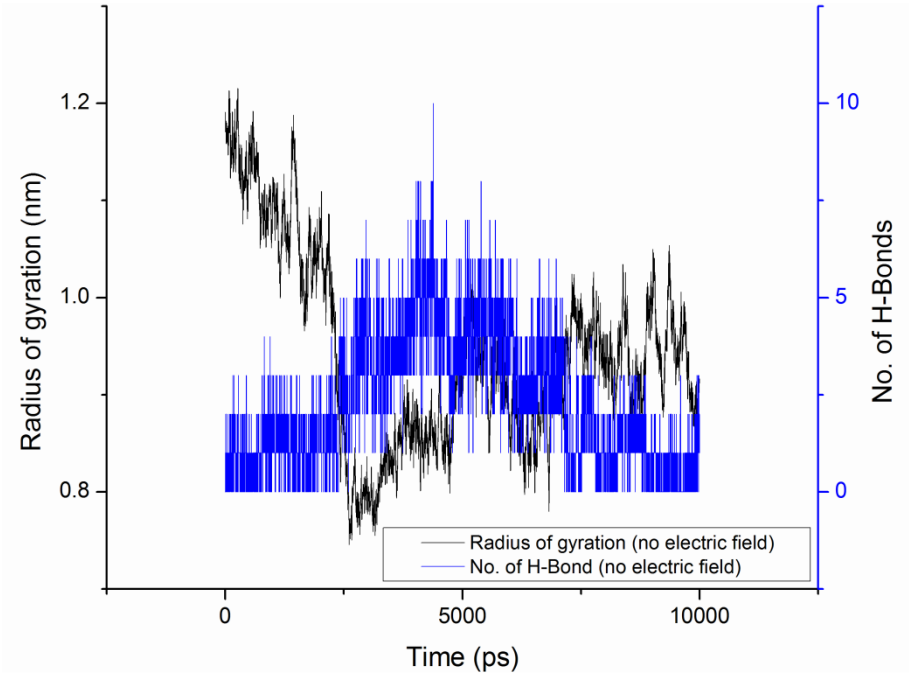
Radius of gyration (nm)
No. of H-Bonds
Time (ps)
1.2
1.0
0.8
10
5
0
0
5000
10000
Radius of gyration (no electric field)
No. of H-Bond (no electric field)

(b)

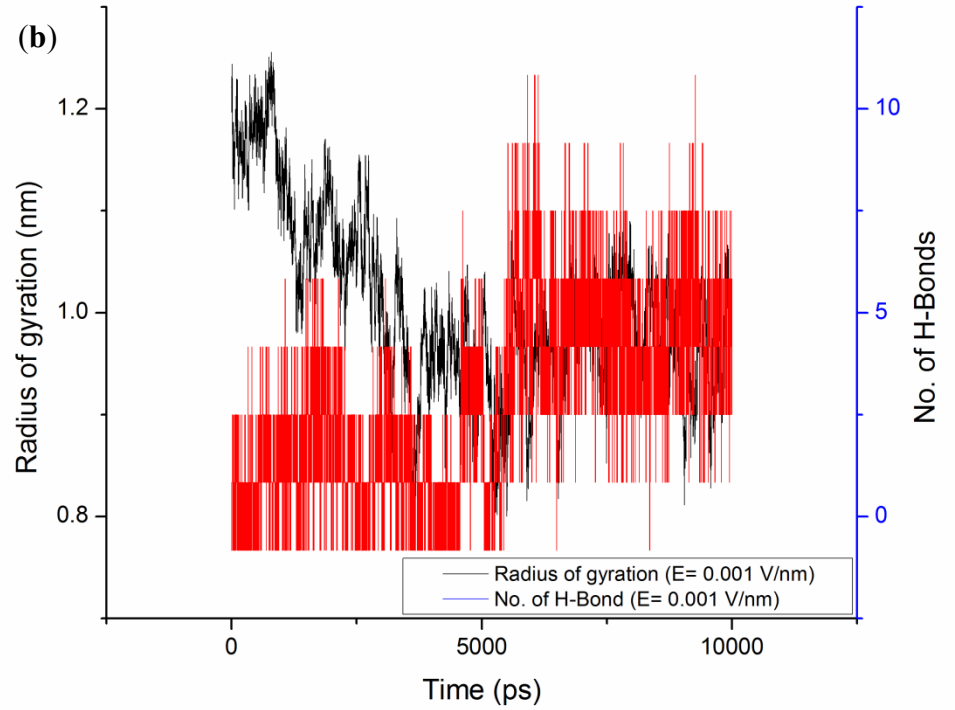
Radius of gyration (nm)
No. of H-Bonds
Time (ps)
1.2
1.0
0.8
10
5
0
0
5000
10000
Radius of gyration (E= 0.001 V/nm)
No. of H-Bond (E= 0.001 V/nm)

Figure 8.7. *Cont.*

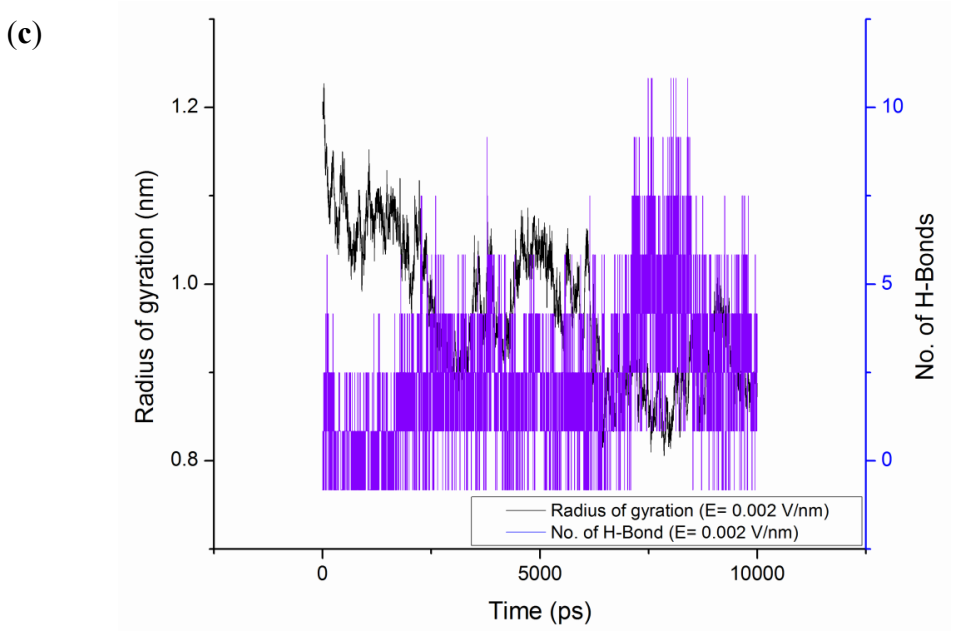

Figure 8.7: Radius of gyration evolution with respect to number of hydrogen bonds; (a) without electric field (b) 0.001V/nm; (c) 0.002 V/nm.

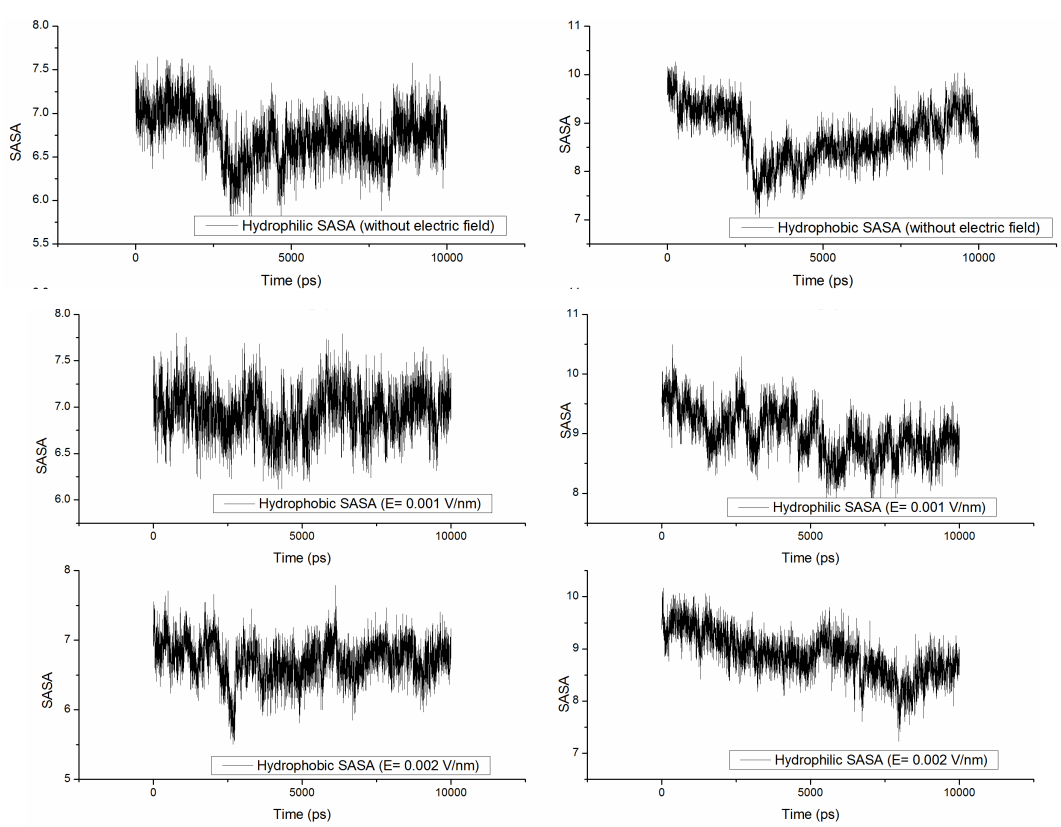

Figure 8.8: Changes in solvent accessible surface area [SASA (nm^2)] under the influence of an external electric field.

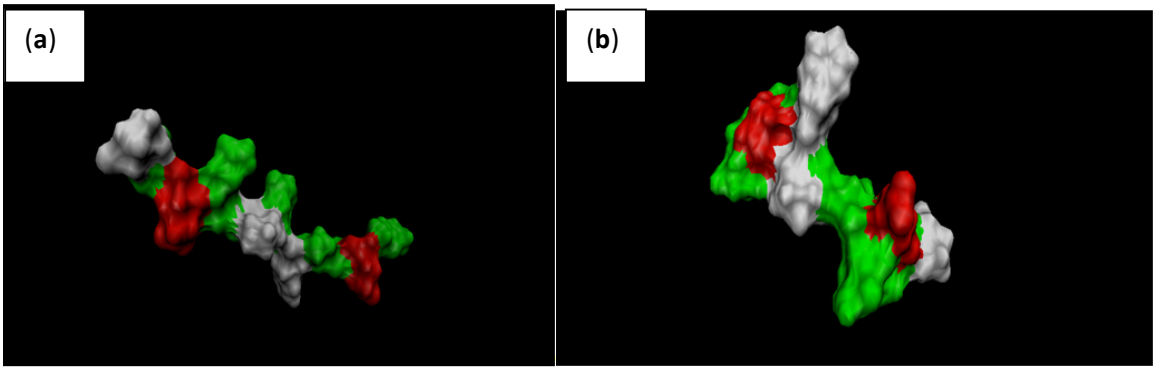

Figure 8.9: Snapshots of gliadin protein surface at the (a) beginning; and (b) end of simulation under external electric field strength of 0.002 V/nm. Note: non-polar residues (white), basic (blue), acidic (red) and polar residues (green).

8.5 Conclusion

The present study explored the effect of static external electric fields of strength 0.001 V/nm and 0.002 V/nm on the structural stability of gliadin protein. It showed that application of an external electric field induced conformational changes in the protein by means of formation of hydrogen bonds between amino acid residues. It was also observed that formation of hydrogen bonds between residues during the course of simulation affected its root mean square deviation and radius of gyration values. Number of hydrogen bonds formed increased with an increase in electric field strength. We can also conclude that more work is required to analyze and evaluate the effect of external electric field stress on the protein structure and its functional properties, but the present study does demonstrate that an electric field can be used to alter the structure of the protein, which will affect its functional properties. Knowledge gained through this MD simulation under static electric field will be useful to explore and explain the effect of novel food processing techniques such as microwave, radiofrequency, pulsed electric field and electrohydrodynamic drying on the biochemical composition of food products.

Connecting Statement

Since MD studies are conducted within the limitation of computational dynamics, it is important to validate and compare their results with experimental ones. Hence in the following chapter an experimental study on the effect of application of external electric field on conformation of wheat gluten protein was carried out using Fourier Transform Infrared Spectroscopy (FT-IR). The results obtained from FT-IR analysis will be compared with observations made through MD technique for validation.

Chapter 9

FT-IR WHEAT GLUTEN:

Effect of High Electric Field on the Secondary Structure of Wheat Gluten

9.1 Abstract

Effect of high electric field on secondary structure conformation of fully hydrated (45.65% wet basis) gluten protein was studied by FT-IR spectroscopy. Three experimental conditions were evaluated including electric field intensity of 0 kV/cm (no treatment), 3.5 kV/cm and 7 kV/cm and treatment time of 30, 60 and 90 minutes. FT-IR spectra of treated and non-treated hydrated gluten protein revealed that high electric field treatment resulted in irreversible changes in the secondary structures. In the Amide I region of the hydrated gluten protein broad shoulders were observed at 1654-1650 cm^{-1}, indicating α-helix conformation. Similar shoulders and minor peaks were observed at 1644 cm^{-1} and 1634 cm^{-1}, indicating presence of random coils and β-sheets. For 30 minutes treatments, no variation was observed for electric field intensities 0 kV and 7 kV; but at 3.5 kV it showed slight reorganization and structural conversion of secondary structures. No variation in spectral pattern was observed for all the high electric field treatments for 60 minutes but major secondary structure reorganization took place for high electric field treatment at 90 minutes. Curve-fitting using Gaussian band shapes and PCA analysis further supported the results. The observations made in this study suggested that application of an external electric field stress influences the hydrogen bonding pattern of the protein resulting in the occurrence of intramolecular hydrogen-bonded antiparallel β-sheet aggregates. The significance of these results has been discussed in relevance to the protein structural changes.

9.2 Introduction

In the past few decades food allergy has become a growing concern in the developed countries due to increasing globalization (Ortolani and Pastorello, 2006). Food allergy is defined as an adverse immune response to food proteins and it is different from food intolerance, which falls under the mechanisms involving non-immunological responses to food (Eigenmann, 2009; Ortolani and Pastorello, 2006). The immune response involves IgE-mediated reactions to food proteins and intolerances fall into categories involving enzymatic or transport deficiencies. One of the most common food based intolerance and allergy can be associated to wheat gluten protein, which is a storage protein complex found in wheat and is of critical importance in determining its bread-making quality. It regulates viscosity, cohesivity, water absorption, and elasticity of the dough (Bekes et al., 1998). It can be divided into two major fractions on the basis of its solubility in aqueous alcohol, gliadin, which is the soluble fraction and plays an important role in the viscous flow behavior of the dough; whereas glutenin the insoluble fraction which contributes to the elasticity of the dough. Both these protein fractions are characterized by their high content of proline and glutamine amino acids (Georget and Belton, 2006). These amino acids not only determine the physical properties of wheat-based products but also play a major role in the patho-physiology of an autoimmune disorder called *Coeliac* disease (Chand and Mihas, 2006; Stoven et al., 2012). It is interesting to note that there is no single laboratory test available to diagnose *Coeliac* disease and most of the clinical diagnosis is based on causal relation between the ingested food and subsequent reaction to it. This is commonly known as double-blind test or placebo-controlled food challenge (Eigenmann, 2009). In recent years several attempts have been made by researchers all around the globe to determine the role of cereal proteins in coeliac disease, and currently for patients suffering from this disorder a strict gluten-free diet is often the most recommended treatment (Chand and Mihas, 2006; Stoven et al., 2012). For food industries involved in producing cereal or wheat based food products the adverse reactions to them comes as a nightmare as it not only limits their ability to cater to the affected population but also adds financial burden involving removal of causal agent and addition of substitutes that can provide similar physico-chemical properties to newly developed food products.

It is well known that the structure of protein governs its physico-chemical properties. And in recent years significant understanding of this structure related functional relationship

garnered through in-vivo and in-vitro studies, has provided means for defining the qualitative and quantitative effect of specific proteins on safety and quality of processed food products (Singh et al., 2013b). Proteins are polymers made of amino-acids and the arrangements of these monomeric amino acids define what spatial conformation a protein will fold into. There are four different levels of protein structure; primary (linear sequence of amino acids), secondary (highly regular local sub-structures including helices, beta-sheets and turns), tertiary (the three dimensional structure) and quaternary structure (three-dimensional structure of a multi-subunit protein). These levels of protein structure can be studied using spectroscopic techniques such as Fourier transform infrared spectroscopy (FT-IR), and recently several researchers have applied FT-IR to study the secondary structures of gluten protein (Belton, 1999; Belton et al., 1995; Georget and Belton, 2006; Wang et al., 2001).

FT-IR spectroscopy is the measurement of wavelength and intensity of the infrared radiation by a protein sample. The spectra obtained from FT-IR are interpreted in terms of the vibrations of the structural repeat units such as polypeptides in proteins. In protein the polypeptide units give rise to nine distinct infrared absorption bands namely, Amide A, B and I-VII (Kong and Yu, 2007). In proteins, the most sensitive IR spectral region is the Amide I region (1700 cm^{-1} -1600 cm^{-1}) due to C=O stretch vibrations of the peptide linkages. The frequency of the Amide I region can be closely correlated to the secondary structural elements of the proteins (Haris and Severcan, 1999; Mangavel et al., 2001). The Amide II is the second most prominent spectral region and it arises mainly due to N-H bending and C-N stretching vibrations. This region of the spectra shows less conformational sensitivity as compared to Amide I (Georget and Belton, 2006). The characteristic IR absorption bands of the protein are listed in Table 9.1. FT-IR analysis of gluten protein has revealed how specific secondary structures such as beta-sheets, helices and turns can determine its physical properties. Wang et al. (2001) reported how beta-sheet changes with change in hydration of gluten protein. In another study, Popineau et al. (1994) reported that in a hydrated gluten protein, containing increasing ratios of gliadins and glutenins, the interaction between glutenin subunits took place via intermolecular beta-sheets because the proportion of intermolecular beta-sheets and alpha-helices increased. In 1999, Belton et al. proposed a "loops-train" model to explain the elasticity of wheat gluten protein. They reported how moisture content determines the formation of secondary structures. In 2006, Georget and Belton studied the effect of temperature on secondary structures of gluten protein under

various hydration conditions. They suggested that dry gluten protein, when exposed to high temperature, does not show any change in its secondary structure, but as the protein is hydrated and heated, changes in the beta-sheet structure occur. They also reported that no permanent changes took place in prolamins at higher temperatures, but they concluded that gluten proteins are conformationally much more sensitive to hydration and heating than other proteins. In this study we have evaluated the effect of externally applied high electric field on the secondary structure conformations of a fully hydrated wheat gluten protein using FT-IR.

Table 9.1: Infrared absorption bands of peptide linkages (Adapted from (Carbonaro and Nucara, 2010; Elliott and Ambrose, 1950; Kong and Yu, 2007; Miyazawa et al., 1956)).

Band	Frequency (cm^{-1})	Description
Amide A	3300	NH stretching
Amide B	3100	NH stretching
Amide I	1690-1600	C=O stretching
Amide II	1575-1480	CN stretching, NH bending
Amide III	1301-1229	CN stretching, NH bending
Amide IV	767-625	OCN bending
Amide V	800-640	Out-of-plane NH bending
Amide VI	606-537	Out-of-plane C=O bending
Amide VII	200	Skeletal torsion

9.3 Materials and Methods

9.3.1 Gluten Protein Sample

Wheat gluten protein was procured from Sigma-Aldrich Canada. The initial moisture content of the gluten protein [7.6 % (wet basis (w.b.))] powder was determined by drying in an oven at 105 °C for 4 h, after which time period weight was constant. The protein sample was fully hydrated (45.65 % moisture content (w.b.)) to replicate the hydration conditions encountered in dough processing by manually mixing it with deionized water. This sample was later subjected to a static high electric field treatment.

9.3.2 Electric Field Treatment

The apparatus utilized to apply the pre-treatment consisted of two parallel electrodes connected to a General Electric Ignition Transformer and a Superior Electric Co. Powerstat adjustable transformer (Figure 9.1). The Powerstat transformer was used to modulate the input AC voltage of the ignition transformer in order to obtain the required electric field strengths of 3.5 and 7 kV/cm between the electrodes. A solid copper wire of diameter 0.05 cm was used as the top electrode and a copper plate was used as the ground electrode. The treatment consisted of placing approximately 1g of the hydrated gluten protein between the electrodes and applying the desired electric field strength of 3.5 and 7 kV/cm for 30, 60 and 90 minutes. The distance between the electrodes was fixed at 1cm and the wire electrode was suspended at approximately 0.8 cm above the sample surface. The samples were then removed and subjected to FT-IR analysis to study structural changes.

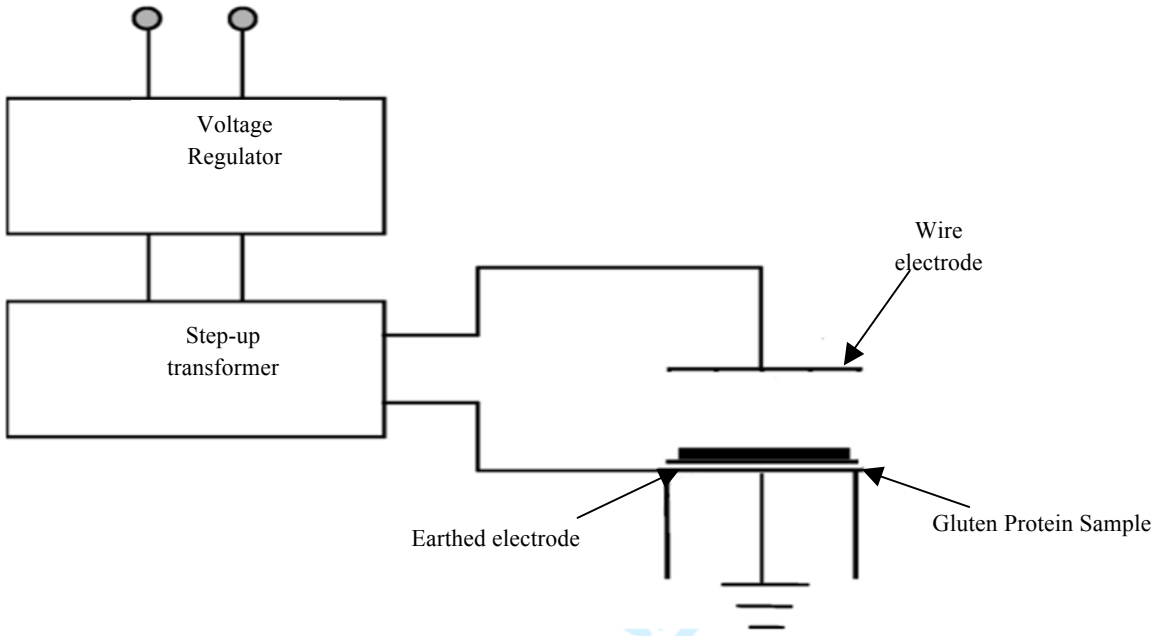

Figure 9.1: Schematic of the static high electric field treatment system.

9.3.3 FT-IR Spectroscopy

FT-IR spectral analysis of gluten protein samples was conducted using Nicolet iS5 ATR-FT-IR spectrometer. The samples were directly applied to the single-reflection diamond ATR (attenuated total reflectance) and pressed down to ensure good contact with the ATR diamond. For each sample, 32 spectra at 4 cm^{-1} resolutions were averaged and the spectra for empty ATR diamond acted as the background reference. The spectra was analyzed using OMNIC software (version 8, Thermo Nicolet Instrument Corp., Madison, WI) and Origin Pro (Version 9, OriginLab Corporation, Northampton, MA, USA) (Georget and Belton, 2006).

9.3.4 Principal Component Analysis

PCA is a widely used chemometric method for data reduction and transformation of data into a new form, which helps to extract relevant information, which is more explicit. PCA helps researchers to obtain a small set of principal components (PC) that can explain the most variability for high dimensional data sets. For this study the principal component analysis with cross validation and cluster analysis (CA), which measures the similarity between samples, were carried out in Unscrambler version 10.3 (Camo Software, AS., Norway) to interpret the FT-IR spectra.

9.4 Results and Discussion

9.4.1 FT-IR Analysis of Conformational Changes in Gluten Protein

In proteins, the Amide I (1700 cm^{-1} -1600 cm^{-1}) region of the IR spectrum is considered as the one of the most sensitive and most useful for secondary structure elucidation (Haris and Severcan, 1999; Kong and Yu, 2007). The Amide I band (Figure 9.2) is the sum of several overlapping component bands including α-helices, β-sheets, β-turns and randomly coiled conformations (Ahmed et al., 2007) which are mainly related to C=O stretching vibrations coupled with the in-plane NH bending. The frequency of this region depends on the nature of the hydrogen bond formed between C=O and NH moieties, which in turn leads to determination of secondary structure backbone configuration and hydrogen bonding patterns (Kong and Yu, 2007). The Amide I band assignment of hydrated gluten protein are presented

in Table 9.2, which are based on previous work (Georget and Belton, 2006; Goormaghtigh et al., 1994; Kong and Yu, 2007; Pelton and McLean, 2000). Figure 9.2 represents a typical FT-IR spectrum of a hydrated wheat gluten protein (4000 cm^{-1} -500 cm^{-1}).

The normalized FT-IR spectra of treated and non-treated hydrated gluten protein revealed that high electric field treatment resulted in irreversible changes in the secondary structures (Figure 9.3). In the Amide I region of the hydrated gluten protein broad shoulders were observed at 1654-1650 cm^{-1}, indicating α-helix conformation. Similar shoulders and minor peaks were observed at 1644 cm^{-1} and 1634 cm^{-1}, indicating presence of random coils and β-sheets (Figure 9.4). For a high electric field treatment of 30 minutes no variation was observed for electric field intensities 0 kV (no treatment) and 7 kV (highest electric field intensity), only at 3.5 kV a slight reorganization and structural conversion of secondary structures was observed. This reorganization may be due to transition of extended structures into α-helices and random coils. Similarly no variation in spectral pattern was observed for all the high electric field treatment at 60 minutes. Our observation of the spectral data revealed that major secondary structure reorganization took place for all electric field treatment at 90 minutes.

Table 9.2: Amide I band frequencies and assignment to protein secondary structure in H_2O media (Adapted from (Georget and Belton, 2006; Goormaghtigh et al., 1994; Kong and Yu, 2007; Pelton and McLean, 2000)).

Secondary structure	**Frequencies (cm^{-1})**	**Average**
α helix	1660-1648	1654
α helix turns	1630	1630
3_{10} Helix	1665-1663	1664
β sheets	1641-1612	1625
	1640-1626	1633
	1697-1670	1682
turns	1684-1662	1673
Random coils	1650-1640	1645

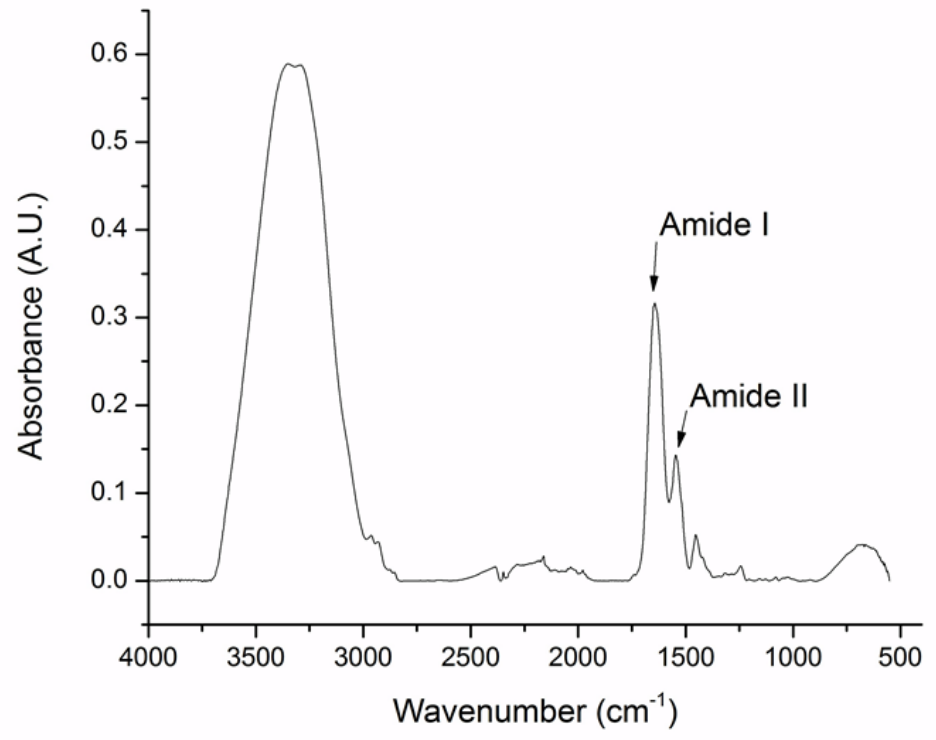

Figure 9.2: Typical FTIR spectra of hydrated wheat gluten protein.

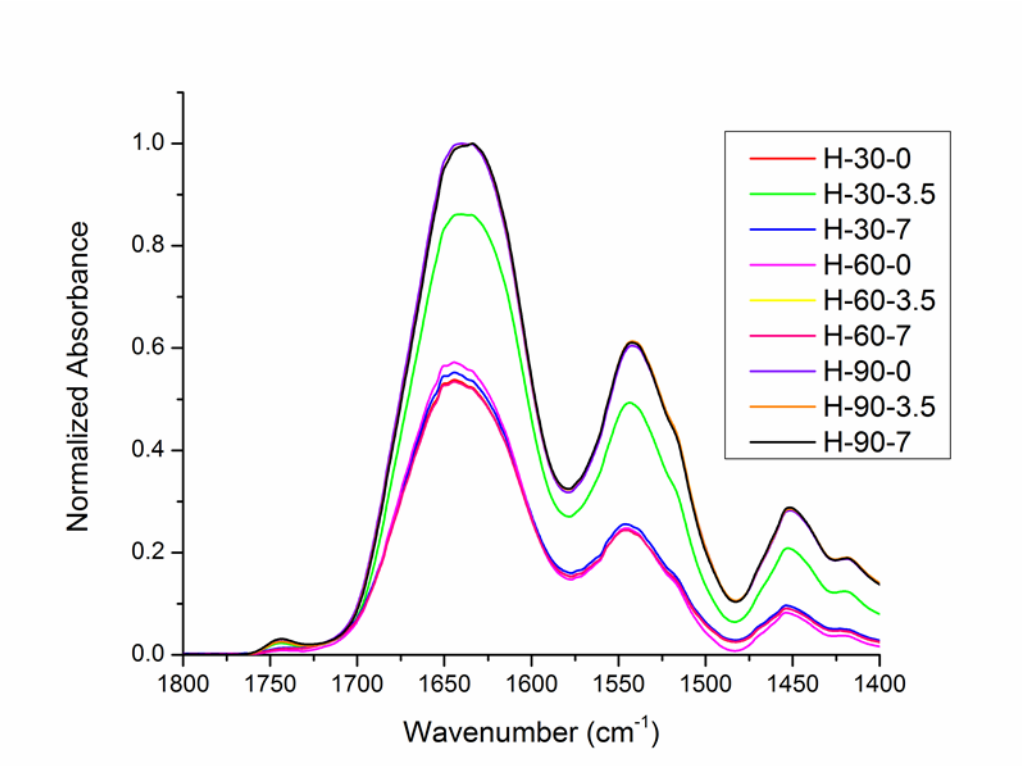

Figure 9.3: FT-IR spectra of hydrated (H) gluten proteins treated with high electric field intensities (0, 3.5 and 7 kV/cm) for set times (30, 60 and 90 minutes)

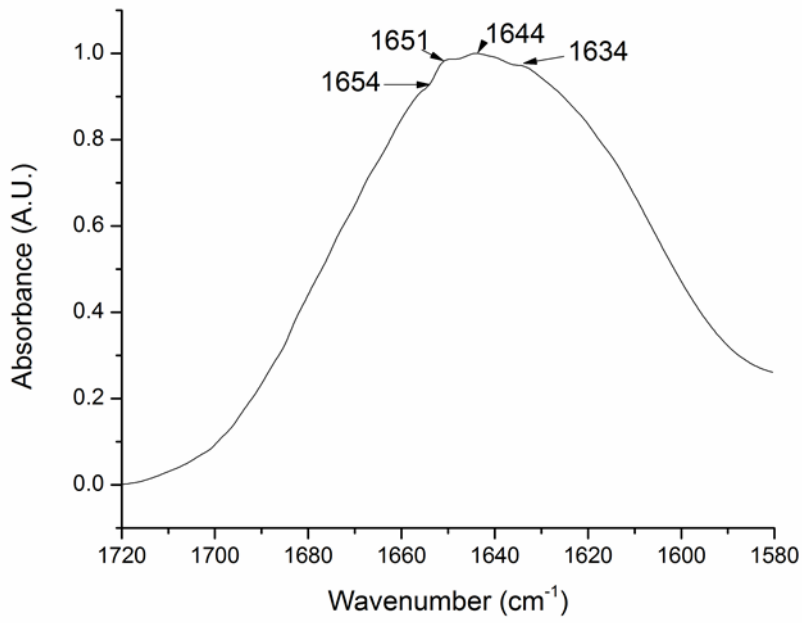

Figure 9.4: Normalized spectra of the Amide I region of hydrated gluten protein

In general it would be expected that as the electric field intensity and treatment time increase, major variations in the secondary structures should normally take place, but this was not the case in the present study. One possible explanation for this observation lies in the effect of the electric field on the texture of the hydrated gluten protein. In the present study the setup used to subject the hydrated gluten protein to electric field treatment was developed for electrohydrodynamic drying of food products. When high voltage is applied to an emitting wire electrode a corona wind is generated that leads to enhancement in drying of food products (Singh et al., 2012). For this setup the velocity of the corona wind is directly proportional to the applied electric field intensity, i.e. the higher the intensity, the more intense is the corona wind; and the longer the sample is subjected to it, the higher the moisture loss would be. Hence we can assume that as the hydrated protein was subjected to the electric field, some moisture would be lost leading to changes in the texture of the gluten protein, i.e. it will hold less moisture than before, and this change in moisture content would also account for variations in the protein structural conformation (Ansari et al., 1992; Halle, 2004). So, as noticed in this study, major structural variations were observed among treatment times; electric field treatment for 90 minutes had significant impact on the

structural conformation as observed by the increase in absorbance intensity (Figure 9.3) as compared to those obtained for 30 and 60 minutes. The reason for minimal spectral absorbance variations between treatment times of 30 and 60 minutes, at all electric field intensities with the exception of treatment at 3.5 kV for 30 minutes, can be attributed to the influence of the electric field on the kinetics of folding and unfolding of the hydrated gluten protein. This theory is still subjected to validation and more intensive work is required to explain the dynamics of protein folding and unfolding under the influence of an external electric field.

To quantify the deviations in the secondary structures in the Amide I band, which consist of overlapped bands, a curve-fitting procedure was applied using Origin Pro (Version 9, OriginLab Corporation, Northampton, MA, USA). Curve-fitting is based on the least-squares minimization procedure, where the software program used attempts to minimize the sum of squares of the difference between the experimental spectra and the computed spectra generated by summation of the component curves (Jackson and Mantsch, 1995; Mangavel et al., 2001). For this study Gaussian band shapes were used to perform the curve-fitting (Figure 9.5) and the component bands were determined using the second derivatives (Figure 9.6) of the normalized FT-IT spectra of the Amide I region.

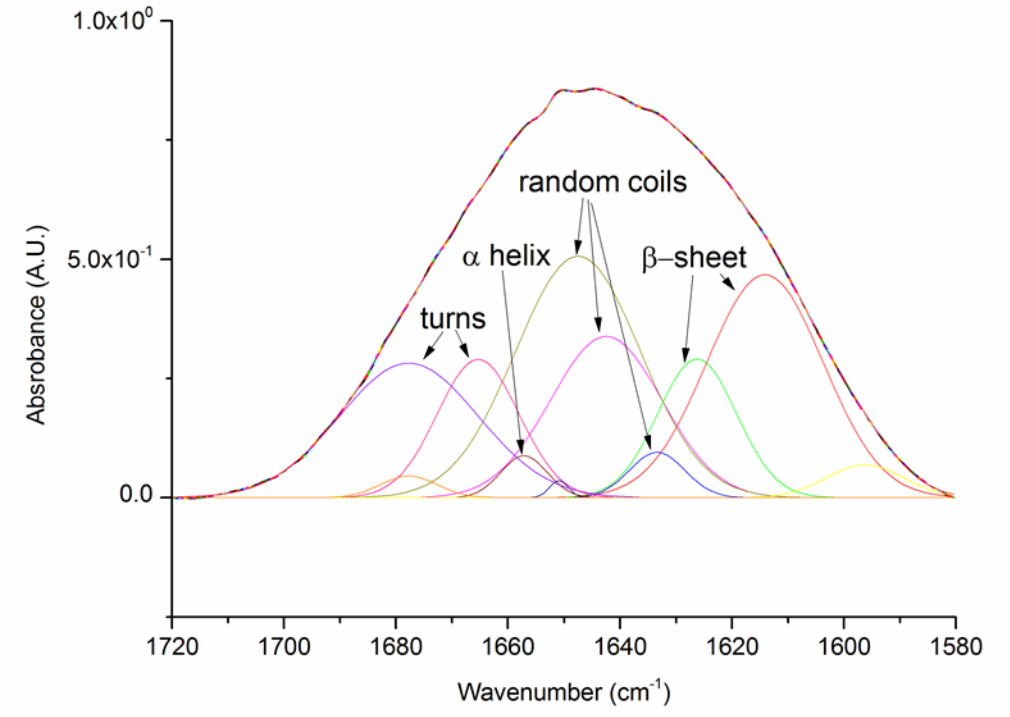

Figure 9.5: Normalized Amide I band of hydrated gluten protein subjected to control conditions of 0kV electric field intensity for 30 minutes fitted with sums of Gaussian bands.

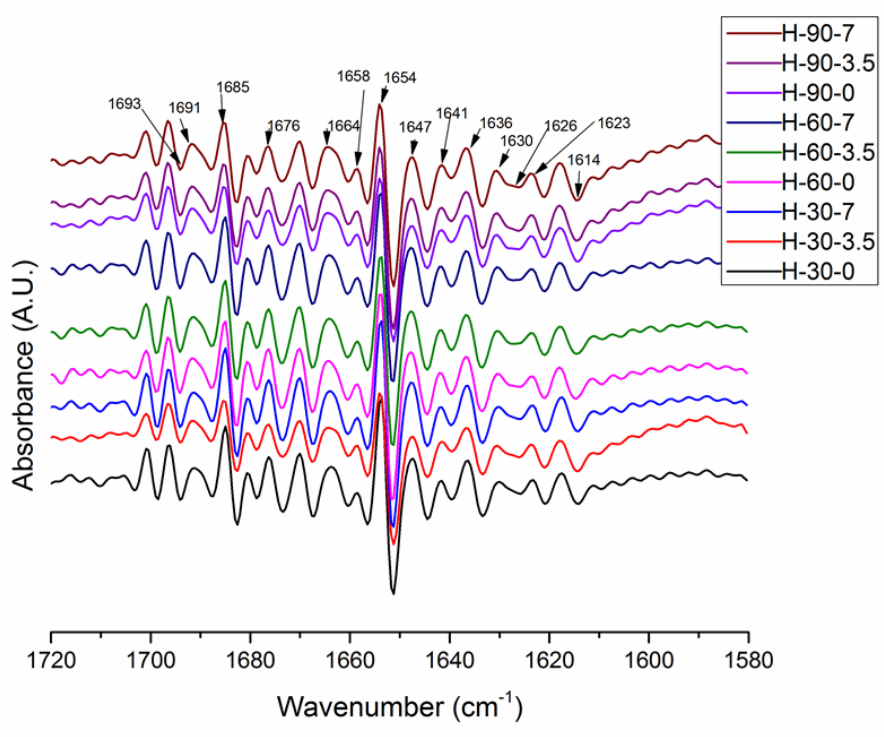

Figure 9.6: Second derivative of normalized spectra showing the valleys and peaks associated with specific secondary structures for all experimental conditions.

Table 9.3 presents the position, relative area and width of the bands fitted to the normalized FT-IR spectra of gluten protein as it was subjected to the varying experimental conditions. From Table 9.3 it was observed that for almost all the experiments conducted for 30 and 90 minutes, random coils and β-sheets were the major secondary structures representing almost 30-40% and 10-15% of the total protein secondary structures respectively. Identification of antiparallel intermolecular hydrogen-bonded β-sheets (1693 cm^{-1}) for the electric field treatment of 30 minutes at 3.5 kV; 60 minutes at 0 kV and 90 minutes at 0-3.5-7 kV revealed the presence of protein aggregates. The 1662-1683 cm^{-1} bands, representing 25-30 % of the total amount of structures, was assigned to secondary structure "turns". The importance of these bands can be related to proline residues in the repetitive domains of the gliadins. In 2001, Mangavel et al. reported that the general features of gliadin film in an FT-IR spectrum are very closely related to wheat gluten protein in its hydrated state. In their analysis of bands fitted to FT-IR deconvoluted spectra of gliadins film dried at different temperatures, they observed bands at 1693 cm^{-1} associated to the presence of antiparallel β-sheets suggesting the presence of protein aggregates.

In the present study, varying influence of experimental conditions on the evolution of secondary structure was observed. For high electric field treatment of 30 minutes at 3.5 kV, the combination of bands at 1650 and 1657.5 cm^{-1}, assigned α-helix, revealed higher relative area (7.12 %) as compared to 1.86 % and 4.91 % obtained for 0 kV and 7 kV treatments. As the treatment time was increased to 60 minutes, no major difference was observed in the relative area of assigned secondary structures except for the presence of antiparallel β-sheets (1693 cm^{-1}) at 0 kV.

With further increase in treatment time to 90 minutes, major variation in the content of α-helical structures of hydrated gluten protein were observed, the relative area obtained were significantly higher compared to treatments conducted for 30 and 60 minutes (10-14% as compared to 1-7%). Figure 9.7 represents the variability in the relative area of protein secondary structures obtained from Gaussian band fitting. It can be observed that for high electric field treatment for 30 minutes at 3.5 kV the relative areas associated with α-helices and β-sheets were higher as compared to 0 kV and 7 kV suggesting that this experimental condition favored α-helices as well as hydrogen bonded β-sheets and antiparallel β-sheets at the expense of random structures and turns. Similar observations can be made for experiments conducted for 60 minutes at 0 kV, where, α-helices were favored more than other secondary structures. As the experimental treatment time was increased to 90 minutes, no major variations were observed between relative areas associated to α-helices and β-sheets but the area values obtained for α-helices were higher compared to other experimental conditions. It is important to know that due to the complexity and amorphous nature of wheat gluten proteins, the understanding of its structural component has been an ongoing battle and only a part of its structural riddle has been solved (Rasheed et al., 2014). As we know that the gluten protein is composed of two component proteins, gliadin (monomeric) and glutenin (polymeric), hence some studies suggest that gluten proteins present a higher ratio of intrinsically disordered regions as compared to structurally organized regions. These observations were supported by studies conducted using circular dichroism, infrared spectroscopy and X-ray scattering (Field et al., 1987; Georget and Belton, 2006; Tatham and Shewry, 1985). In 2013 Singh et al. conducted a molecular dynamic (MD) study on the effect of external electric field on the conformation of gliadin protein. Within the limitation of the MD simulation they suggested that application of an external electric field resulted in changes in the hydrogen bond evolution of gliadin protein and since gliadin protein present

similar structural conformation as a hydrated gluten protein, their result can be validated with the observations made in this study. Appearance of antiparallel β-sheets and increase in the relative areas of α-helices and β-sheets confirm that under the influence of an electric field and depending on the treatment time, the hydrogen bonding pattern of gluten protein leads to the formation of certain secondary structures at the expense of others.

Table 9.3 Positions, width and areas of the bands fitted to the normalized FT-IR spectra of hydrated gluten protein (1720 cm^{-1} – 1580 cm^{-1}) subjected to different electric field intensities and treatment time.

Experimental conditions								
H-30-0			**H-30-3.5**			**H-30-7**		
Pos (cm^{-1})	**Area (%)**	**Width (cm^{-1})**	**Pos (cm^{-1})**	**Area (%)**	**Width (cm^{-1})**	**Pos (cm^{-1})**	**Area (%)**	**Width (cm^{-1})**
1614	21.02	24.51	1615	24.34	24.36	1614	20.88	24.68
1626	8.90	16.62	1625.5	7.62	15.46	1627	9.45	17.95
1633	2.14	11.75	1633	4.05	12.99	1633	0.57	9.04
1642	14.42	23.33	1644	12.14	24.30	1643	16.20	26.99
1647	24.25	26.09	1645	23.17	23.72	1646	23.61	25.81
1650	0.26	4.03	1650	0.10	3.74	1650	0.22	3.78
1657	1.60	9.74	1657.5	7.02	15.22	1658	3.79	12.02
1665	9.21	17.17	1668	12.48	17.85	1667	7.73	15.26
1677	15.14	29.24	1680.5	5.69	16.27	1678	14.10	28.61
			1693	0.87	11.95			

Table 9.3 Continued

Experimental conditions								
H-60-0			**H-60-3.5**			**H-60-7**		
Pos (cm^{-1})	**Area (%)**	**Width (cm^{-1})**	**Pos (cm^{-1})**	**Area (%)**	**Width (cm^{-1})**	**Pos (cm^{-1})**	**Area (%)**	**Width (cm^{-1})**
1615	21.68	24.99	1615	21.79	25.11	1615	22.06	25.07
1629.5	16.49	18.88	1625	10.78	17.97	1623	11.89	14.35
1637	8.06	12.69	1633	0.05	3.62	1633	19.72	19.49
1640	0.13	4.63	1645.5	19.57	17.88	1647	22.04	18.93
1645	10.29	11.37	1651	0.22	3.79	1651	0.21	3.75
1651	0.33	4.25	1657	2.60	9.95	1657	1.01	9.06
1653.5	11.10	13.19	1663	14.55	17.25	1663	18.45	20.07
1662	10.32	16.68	1675.5	5.72	16.76	1677.5	2.25	14.60
1674	17.80	25.13	1683	8.80	25.96	1682	9.99	26.63
1693	1.71	19.72						
H-90-0			**H-90-3.5**			**H-90-7**		
Pos (cm^{-1})	**Area (%)**	**Width (cm^{-1})**	**Pos (cm^{-1})**	**Area (%)**	**Width (cm^{-1})**	**Pos (cm^{-1})**	**Area (%)**	**Width (cm^{-1})**
1613	19.39	21.94	1615	24.33	24.26	1615	24.19	24.07
1626	14.47	17.41	1626	9.75	15.84	1627	10.45	16.26
1634	5.61	13.70	1633	3.57	12.57	1633	2.78	12.23
1643.5	18.08	19.20	1641	12.12	19.18	1641	12.44	20.11
1650.5	0.10	3.73	1645	17.42	22.28	1645	17.52	21.83
1657	10.13	15.98	1651	0.10	3.60	1651	0.10	3.66
1667.5	15.36	19.93	1657	12.37	17.73	1658	12.29	17.41
1682	5.58	16.80	1670	12.81	19.15	1670	12.68	18.89
1693	1.04	12.59	1683	4.21	15.38	1683	3.99	14.73
			1693	0.88	11.34	1693	0.86	11.00

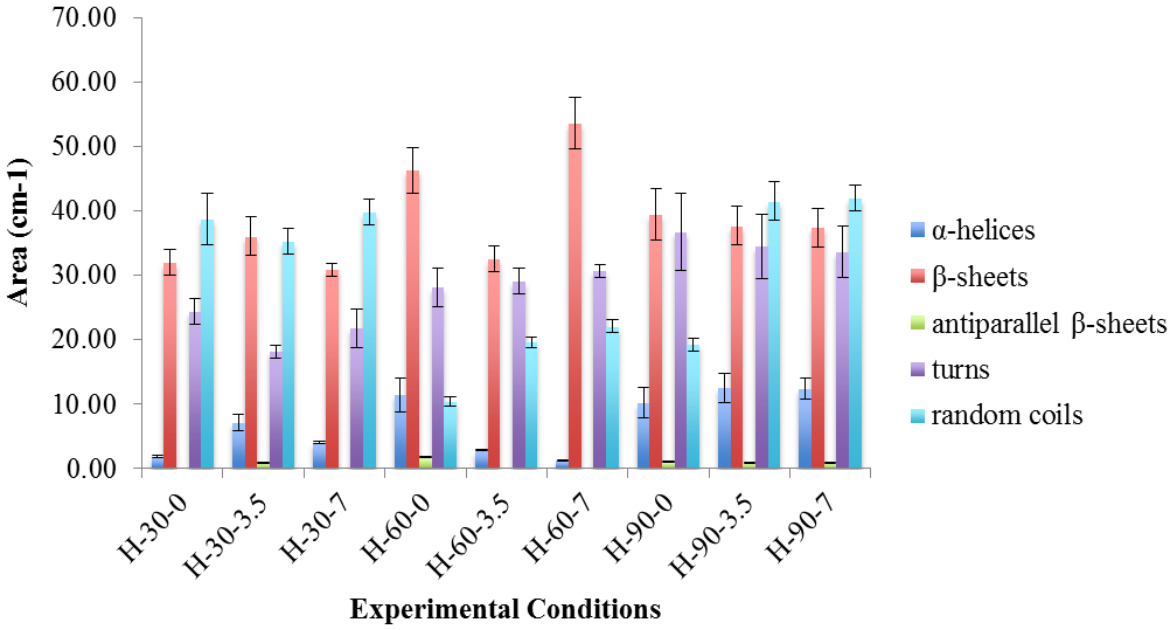

Figure 9.7: Variations in relative areas of the bands fitted to the normalized FT-IT spectra of Amide I region (1720 cm^{-1} – 1580 cm^{-1}) of gluten protein.

9.4.2 PCA Analysis

PCA analysis of the normalized spectral data within 1720-1580 cm^{-1} Amide I region supported the aforementioned findings. PCA was conducted to provide an interpretable overview of the information present in the multidimensional FT-IR datasets. Figure 9.8 present the loading plot obtained from the PCA analysis.

The PCA analysis suggested that principal component 1 (PC1) explained about 98% of the total variability among the samples and principal component 2 (PC2) explained 1%. No variability was observed between the experimental replicates. From PCA score plot (data not shown) it was apparent that all nine sets of sample spectra clustered appropriately with only samples treated under high electric field intensity of 3.5 kV and 7 kV for 60 minutes showing significant overlap. It was also observed that high electric field treatment for 90 minutes under all electric field intensities and one conducted for 30 minutes at 3.5 kV were grouped on the negative side of PC1 suggesting similarities among them and others were grouped along the positive side of PC1.

Analysis of the PCA loadings plot indicated that maximum contribution to the spectral differences was due to the variability between α-helices (1652-1653 cm^{-1}) and the presence of antiparallel β-sheets explained both by PC1 and PC2 (Figure 9.8). PC2 alone was able to

explain the variability in the absorbance of turns (1672 cm^{-1}, 1667 cm^{-1}) and β-sheets (1620 cm^{-1}, 1627 cm^{-1} and 1633 cm^{-1}). A significant limitation for this study was the strength of the electric field applied on the protein sample. Further studies are required with higher electric field intensities in the range of 50-60 kV for significant conformational changes in proteins.

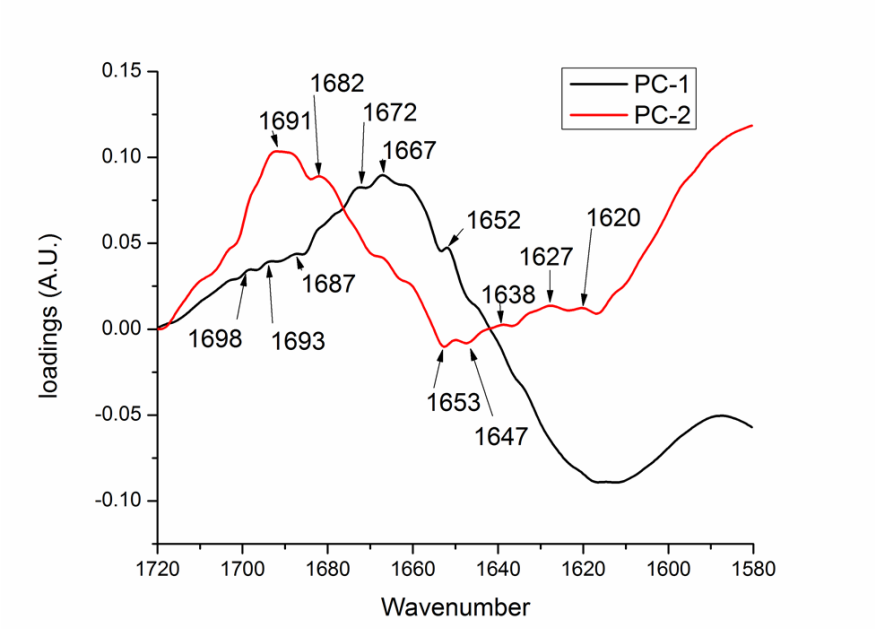

Figure 9.8: PCA loadings plots of the FT-IR spectra in the 1720-1580 cm-1 Amide I region.

9.5 Conclusion

This study clearly showed that protein conformation is influenced by external factors including applied electric field and treatment time. As the treatment time increased the intensity of the Amide I bands (1720-1580 cm^{-1}) increased suggesting conformational changes. The results were further supported by band fitting using Gaussian band shapes and PCA analysis. The observations made in this study suggest that application of an external electric field stress influences the hydrogen bonding pattern of the protein resulting in the occurrence of intramolecular hydrogen-bonded antiparallel β-sheet aggregates. To improve our understanding of the effect of an electric field on gluten protein, further studies need to be conducted with the application of higher electric field intensities in the range of 50-60 kV as they are widely applied in novel food processing techniques such as pulsed electric field and electrohydrodynamic drying.

Chapter 10

Summary, Conclusions, Contribution to Knowledge and Future Work.

10.1 Summary

This thesis pertains to a novel and non-thermal drying process "Electrohydrodynamic (EHD) drying". EHD is a method of inducing electric wind that is generated by gaseous ions under the influence of a high-voltage electric field. Through the review of literatures it was established that corona current increased linearly with an increase in applied voltage (kV) for both positive and negative polarities; and the negative corona discharge produced a larger corona current as compared to a positive corona discharge. It was also revealed that the specific energy consumption increased with an increase in applied voltage for both polarities but was lower when compared to conventional drying processes such as fluidized bed drying, but it was observed that the specific energy consumed by EHD process was lower than that of latent heat of vaporization, indicating the removal of water from the surface of sample by other means in addition to evaporation. Electrode configuration plays an important role in determining the efficiency of the EHD process; the multiple needle electrode configurations had better efficiency than wire and single electrode configuration. The benefit of using EHD for food and bioprocessing due to its unique properties and advantages over conventional drying methods supported the feasibility and applicability of EHD as a suitable alternative for processing thermally sensitive biological materials.

Prior to conducting EHD studies it was important to gain experience and understand the effect of high electric field on food materials. to achieve this goal a study was conducted to evaluate the effect of static high electric field intensity of 4 kV/cm on drying kinetics of microwave-convective and hot air drying systems. The studied electric field intensity had minimal to no effect on the drying kinetics of the potato slices. Less to no curling was observed for high electric field pretreated samples compared to microwave-convective and hot air dried samples. This characteristic was attributed to membrane permeabilization induced by application of high electric field.

After gaining experience in application of high electric field and understanding of EHD drying process at University of Oklahoma an EHD applicator was designed and developed to dry wheat samples. After the design step was complete, the applicability of the EHD system was assessed by conducting an experiment to evaluate the effect of process parameters including electrode gap, applied voltage and cross-flow on drying kinetics of sand. A central composite design was used to evaluate the interactions between the factors and their effect on response variables including, percentage water removed (%), Sherwood Number, EHD Number and Specific energy consumed (kJ/kg). Analysis of results using response surface methodology revealed that maximum drying was obtained at air velocity (2 m/s), electrode gap (1.5 cm) and applied voltage (15 kV). Air velocity and electric field intensity had significant effect on percentage water removed (%) and Sherwood number but in the case of EHD number and specific energy consumed, all process parameters had significant effect. This study also suggested that the EHD drying process in combination with cross-flow will lead to higher drying rate and lower energy consumption under ambient conditions.

Once the effectiveness of the designed EHD applicator was set, EHD drying of wheat sample was conducted. This study investigates the electrohydrodynamic drying characteristics of wheat and its effect on the conformation of wheat protein using Fourier Transform Infrared Spectroscopy (FTIR). It was observed that the drying rate of EHD dried wheat was significantly higher than that of control. A single wire electrode EHD system was used with set electrode gap of 1.5 cm, applied voltages of 10 kV, 12.5 kV and 15 kV in combination with cross-flow with air velocity 1m/s, 1.5 m/s and 2m/s. It was also observed that the drying rate of wheat sample was significantly affected by applied voltage and air velocity. The drying rate increased with an increase in air velocity and applied voltage. The exponential equation showed good agreement with the EHD drying kinetics of wheat.

FT-IR analysis of wheat flour showed that wheat protein conformation was significantly affected by EHD drying. The analysis of Amide I region (1720-1580 cm^{-1}) of wheat protein FT-IR spectra revealed distinct valleys were observed at 1682 - 1686 cm^{-1} (β-sheets), 1674 cm^{-1} (β-sheets), 1664 -1667 cm^{-1} (turns), 1654 - 1657 cm^{-1} (α-helices), 1651 cm^{-1} (α-helices), 1645 - 1647 cm^{-1} (Random coils) and 1633 - 1634 cm^{-1} (β-sheets). Peak fitting using Gaussian band shapes suggested that exposure to electric field influenced the hydrogen bonding pattern of wheat protein resulting in shifts between low and high frequency bands which further supported these results. Thermal analysis of EHD dried wheat sample did not

provide any conclusive results.

To elucidate the effect of external electric field on protein conformation and its surface properties molecular dynamic (MD) modeling approach was applied. The software GROMACS used for MD studies required modification of its code to implement the effect of electric field. As a test run soybean hydrophobic protein enclosed inside a simulated water box was subjected to nominal electric field strengths of 0.002 V/nm and 0.004 V/nm. It was observed that nominal electric field had no major effect on the structure and surface properties of the protein isolate but when higher electric field strength of 3 V/nm was applied significant changes in the protein conformation and solvent accessible surface area were observed. Once the methodology of MD simulation was established for application of electric field stress, wheat gliadin protein was subjected to static electric field of strengths of 0.001 V/nm and 0.002 V/nm. It was observed that the lack of secondary structures in the starting protein ensemble resulted in a non-conclusive result for analysis of surface properties. Hence to validate the effect of electric field, study on hydrogen bond evolution during the course of simulation was conducted. The study revealed that the root mean square deviation, radius of gyration and secondary structure formation, all depend significantly on the number hydrogen bonds formed. Both of the aforementioned studies demonstrated that it is necessary to gain insight into protein dynamics under external electric field stress, in order to develop the novel food processing techniques that can be potentially used towards reducing or eradication of food allergens.

Since MD simulation is conducted within the limitations of computational and statistical mechanics, it is important to validate the findings of the simulation study through an experiment. Hence a FT-IR study was conducted to evaluate the effect of high electric field on secondary structure conformation of fully hydrated (45.7% wet basis) gluten protein. Three experimental conditions were evaluated including electric field intensity of 0 kV (no treatment), 3.5 kV and 7 kV and treatment time of 30, 60 and 90 minutes. FT-IR spectra of treated and non-treated hydrated gluten protein revealed that high electric field treatment resulted in irreversible changes in the secondary structures. In the Amide I region of the hydrated gluten protein broad shoulders were observed at 1654-1650 cm^{-1}, indicating α-helix conformation. Similar shoulders and minor peaks were observed at 1644 cm^{-1} and 1634 cm^{-1}, indicating presence of random coils and β-sheets. For 30 minutes treatment no variation was observed for electric field intensities at 0 kV and 7 kV; but at 3.5 kV it showed slight reorganization and structural conversion of secondary structures. No variation in spectral

pattern was observed for all the high electric field treatments for 60 minutes but major secondary structure reorganization took place for high electric field treatment at 90 minutes. Curve-fitting using Gaussian band shapes and PCA analysis further supported the results. The observations made in this study suggested that application of an external electric field stress influences the hydrogen bonding pattern of the protein resulting in the occurrence of intramolecular hydrogen-bonded antiparallel β-sheet aggregates. The significance of these results was extensively discussed in relevance to the protein structural changes.

10.2 Conclusion

In Part I of this thesis I have explored the mechanisms, applicability and efficiency of electrohydrodynamic drying. A thorough review of available literature was conducted to understand the mechanisms involved in the EHD drying process. It was found that most of the researchers who have studied EHD drying process have used either multiple needle point-plane electrode, single needle point-plane electrodes or wire electrodes; application of parallel plate electrode has been limited to shelf life studies and the mechanisms involved in the generation of an electric wind still need better investigation. The energy efficiency and other advantages, such as low implementation and maintenance costs make EHD an interesting alternative to conventional drying processes. It was also concluded that the specific energy consumed during an EHD drying process is 2-3 times lower than for a conventional drying process such as spouted bed drying. For the development of an industrial scale EHD dryer a thorough life cycle assessment and validation of safety (both operational and environmental) and stability of the EHD dryer at a pilot plant scale is required. A successful assessment of these attributes demands an extensive research on design and application of EHD for varied products from different industrial sectors including food, pharmaceutical, mechanical and chemical industries.

In order to gain experience and investigate the effect of electric field on biological samples, high electric field was applied as a pre-treatment prior to microwave-assisted drying of potato slices. In this study it was observed that pre-treatment had minimal effect on the drying kinetics and effective moisture diffusivity. Microwave-convective drying and hot air drying had significant effect on the color characteristics of potato slices. For textural properties, it was observed that pretreated potato slices were less curled and had uniform

distribution of moisture within the potato slices. The reason for uniform distribution was attributed to pore formation under the influence of the applied electric field, but since a parallel plate electrode was used for the pre-treatment, it was hypothesized that it was just the electric field which had played a role here as no corona wind was generated because of the huge surface area of the parallel plate electrode. It was noted that the quality of the potato slices was very good.

After evaluating the effect of high electric field pretreatment on the microwave assisted drying kinetics of potato slices an electrohydrodynamic drying unit was designed and developed. The unit was used to study the effect of process parameters such as air velocity, electrode gap and applied voltage on EHD drying kinetics and efficiency, using a wire electrode. Standard Ottawa sand was used as the test sample. The sample was completely saturated with known mass of water and EHD drying was conducted. From the study it was concluded that the percentage of water removed was dependent on the strength of the applied electric field (i.e. electric field intensity) and air velocity. It was also observed that the amount of energy (kJ) consumed to dry a kg of water increased linearly with an increase in applied voltage but decreased when air speed was increased, suggesting that EHD drying in combination with a cross flow consumes less energy and provides better drying efficiency. This observation was critical because several researchers have suggested that a cross-flow suppresses the corona wind and will eventually decrease the drying rate. But, in our study we were able to achieve higher drying efficiency when cross flow and electric field intensities were set to the highest value, suggesting that if we intend to use cross-flow, its optimal to use high applied voltage with smallest electrode gap.

From the gained insight into the interaction between the process parameters and the applicability of EHD drying, it was noted that the moisture available for removal was mostly surficial or loosely bound on the surface of the sand sample or between the pores of the sand particles. Hence, we conducted a thorough study to evaluate the effectiveness of EHD on bound moisture as found within biological samples. In this study, wheat was the test sample. The wheat sample was dried using a single wire electrode system and it was observed that the drying rate of wheat samples was significantly affected by applied voltage and air velocity. The drying rate increased with an increase in air velocity and applied voltage as observed for sand samples. The exponential equation showed good agreement with the EHD drying kinetics of wheat. From the results obtained on the drying kinetics of the wheat we

were able to conclude that we can use EHD for drying of biological samples and that electric field intensity and cross-flow used in combination provided the best drying results.

Food processing conditions can have both favorable and detrimental effects on the food constituents. Hence to evaluate the effect of EHD drying of wheat on the wheat protein, Fourier Transform Infrared Spectroscopy was used to study the conformational changes of the protein during the drying process. FT-IR study showed that wheat protein conformation was significantly affected by EHD drying. Analysis of Amide I region of wheat protein FT-IR spectra suggested that exposure to electric field influenced the hydrogen bonding pattern resulting in shifts between low and high frequency bands. Peak fitting using Gaussian band shapes further supported these results. Thermal analysis of EHD dried wheat sample showed some evidence through heat flow changes due to EHD.

In Part II of the thesis, we explored the behavior of food proteins under applied external electric field using Molecular dynamic (MD) modeling approach. Multiple MD simulations were performed to study the effect of an applied external electric field on the conformation and surface properties of food proteins. The first test protein used in this study was soybean hydrophobic protein (SHP). The three-dimensional tertiary structure of the protein was obtained from Protein Data Bank and MD simulations were carried under varying electric field intensities. For soybean protein isolate, we subjected the protein to electric field intensities of 0.002 V/nm, 0.004 V/nm and 3 V/nm. The application of static electric field was shown to affect the behavior of SHP protein as it aligns itself with respect to the direction of the electric field. This alignment was attributed to the coupling between the electric field and the protein's helical dipole moment. Our observation indicates that the effect lower intensity electric field had no major effect on the secondary structures of the protein, but under 3V/nm, the protein unfolded and almost all the helical structures were lost during simulation.

Similar study was performed for wheat gliadin protein. In this study effect of static external electric fields of strength 0.001 V/nm and 0.002 V/nm were evaluated. It was observed that application of an external electric field induced conformational changes in the protein by means of formation of hydrogen bonds between amino acid residues. It was also observed that formation of hydrogen bonds between residues during the course of simulation affected its root mean square deviation and radius of gyration values.

The results obtained from the MD simulation studies suggested that the electric field

affects the flexibility of secondary structures by affecting the hydrogen bonding pattern of the protein. To validate our findings from MD simulation studies we subjected hydrated wheat gluten protein (simulating the conditions used for MD studies) to different electric field intensities for varying amounts of time. From this study we were able to show that protein conformation is influenced by external factors including electric field and treatment time. As the treatment time increased the intensity of the Amide I bands (1720-1580 cm^{-1}) increased suggesting conformational changes. The results were further supported by band fitting using Gaussian band shapes and PCA analysis. The observations made in this study suggest that application of an external electric field stress influences the hydrogen bonding pattern of the protein resulting in the occurrence of intramolecular hydrogen-bonded antiparallel β-sheet aggregates; these observations were similar to those obtained for the MD simulation of gliadin protein, where it was concluded that the external electric field influenced the hydrogen-bonding pattern of the protein.

10.3 Contribution to Knowledge

The major contributions to the knowledge from the study are as follows:

1. Majority of research on electrohydrodynamic (EHD) till date have focused on its applicability alone, but this thesis provides an insight into the mechanism involved and also the relation between the process parameters that define its efficiency.
2. While defining the quality of food, industries focus on the quantity of its constituents such as total protein, total antioxidant etc. but hardly any focus is given on the quality of its constituents. This thesis emphasizes the importance of protein quality as a function of its structure, which governs its functional properties.
3. For the first time, molecular dynamics simulation technique has been applied to gain an insight into the effect of external electrical stress on the structure of food proteins.
4. This thesis also targets wheat gluten protein and shows how application of an external electric field can affect its structure, with a hope of creating a possibility for future work on development of processing techniques targeted at changing the conformation of protein within food products in order to improve digestibility, functional properties and reduce or completely eradicate its ability to induce allergenic responses.

10.4 Future Work

Electrohydrodynamic drying is a novel drying technique and is still at its novice state. In this study we have explored its applicability in the drying of biological samples. However we still require some extensive studies to improve its efficiency and applicability at the industrial scale. Some of the recommendations for future work are given below:

1. Design, development and optimization of an industrial scale EHD applicator.
2. Since corona wind generation depends on the electrode shape, a thorough study needs to be conducted on the performance and application potential of different shaped electrodes.
3. In this thesis the static electric field was introduced using a single wire electrode, to make it more viable for industrial use, we need to evaluate the use of multiple electrode systems, which can be of a single shape or multiple.
4. More biological samples need to studied for better evaluation of drying efficiency of EHD technique and emphasis should be given to all quality attributes.

In this thesis we also explored the applicability of molecular dynamic (MD) simulation to study the effect of external stress on structural and surface properties of food proteins. Based on the findings made in this project, following future works can be conducted:

1. A thorough investigation needs to be carried out to understand the precise nature of the conformational changes that occur in proteins under the influence of external stresses.
2. Effects of other external stresses such as oscillating electric field, chemical and thermal on various food proteins needs to be assessed and results validated.
3. MD technique study of other food constituents such as starch, organic and inorganic compounds needs to be carried out.
4. At present almost all MD simulations are carried out on proteins to study the dynamics and interactions with other proteins. The software used for conducting MD simulations needs to be overhauled to study the interaction between different macromolecules like starch-protein. If this is achieved, we may be able to simulate the whole food and study how food-processing parameters affect the constituents.

Bibliography

1. Official methods of analysis of the Association of official analytical chemists (17th ed.) 2000, AOAC International, Gaithersburg, MD, USA, Official Method 925.10
2. Aghbashlo, M., M. H. Kianmehr, and H. Samimi-Akhijahani. 2008. Influence of drying conditions on the effective moisture diffusivity, energy of activation and energy consumption during the thin-layer drying of berberis fruit (*Berberidaceae*). Energy Convers. Manage.49: 2865–2871.
3. Adcock, S. A. and J. A. McCammon 2006. Molecular dynamics: Survey of methods for simulating the activity of proteins. Chemical Reviews 106: 1589-1615.
4. Ade-Omowaye, B. I. O., N. K. Rastogi, A. Angersbach and D. Knorr 2003. Combined effects of pulsed electric field pre-treatment and partial osmotic dehydration on air drying behaviour of red bell pepper. Journal of Food Engineering 60: 89-98.
5. Ahmed, J., H. S. Ramaswamy, A. Ayad, I. Alli and P. Alvarez 2007. Effect of high-pressure treatment on rheological, thermal and structural changes in Basmati rice flour slurry. Journal of Cereal Science 46: 148-156.
6. Alder, B. J. and T. E. Wainwright 1959a. Studies in molecular dynamics. I. General method. The Journal of Chemical Physics 31: 459-466.
7. Alder, Berni J and TE Wainwright 1959b. Studies in molecular dynamics. I. General method. The Journal of Chemical Physics 31: 459.
8. Alem-Rajabi, A. and F. C. Lai 2005. EHD-enhanced drying of partially wetted glass beads. Drying Technology 23: 597-609.
9. Ames, Jennifer M 1998. Applications of the Maillard reaction in the food industry. Food Chemistry 62: 431-439.
10. Angersbach, A., V. Heinz and D. Knorr 2000. Effects of pulsed electric fields on cell membranes in real food systems. Innovative Food Science and Emerging Technologies 1: 135-149.
11. Ansari, A, CM Jones, ER Henry, J Hofrichter and WA Eaton 1992. The role of solvent viscosity in the dynamics of protein conformational changes. Science 256: 1796-1798.
12. Arevalo, P., M. O. Ngadi, M. I. Bazhal and G. S. V. Raghavan 2004. Impact of pulsed electric fields on the dehydration and physical properties of apple and potato slices.

Drying Technology 22: 1233-1246.

13. Arntfield, S. D. and E. D. Murray 1981. The influence of processing parameters on food protein functionality. I. Differential scanning calorimetry as an indicator of protein denaturation. Can. Inst. Food Sci. Technol. J. 14: 289-294.
14. Asakawa, Y. 1976. Promotion and retardation of heat transfer by electric fields. Nature 261: 220-221.
15. Astrakas, L. G., C. Gousias and M. Tzaphlidou 2012. Structural destabilization of chignolin under the influence of oscillating electric fields. Journal of Applied Physics 111.
16. Astrakas, L., C. Gousias and M. Tzaphlidou 2011a. Electric field effects on chignolin conformation. Journal of Applied Physics 109.
17. Astrakas, Loukas, Christos Gousias and Margaret Tzaphlidou 2011b. Electric field effects on chignolin conformation. Journal of Applied Physics 109: 094702-094702-094705.
18. Atungulu, G., Y. Nishiyama and S. Koide 2004. Respiration and climacteric patterns of apples treated with continuous and intermittent direct current electric field. Journal of Food Engineering 63: 1-8.
19. Bai, Y. X. and B. Sun 2011. Study of electrohydrodynamic (EHD) drying technique for shrimps. Journal of Food Processing and Preservation 35: 891-897.
20. Bai, Y., B. Sun and G. Yang 2011. Drying characteristics of Spanish mackerel during electrohydrodynamic (EHD) drying. In Drying characteristics of Spanish mackerel during electrohydrodynamic (EHD) drying.
21. Bajgai, T. R. and F. Hashinaga 2001a. Drying of spinach with a high electric field. Drying Technology 19: 2331-2341.
22. Bajgai, T. R. and F. Hashinaga 2001b. High electric field drying of Japanese radish. Drying Technology 19: 2291-2302.
23. Bajgai, T. R., F. Hashinaga, S. Isobe, G. S. Vijaya Raghavan and M. O. Ngadi 2006a. Application of high electric field (HEF) on the shelf-life extension of emblic fruit (Phyllanthus emblica L.). Journal of Food Engineering 74: 308-313.
24. Bajgai, T. R., G. S. V. Raghavan, F. Hashinaga and M. O. Ngadi 2006b. Electrohydrodynamic drying - A concise overview. Drying Technology 24: 905-910.
25. Bajgai, Tirtha R., G. S. Vijaya Raghavan, Fumio Hashinaga and Michael O. Ngadi 2006c. Electrohydrodynamic Drying—A Concise Overview. Drying Technology 24:

905-910.

26. Balasubramaniam, VM and D Farkas 2008. High-pressure food processing. Food Science and Technology International 14: 413-418.
27. Balcer, B. E. and F. C. Lai 2004. EHD-enhanced drying with multiple-wire electrode. Drying Technology 22: 821-836.
28. Ball Jr, Hershell R, Mohammad-HH Samimi and Kenneth R Swartzel 1997. Method for the pasteurization of egg products using radio waves. In Method for the pasteurization of egg products using radio waves: Google Patents.
29. Barthakur, N. N. 1989. Electrostatic method of drying saline water. Drying Technology 7: 503-521.
30. Barthakur, N. N. 1990. Electrohydrodynamic enhancement of evaporation from NaCl solutions. Desalination 78: 455-465.
31. Barthakur, N. N. and T. Al-Kanani 1989. Impact of air ions of both polarity on evaporation of certain organic and inorganic liquids. International Journal of Biometeorology 33: 136-141.
32. Basiry, M. and A. Esehaghbeygi 2010. Electrohydrodynamic (EHD) drying of rapeseed (Brassica napus L.). Journal of Electrostatics 68: 360-363.
33. Bekes, F., L. Tamas, P. W. Gras, P. R. Shewry, O. Anderson and R. Appels 1998. Functional domain within the glutenin subunits of wheat. Proceedings of the 9th International Wheat Genetics Symposium 4: 136-138.
34. Bekker, H., E. J. Dijkstra, M. K. R. Renardus and H. J. C. Berendsen 1995. An Efficient, Box Shape Independent Non-Bonded Force and Virial Algorithm for Molecular Dynamics. Mol. Simul. 14: 137-151.
35. Belton, P. S. 1999. On the elasticity of wheat gluten. Journal of Cereal Science 29: 103-107.
36. Belton, P. S., I. J. Colquhoun, A. Grant, N. Wellner, J. M. Field, P. R. Shewry and A. S. Tatham 1995. FTIR and NMR studies on the hydration of a high-Mr subunit of glutenin. International Journal of Biological Macromolecules 17: 74-80.
37. Berendsen, H. J. C., J. P. M. Postma, W. F. Van Gunsteren, A. Dinola and J. R. Haak 1984. Molecular dynamics with coupling to an external bath. The Journal of Chemical Physics 81: 3684-3690.
38. Bouraoui, M., P. Richard and T. Durance 1994. Microwave and convective drying of potato slices. Journal of Food Process Engineering 17: 353-363.

39. Bracken, T. D. 1987. Small air ion properties. In Air Ions: Physical and Biological Aspects. Jonathan, M. J. M.; Kavet, R., Eds, CRC Press, Boca Raton, FL: 1-12
40. Breiteneder, Heimo and Christian Radauer 2004. A classification of plant food allergens. Journal of Allergy and Clinical Immunology 113: 821-830.
41. Brooks, B. R., R. E. Bruccoleri, B. D. Olafson, D. J. States, S. Swaminathan and M. Karplus 1983. CHARMM: A program for macromolecular energy, minimization, and dynamics calculations. J. Comput. Chem. 4: 187-217.
42. Budi, A., F. S. Legge, H. Treutlein and I. Yarovsky 2008. Comparative study of insulin chain-B in isolated and monomeric environments under external stress. Journal of Physical Chemistry B 112: 7916-7924.
43. Budi, A., S. Legge, H. Treutlein and I. Yarovsky 2004. Effect of external stresses on protein conformation: A computer modelling study. European Biophysics Journal 33: 121-129.
44. Budi, Akin, F. Sue Legge, Herbert Treutlein and Irene Yarovsky 2007. Effect of Frequency on Insulin Response to Electric Field Stress. The Journal of Physical Chemistry B 111: 5748-5756.
45. Budi, Akin, F. Sue Legge, Herbert Treutlein and Irene Yarovsky 2005. Electric Field Effects on Insulin Chain-B Conformation. The Journal of Physical Chemistry B 109: 22641-22648.
46. Caixeta, A. T., R. Moreira and M. E. Castell-Perez 2002. Impingement drying of potato chips. Journal of Food Process Engineering 25: 63-90.
47. Califano, A. N. and A. Calvelo 1987. Adjustment of surface concentration of reducing sugars before frying of potato strips. Journal of Food Processing and Preservation 12: 1-9.
48. Cao, W., Y. Nishiyama and S. Koide 2004a. Electrohydrodynamic drying characteristics of wheat using high voltage electrostatic field. Journal of Food Engineering 62: 209-213.
49. Cao, W., Y. Nishiyama, S. Koide and Z. H. Lu 2004b. Drying enhancement of rough rice by an electric field. Biosystems Engineering 87: 445-451.
50. Case, D. A., T. E. Cheatham Iii, T. Darden, H. Gohlke, R. Luo, K. M. Merz Jr, A. Onufriev, C. Simmerling, B. Wang and R. J. Woods 2005. The Amber biomolecular simulation programs. Journal of computational chemistry 26: 1668-1688.
51. Chand, N. and A. A. Mihas 2006. Celiac disease: Current concepts in diagnosis and treatment. Journal of Clinical Gastroenterology 40: 3-14.

52. Chen, Y. H. and N. N. Barthakur 1991. Potato slab dehydration by air ions from corona discharge. International Journal of Biometeorology 35: 67-70.
53. Chen, Y., N. N. Barthakur and N. P. Arnold 1994. Electrohydrodynamic (EHD) drying of potato slabs. Journal of Food Engineering 23: 107-119.
54. Christen, M., P. H. Hünenberger, D. Bakowies, R. Baron, R. Bürgi, D. P. Geerke, T. N. Heinz, M. A. Kastenholz, V. Kräutler, C. Oostenbrink, C. Peter, D. Trzesniak and W. F. Van Gunsteren 2005. The GROMOS software for biomolecular simulation: GROMOS05. Journal of computational chemistry 26: 1719-1751.
55. Colombo, Marcio F, Donald C Rau and V Adrian Parsegian 1992. Protein solvation in allosteric regulation: a water effect on hemoglobin. Science 256: 655-659.
56. Corey, Robert B and Linus Pauling 1953. Molecular models of amino acids, peptides, and proteins. Review of Scientific Instruments 24: 621-627.
57. Crank, J. 1975. The Mathematics of Diffusion. 2nd Ed.; Clarendon, Oxford
58. Damodaran, S. 1994. Structure-function relationship of food proteins. Protein Functionality in Food Systems: 1-37.
59. Damodaran, Srinivasan and Alain Paraf 1997. Food proteins and their applications: CRC Press.
60. Davidson, J. H. and E. J. Shaughnessy 1986. Turbulence generation by electric body forces. Experiments in Fluids 4: 17-26.
61. De Pomerai, D. I., B. Smith, A. Dawe, K. North, T. Smith, D. B. Archer, I. R. Duce, D. Jones and E. P. M. Candido 2003. Microwave radiation can alter protein conformation without bulk heating. FEBS letters 543: 93-97.
62. Debnath, S., K. K. Bhat and N. K. Rastogi 2003. Effect of pre-drying on kinetics of moisture loss and oil uptake during deep fat frying of chickpea flour-based snack food. LWT - Food Science and Technology 36: 91-98.
63. Delben, F. and Crescenzi, V. 1969. Thermal denaturation of lysozyme. A differential scanning calorimetry investigation. Biochimica et Biophysica Acta 194: 615.
64. Denmat, M, M Anton and G Gandemer 1999. Protein denaturation and emulsifying properties of plasma and granules of egg yolk as related to heat treatment. Journal of Food Science 64: 194-197.
65. Dev, S. R. S., G. S. V. Raghavan and Y. Gariepy 2008b. Dielectric properties of egg components and microwave heating for in-shell pasteurization of eggs. Journal of Food Engineering 86: 207-214.

66. Dev, S. R. S., T. Padmini, A. Adedeji, Y. Gariépy and G. S. V. Raghavan 2008a. A comparative study on the effect of chemical, microwave, and pulsed electric pretreatments on convective drying and quality of raisins. Drying Technology 26: 1238-1243.
67. Dunker, A. K., C. J. Brown, J. D. Lawson, L. M. Iakoucheva and Z. Obradović 2002. Intrinsic disorder and protein function. Biochemistry 41: 6573-6582.
68. Dutta, B., G. S. V. Raghavan, S. R. S. Dev, P. Liplap, R. Murugesan, K. Anekella and T. Kaushal 2012. A Comparative Study on the Effects of Microwave and High Electric Field Pretreatments on Drying Kinetics and Quality of Mushrooms. Drying Technology 30: 891-897.
69. Eigenmann, P. A. 2009. Mechanisms of food allergy. Pediatric Allergy and Immunology 20: 5-11.
70. Eisenberg, David 2003. The discovery of the α-helix and β-sheet, the principal structural features of proteins. Proceedings of the National Academy of Sciences 100: 11207-11210.
71. Eliasson, A. C. and P. O. Hegg 1980. Thermal stability of wheat gluten. Cereal Chem. 57: 436-437.
72. Elizabeth, P., S. Tibor and M. Arun 2006. Spouted bed drying. Handbook of Industrial Drying: 453-488.
73. Esehaghbeygi, A. and M. Basiry 2011. Electrohydrodynamic (EHD) drying of tomato slices (Lycopersicon esculentum). Journal of Food Engineering 104: 628-631.
74. Fabiola, F., R. Bertram, A. Korostelev and M. S. Chapman 2002. An improved hydrogen bond potential: Impact on medium resolution protein structures. Protein Science 11: 1415-1423.
75. Fenimore, P. W., H. Frauenfelder, B. H. McMahon and F. G. Parak 2002. Slaving: Solvent fluctuations dominate protein dynamics and functions. Proceedings of the National Academy of Sciences 99: 16047-16051.
76. Fernandez-Diaz, M. D., L. Barsotti, E. Dumay and J. C. Cheftel 2000. Effects of pulsed electric fields on ovalbumin solutions and dialyzed egg white. Journal of Agricultural and Food Chemistry 48: 2332-2339.
77. Fincan, M. and P. Dejmek 2003. Effect of osmotic pretreatment and pulsed electric field on the viscoelastic properties of potato tissue. Journal of Food Engineering 59: 169-175.
78. Fincan, M., F. DeVito and P. Dejmek 2004. Pulsed electric field treatment for solid-

liquid extraction of red beetroot pigment. Journal of Food Engineering 64: 381-388.
79. Froning, Glenn W and United Egg Producers 2002. International egg pasteurization manual: United Egg Producers.
80. Fruton, Joseph S 1972. Molecules and life. Wiley Interscience
81. Garayo, Jagoba and Rosana Moreira 2002. Vacuum frying of potato chips. Journal of Food Engineering 55: 181-191.
82. Georget, D. M. R. and P. S. Belton 2006a. Effects of temperature and water content on the secondary structure of wheat gluten studied by FTIR spectroscopy. Biomacromolecules 7: 469-475.
83. Georget, Dominique MR and Peter S Belton 2006b. Effects of temperature and water content on the secondary structure of wheat gluten studied by FTIR spectroscopy. Biomacromolecules 7: 469-475.
84. Gilquin, Bernard, Christophe Guilbert and David Perahia 2000. Unfolding of hen egg lysozyme by molecular dynamics simulations at 300K: Insight into the role of the interdomain interface. Proteins: Structure, Function, and Bioinformatics 41: 58-74.
85. Goodenough, T. I. J., P. W. Goodenough and S. M. Goodenough 2007. The efficiency of corona wind drying and its application to the food industry. Journal of Food Engineering 80: 1233-1238.
86. Goormaghtigh, E., V. Cabiaux and J. M. Ruysschaert 1994. Determination of soluble and membrane protein structure by Fourier transform infrared spectroscopy. III. Secondary structures. Sub-cellular biochemistry 23: 405-450.
87. Granda, C., R. G. Moreira and S. E. Tichy 2004. Reduction of acrylamide formation in potato chips by low-temperature vacuum frying. Journal of Food Science 69: E405-E411.
88. Grubmüller, Helmut, Helmut Heller, Andreas Windemuth and Klaus Schulten 1991. Generalized Verlet algorithm for efficient molecular dynamics simulations with long-range interactions. Molecular Simulation 6: 121-142.
89. Gu, Jenny and Philip E Bourne 2009. Structural bioinformatics: John Wiley & Sons.
90. Halle, Bertil 2004. Protein hydration dynamics in solution: a critical survey. Philosophical Transactions of the Royal Society of London. Series B: Biological Sciences 359: 1207-1224.
91. Han, Z. and H. Fumio 1997. Effect of high electric field on the quality of satsuma mandarin fruits. Journal of Shita 9: 107-113.

92. Han, Zhong, Xin-an Zeng, Ben-shan Zhang and Shu-juan Yu 2009. Effects of pulsed electric fields (PEF) treatment on the properties of corn starch. Journal of Food Engineering 93: 318-323.
93. Haris, P. I. and F. Severcan 1999. FTIR spectroscopic characterization of protein structure in aqueous and non-aqueous media. Journal of Molecular Catalysis - B Enzymatic 7: 207-221.
94. Hart, F. X. and Ch H. Bachman 1968. The effect of air ions on liquid evaporation rates. International Journal of Biometeorology 12: 251-261.
95. Harwalkar, V. R. and C. Y. Ma 1987. Study of thermal properties of oat globulin by differential scanning calorimetry. J. Food Sci. 52: 394-398.
96. Hashinaga, F., T. R. Bajgai, S. Isobe and N. N. Barthakur 1999. Electrohydrodynamic (EHD) drying of apple slices. Drying Technology 17: 479-495.
97. Heinig, M. and D. Frishman 2004. STRIDE: A web server for secondary structure assignment from known atomic coordinates of proteins. Nucleic Acids Research 32: W500-W502.
98. Henderson, Kate N., Jason A. Tye-Din, Hugh H. Reid, Zhenjun Chen, Natalie A. Borg, Tim Beissbarth, Arthur Tatham, Stuart I. Mannering, Anthony W. Purcell, Nadine L. Dudek, David A. van Heel, James McCluskey, Jamie Rossjohn and Robert P. Anderson 2007. A Structural and Immunological Basis for the Role of Human Leukocyte Antigen DQ8 in Celiac Disease. Immunity 27: 23-34.
99. Humphrey, W., A. Dalke and K. Schulten 1996. VMD: Visual molecular dynamics. Journal of molecular graphics 14: 33-38.
100. Jackson, M. and H. H. Mantsch 1995. The use and misuse of FTIR spectroscopy in the determination of protein structure. Critical Reviews in Biochemistry and Molecular Biology 30: 95-120.
101. Jafar Dalvand, Mohammad, Seyed Saeid Mohtasebi and Shahin Rafiee 2013. Effect of needle number on drying rate of kiwi fruit in EHD drying process. Agricultural Sciences 4.
102. Joyce, I. Boye and S. H. Rajamohamed 2009. Novel Techniques for the Processing of Soybeans. In Novel Food Processing, 373-401: CRC Press.
103. Kalé, L., R. Skeel, M. Bhandarkar, R. Brunner, A. Gursoy, N. Krawetz, J. Phillips, A. Shinozaki, K. Varadarajan and K. Schulten 1999. NAMD2: Greater Scalability for Parallel Molecular Dynamics. Journal of Computational Physics 151: 283-312.

104. Karino, Yasuhito and Nobuyuki Matubayasi 2011. Communication: Free-energy analysis of hydration effect on protein with explicit solvent: Equilibrium fluctuation of cytochrome c. The Journal of Chemical Physics 134
105. Karplus, Martin and J Andrew McCammon 2002. Molecular dynamics simulations of biomolecules. Nature Structural & Molecular Biology 9: 646-652.
106. Kharel, G. P. and F. Hashinaga 1996. Effect of high electric field on shelf life of strawberries. Food Sci. Technol. Int. 2: 198-202.
107. Kharel, G. P., F. Hashinaga and R. Shintani 1996. Effect of high electric field on some fruits and vegetables. Journal of the Japanese Society of Cold Food Preservation 22: 17-22.
108. Kinsella, J. E. 1979. Functional properties of soy proteins. Journal of the American Oil Chemists' Society 56: 242-258.
109. Koltun, Walter L. 1965. Precision space-filling atomic models. Biopolymers 3: 665-679.
110. Kong, J. and S. Yu 2007. Fourier transform infrared spectroscopic analysis of protein secondary structures. Acta Biochimica et Biophysica Sinica 39: 549-559.
111. Kortemme, Tanja, Alexandre V. Morozov and David Baker 2003. An Orientation-dependent Hydrogen Bonding Potential Improves Prediction of Specificity and Structure for Proteins and Protein–Protein Complexes. Journal of Molecular Biology 326: 1239-1259.
112. Kulacki, F. A. and J. A. Daumenmier 1978. A preliminary study of electrohydrodynamic augmented baking. Journal of Electrostatics 5: 325-336.
113. Lai, F. C. 2010. A prototype of EHD-enhanced drying system. Journal of Electrostatics 68: 101-104.
114. Lai, F. C. and D. S. Wong 2003. EHD-enhanced drying with needle electrode. Drying Technology 21: 1291-1306.
115. Lai, F. C. and K. W. Lai 2002. EHD-Enhanced drying with wire electrode. Drying Technology 20: 1393-1405.
116. Lai, F. C. and R. K. Sharma 2005. EHD-enhanced drying with multiple needle electrode. Journal of Electrostatics 63: 223-237.
117. Lai, F. C., P. J. McKinney and J. H. Davidson 1995. Oscillatory electrohydrodynamic gas flows. Journal of Fluids Engineering, Transactions of the ASME 117: 491-497.
118. Laurence, J. A., P. W. French, R. A. Lindner and D. R. McKenzie 2000. Biological

effects of electromagnetic fields - Mechanisms for the effects of pulsed microwave radiation on protein conformation. Journal of Theoretical Biology 206: 291-298.

119. Lebovka, N. I., I. Praporscic, S. Ghnimi and E. Vorobiev 2005. Temperature enhanced electroporation under the pulsed electric field treatment of food tissue. Journal of Food Engineering 69: 177-184.

120. Lebovka, N. I., M. I. Bazhal and E. Vorobiev 2000. Simulation and experimental investigation of food material breakage using pulsed electric field treatment. Journal of Food Engineering 44: 213-223.

121. Lebovka, N. I., M. I. Bazhal and E. Vorobiev 2001. Pulsed electric field breakage of cellular tissues: Visualisation of percolative properties. Innovative Food Science and Emerging Technologies 2: 113-125.

122. Lebovka, N. I., N. V. Shynkaryk and E. Vorobiev 2007. Pulsed electric field enhanced drying of potato tissue. Journal of Food Engineering 78: 606-613.

123. Leeratanarak, N., S. Devahastin and N. Chiewchan 2006. Drying kinetics and quality of potato chips undergoing different drying techniques. Journal of Food Engineering 77: 635-643.

124. Leimkuhler, B. J. 1994. Symplectic numerical integrators in constrained Hamiltonian systems. Journal of Computational Physics 112: 117-125.

125. Leon, A., C. M. Rosell and C. B. De Barber 2003. A differential scanning calorimetry study of wheat proteins. European Food Research and Technology 217: 13-16.

126. Levy, Yaakov and José N. Onuchic 2004. Water and proteins: A love–hate relationship. Proceedings of the National Academy of Sciences of the United States of America 101: 3325-3326.

127. Li, F. D., L. T. Li, J. F. Sun and E. Tatsumi 2005. Electrohydrodynamic (EHD) drying characteristic of okara cake. Drying Technology 23: 565-580.

128. Li, F. D., L. T. Li, J. F. Sun and E. Tatsumi 2006. Effect of electrohydrodynamic (EHD) technique on drying process and appearance of okara cake. Journal of Food Engineering 77: 275-280.

129. Lindahl, E., B. Hess and D. van der Spoel 2001. GROMACS 3.0: A package for molecular simulation and trajectory analysis. Journal of Molecular Modeling 7: 306-317.

130. Ma, C. Y. 1990. Thermal analysis of vegetable proteins and vegetable protein-based food products. Thermal Analysis of Food: 149-167.

131. Maiuri, L., C. Ciacci, I. Ricciardelli, L. Vacca, V. Raia, S. Auricchio, J. Picard, M.

Osman, S. Quaratino and M. Londei 2003. Association between innate response to gliadin and activation of pathogenic T cells in coeliac disease. Lancet 362: 30-37.

132. Mangavel, C., J. Barbot, Y. Popineau and J. Guéguen 2001. Evolution of wheat gliadins conformation during film formation: A Fourier transform infrared study. Journal of Agricultural and Food Chemistry 49: 867-872.

133. Mark, Alan E. and Wilfred F. Van Gunsteren 1992. Simulation of the thermal denaturation of hen egg white lysozyme: trapping the molten globule state. Biochemistry 31: 7745-7748.

134. Mata, I., E. Molins, I. Alkorta and E. Espinosa 2009. Effect of an external electric field on the dissociation energy and the electron density properties: The case of the hydrogen bonded dimer HF···HF. Journal of Chemical Physics 130.

135. Meade, Susie J, Elizabeth A Reid and Juliet A Gerrard 2005. The impact of processing on the nutritional quality of food proteins. Journal of AOAC International 88: 904-922.

136. Micaêlo, Nuno M. and Cláudio M. Soares 2007. Modeling hydration mechanisms of enzymes in nonpolar and polar organic solvents. FEBS Journal 274: 2424-2436.

137. Micard, V. and S. Guilbert 2000. Thermal behavior of native and hydrophobized wheat gluten, gliadin and glutenin-rich fractions by modulated DSC. International Journal of Biological Macromolecules 27: 229-236.

138. Min, BR, KC Nam, EJ Lee, GY Ko, DW Trampel and DU Ahn 2005. Effect of irradiating shell eggs on quality attributes and functional properties of yolk and white. Poultry science 84: 1791-1796.

139. Mobley, David L., Christopher I. Bayly, Matthew D. Cooper, Michael R. Shirts and Ken A. Dill 2009. Small Molecule Hydration Free Energies in Explicit Solvent: An Extensive Test of Fixed-Charge Atomistic Simulations. Journal of chemical theory and computation 5: 350-358.

140. Nair, GR, P. Liplap, Y. Gariepy and GSV Raghavan 2011. Microwave Drying of Flax Fibre at Controlled Temperatures. Journal of Agricultural Science and Technology B 1: 9-21.

141. Ogata, J. and A. Yabe 1993. Augmentation of boiling heat transfer by utilizing the EHD effect-EHD behaviour of boiling bubbles and heat transfer characteristics. International Journal of Heat and Mass Transfer 36: 783-791.

142. Ortolani, C. and E. A. Pastorello 2006. Food allergies and food intolerances. Best Practice and Research: Clinical Gastroenterology 20: 467-483.

143. Palanimuthu, V., P. Rajkumar, V. Orsat, Y. Gariépy and G. S. V. Raghavan 2009. Improving cranberry shelf-life using high voltage electric field treatment. Journal of Food Engineering 90: 365-371.

144. Panofsky, W. K. H. and M. Phillips 1962. Classical Electricity and Magnetism.

145. Paschkewitz, J. S. and D. M. Pratt 2000. The influence of fluid properties on electrohydrodynamic heat transfer enhancement in liquids under viscous and electrically dominated flow conditions. Experimental Thermal and Fluid Science 21: 187-197.

146. Pedreschi, F. and P. Moyano 2005. Effect of pre-drying on texture and oil uptake of potato chips. LWT - Food Science and Technology 38: 599-604.

147. Pelton, J. T. and L. R. McLean 2000. Spectroscopic methods for analysis of protein secondary structure. Analytical Biochemistry 277: 167-176.

148. Pereira, R. N. and A. A. Vicente 2010. Environmental impact of novel thermal and non-thermal technologies in food processing. Food Research International 43: 1936-1943.

149. Petersen, H. G. 1995. Accuracy and efficiency of the particle mesh Ewald method. The Journal of Chemical Physics 103: 3668-3679.

150. Popineau, Y., S. Bonenfant, M. Cornec and M. Pezolet 1994. A Study by Infrared Spectroscopy of the Conformations of Gluten Proteins Differing in their Gliadin and Glutenin Compositions. Journal of Cereal Science 20: 15-22.

151. Pravisani, C. I. and A. Calvelo 1986. Minimum cooking time for potato strip frying. Journal of Food Science 51: 614-617.

152. Privalov, P. L. and Khechinashvili, N. N. 1974. A thermodynamic approach to the problem of stabilization of globular protein structure: a calorimetric study. Journal of Molecular Biology 86: 665.

153. Puppo, C., N. Chapleau, F. Speroni, M. De Lamballerie-Anton, F. Michel, C. Añón and M. Anton 2004. Physicochemical Modifications of High-Pressure-Treated Soybean Protein Isolates. Journal of Agricultural and Food Chemistry 52: 1564-1571.

154. Purcell, J. M., D. D. Kasarda and C. S. C. Wu 1988. Secondary structures of wheat α- and ω-gliadin proteins: Fourier transform infrared spectroscopy. Journal of Cereal Science 7: 21-32.

155. Raghavan, G. S. V., T. J. Rennie, P. S. Sunjka, V. Orsat, W. Phaphuangwittayakul and P. Terdtoon 2005a. Overview of new techniques for drying biological materials with emphasis on energy aspects. Brazilian Journal of Chemical Engineering 22: 195-201.

156. Raghavan, GSV, TJ Rennie, PS Sunjka, V Orsat, W Phaphuangwittayakul and P Terdtoon 2005b. Overview of new techniques for drying biological materials with emphasis on energy aspects. Brazilian Journal of Chemical Engineering 22: 195-201.

157. Richardson, Philip 2001. Thermal technologies in food processing. In Thermal technologies in food processing. Boca Raton, Fla.; Cambridge, England: CRC Press ; Woodhead Pub.

158. Rohs, R., C. Etchebest and R. Lavery 1999. Unraveling proteins: A molecular mechanics study. Biophysical Journal 76: 2760-2768.

159. Roupassov, D. V., A. A. Nikipelov, M. M. Nudnova and A. Yu Starikovskii 2009. Flow separation control by plasma actuator with nanosecond pulsed-periodic discharge. AIAA Journal 47: 168-185.

160. Roy, Susmita and Biman Bagchi 2012. Free Energy Barriers for Escape of Water Molecules from Protein Hydration Layer. The Journal of Physical Chemistry B 116: 2958-2968.

161. Rupley, John A and Giorgio Careri 1991. Protein hydration and function. Advances in protein chemistry 41: 37.

162. Sadek, S. E. and M. Hurwitz 1972. Influence of electric fields on convective heat and mass transfer from a horizontal surface under forced convection. Journal of Heat Transfer, Transactions ASME 94 Ser C: 144-148.

163. Sagar, VR and P Suresh Kumar 2010. Recent advances in drying and dehydration of fruits and vegetables: a review. Journal of food science and technology 47: 15-26.

164. Sagui, Celeste and Thomas A Darden 1999. Molecular dynamics simulations of biomolecules: long-range electrostatic effects. Annual review of biophysics and biomolecular structure 28: 155-179.

165. Sanger, Frederick 1952. The arrangement of amino acids in proteins. Advances in protein chemistry 7: 1.

166. Senadeera, W., B. Bhandari, G. Young and B. Wijesinghe 2000. Physical property changes of fruits and vegetables during hot air drying. Drying Technology in Agriculture and Food Sciences: 149-166.

167. Singh, A., V. Orsat and V. Raghavan 2012. A Comprehensive Review on Electrohydrodynamic Drying and High-Voltage Electric Field in the Context of Food and Bioprocessing. Drying Technology 30: 1812-1820.

168. Singh, Ashutosh, Gopu Raveendran Nair, Jamshid Rahimi, Yvan Gariepy and Vijaya

Raghavan 2013b. Effect of Static High Electric Field Pre-Treatment on Microwave-Assisted Drying of Potato Slices. Drying Technology 31: 1960-1968.

169. Singh, Ashutosh, Kebba Sabally, Stan Kubow, Danielle J Donnelly, Yvan Gariepy, Valérie Orsat and GSV Raghavan 2011. Microwave-assisted extraction of phenolic antioxidants from potato peels. Molecules 16: 2218-2232.

170. Singh, Ashutosh, Shirin Munshi and Vijaya Raghavan 2013a. Effect of External Electric Field Stress on Gliadin Protein Conformation. Proteomes 1: 25-39.

171. Singh, Ashutosh, Valérie Orsat and Vijaya Raghavan 2013c. Soybean Hydrophobic Protein Response to External Electric Field: A Molecular Modeling Approach. Biomolecules 3: 168-179.

172. Singh, Harjinder 1991. Modification of food proteins by covalent crosslinking. Trends in Food Science & Technology 2: 196-200.

173. Sorgentini, D. A., J. R. Wagner and M. C. Añón 1995. Effects of thermal treatment of soy protein isolate on the characteristics and structure-function relationship of soluble and insoluble fractions. Journal of Agricultural and Food Chemistry 43: 2471-2479.

174. Sourice, S., A. Nisole, J. Guéguen, Y. Popineau and K. Elmorjani 2003. High microbial production and characterization of strictly periodic polymers modelled on the repetitive domain of wheat gliadins. Biochemical and Biophysical Research Communications 312: 989-996.

175. Stoven, S., J. A. Murray and E. Marietta 2012. Celiac Disease: Advances in Treatment via Gluten Modification. Clinical Gastroenterology and Hepatology 10: 859-862.

176. Stuetzer, O. M. 1959. Instability of certain electrohydrodynamic systems. Physics of Fluids 2: 642-648.

177. Stuetzer, O. M. 1960. Ion drag pumps. Journal of Applied Physics 31: 136-146.

178. Subirade, M., I. Kelly, J. Guéguen and M. Pézolet 1998. Molecular basis of film formation from a soybean protein: Comparison between the conformation of glycinin in aqueous solution and in films. International Journal of Biological Macromolecules 23: 241-249.

179. Sunjka, P. S., T. J. Rennie, C. Beaudry and G. S. V. Raghavan 2004. Microwave-convective and microwave-vacuum drying of cranberries: A comparative study. Drying Technology 22: 1217-1231.

180. Surewicz, W. K., H. H. Mantsch and D. Chapman 1993. Determination of protein secondary structure by Fourier transform infrared spectroscopy: A critical assessment.

Biochemistry 32: 389-394.

181. Toda, S. 1990. Preservation of foods and vegetables by application of electric field. Shokuhin Rhytsu Gijitsu 19: 62-64.

182. Vader, L. Willemijn, Dariusz T. Stepniak, Evelien M. Bunnik, Yvonne M. C. Kooy, Willeke De Haan, Jan Wouter Drijfhout, Peter A. Van Veelen and Frits Koning 2003. Characterization of cereal toxicity for celiac disease patients based on protein homology in grains. Gastroenterology 125: 1105-1113.

183. van der Spoel, David, Erik Lindahl, Berk Hess, AR Van Buuren, E Apol, PJ Meulenhoff, DP Tieleman, ALTM Sijbers, KA Feenstra and Rudi van Drunen 2008. GROMACS user manual version 3.3.

184. Van Der Spoel, David, Erik Lindahl, Berk Hess, Gerrit Groenhof, Alan E Mark and Herman JC Berendsen 2005a. GROMACS: fast, flexible, and free. Journal of computational chemistry 26: 1701-1718.

185. Van Der Spoel, David, Erik Lindahl, Berk Hess, Gerrit Groenhof, Alan E. Mark and Herman J. C. Berendsen 2005b. GROMACS: Fast, flexible, and free. Journal of computational chemistry 26: 1701-1718.

186. Van Velzen, E. J. J., J. P. M. Van Duynhoven, P. Pudney, P. L. Weegels and J. H. Van der Maas 2003. Factors associated with dough stickiness as sensed by attenuated total reflectance infrared spectroscopy. Cereal Chemistry 80: 378-382.

187. Wang, Yulan, Peter S. Belton, Helene Bridon, Elisabeth Garanger, Nikolaus Wellner, Mary L. Parker, Alex Grant, Pierre Feillet and Tim R. Noel 2001. Physicochemical Studies of Caroubin: A Gluten-like Protein. Journal of Agricultural and Food Chemistry 49: 3414-3419.

188. Wangnipparnto, S., J. Tiansuwan, S. Jiracheewanun, T. Kiatsiriroat and C. C. Wang 2002. Air side performance of thermosyphon heat exchanger in low Reynolds number region: With and without electric field. Energy Conversion and Management 43: 1791-1800.

189. Wellner, N., E. N. C. Mills, G. Brownsey, R. H. Wilson, N. Brown, J. Freeman, N. G. Halford, P. R. Shewry and P. S. Belton 2005. Changes in protein secondary structure during gluten deformation studied by dynamic fourier transform infrared spectroscopy. Biomacromolecules 6: 255-261.

190. Were, L., N. S. Hettiarachchy and U. Kalapathy 1997. Modified Soy Proteins with Improved Foaming and Water Hydration Properties. Journal of Food Science 62: 821-

824.

191. Wolny, A. 1992. Intensification of the evaporation process by electric field. Chemical Engineering Science 47: 551-554.

192. Wolny, A. and R. Kaniuk 1996. The effect of electric field on heat and mass transfer. Drying Technology 14: 195-216.

193. Xiang, BY, MO Ngadi, BK Simpson and MV Simpson 2011. Pulsed electric field induced structural modification of soy protein isolate as studied by fluorescence spectroscopy. Journal of Food Processing and Preservation 35: 563-570.

194. Xue, G. R., T. Uchino and M. Matsuo 1994. Drying promoting of radish using corona discharge. Journal of the Japanese Society of Agricultural Machinery 56: 35-42.

195. Xue, X., N. N. Barthakur and I. Alli 1999. Electrohydrodynamically-dried whey protein: An electrophoretic and differential calorimetric analysis. Drying Technology 17: 467-478.

196. Ya-xiang, B., L. Jing, M. Yan and K. Dong-mei 2008. Experiment of drying kelp with high voltage electric fields. International Conference on High Voltage Engineering and Application: 732-734.

197. Yamashita, K., M. Kumagai, S. Sekita, A. Yabe, T. Taketani and K. Kikuchi 1991. Heat transfer characteristics on an EHD condenser. Proc. ASME/JSME Thermal Eng. 3: 61-67.

198. Yaxiang, B., Y. Hu, X. Li and J. Li 2009. Experiment study of electrohydrodynamic (EHD) drying scallop. Power and Energy Engineering Conference: 2803-2806.

199. Yaxiang, Bai, Hu Yucai and Li Xinjun 2010. The Tofu's Characteristics of Electrohydrodynamic Drying with Wire Electrode. Power and Energy Engineering Conference (APPEEC), 2010 Asia-Pacific, 1-4.

200. Zheng, D. J., Y. Q. Cheng, H. J. Liu and L. T. Li 2011. Investigation of EHD-enhanced water evaporation and a novel empirical model. International Journal of Food Engineering 7.